

**The origin of electron density
accumulation within CH,HC contacts in
biphenyl: a theoretical study**

by

Thomas Günter Bates

Supervisor: Dr. Jurgens de Lange

Co-Supervisor: Prof. Ignacy Cukrowski

Submitted in fulfilment of the requirements for the degree

Master of Science (Chemistry)

In the Faculty of Natural & Agricultural Sciences

University of Pretoria

Pretoria, South Africa

May 2021

Declaration

Declaration

I, Thomas Günter Bates, declare that the dissertation, which I hereby submit for the degree Master of Science (Chemistry) at the University of Pretoria, is my own work and has not previously been submitted by me for a degree at this or any other tertiary institution.

SIGNATURE: _____



DATE: 20th May 2021

Abstract

The primary focus of this work is the investigation into the nature and origin of the electron density between the *ortho*-hydrogens in the higher energy, planar transition state of biphenyl. This interaction has been the subject of debate within the scientific community for almost three decades with no clear consensus being made. Since the distance between these hydrogens is smaller than their summed van der Waals radii (2.4 Å), classically one can assume that they partake in a steric clash, however the Quantum Theory of Atoms in Molecules (QTAIM) depicts a bond path for this H,H contact. This presence of a bond path caused the rift in the scientific community.

To investigate the problem, we made use of cross-section decomposition analysis whereby the electron density at any given coordinate is decomposed into the components that contribute to its presence. In this dissertation, three methods using this analysis were made, namely (i) MO-ED, (ii) FALDI-ED, and (iii) NBO-ED. These represent the decomposition products that the density is decomposed into; the MO-ED method decomposed the density between the *ortho*-hydrogens into its molecular orbital (MO) contributions, the FALDI-ED method decomposed the density into fragment *and* diatomic contributions, and the NBO-ED method decomposed the density into its natural bond orbital (NBO) contributions.

With all three methods, when decomposing the density along the λ_2 -eigenvector from the bond critical point (BCP) between the *ortho*-hydrogens in the planar conformer, it was found that the total electron density is concentrating, shown by the directional second partial derivative. This means that the electron density is purposefully accumulated in the H,H contact rather than dissipated as one would expect from a classical steric clash. Furthermore, this density decomposition analysis revealed that this density is due to a large molecular-wide delocalisation, rather than a classical 2-centred approach, with the largest contributions (in both conformers) being from the two covalent *ortho* C-H bonds. This delocalisation forms a density

Abstract

channel between two hydrogens, of an overwhelmingly concentrating/bonding nature, forming a weak covalent bond. Due to these findings, it is clear that the classical idea of a steric clash cannot be the case for this system, and that QTAIM correctly predicts the bond path between these *ortho*-hydrogens.

Outputs of this Work

Journal Publications

1. Cukrowski, I.; de Lange, J.H.; van Niekerk, D.M.; Bates, T.G. Molecular Orbitals Support Energy-Stabilizing ‘Bonding’ Nature of Bader’s Bond Paths. *J. Phys. Chem. A* **2020**, *124*, 5523-5533. DOI: 10.1021/acs.jpca.0c02234.
2. Bates, T.G.; de Lange, J.H.; Cukrowski, I. The CH···HC interaction in biphenyl is a delocalized, molecular-wide and entirely non-classical interaction: results from FALDI analysis. *J. Comput. Chem.* **2021**. DOI: 10.1002/jcc.26491.

Conference Presentations

1. Bates, T.G.; de Lange, J.H. Bridging quantum chemical topology (QCT) and molecular orbital (MO) based interpretations in explaining the absence/presence of Bader’s bond paths. *Proceedings of the South African Chemical Institute Young Chemists’ Symposium 2019*, Thohoyandou, South Africa. (*Oral, received 1st prize for best presentation*).
2. Bates, T.G.; de Lange, J.H.; Cukrowski, I. The CH···HC Interaction In Biphenyl Is A Delocalized, Molecular-Wide And Entirely Non-Classical Interaction: Results From FALDI Analysis. *Proceedings of the 4th International Symposium On Halogen Bonding 2020*, Stellenbosch, South Africa. (*Poster, received honourable mention*).

Table of Contents	Page
Abstract	iii
Outputs of this work	v
Table of Contents	vi
List of Figures	x
List of Tables	xv
List of Abbreviations	xviii
Chapter 1. Introduction	1
1.1. Chemical Bonding	2
1.2. Previous Studies on Biphenyl	4
1.3. Meaning of a Bond Path	6
1.4. Aims and General Approach	7
1.5. Overview of this Dissertation	7
1.6. References	12
Chapter 2. Theoretical Background	14
2.1. Introduction	15
2.2. Electronic Structure Methods	16
2.2.1. Levels of Theory	16
2.2.1.1. Hartree-Fock Approximations	16
2.2.1.2. Density Functional Theory	21
2.2.2. Basis Sets	23
2.3. Quantum Chemical Topology	26
2.3.1. QTAIM	26
2.3.1.1. Background	26
2.3.1.2. Critical Points, Curvatures, and Bond Paths	27
2.3.1.3. Zero Flux Surface, Gradient Vector Field, and Atomic Boundaries	29
2.3.1.4. Electron (de)localisation	30
2.3.2. FALDI Background	32
2.3.2.1. Original Reason for FALDI Development	32

Table of Contents

2.3.2.2. Electron Density and Pair Density	33
2.3.2.3. Domain Averaged Fermi Holes	35
2.3.2.4. FALDI Decomposition Development	37
2.4. Orbital Analysis	39
2.4.1. Molecular Orbitals	39
2.4.2. Natural Bond Orbitals	40
2.5. New Theoretical Developments	40
2.5.1. Cross-Section Decomposition of Electron Density	40
2.5.2. $CP(\mathbf{r})$ Function	42
2.5.3. MO–DI	43
2.6. References	46
Chapter 3. Molecular Orbitals Support Energy-Stabilizing ‘Bonding’ Nature of Bader’s Bond Paths	47
3.1. Abstract	48
3.2. Introduction	49
3.3. Methods	51
3.3.1. Theoretical Background	51
3.3.2. Computational Details	53
3.4. Results and Discussion	53
3.4.1. MO-based picture of the C1-C12 and C19-H22 covalent bonds in the planar conformer	55
3.4.2. MO-based interpretation of absence and presence of a DB between H–atoms of a bay in Bph conformers	58
3.4.3. MO-based nature of the hydride H,H DBs in cubic Li_4H_4	63
3.5. Conclusions	65
3.6. Associated Content	69
3.6.1. Supporting Information	69
3.7. Acknowledgments	69
3.8. References	70

Chapter 4. The CH \cdots HC interaction in biphenyl is a delocalized, molecular wide and entirely non-classical interaction: results from FALDI analysis	76
4.1. Abstract	77
4.2. Introduction	78
4.3. Theoretical Background	81
4.4. Computational Methods	87
4.5. Results and Discussion	87
4.5.1. FALDI Fragment analysis of planar and twisted biphenyl	91
4.5.2. FALDI diatomic analysis of planar and twisted biphenyl	97
4.6. Conclusions	100
4.7. Conflicts of interest	101
4.8. Acknowledgments	102
4.9. References	102
Chapter 5. NBOs Support MO and FALDI based ‘Bonding’ Description of CH \cdots HC Bond Paths in Planar Biphenyl	106
5.1. Abstract	107
5.2. Introduction	108
5.3. Theoretical Background	111
5.4. Computational Methods	112
5.5. Results and Discussion	113
5.6. Conclusions	120
5.7. References	122
Chapter 6. Conclusions	124
6.1. Summary	125
6.2. Future Work	133
6.3. References	134
Appendix I Molecular Orbitals Support Energy-Stabilizing ‘Bonding’ Nature of Bader’s Bond Paths	135

Appendix II	The CH \cdots HC interaction in biphenyl is a delocalized, molecular wide and entirely non-classical interaction: results from FALDI analysis	182
Appendix III	NBOs Support MO and FALDI based 'Bonding' Description of CH \cdots HC Bond Paths in Planar Biphenyl	201

List of Figures		Page
Chapter 1.	Introduction	
Scheme 1.	Molecular graph of planar biphenyl, with corresponding bond paths between the ortho-hydrogens.	4
Chapter 2.	Theoretical Background	
Scheme 1	Molecular graph of planar biphenyl. The lines represent bond paths, as well as critical points.	28
Chapter 3.	Molecular Orbitals Support Energy-Stabilizing ‘Bonding’ Nature of Bader’s Bond Paths	
Figure 1.	Molecular graphs of planar biphenyl and equilibrium structures of cubic Li ₄ H ₄ .	50
Figure 2.	Cross-sections along the λ_2 -eigenvector in the C1,C12 and C19,H22 inter-nuclear regions.	56
Figure 3.	Decomposition of the directional partial second and derivatives along the λ_2 -eigenvector in the H7,H18 inter-nuclear region in planar and twisted biphenyl, on selected individual MOs.	60
Figure 4.	Shapes of the eight MOs in cubic Li ₄ H ₄ .	63
Figure 5.	The partial directional 2nd-derivative, ED contributions made by higher-energy MOs and lower-energy MOs and the CP(r) function as cross-sections along the λ_2 -eigenvector for atom-pair H2,H5 in Li ₄ H ₄ .	64

Chapter 4.	The CH···HC interaction in biphenyl is a delocalized, molecular wide and entirely non-classical interaction: results from FALDI analysis	
Figure 1.	Decomposition of the electron density at the CP(H7,H18) in planar biphenyl into concentrating density and depleting density, as well as the decomposition of these densities into MO contributions.	79
Scheme 1.	Definition of fragments for FALDI analysis.	88
Figure 2.	Decomposition of the 2 nd derivative $\rho(\text{tot})$ in planar conformation, and of the Total-ED in twisted conformation of both MO-ED and FALDI-ED along the 2 nd eigenvector crossing the CP(H7,H18) in the planar and MDP(H7,H18) in twisted, as well as showing the $CP(\mathbf{r})$ function in planar and twisted conformation for the MO-ED and FALDI-ED method.	90
Figure 3.	Decompositions showing the leading and remaining major FALDI fragment contributions to the ED of the CP(H7,H18) along the λ_2 -eigenvector in planar biphenyl.	93
Figure 4.	Isosurfaces of less significant, but noteworthy contributions in planar and twisted biphenyl.	94
Figure 5.	Decompositions showing the leading and remaining major FALDI fragment contributions to the ED of the MDP(H7,H18) along the λ_2 -eigenvector in twisted biphenyl.	96
Chapter 5.	NBOs Support MO and FALDI based ‘Bonding’ Description of CH···HC Bond Paths in Planar Biphenyl	
Scheme 1.	Molecular graph of planar biphenyl.	108

Figure 1.	Cross-section comparison between FALDI-ED and NBO-ED analysis along λ_2 -eigenvector, crossing the BCP(H7,H18) and MDP(H7,H18) where applicable in planar and twisted biphenyl, respectively.	115
Scheme 2.	Atom numbering of biphenyl.	116
Chapter 6.	Conclusions	
Scheme 1.	Atom numbering of biphenyl.	125
Scheme 2.	Definition of fragments for FALDI analysis.	129
Scheme 3.	Illustration of the major atom-pair contributions.	129
Appendix I.	Molecular Orbitals Support Energy-Stabilizing ‘Bonding’ Nature of Bader’s Bond Paths	
Figure S1.	Delocalized matrix for N_2 , as calculated at HF/6-311++G(2df,2pd) level.	144
Figure S2.	3D-isosurfaces of MOs of N_2 at the HF/6-311++g(2df,2pd) level. Percentage contributions to the $DI(N,N)$ as well as to the electron density at the (3,-1) CP(N,N) are also shown.	145
Figure S3.	Decomposition of the total-ED, first derivative and directional second partial derivatives along the λ_2 -eigenvector in the C1,C12 inter-nuclear region in planar biphenyl, as well as the subsequent decomposition of the concentrating density into the largest MO contributions.	169
Figure S4.	Decomposition of the total-ED, first derivative and directional second partial derivatives along the λ_2 -eigenvector in the C19,H22 inter-nuclear region in planar biphenyl, as well as the subsequent decomposition of the concentrating density into the largest MO contributions.	170

Figure S5.	Decomposition of the total-ED, first derivative and directional second partial derivatives along the λ_2 -eigenvector in the H7,H18 inter-nuclear region in planar biphenyl, as well as the subsequent decomposition of the concentrating density into the largest MO contributions.	176
Figure S6.	Decomposition of the total-ED, first derivative and directional second partial derivatives along the λ_2 -eigenvector in the H7,H18 inter-nuclear region in twisted biphenyl, as well as the subsequent decomposition of the concentrating density into the largest MO contributions.	177
Figure S7	Decomposition of the total-ED, first derivative and directional second partial derivatives along the λ_2 -eigenvector in the H2,H5 inter-nuclear region in Li ₄ H ₄ , as well as the subsequent decomposition of the concentrating density into the largest MO contributions	181
Appendix II.	The CH \cdots HC interaction in biphenyl is a delocalized, molecular wide and entirely non-classical interaction: results from FALDI analysis	
Figure S1.	Decomposition of the directional second partial derivative $\rho(\text{tot})$ along the λ_2 -eigenvector crossing the CP(H7,H18) in planar conformer and MDP(H7,H18) in twisted conformer of biphenyl to major contributions (concentrating, depleting, and removing) using MO and FALDI densities.	186
Figure S2.	Decomposition of the $\rho(\text{tot})$ along the λ_2 -eigenvector crossing the CP(H7,H18) in planar conformer and MDP(H7,H18) in twisted conformer of biphenyl to major contributions (concentrating, depleting, and removing) using MO and FALDI densities.	187

Figure S3.	<i>CP</i> (r) function cross-sections along the λ_2 -eigenvector crossing the CP(H7,H18) in the planar conformer and MDP(H7,H18) in twisted conformer of biphenyl using MO and FALDI densities.	188
Scheme S1.	Definition of fragments for FALDI analysis.	189
Figure S4.	Decomposition of the major and minor FALDI fragment contributions to the ED of the CP(H7,H18) along the λ_2 -eigenvector in planar biphenyl.	190
Figure S5.	Decomposition of the major and minor FALDI fragment contributions to the ED of the MDP(H7,H18) along the λ_2 -eigenvector in twisted biphenyl.	192
 Appendix III. NBOs Support MO and FALDI based ‘Bonding’ Description of CH\cdotsHC Bond Paths in Planar Biphenyl		
Figure S1.	Decomposition of the directional second partial derivative ρ (tot) along the λ_2 -eigenvector crossing the CP(H7,H18) in planar conformer and MDP(H7,H18) in twisted conformer of biphenyl to major contributions (concentrating, depleting, and removing) using FALDI and NBO methods.	205
Figure S2.	Decomposition of the ρ (tot) along the λ_2 -eigenvector crossing the CP(H7,H18) in planar conformer and MDP(H7,H18) in twisted conformer of biphenyl to major contributions (concentrating, depleting, and removing) using FALDI and NBO methods.	206
Figure S3.	<i>CP</i> (r) function cross-sections along the λ_2 -eigenvector crossing the CP(H7,H18) in the planar conformer and MDP(H7,H18) in twisted conformer of biphenyl using FALDI and NBO methods.	207

List of Tables	Page
Chapter 3. Molecular Orbitals Support Energy-Stabilizing ‘Bonding’ Nature of Bader’s Bond Paths	
Table 1. Selected top-views of MOs in planar Bph. Percentage contributions to ED at relevant BCPs and DI for interactions of interest are also shown.	54
Chapter 4. The CH···HC interaction in biphenyl is a delocalized, molecular wide and entirely non-classical interaction: results from FALDI analysis	
Table 1. Isosurfaces of the most significant FALDI atom-pair contributions of concentrating, depleting, and removing nature to the electron density at the (3,-1) CP(H7,H18) and MDP(H7,H18) in planar and twisted biphenyl, respectively.	98
Table 2. Most notable FALDI-ED contributions and %-fractions to the (3,-1) CP(H7,H18) and MDP(H7,H18) in planar and twisted biphenyl, respectively, for concentrating, depleting, and removing density.	99
Chapter 5. NBOs Support MO and FALDI based ‘Bonding’ Description of CH···HC Bond Paths in Planar Biphenyl	
Table 1. Electron density contribution (a.u.) with its corresponding %-fraction for the major NBOs contributing to concentrating and depleting density at the BCP(H7,H18) in planar and MDP(H7,H18) in twisted biphenyl.	117

Table 2.	Isosurfaces of the most significant (above 5% contribution) NBO contributions at the (3,-1) CP(H7,H18) and MDP(H7,H18) in planar and twisted biphenyl, respectively.	119
Appendix I. Molecular Orbitals Support Energy-Stabilizing ‘Bonding’ Nature of Bader’s Bond Paths		
Table S1.	Cartesian coordinates of planar biphenyl at the B3LYP/6-311++g(2df,2pd)/GD3 level.	147
Table S2.	Cartesian coordinates of twisted biphenyl at the B3LYP/6-311++g(2df,2pd)/GD3 level.	148
Table S3.	Cartesian coordinates of cubic Li ₄ H ₄ at the B3LYP/6-311++g(2df,2pd)/GD3 level.	149
Table S4.	Full list of MOs in the planar biphenyl.	150
Table S5.	Full list of MOs in the twisted biphenyl.	157
Table S6.	MO-ED data at (3,-1) CP(C1,C12) & CP(C19,H22) in the planar biphenyl.	164
Table S7.	MO-DI data (in e ⁻ -pairs) for covalent bond C1–C12 in the planar biphenyl.	166
Table S8.	MO-DI data (in e ⁻ -pairs) for covalent bond C19–H22 in planar biphenyl.	167
Table S9.	Summary of MO-ED & MO-DI data, for covalent bonds C1,C12 & C19,H22 in planar biphenyl.	168
Table S10.	MO-ED data at (3,-1) CP(H7,H18) in planar and at MDP(H7,H18) in twisted biphenyl.	171
Table S11.	MO-DI data (in e ⁻ -pairs) for noncovalent interaction H7⋯H18 in the planar biphenyl.	173
Table S12.	MO-DI data (in e ⁻ -pairs) for noncovalent interaction H7⋯H18 in the twisted biphenyl.	174
Table S13.	Summary of MO-ED & MO-DI data for H7⋯H18 in planar and twisted biphenyl.	175
Table S14.	MO-ED data at (3,-1) CP(H2,H4), CP(H2,H5) and CP(H4,H5) in Li ₄ H ₄ .	178
Table S15.	MO-DI data for the H2,H5 atom-pair in Li ₄ H ₄ .	179

Table S16.	Summary of MO-ED and MO-DI data for three H \cdots H density bridges in Li ₄ H ₄ .	180
Appendix II.	The CH \cdots HC interaction in biphenyl is a delocalized, molecular wide and entirely non-classical interaction: results from FALDI analysis	
Table S1.	Cartesian coordinates of planar biphenyl at the B3LYP/cc-pVDZ level.	184
Table S2.	Cartesian coordinates of twisted biphenyl at the B3LYP/cc-pVDZ level.	185
Table S3.	FALDI fragment data at (3,-1) CP(H7,H18) or MDP(H7,H18) in planar and twisted biphenyl, respectively.	193
Table S4.	FALDI diatomic data at (3,-1) CP(H7,H18) or MDP(H7,H18) in planar and twisted biphenyl, respectively.	194
Appendix III.	NBOs Support MO and FALDI based ‘Bonding’ Description of CH \cdots HC Bond Paths in Planar Biphenyl	
Table S1.	Cartesian coordinates of planar biphenyl at the B3LYP/cc-pVDZ level.	203
Table S2.	Cartesian coordinates of twisted biphenyl at the B3LYP/cc-pVDZ level.	204
Table S3.	Isosurfaces of the most significant NBO contributions the (3,-1) CP(H7,H18) and MDP(H7,H18) in planar and twisted biphenyl, respectively.	208

List of Abbreviations

a.u.	Atomic Units
AOM	Atomic Overlap Matrix
AOM	Atomic Orbital
B3LYP	Becke, 3-Parameter, Lee-Yang-Parr
BCP	Bond Critical Point
BP	Bond Path
Bph	Biphenyl
CCP	Cage Critical Point
CHPC	Centre for High Performance Computing
CP	Critical Point
CSD	Cambridge Structural Database
DAFH	Domain Averaged Fermi Hole
DB	Density Bridge
DD	Deformation Density
DFT	Density Functional Theory
DI	Delocalisation Index
ED	Electron Density
EDA	Energy Decomposition Analysis
ETS	Extended Transition State
FALDI	Fragment, Atomic, Localised, Delocalised, Intra- & Inter-atomic
FAMSEC	Fragment Attributed Molecular System Energy Change
FOHI	Fractional Occupation Iterative Hirshfeld
HF	Hartree-Fock
IQA	Interacting Quantum Atoms
LBT	Lewis Bond Theory
LDO	Localised-Delocalised Overlap
LI	Localisation Index
MDP	Minimum Density Point
MO	Molecular Orbital
NBO	Natural Bond Orbital
NCP	Nuclear Critical Point
NOCV	Natural Orbitals for Chemical Valence

List of Abbreviations

PD	Pair-Density
QM	Quantum Mechanics
QTAIM	Quantum Theory of Atoms in Molecules
QTC	Quantum Chemical Topology
RCP	Ring Critical Point
REG	Relative Energy Gradient
SCF	Self-Consistent Field
VB	Valence Bond
vdW	van der Waals
XC	Exchange-Correlation

Chapter 1

Introduction

1.1. Chemical Bonding

The term *chemical bond* and what it refers to, is immediately understood by chemists. However, when one tries to define a chemical bond and what defining features are needed to characterise it, conflict arises.

A chemical bond could be described as a phenomenon (having a set of physical-chemical properties) leading to the lowering of energy between two atomic nuclei, and as a whole, it is an energy minimising contribution to a molecular system.^[1] This concept of a chemical bond is thoroughly defined for diatomic molecules, in which one can measure the stabilisation of energy of two atoms that are brought together from an infinite distance.

For polyatomic molecules however, we expand our knowledge from diatomic theory to understand polyatomic molecular bonding. If one takes CO₂ as example, one could say that the carbon is attracted to the one oxygen (O1), but what about the second (O2)? Is O2 attracted to the carbon atom, or to the whole delocalised system of the already established C-O1 bond? Classically, one can explain this conundrum using Lewis Bond Theory (LBT), but on a quantum mechanics (QM) level, the electrons that were once localised to the carbon atom are now delocalised with the one oxygen atom. This makes bonding in polyatomic molecules more complex.

There are traditionally two major models for the calculation of chemical bonds and molecular structures, namely valence bond (VB) theory^[2-5] and molecular orbital (MO) theory.^[2-3, 6] There is however a third approach that will be discussed in this project along with MO theory, which is natural bond orbital (NBO) theory.^[7-9]

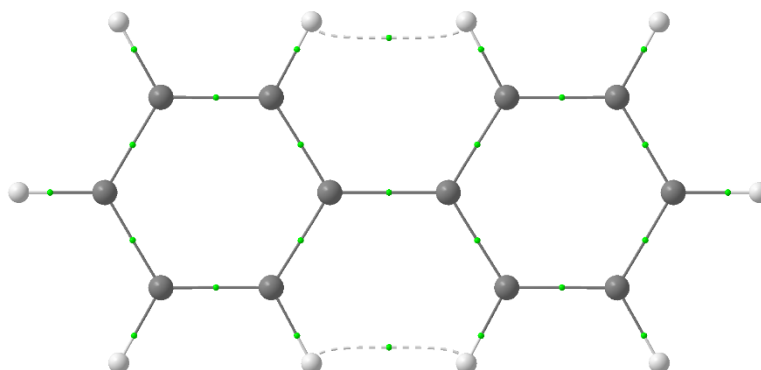
VB theory was the first successful method for calculating molecular energy, achieved by Heitler and London's H₂ calculation, but was not adequate for describing larger molecules. Due to this shortcoming, it was overshadowed by Friedrich Hund and Robert Muliken's theory of MOs. Today nearly all computational chemistry calculations make use of MO theory to

calculate electronic structures of atoms and molecules.^[6] The main view of MO theory is to disregard the notion of electrons being fixed to one specific bond, but rather be free to delocalise them throughout the entire molecule, in stark contrast to LBT. Although it has been shown to be highly accurate for small molecules, the main concepts of MOs in polyatomic molecules are merely extensions of the theory based on homonuclear diatomic molecules/ions. The third approach to chemical bonding is NBO, which intrinsically views electronic wave functions as localised Lewis-like chemical bonds. These can be split further into Lewis members or non-Lewis members that describe the lone pairs or bond pairs as you would typically see in a Lewis-dot structure and resonance delocalisation. In order to fulfil the restriction of its electronic wave function to form Lewis-like chemical bonds however, the orbitals are forced to be doubly occupied, likewise to MOs calculated using the Hartree-Fock approximation or Density Functional Theory for example.

Modern theories have been developed on the basis of QM to describe chemical bonding, in which a successful theory arose, developed by Richard Bader, called the Quantum Theory of Atoms in Molecules (QTAIM)^[10] – this will be discussed in more detail in Chapter 2. In short, QTAIM describes atoms and bonds directly from the quantum observable electron density (ED), rather than from the electronic wavefunction.

What happens, however, if a modern theory disagrees with classical interpretations or intuition? As an example, what if QTAIM would contradict (to a certain extent) LBT? This is the case about two conformations (equilibrium/twisted and planar) of biphenyl (Bph, Scheme 1) which has led to a scientific debate for almost three decades.^[11-28] The contention largely came about when Matta *et al* suggested with the aid of QTAIM that the *ortho*-hydrogen atoms are in-fact “bonded” in the bay-region of planar Bph, contradicting our intuition as a chemist.^[12] Note that this phenomenon is not exclusive to Bph; there are many systems that

resemble this “bond”, such as in phenanthrene and *cis*-2-butene. This will be elaborated on further in the following sections.



Scheme 1. Molecular graph of planar Bph, with corresponding bond paths between the *ortho*-hydrogens.

1.2. Previous Studies on Biphenyl

Bph exists at equilibrium as twisted, with a dihedral angle (ϕ) of $\pm 42^\circ$ between the rings and has a rotation barrier of $2.1 \text{ kcal.mol}^{-1}$ between the equilibrium conformation and its planar transition state.^[29] Furthermore, in the planar conformation, the *ortho*-hydrogens are separated by $\pm 1.94767 \text{ \AA}$, whereas the van der Waals radii of the two hydrogens sums to 2.4 \AA . Due to this, one of the first interpretations for the twisted conformation to be lower in energy was made in 1944 by Karle *et al.*,^[30] stating that it avoids the steric hindrance between the *ortho*-hydrogen atoms in the planar conformation.

The debate about the bonding nature of this interaction between the aforementioned hydrogens uses approaches routed in two major families of QM methods. The one grouping belongs to an orbital-based method including the use of MOs and NBOs, and the second grouping belongs to an ED-based method incorporating QTAIM and interacting quantum atoms (IQA).^[31] In general, the arguments made *for* the bonding nature of the hydrogens are routed in density-based approaches, and arguments made *against* the bonding nature are routed in orbital-based approaches. This division leads to the speculation of why one family of QM

methods forms a different conclusion to that of the other, and whether or not these two families can be reconciled.

Cioslowski and Mixon^[11] studied planar and twisted Bph back in 1992 with QTAIM, but they took a more neutral approach in their conclusion – the presence of a bond path (BP) does not inherently imply bonding. As previously mentioned, the debate mainly surfaced when Matta *et al*^[12] suggested that the BP between the *ortho*-hydrogens actually stabilises the molecule in the planar conformation, rather than destabilising it by steric hindrance. However, Poater *et al*^[13] disputed Matta’s claims by concluding that the Pauli repulsion from Kohn-Sham MO theory is at a maximum in the planar conformation after adjusting the bond distance of the carbon-carbon linkers. They further ‘validated’ their claim by cutting the four *ortho*-hydrogens from Bph to form a tetra-radical system and observing that this system optimises to the planar conformation. Poater however, was quickly rebutted by Bader^[14] on the basis that the former authors arbitrarily chose “non-physical reference states that violate all of the rules of physics.”

If we look at more recent studies, Hancock *et al*^[21] investigated the stabilities between the two structural isomers phenanthrene and anthracene (phenanthrene contains an H···H interaction similar to planar Bph). They attributed the increased stability of phenanthrene to the increased aromatic stabilisation of its π -orbitals and that its corresponding H···H interaction actually destabilises the molecule. Weinhold *et al*^[23] studied another similar system, *cis*-2-butene, whereby a BP is present between two hydrogens on the terminal carbons if the hydrogens point towards each other. Weinhold approached this system using another orbital-based method, namely NBO. Although he claimed that “there is evidently a germ of truth” in the QTAIM view (BP existing between the hydrogens), he concluded that according to NBO analysis, the hydrogens are nevertheless repulsive/sterically hindered. On the opposing side of this dispute, Eskandari and Van Alsenoy^[22] agreed with Matta and Bader’s hypothesis that the *ortho*-hydrogens in planar Bph have a bonding mechanism. After using IQA to study the energy

components, they discovered that the *ortho*-hydrogens have a net attractive interaction to each other. Popelier *et al*^[28] also studied the energetics of planar Bph, and similarly concluded that the *ortho*-hydrogens form a weak covalent bond between the two, to a degree counteracting the net destabilisation of the planar conformation.

There are many more studies that could be thoroughly discussed, but for the purpose of this discussion, the main focus is to show that the density-based approach leads to a ‘bonding’ conclusion, and that an orbital-based approach leads to a ‘non-bonding’ conclusion.

1.3. Meaning of a Bond Path

Throughout this long scientific debate, the question arises (either directly or indirectly) of what the chemical meaning a BP is (as QTAIM defines it). A BP first and foremost is a line of maximum ED, linking two nuclei with a corresponding bond critical point (BCP) between them. Richard Bader eloquently addressed this^[32-33] clarifying that a BP is not a chemical bond; As briefly discussed in the beginning of this chapter, giving a precise definition for a chemical bond with a set of physical parameters is difficult, but arguably the most important aspect of a chemical bond is that it is an aid to chemical concepts – it is not a real or measurable property. On the other hand, a BP is precise in its definition, in line with physics, and since ED is measurable, a BP is a measurable property of a system which is becoming common practice today.^[34-35] Because all BP’s share common quantum mechanical properties, a BP is an indicator of *bonding* between atoms, not a *bond* between atoms, the former being a mechanism of stabilising/lowering the energy the molecule/molecular environment and the latter being a physical object.

In support of QTAIM, Pendás *et al*^[19] sought to determine the further meaning and implications of a BP, and concluded that BPs indicate the presence of privileged exchange-channels, or to put it otherwise, carriers of quantum-mechanical exchange. They give a criterion of two factors that lead to the formation of a BP, (i) that direct exchange must occur

between the respective atoms, with no other atoms in its close environment to compete and (ii) that out of all possibilities, the V_{XC} term must be largest for the given BP.

This was, however, shown not to be the case, as de Lange *et al*^[36] investigated the FALDI-based criterion for the origin of an ED bridge. They showed that the bicentric approach of setting parameters for the presence of a BP distorts the topology of the ED; rather its presence is due to the multicentred nature of the molecular environment. They state that the notion of privileged exchange-channels put forward by Pendás *et al* should be refined to incorporate the multicentred nature of the molecule, taking into account multiple exchange-channels.

1.4. Aims and General Approach

This dissertation aims to (i) explain the presence and absence of a BP in planar and twisted Bph, respectively, (ii) determine the origin of the density of the H,H contact, (iii) determine the nature of this H \cdots H interaction and (iv) reconcile the orbital- and density-based disparity in their interpretations of the nature of the BP in planar Bph. The term ‘nature of this H \cdots H interaction’ refers to whether the density is concentrating, depleting, or removing, which is synonymous with bonding, nonbonding or antibonding, respectively. In order to achieve these aims, we utilise an in-house developed density decomposition cross-section analysis. Cross-section analysis allows us to decompose the density at a specific point in space (densities that can be decomposed from a number of sources) into individual contributors, allowing us to investigate the origin and nature of the specific density by observing what factors are at play.

1.5. Overview of this Dissertation

Each of the results-containing chapters, Chapters 3 through 5 (as well as Appendices I through III), are presented as the manuscripts for publication whereby Chapter 3 has been published in the Journal of Physical Chemistry A,^[37] and Chapter 4 has been submitted at the time of writing to Physical Chemistry Chemical Physics.^[38] Chapter 5 is being prepared for submission to the Journal of Computational Chemistry. Each appendix is presented as the supplementary

information pertaining to its relative chapter, i.e. Appendix I relates to Chapter 3, and so on. Note that the manuscripts for Chapters 3 and 4 are included as they were submitted for publication.

This dissertation tells a ‘story’ if you will, investigating the density at the BCP and minimum density point (MDP) of H···H in the planar and twisted conformation, respectively, from different methods. A brief overview of each chapter is explained below.

Chapter 2 provides the Theoretical Background relating to this present work. It is split into four sections. The first section covers some background in “Electronic Structure Methods” which include the following topics: (i) Levels of Theory and (ii) Basis Sets. In the second section, “Quantum Chemical Topology” is addressed, covering the crucial background and fundamentals of (i) QTAIM^[10] and (ii) FALDI^[36, 39-42]. The third section departs from electron density focused methods and moves on to wavefunction methods in “Orbital Analysis” covering (i) Molecular Orbitals and (ii) Natural Bond Orbitals. Finally, “New Theoretical Developments” is discussed in the fourth section covering (i) Cross-Section Decomposition of Electron Density, (ii) a function to describe the presence of a BP ($CP(\mathbf{r})$ Function) and (iii) a method for decomposing QTAIM delocalisation indices (DI) in terms of MOs, also known as the MO-DI method.

Chapter 3, titled “Molecular Orbitals Support Energy-Stabilising ‘Bonding’ Nature of Bader’s Bond Paths”^[37] is the first chapter in the investigation of the BP between the *ortho*-hydrogens in planar Bph, published in the Journal of Physical Chemistry A. This chapter utilises cross-section decomposition of electron density as well as the MO-DI method to break down the densities at the BCP between two non-controversial, traditional covalent bonds. These results are then compared to the BCP(H,H) and MDP(H,H) in the planar and twisted conformation of Bph, respectively. Further investigation was done on another H···H

interaction, but rather than the two hydrogens having net positive charges (δ^+) as is the case in Bph, these hydrogens have net negative charges (δ^-) in cubic Li_4H_4 .

The densities for this study are decomposed from MO distributions, and by utilising cross-section analysis, the density at the aforementioned points in space can be decomposed into MO contributions. This allows one to determine which MOs contribute (and to what extent) to the density, and whether they are either concentrating or depleting. The MO-DI method, however, decomposes the QTAIM DI into MO contributions. This creates valuable insights to the extent of electron density ‘donation’ from all MOs, but also to determine the nature at which the MOs interrelate – if they increase the delocalised electron pairs through constructive interference or decrease the delocalised electron pairs through deconstructive interference. This chapter’s supplementary information is provided in Appendix I.

Chapter 4, titled “The $\text{CH}\cdots\text{HC}$ interaction in biphenyl is a delocalized, molecular-wide and entirely non-classical interaction: results from FALDI analysis”, takes a similar approach to Chapter 3, published in the Journal of Computational Chemistry. However, rather than the ED being decomposed into contributing MOs, the ED is decomposed into FALDI components. These cross-section decomposition results are then compared to the investigation of the MO description. The analysis done through FALDI density decomposition decomposes the electron density into concentrating, depleting, or removing density at BCP(H,H) and MDP(H,H) in the planar and twisted conformation of Bph, respectively. FALDI also allows one to decompose the densities into two different types of contributions: into (i) fragment contributions and (ii) diatomic contributions. Decomposition into FALDI-fragments allows for unique analysis, as FALDI allows one to maintain the integrity of the molecule whilst still forming fragments, i.e. the molecular wide electronic environment is not shattered by breaking the molecule into radical states. We can then determine which fragments contribute (and to what extent) to the density measured. Decomposition into FALDI-atom pairs decomposes the density into Bph’s

231 atom pair contributions. Not only does this provide a higher resolution into the effects at play (compared to Bph's 41 MOs), it provides insight in chemically intuitive terms. This chapters supplementary information is provided in Appendix II.

Chapter 5, titled “NBOs Support MO and FALDI based ‘Bonding’ Description of CH···HC Bond Paths in Planar Biphenyl”, is the final results chapter of this study. In previous studies, the BP in planar Bph had been investigated on the basis of electron density, as well as orbital analysis by the likes of MOs and NBOs, and up until now only MO- and density-based studies in our work have been conducted. Just as MO-based studies concluded a non-bonding nature of the H···H interaction, so too did NBO-based studies, and as such this dissertation is concluded by undergoing cross-section decomposition of the electron density from NBOs. In doing so, these results are compared to FALDI-based cross-sections. Due to the fact that NBO wavefunctions are constricted into resembling Lewis-like bonds and that there are 240 individual NBOs, this decomposition provides somewhat chemically intuitive contributions and a higher resolution than MO decomposition does. This chapters supplementary information is provided in Appendix III.

Chapter 6, Conclusions, concludes the major observations and outputs of this dissertation, as well as future work to be conducted.

Appendix I, titled “Molecular Orbitals Support Energy-Stabilising ‘Bonding’ Nature of Bader’s Bond Paths”, is the supplementary information for Chapter 3 which has been published in the Journal of Physical Chemistry A.^[37] This is split into six parts: (i) Theoretical background, (ii) Cartesian coordinates of molecules studies, (iii) Canonical molecular orbitals in biphenyl, (iv) Data pertaining to covalent bonds in biphenyl, (v) Data pertaining to BCP/MDP(H7,H18) in the planar/twisted biphenyl, and (vi) Data pertaining to H···H density bridges in Li₄H₄.

Appendix II, titled “The CH \cdots HC interaction in biphenyl is a delocalized, molecular-wide and entirely non-classical interaction: results from FALDI analysis”, is the supplementary information for Chapter 4 which has been published in the Journal of Computational Chemistry. This is split into four parts: (i) Cartesian coordinates of all molecules studied, (ii) Cross-section comparison between MO- and FALDI-ED method for biphenyl, (iii) Alternate fragment partitioning scheme, and (iv) FALDI-ED data for H7 \cdots H18 interaction in biphenyl.

Appendix III, titled “NBOs Support MO and FALDI based ‘Bonding’ Description of CH \cdots HC Bond Paths in Planar Biphenyl”, is the supplementary information for Chapter 5 which is being prepared for submission to the Journal of Computational Chemistry. This is split into three parts: (i) Cartesian coordinates of all molecules studies, (ii) Cross-section comparison between FALDI- and NBO-ED method for biphenyl, and (iii) Isosurfaces of the major NBO contributions.

1.6. References

1. Boča, R.; Linert, W. *Monatsh. Chem.* **2005**, *136*, 881-923.
2. Frenking, G.; Shaik, S. *The Chemical Bond: Fundamental Aspects of Chemical Bonding*, 1; Wiley-VCH: Weinheim, 2014.
3. Frenking, G.; Shaik, S. *The Chemical Bond: Chemical Bonding Across the Periodic Table*, 1; John Wiley & Sons: 2014; 2.
4. Wu, W.; Song, L.; Cao, Z.; Zhang, Q.; Shaik, S. *J. Phys. Chem. A* **2002**, *106*, 2721-2726.
5. Song, L.; Wu, W.; Zhang, Q.; Shaik, S. *J. Comput. Chem.* **2004**, *25*, 472-478.
6. Murrell, J.N. *Int. J. Quantum. Chem.* **2012**, *112*, 2875-2879.
7. Weinhold, F.; Landis, C.R. *Chem. Educ. Res. Pract.* **2001**, *2*, 91-104.
8. Weinhold, F.; Landis, C.R. *Valency and Bonding: A Natural Bond Orbital Donor-Acceptor Perspective*; Cambridge University Press: Cambridge, 2005.
9. Glendening, E.D.; Landis, C.R.; Weinhold, F. *Wiley Interdiscip. Rev. Comput. Mol. Sci.* **2012**, *2*, 1-42.
10. Bader, R.F.W. *Atoms in Molecules: A Quantum Theory*; Oxford University Press: Oxford, 1990.
11. Cioslowski, J.; Mixon, S.T. *Can. J. Chem.* **1992**, *70*, 443-449.
12. Matta, C.F.; Hernández-Trujillo, J.; Tang, T.H.; Bader, R.F.W. *Chem. Eur. J.* **2003**, *9*, 1940-1951.
13. Poater, J.; Solà, M.; Bickelhaupt, F.M. *Chem. Eur. J.* **2006**, *12*, 2889-2895.
14. Bader, R.F.W. *Chem. Eur. J.* **2006**, *12*, 2896-2901.
15. Poater, J.; Solà, M.; Bickelhaupt, F.M. *Chem. Eur. J.* **2006**, *12*, 2902-2905.
16. Pacios, L.F.; Gómez, L. *Chem. Phys. Lett.* **2006**, *432*, 414-420.
17. Hernández-Trujillo, J.; Matta, C.F. *Struct. Chem.* **2007**, *18*, 849-857.
18. Pacios, L.F. *Struct. Chem.* **2007**, *18*, 785-795.
19. Pendás, A.M.; Francisco, E.; Blanco, M.A.; Gatti, C. *Chem. Eur. J.* **2007**, *13*, 9362-9371.
20. Echeverría, J.; Aullón, G.; Danovich, D.; Sharik, S.; Alvarez, S. *Nat. Chem.* **2011**, *3*, 323-330.
21. Hancock, R.D.; Nikolayenko, I.V. *J. Phys. Chem. A* **2012**, *116*, 8572-8583.
22. Eskandari, K.; Van Alsenoy, C. *J. Comput. Chem.* **2014**, *35*, 1883-1889.
23. Weinhold, F.; Schleyer, P.v.R.; McKee, W.C. *J. Comput. Chem.* **2014**, *35*, 1499-1508.
24. Jenkins, S.; Maza, J.R.; Xu, T.; Jianjun, D.; Kirk, S.R. *Int. J. Quantum. Chem.* **2015**, *115*, 1678-1690.

25. Jiajun, D.; Xu, Y.; Xu, T.; Momen, R.; Kirk, S.R.; Jenkins, S. *Chem. Phys. Lett.* **2016**, *651*, 251-256.
26. Li, J.; Huang, W.; Xu, T.; Kirk, S.R.; Jenkins, S. *Chem. Phys. Lett.* **2018**, *702*, 32-37.
27. Jara-Cortés, J.; Hernández-Trujillo, J. *J. Comput. Chem.* **2018**, *39*, 1103-1111.
28. Popelier, P.L.; Maxwell, P.I.; Thacker, J.C.; Alkorta, I. *Theor. Chem. Acc.* **2019**, *138*, 12.
29. Hargreaves, A.T.; Rizvi, S.H. *Acta Crystallogr.* **1962**, *15*, 365-373.
30. Karle, I.L.; Brockway, L.O. *J. Am. Chem. Soc.* **1944**, *66*, 1974-1979.
31. Blanco, M.A.; Martín Pendás, A.; Francisco, E. *J. Chem. Theory Comput.* **2005**, *1*, 1096-1109.
32. Bader, R.F.W. *J. Phys. Chem. A* **1998**, *102*, 7314-7323.
33. Bader, R.F.W. *J. Phys. Chem. A* **2009**, *113*, 10391-10396.
34. Coppens, P. *X-ray charge densities and chemical bonding*; International Union of Crystallography: Oxford, 1997.
35. Coppens, P. *Angew. Chem. Int. Ed.* **2005**, *44*, 6810-6811.
36. de Lange, J.H.; van Niekerk, D.M.; Cukrowski, I. *J. Comput. Chem.* **2018**, *39*, 2283-2299.
37. Cukrowski, I.; de Lange, J.H.; van Niekerk, D.M.; Bates, T.G. *J. Phys. Chem. A* **2020**, *124*, 5523-5533.
38. Bates, T.G.; de Lange, J.H.; Cukrowski, I. *Submitted to Phys. Chem. Chem. Phys.* **2020**.
39. de Lange, J.H.; Cukrowski, I. *J. Comput. Chem.* **2017**, *38*, 981-997.
40. Cukrowski, I.; van Niekerk, D.M.; de Lange, J.H. *Struct. Chem.* **2017**, *28*, 1429-1444.
41. de Lange, J.H.; van Niekerk, D.M.; Cukrowski, I. *J. Comput. Chem.* **2018**, *39*, 973-985.
42. de Lange, J.H.; Cukrowski, I. *J. Comput. Chem.* **2018**, *39*, 1517-1530.

Chapter 2

Theoretical Background

2.1. Introduction

This chapter gives a contextual background on *electronic structure methods*, in which the concept of a level of theory/theoretical model is discussed, as well as a more in-depth elaboration of the Hartree-Fock approximation and Density Functional Theory. This subsection is concluded with a discussion of basis sets and its anatomy. Following this section, we discuss electron density methods in *Quantum Chemical Topology* which gives an overview of the well-established and highly successful QTAIM^[1] method, as well as the relatively new in-house technique, FALDI.^[2-6] The next section provides a brief overview of *Orbital Analysis* which briefly covers molecular orbitals and natural bond orbitals. The final section gives a background to *New Theoretical Developments* which discusses techniques developed in-house. These in-house developments include novel functions and indicators for the detection of bond paths and bond critical points which can be used in a variety of different systems to decompose the electron density. This allows one to more clearly investigate the origins of density, as well as its nature. These developments include the cross-section decomposition of the electron density, the $CP(\mathbf{r})$ function, and the MO-DI method.

The work covered in 2.2. *Electronic Structure Methods* of this chapter follows extracts from three comprehensive textbooks, namely *Exploring Chemistry with Electronic Structure Methods* by Foresman and Frisch,^[7] *A Chemist's Guide to Density Functional Theory* by Kock and Holthausen,^[8] and *Essentials of Computational Chemistry: Theories and Models* by Cramer.^[9] The section on electronic structure methods are reported in numerous works and are well known. The purpose of this is to give context to the rest of the work.

2.2. Electronic Structure Methods

2.2.1. Levels of Theory

Levels of theory are known as a hierarchy of procedures that correlate to different approximation methods to approximate the Schrödinger equation. Common levels of theory include Hartree-Fock (HF) theory, and Density Functional Theory (DFT), in which multiple functions are included, such as the well-known B3LYP function. We will delve deeper into HF and DFT in the forthcoming sections.

Levels of theory represent different theoretical models which hold a number of implications:

- (i) should be uniquely defined for any system of any arrangement of nuclei and electrons, and
- (ii) should be unbiased, where no special assumptions or considerations are to be made for certain chemical systems/structures.

2.2.1.1. Hartree-Fock Approximation

To delve into the HF approximation, we must go through the development that precedes it. By looking at the Schrödinger equation (Eq 1) with regards to its one-electron Hamiltonian

$$E\Psi = \hat{H}\Psi = \frac{-\hbar^2}{2m}\nabla^2\Psi + V(x)\Psi \quad (2-1)$$

if it only constitutes the one-electron kinetic energy and nuclear attraction, we can obtain the operator

$$\hat{H} = \sum_{i=1}^N \hat{h}_i \quad (2-2)$$

in which N represents the total number of electrons and \hat{h}_i is the one-electron Hamiltonian. This equation is separable and is the sum of all one-electron Hamiltonians for the total number of electrons in the system. The term \hat{h}_i is defined as

$$\hat{h}_i = -\frac{1}{2}\nabla_i^2 - \sum_{k=1}^M \frac{Z_k}{r_{ik}} \quad (2-3)$$

in which M represents the total number of nuclei. For the eigenfunctions in the above one-electron Hamiltonian to be real, it must satisfy the one-electron Schrödinger equation

$$\hat{h}_i \psi_i = \varepsilon_i \psi_i \quad (2-4)$$

As previously stated, the Hamiltonian operator is separable, and because of this, it allows one to construct many-electron eigenfunctions which are merely the products of one-electron eigenfunctions

$$\Psi_{HP} = \psi_1 \psi_2 \cdots \psi_N \quad (2-5)$$

The wavefunction term Ψ_{HP} is known as the Hartree-product wavefunction, which was the groundwork for further methods to be developed. We can determine the eigenvalue from the Hartree-product by incorporating the operator from Eq. 2 into Eq. 5

$$\begin{aligned} \hat{H} \Psi_{HP} &= \hat{H} \psi_1 \psi_2 \cdots \psi_N \\ &= \left(\sum_{i=1}^N \varepsilon_i \right) \Psi_{HP} \end{aligned} \quad (2-6)$$

We must take note, although intuitive, that Eq. 2 and 3 does not take interelectronic repulsion into account as that depends on all pairwise interactions, where Eq. 2 and 3 only describes the *one-electron* Hamiltonian. In turn, a question arises to how accurately the Hartree-product wave function can compute the energies of the true Hamiltonian; in other words, we need to find which orbitals (ψ) minimise $\langle \Psi_{HP} | \hat{H} | \Psi_{HP} \rangle$. We show that each ψ is an eigenfunction of the operator \hat{h}_i

$$\hat{h}_i = -\frac{1}{2} \nabla_i^2 - \sum_{k=1}^M \frac{Z_k}{r_{ik}} + V_i\{J\} \quad (2-7)$$

where

$$V_i\{J\} = \sum_{j \neq i} \int \frac{\rho_j}{r_{ij}} d\mathbf{r} \quad (2-8)$$

The third term in Eq. 7 represents the interaction potential of an electron with all other electrons in orbitals $\{j\}$, and ρ_j represents the charge density linked with electron j .

However, another problem arises from the first problem stated; we want to find the ψ 's that minimises the energy, $\langle \Psi_{HP} | \hat{H} | \Psi_{HP} \rangle$, but then again the ψ needs to be used in the one-electron Hamiltonian. So how can they be used before they are inherently calculated? This problem was resolved when Hartree suggested the self-consistent field (SCF) method. This allowed the calculation of ψ that minimises the energy from an initial guess of the ψ , and reiterating the method until the difference between the new energy and the previous energy is below an arbitrary threshold, which is termed to be 'converged'.

If we now place two electrons in an orbital, there are two possible orientations that they can present – if their spins are paired (i.e. one-electron spin up, and one-electron spin down), or if they have parallel spins (either both spin up or spin down). Thus, these electrons can be characterised by their spin quantum number, denoted as α and β , and due to the Pauli exclusion principle, no two electrons may be characterised by the same quantum numbers. As a result, in a doubly occupied orbital, the electrons must be paired.

Let's say that a Hartree-product wave function is constructed whereby the electrons hold the same spin, α , we can define it as

$${}^3\Psi_{HP} = \psi_a(1)\alpha(1)\psi_b(2)\alpha(2) \quad (2-9)$$

where the superscript 3 denotes that the Hartree-product exists in a triplet electronic state, and ψ_a and ψ_b represent two different orbitals (as a result of the Pauli-exclusion principle) and are orthonormal. However, for an electronic wavefunction to be valid, the Pauli-exclusion principle says that it must *change sign* if the coordinates of two electrons are switched, or in other words to be *antisymmetric*. This does not hold true for our triplet state Hartree-product in Eq. 9. To illustrate this, we can define a permutation operator \hat{P}_{ij} as an operator that switches the coordinates of electron i and j

$$\begin{aligned} \hat{P}_{12}[\psi_a(1)\alpha(1)\psi_b(2)\alpha(2)] &= \psi_b(1)\alpha(1)\psi_a(2)\alpha(2) \\ &\neq -\psi_a(1)\alpha(1)\psi_b(2)\alpha(2) \end{aligned} \quad (2-10)$$

With a small modification to the Hartree-product wave function however, the Ψ_{HP} can be made to be antisymmetric, which we term the Slater determinant

$${}^3\Psi_{SD} = \frac{1}{\sqrt{2}} [\psi_a(1)\alpha(1)\psi_b(2)\alpha(2) - \psi_a(2)\alpha(2)\psi_b(1)\alpha(1)] \quad (2-11)$$

which can be denoted differently as

$${}^3\Psi_{SD} = \frac{1}{\sqrt{2}} \begin{vmatrix} \psi_a(1)\alpha(1) & \psi_b(1)\alpha(1) \\ \psi_a(2)\alpha(2) & \psi_b(2)\alpha(2) \end{vmatrix} \quad (2-12)$$

and can be further denoted more compactly as

$$\Psi_{SD} = \frac{1}{\sqrt{N!}} \begin{vmatrix} \chi_1(1) & \chi_2(1) & \cdots & \chi_N(1) \\ \chi_1(2) & \chi_2(2) & \cdots & \chi_N(2) \\ \vdots & \vdots & \ddots & \vdots \\ \chi_1(N) & \chi_2(N) & \cdots & \chi_N(N) \end{vmatrix} \quad (2-13)$$

where χ is the spin orbital, as the product of the spatial orbital (ψ) and electron spin eigenfunction (α or β).

Similarly to how the Hartree-product orbitals can be determined as eigenfunctions as the product of one-electron Hamiltonian operators, so too can the HF orbitals, with the difference being, that each electron interacting with a potential field of all other electrons now *includes* exchange effects on the Coulomb repulsion – previously the modification of the Hartree-product wave function into the Slater determinant did not include exchange effects for paired electron spins.

Up until now, we have only worked with spin orbitals χ and their individual components, though the spin orbitals are constructed from a combination of basis function (weighted by their coefficients)

$$\chi_j = \sum_{i=1}^N a_{ij}\varphi_i \quad (2-14)$$

whereby if introduced into the equations discussed so far, it gives rise to Roothan equations, which describes HF calculations in the form of matrix algebraic equations.

We can define the one-electron Fock operator for electron i as

$$\hat{f}_i = -\frac{1}{2}\nabla_i^2 - \sum_k^M \frac{Z_k}{r_{ik}} + V_i^{HF}\{j\} \quad (2-15)$$

which allows us to calculate the HF molecular orbitals (MO) by solving the secular equation as part of the Roothan approach

$$\begin{vmatrix} F_{11} - ES_{11} & F_{12} - ES_{12} & \cdots & F_{1N} - ES_{1N} \\ F_{21} - ES_{21} & F_{22} - ES_{22} & \cdots & F_{2N} - ES_{2N} \\ \vdots & \vdots & \ddots & \vdots \\ F_{N1} - ES_{N1} & F_{N2} - ES_{N2} & \cdots & F_{NN} - ES_{NN} \end{vmatrix} = 0 \quad (2-16)$$

Matrix element S represents overlap matrix elements, and F represents Fock matrix elements which is defined as

$$F_{\mu\nu} = \langle \mu | -\frac{1}{2}\nabla^2 | \nu \rangle - \sum_k^M Z_k \langle \mu | \frac{1}{r_k} | \nu \rangle + \sum_{\lambda\sigma} \mathbf{P}_{\lambda\sigma} \left[(\mu\nu|\lambda\sigma) - \frac{1}{2}(\mu\lambda|\nu\sigma) \right] \quad (2-17)$$

where \mathbf{P} is the density matrix

$$\mathbf{P}_{\lambda\sigma} = 2 \sum_i^{\text{occupied}} a_{\lambda i} a_{\sigma i} \quad (2-18)$$

The coefficients in the density matrix ($a_{\zeta i}$) weigh the contribution that each basis function makes to the MO i .

The final term on the right-hand side of Eq. 17 gives the electron-electron repulsion integrals, where $(\mu\nu|\lambda\sigma)$ gives the Coulomb repulsion, and $(\mu\lambda|\nu\sigma)$ gives the Exchange energy (halved because it only affects half of the electrons).

The same characteristic paradox is present when solving the secular determinant/equation as with the one-electron Hamiltonian method, that we need to know the orbital coefficients

($a_{\zeta i}$) to calculate the density matrix P . This in turn is used in the Fock matrix element F , however the main purpose of the secular equation is to determine the values of these orbital coefficients. This is overcome by referring to the SCF procedure mentioned earlier, in which an initial guess is made of these orbital coefficients, and then iterated through the SCF procedure until the energies converge.

Although the HF theory is extremely useful in giving initial base-level predictions for a number of systems, it is however limited to the extent that it ignores all electron correlation (apart from for exchange correlation) due to the one-electron nature of the Fock operator (Eq 16). This is in part due to the severe approximation made in HF theory, that each electron exists within the domain of a nuclei, and that their movements and interactions are influenced in an *averaged* way from all other electrons of the same spin, ignoring how the electrons of the opposite spin may affect it. Nonetheless, it primed the expansion and development of other computational models that exist today.

2.2.1.2. Density Functional Theory

Our goal in HF theory is to find the wave function of its Schrödinger approximation and from that, obtain the densities, however in DFT, the inverse is true; we first find the density, and then obtain the wave functions.

DFT as we know it today arose in 1964 from Hohenberg and Kohn, where they presented two theorems which form the pillars of all density functional theories that have been developed and exist today.

The first theorem inherently states that the electron density (ED) of a system can be used directly to determine the Hamiltonian operator, and from this we can obtain all properties of said system. We can break down the Hamiltonian operator into the following:

$$\hat{H} = \hat{T} + \hat{V}_{ee} + \hat{V}_{ext} \quad (2-19)$$

where \hat{T} is the kinetic energy operator, \hat{V}_{ee} is the electron-electron repulsion operator, and \hat{V}_{ext} is the external potential operator.

This theorem proves that the ground state ED can only be described by one V_{ext} , or otherwise stated, that the ground state ED *uniquely* defines V_{ext} . And so, from the ground state ED (ρ_0), we can obtain the Hamiltonian operator, which one can then use to obtain the wave function, and in conclusion we can obtain the energy, shown as a depiction below

$$\rho_0 \Rightarrow \hat{H} \Rightarrow \Psi_0 \Rightarrow E_0$$

and since the ground state energy is a function of the ground state ED, the components that make up this energy will too be a function of the ground state ED.

$$E_0[\rho_0] = T[\rho_0] + E_{ee}[\rho_0] + E_{ne}[\rho_0] \quad (2-20)$$

This energy expression can further be separated into components that depend on the system in question, and components that are independent of the system.

$$E_0[\rho_0] = \int \rho_0(\mathbf{r})V_{ne}d\mathbf{r} + T[\rho_0] + E_{ee}[\rho_0] \quad (2-21)$$

where the first term is system dependent and the second and third term is system independent. Terms two and three can be grouped, to form a functional known as the *Hohenberg-Kohn functional* $F_{HK}[\rho_0]$

$$E_0[\rho_0] = \int \rho_0(\mathbf{r})V_{ne}d\mathbf{r} + F_{HK}[\rho_0] \quad (2-22)$$

This Hohenberg-Kohn functional allows us to obtain the ground state wave function when given an arbitrary density, and so one can define this functional further as

$$F_{HK}[\rho] = T[\rho] + E_{ee}[\rho] = \langle \Psi | \hat{T} + \hat{V}_{ee} | \Psi \rangle \quad (2-23)$$

This functional forms the basis of density functional theory, and if known exactly, we would have an exact solution to the Schrödinger equation, rather than a mere approximation.

The second theorem adds on to this with the use of the variational principle, stating that the Hohenberg-Kohn functional will only give the lowest energy of the system if the density given is truly the ground state density. We can express the variational principle as follows

$$E_0 \leq E[\tilde{\rho}] = T[\tilde{\rho}] + E_{ne}[\tilde{\rho}] + E_{ee}[\tilde{\rho}] \quad (2-24)$$

This states that if the boundary conditions $\tilde{\rho}(\mathbf{r}) \geq 0$ and $\int \tilde{\rho}(\mathbf{r})d\mathbf{r} = N$ are met, then for any trial density $\tilde{\rho}(\mathbf{r})$, the energy that we receive from Eq 20 will be the upper limit to the true ground state energy. We will only get the true ground state energy if the trial density is in fact the true ground state density.

Up until this point, we have a powerful tool with the use of the Hohenberg-Kohn functional to obtain the nuclear-electron attraction, and the classical electron-electron repulsion, but there is an important electron interaction missing, specifically the non-classical portion called the electron exchange correlation, E_{XC} . For this, further functions have been developed to add onto the DFT method to best approximate this correlation, and we can say that the quality of the density function lies to a large part in the quality and accuracy of such an approximation. There have been many functions developed, but up to now, the most popular function is a hybrid functional known as B3LYP (Becke, 3-parameter, Lee-Yang-Parr) as it has shown major success in a wide variety of different chemical states and systems.

2.2.2. Basis Sets

Following from levels of theory one must amalgamate *basis sets*, and each unique combination approximates the Schrödinger equation in a slightly different way. Some combinations may be more accurate than others, as smaller basis sets have reduced degrees of freedom than larger ones.

The degrees of freedom links to the idea of cost versus accuracy, and by cost we refer to computational time. The smaller the basis set, the less degrees of freedom are available, and thus the approximation of the Schrödinger equation is less accurate, however, faster to

calculate. On the other hand, if we make use of a larger basis set, the computational time increases, however our approximation of the Schrödinger equation becomes closer to the true state of the system. In computational comparisons between systems, for the sake of consistency, one must calculate the system using identical model chemistries, i.e. the same level of theory and basis set.

To focus down to *basis sets*, they are defined as the mathematical description of each orbital, typically MO. These orbitals are then combined to approximate a part of the Schrödinger equation, the total electronic wavefunction Ψ . Within basis sets exist individual specific pre-defined functions, termed *basis functions*, which are applied to each atom in the molecular system to approximate the orbitals in one way or another.

Two general types of basis functions are used to construct basis sets, namely (i) Slater-type functions, and (ii) Gaussian-type functions. Slater-type functions are a specialised mathematical function that describes the ‘tail’ of the real ED more accurately. In other words, as will be described in following sections, the ED is maximum at the nuclei and as the ED trails off to infinity, the Slater-type functions describe this more accurately than Gaussian functions would. A Gaussian-type function is simply a gaussian/bell-curve in three dimensions. These bell-curves are much easier to integrate, and therefore much quicker to calculate, however at the cost of reduced accuracy, and therefore uses many basis functions to cover this downfall. Slater-type functions use fewer basis functions, because they are more accurate, but their integration can become troublesome, increasing the time to compute. From here on, we will cover Gaussian-type functions exclusively.

There are two classes that we will cover, (i) Pople type basis sets which include basis sets such as 6-311G, and (ii) Dunning correlation consistent basis sets which include basis sets such as cc-pVDZ.

There are *minimal basis sets*, which within them are restricted to the minimum number of basis functions for each atom in the system. They make no change to the shape or size of the orbitals. The first step to making these basis sets larger however is to add *split valence basis sets*. If we take 3-21G and 6-31G as examples, the dash separating the two basis functions represent the split valence basis sets. The functions before the dash represent the core orbitals and the functions after the dash represent the valence orbitals, hence *split valence*. These add the number of primitives to calculate, which comes down to cost versus accuracy; they add more degrees of freedom and so increases the accuracy of the calculation, but at the cost of the computing time. In using the Pople type basis set 6-31G as example, one refers to it as a double-zeta basis set and 6-311G as a triple-zeta basis set. If one refers to Dunning correlation consistent basis set, a double-zeta basis set is represented as pVDZ, and triple-zeta basis set as pVTZ.

The next step to making the basis sets larger is to add *polarised basis sets*. As opposed to split valence basis sets, these change the shapes of the orbitals by adding further angular momentum to the orbitals. To understand this more clearly, consider the basis set 6-31(d,p) where the underlined refers to the polarised basis set. This adds d orbital functions to heavy atoms (all atoms other than hydrogen) and adds p orbital functions to hydrogen atoms. Therefore, one can obtain a p orbital which partly has d orbital character, or an s orbital which partly has p orbital character. One can further add more polarised basis sets, such as 6-311G(3df,3pd), where one adds three ‘d’ functions and one ‘f’ function to each heavy atom, and three ‘p’ functions and one ‘d’ function to hydrogen atoms. This can be referred to as *high angular momentum basis sets*.

The last basis function to cover that can be added, is the addition of *diffuse functions*. With regards to Pople type basis sets, the diffuse functions are represented as a “+”, for example 6-311G+(d), and in Dunning correlation consistent as “aug”, for example aug-cc-pVDZ. These

diffuse functions allow orbitals to occupy a larger region of space, to allow electrons to be dispersed further from the nuclei. This is important for systems that include lone pairs, excited states, and in the case of this dissertation, to describe intramolecular hydrogen bonding, as well as other systems. For Pople type basis sets, we can describe the diffuse function in two ways; (i) a single “+”, e.g. 6-311G+(d), and (ii) a double “+”, e.g. 6-311G++(d). The first “+” adds the diffuse function only to heavy atoms, however the second “+” adds diffuse functions to the hydrogens as well.

All the discussed basis functions are dependent of the system that one is calculating. One must always take into consideration the different chemical properties of the system, as well as cost versus accuracy.

2.3. Quantum Chemical Topology

2.3.1. QTAIM

2.3.1.1. Background

The Quantum Theory of Atoms in Molecules (QTAIM)^[1] recovers from the topology of the ED distribution, our elementary chemical concepts of atoms and bonds. In other words, QTAIM fully defines atomic basins and bonds (which are referred to as bond paths (BP) in QTAIM) from the quantum observable ED, $\rho(\mathbf{r})$. The ED recovers, to a large extent, the chemical bonds that we would draw from our classical chemical concepts. The topology of the ED is controlled by nuclei attraction, in line with Feynman’s theorems,^[10] where one will find a maximum in ED at the nuclei positions. ED is then dispersed throughout the system in a fashion to lower the energy of the molecule. Due to this inherent accumulation of ED on the nucleus, we can obtain an atomic definition with a well-defined atomic volume and boundaries in which, from an ED perspective, we can define as the specific atomic basin. Before this is further explained, a few crucial concepts must first be clarified.

2.3.1.2. Critical Points, Curvatures, and Bond Paths

The first concept is how we define a critical point (CP). A CP within the ED is defined as a point in real space \mathbf{r} that is characterised by a zero-gradient, meaning that the first derivatives of the density vanish.^[1]

$$\nabla\rho = i\frac{d\rho}{dx} + j\frac{d\rho}{dy} + k\frac{d\rho}{dz} \rightarrow \begin{cases} = \vec{0} & (\text{At critical points}) \\ \text{Generally} \neq \vec{0} & (\text{At all other points}) \end{cases} \quad (2-25)$$

Eq. 25 above shows that each component in the gradient operator, $\nabla\rho$, must be zero and not just the sum of all components.

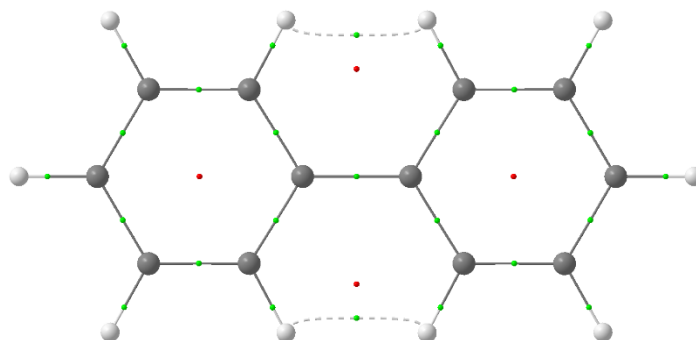
CP's can be classified in a (ω, σ) manner, in which ω and σ are referred to as the *rank* and *signature*, respectively. To understand this classification, we need to bring in the concept of curvature. The curvature is represented by the diagonalised Hessian Matrix in Eq. 26. The curvature is due to the three eigenvalues, λ_1 , λ_2 , and λ_3 , of the density with respect to the three principle axes x' , y' and z' (the coordinate system resulting from the diagonalisation of the Hessian Matrix). This represents the curvature of the ED in 3-dimensions.

$$\Lambda = \left(\begin{array}{ccc} \frac{\partial^2\rho}{\partial x'^2} & 0 & 0 \\ 0 & \frac{\partial^2\rho}{\partial y'^2} & 0 \\ 0 & 0 & \frac{\partial^2\rho}{\partial z'^2} \end{array} \right)_{r'=r_c} = \begin{pmatrix} \lambda_1 & 0 & 0 \\ 0 & \lambda_2 & 0 \\ 0 & 0 & \lambda_3 \end{pmatrix} \quad (2-26)$$

The curvature at a local maximum has a negative value, and at a local minimum has a positive value. Therefore, we can explain the (ω, σ) nomenclature with more context. The rank (ω) is defined as the amount of non-zero curvatures, in which $\omega = 3$ in most occurrences, where if the rank is less than 3, the system is generally unstable. The signature (σ) is the sum of the *signs* of the curvature in three dimensions. The curvature therefore contributes ± 1 to the signature. There are four CP's that exist:^[11]

- 1) (3,-3) CP - This denotes the *nuclear critical point* (NCP). At the NCP, there exists a global maximum ED in three dimensions, therefore there are three negative curvatures.
- 2) (3,-1) CP - This denotes the *bond critical point* (BCP). At the BCP, there are two negative curvatures and one positive curvature, which implies a maximum ED in two directions, and a minimum ED in the third. The BCP exists along the BP between two nuclei, whereby we go from a maximum ED (nucleus A) to a minimum (where the BCP is present) to another maximum ED (nucleus B).
- 3) (3,+1) CP - This denotes the *ring critical point* (RCP). At the RCP, there are two positive curvatures and one negative curvature, which implies a minimum ED in two directions and a maximum ED in the third. The RCP exists consistently as the name suggests, within ring systems.
- 4) (3,+3) CP - This denotes the *cage critical point* (CCP). At the CCP, all curvatures are positive, implying a minimum ED in all directions. When multiple ring systems are chemically bonded in such a way that it encompasses an interstitial space, we observe a CCP where there is a minimum ED in all directions.

In Scheme 1 below we depict a molecular graph of planar biphenyl. A molecular graph is a combination of BPs linking nuclei together with respective critical points.^[11]



Scheme 1. Molecular graph of planar biphenyl. The lines represent bond paths, as well as critical points which are colour coded: nuclear CP (C = grey, H = white), bond CP (green), and ring CP (red).

A BP is a line depicting the maximum density between two nuclei, that passes through a minimum density, a point referred to as the BCP.^[12] From Scheme 1 above we observe BPs linking nuclei together, which correspond directly to what a chemist would traditionally draw.

The BPs observed represent a line of density between two nuclei that are related to a minimisation of energy for the interaction between two atoms, and typically represent chemically covalent bonds. However the term BP is swarmed with critical debate, in which Bader clarified that a BP “is not to be understood as representing a bond”, but to represent that the atoms linked by a BP are chemically bonded to one another.^[13] Due to this debate surrounding the terminology and physical meaning of BPs, we choose to rather refer to this energy lowering line of density as a density bridge (DB), as this term is fully applicable and unambiguous, and makes no assumption on the readers behalf regarding the nature of the interaction between the linked atoms. However, regarding the term ‘*bond critical point*’, it has been suggested to call it a *line* critical point, or a *path* critical point, however from here on out it shall be referred to as (3,-1) CP until we can find a better term.

2.3.1.3. Zero Flux Surface, Gradient Vector Field, and Atomic Boundaries

Due to the topology of ED encompassing the entire system and maximums of ED at the nuclei, we can divide the densities into separate mononuclear regions, which we identify as an atom/atomic basin (Ω). We call the boundaries from the partitioning of atoms in a molecule as one of *zero flux* in a gradient vector field of ED.^[11] This means that it isn't crossed by any gradient vector field lines from its own atomic basin or neighbouring atomic basins. These zero flux surfaces terminate at the (3,-1) CP between nuclei and thus to reiterate, the regions of zero flux act as boundaries. In this way, one can define an atom from the basis of ED with its boundaries originating from the (3,-1) CPs around the nucleus. The gradient vector $[\nabla\rho(\mathbf{r})]$ field lines are lines representing the paths of first derivative ED, that converge to its respective nucleus, which do not cross the regions of zero flux. This mononuclear partitioning of the ED

into the topological definition of an atom is entrenched in quantum mechanics, and as such to be connected to that of a quantum subsystem.

2.3.1.4. Electron (de)localisation

Since we now have an ED based definition of an atom, this allows QTAIM to calculate the extent of electron sharing between two atoms, termed the delocalisation index (DI), as well as the electrons localised to only one atom, termed the localisation index (LI).

One can express the DI and LI in QTAIM as a function of the overlap integrals of two spin orbitals and the Fermi correlation,^[11] or one can make use of MO overlaps. For the remainder of this section, an MO based approach will be expressed to dictate the electron (de)localisation from QTAIM.

To start with, QTAIM calculates the atomic electron population, $N(A)$, of an atom by calculating the ED over the atom. This can be done by integrating the overlap of all MO pairs over a specific atomic basin, $\Omega(A)$

$$N(A) = \sum_i^{N_{MO}} \int_A v_i |\chi_i(\mathbf{r})|^2 d\mathbf{r} \quad (2-27)$$

This integration over $\Omega(A)$ can otherwise make use of atomic overlap matrices (AOM) to simplify the real space calculation on atom A, S^A .

$$S_{ij}^A = \int_A \chi_i^*(\mathbf{r}) \chi_j(\mathbf{r}) d\mathbf{r} \quad (2-28)$$

This AOM provides valuable information since the diagonal components (normalised MO) and off-diagonal components (pair of MOs) provide information on how they contribute to the density distribution within the confounds of atom A. Therefore, one can express the atomic electron population as a function of the trace of the AOM, weighted by the MOs corresponding occupation:

$$N(A) = \sum_i^{N_{MO}} v_i S_{ii}^A \quad (2-29)$$

Although the atomic electron population exclusively uses the diagonal elements, one can gather information from its off-diagonal elements, where one can see how the MOs interfere, either constructively or destructively within the confines of an atomic basin.

By integrating all MO-pairs over two atomic basins, A & B, one obtains the total delocalisation, or electron sharing, between both atoms. Again, AOM can be used for this:

$$\delta(A, B) = 2 \sum_{ij} \sqrt{v_i v_j} S_{ij}^A S_{ji}^B \quad (2-30)$$

where v is the occupation of the respective MOs i and j – in the case of my current work with HF and DFT, we assume double occupation because it is both restricted and a closed-shell system, and because it is a single determinant method. This $\delta(A, B)$ function is known as the DI, and represents the *electron pair* sharing between the two basins, and is a measure of bond strength.^[11]

Just as one calculates the delocalisation by integrating all MO-pairs over two atomic basins, one can obtain the number of electron pairs localised to one atomic basin, LI [$\lambda(A)$], by integrating the off-diagonal elements of the AOM over one atomic basin, A:

$$\lambda(A) = \sum_{ij} \sqrt{v_i v_j} S_{ij}^A S_{ji}^A \quad (2-31)$$

where $\lambda(A)$ is the LI of $\Omega(A)$.

Therefore, from the atomic electron population, QTAIM can decompose the ED into the LI of atom A, and DI between A & B.

2.3.2. FALDI Background

2.3.2.1. Original Reason for FALDI Development

Many intermolecular and intramolecular interactions are known to chemists, however theoretical research suggests that their nature and properties are not as well defined in terms of classical chemistry as suspected. There have been many debates on such interactions, notably on the nature of the weak H \cdots H intramolecular interaction in systems such as biphenyl and phenanthrene sparked by Matta *et al*^[14] that spans almost three decades. Although previously we thought that we had a clear enough understanding of a chemical bond, these debates have made it clear to how lacking our fundamental understanding of a chemical bond and chemical interactions are.

In this light, many methods have been developed over the course of a few decades to increase our understanding of certain facets of weak interactions, though whilst we gain insight into intermolecular interactions, our intramolecular interactions remain a cause of debate. To this end, QTAIM^[1] showed to be near perfect; by making use of measuring the topology of the ED distribution, it could recover our ideas of atoms and bonds, although this methodology is still thoroughly debated. Surrounding this fundamental underdevelopment in the understanding of intramolecular interactions, but knowing that the ED is a good measure of charge distribution in a molecule, the use of deformation densities (DD) became common to measure the accumulation or depletion in electron densities as a description of how the ED changes between two states of a molecule.

The deformation density measures the change in ED ($\Delta\rho$) at a given coordinate \mathbf{r} between the final (*fin*) and reference (*ref*) state, whereby the reference state represents the initial state.

$$\Delta\rho(\mathbf{r}) = \rho(\mathbf{r}) - \rho^0(\mathbf{r}) \quad (2-32)$$

The reasons why deformation densities are beneficial are because, not only do they clearly show the difference in ED inside the bonding region, but also the difference in ED outside the

bonding region, whereby we can detect polarisations and charge transfers in the molecular system. Foregoing these benefits, a few drawbacks exist. The first is that the coordinate system in the *fin* state needs to be identical to the *ref* state. This means that each atomic/nuclear position in the *fin* system must be identical to that of the *ref* system. Although the ED changes between the two systems, which one can then detect with the deformation densities, it limits the true distribution of ED between two configurations/conformations that differ in nuclear positions. The second drawback is that molecular *ref* systems are typically not available in the study of intramolecular interactions, and it is typically necessary to fragment the system into unchemical systems, commonly being radicals.

Our in-house FALDI^[2-6] (Fragment, Atomic, Localised, Delocalised, and Intra- & Interatomic) density decomposition scheme allows for the study of intramolecular interactions without being confined to the use of unchemical *ref* systems. The current need to break bonds into radical states to understand the formation, nature, and properties of an intramolecular interaction is clearly disadvantageous and a technique such as FALDI is a distinct benefit. With this technique, we are able to gain the *atom*-DD (how the ED distribution changes from one atomic basin), *frag*-DD (how the ED distribution changes from a fragment group in the molecule), and *tot*-DD (how the ED distribution changes throughout the whole molecule) from a conformational *ref*→*fin* transformation.

The next subsections of “FALDI Background” cover the derivation of individual FALDI components.

2.3.2.2. *Electron Density and Pair Density*

The ED (ρ) is an important feature in the field of quantum chemistry as its spin-independent description is related to a wide range of chemical phenomena. There are multiple ways to calculate the ED, however it is primarily calculated by the multiplication of the occupancy of its respective MO over the total number of occupied MOs:

$$\rho(\mathbf{r}) = \sum_i^{N_{MO}} v_i |\chi_i(\mathbf{r})|^2 \quad (2-33)$$

where $\chi_i(\mathbf{r})$ is the i th MO, v_i is its occupancy and N_{MO} is the total number of MOs.

The ED in Eq. 33 is dependent on the correlated movement of electrons within a system, whereby we can study the electron correlation of the pair-density (PD) directly between two electrons in two different regions of space

$$\rho_2(\mathbf{r}_1, \mathbf{r}_2) = \rho(\mathbf{r}_1)\rho(\mathbf{r}_2)[1 + f(\mathbf{r}_1; \mathbf{r}_2)] \quad (2-34)$$

where $\rho_2(\mathbf{r}_1, \mathbf{r}_2)$ is the PD and $f(\mathbf{r}_1; \mathbf{r}_2)$ is the correlation factor between two electrons at two spatial coordinates. Since all electrons in a molecular system are correlated, $f(\mathbf{r}_1; \mathbf{r}_2) \neq 0$, and due to the repulsion between electrons, the correlation factor generally leads to a *decrease* in PD, approaching zero as the distance between \mathbf{r}_1 and \mathbf{r}_2 decreases.

We now need to define another important ED component, namely *conditional probability*. This is defined as the probability of finding an electron at \mathbf{r}_1 given that there is an electron at \mathbf{r}_2 .

$$\rho^{cond}(\mathbf{r}_1; \mathbf{r}_2) = \frac{\rho_2(\mathbf{r}_1, \mathbf{r}_2)}{\rho(\mathbf{r}_2)} \quad (2-35)$$

If electrons were not correlated, then $\rho^{cond}(\mathbf{r}_1; \mathbf{r}_2) = \rho(\mathbf{r}_1)$ because the ED at \mathbf{r}_1 would not be influenced by an electron at \mathbf{r}_2 . The difference between the uncorrelated and correlated ED for an electron at \mathbf{r}_1 describes the *electron hole* function, or more commonly known as the exchange-correlation (XC) hole.

$$\rho^{Hole}(\mathbf{r}_1; \mathbf{r}_2) = \rho(\mathbf{r}_1) - \frac{\rho_2(\mathbf{r}_1, \mathbf{r}_2)}{\rho(\mathbf{r}_2)} \quad (2-36)$$

This $\rho^{\text{Hole}}(\mathbf{r}_1; \mathbf{r}_2)$ function defines how the ED accumulates or depletes at the spatial coordinate \mathbf{r}_1 as a result of the presence of an electron at \mathbf{r}_2 , and in general, to what extent an electron is *excluded* in spatial coordinate \mathbf{r}_1 as a result of an electron at \mathbf{r}_2 .

2.3.2.3. Domain Averaged Fermi Holes

The Domain Averaged Fermi Hole (DAFH)^[15-16] is a powerful technique which aims to discover how a specific electron-pair is localised or delocalised if one electron is defined by its average distribution within an explicit domain. In other words, we can take the electron hole function from Eq. 36 wherein one of the electrons in a spatial coordinate is averaged over a specified domain. While DAFH allows for any domain to be chosen, this work will consider QTAIM's^[1] atomic-basins as the domain of choice.

DAFH has a key function, the $g_A(\mathbf{r})$ function.

$$g_A(\mathbf{r}_1) = \int_A \rho(\mathbf{r}_2) \rho^{\text{Hole}}(\mathbf{r}_1; \mathbf{r}_2) d\mathbf{r}_2 \quad (2-37)$$

This function integrates the spatial coordinates of the XC-hole over a specific atomic basin (A), weighted by the charge density of the integrated coordinate of $\rho(\mathbf{r}_2)$. This allows for an evaluation of the total charge *at* \mathbf{r}_2 . Since we take the XC-hole into the equation, $g_A(\mathbf{r})$ function essentially gives the total number of electrons that are *excluded* within the averaged region due to the electron found within that domain (Ω_A). In other words, our DAFH function retrieved the ED contribution at spatial coordinate \mathbf{r} from atom A due to delocalisations in the system. Because of this, we are able to retrieve a comprehensive ED decomposition at \mathbf{r} :

$$\rho(\mathbf{r}) = \sum_A^M g_A(\mathbf{r}) \quad (2-38)$$

Between DAFH's $g_A(\mathbf{r})$ function and QTAIM's population analysis, there are some key associations that must be stated.

- (a) If we integrate the $g_A(\mathbf{r})$ function over the entire molecule/system (expression to the right of Eq. 39 below), then we can obtain the atomic population of A, N_A , in comparison to the left hand expression which is the QTAIM based calculation for the atomic population.

$$N(A) = \int_A \rho(\mathbf{r})d\mathbf{r} = \int_{-\infty}^{\infty} g_A(\mathbf{r}) d\mathbf{r} \quad (2-39)$$

As $N(A)$ measures the atomic populations in the atomic basin of atom A (Ω_A), $g_A(\mathbf{r})$ measures how these electrons are delocalised from Ω_A into the remaining system due to XC effects.

- (b) We can recover QTAIM's LI of Ω_A if we integrate $g_A(\mathbf{r})$ over Ω_A :

$$\lambda(A) = \int_A g_A(\mathbf{r})d\mathbf{r} \quad (2-40)$$

which gives the number of electrons that are exclusively *localised* to atom A.

- (c) We can recover QTAIM's half- DI if we integrate $g_A(\mathbf{r})$ over any other atomic basin:

$$\frac{1}{2}\delta(A, B) = \int_B g_A(\mathbf{r})d\mathbf{r} = \int_A g_B(\mathbf{r})d\mathbf{r} \quad (2-41)$$

which simply shows us how electrons belonging to Ω_A are delocalised and contribute to Ω_B , whereby the reverse it also true. In other words, Eq. 41 explains how Ω_A 's electrons contribute to Ω_B 's expected $N(B)$.

- (d) We can further decompose $N(A)$ in terms of $g_A(\mathbf{r})$:

$$\begin{aligned} N(A) &= \int_A g_A(\mathbf{r})d\mathbf{r} + \sum_{B \neq A}^{M-1} \int_B g_A(\mathbf{r})d\mathbf{r} \\ &= \int_A g_A(\mathbf{r})d\mathbf{r} + \sum_{B \neq A}^{M-1} \int_A g_B(\mathbf{r})d\mathbf{r} \end{aligned} \quad (2-42)$$

whereby Eq. 42 essentially shows that the atomic electron population of Ω_A can be decomposed into the localised electrons of Ω_A (first term in the expression) plus the delocalised electrons that Ω_A makes to all other atoms in the system.

Properties (a)-(d) show us how useful DAFH is to understand the atomic electron populations $N(A)$, as well as its delocalisation, due to $g_A(\mathbf{r})$ being effectively used to describe $N(A)$.

Since $g_A(\mathbf{r})$ calculation can typically be an exhaustive calculation, we can simplify the matter by using AOM elements:

$$g_A(\mathbf{r}) = \sum_{ij} \sqrt{v_i} \sqrt{v_j} \chi_i^*(\mathbf{r}) \chi_j(\mathbf{r}) S_{ji}^A \quad (2-43)$$

where

$$S_{ji}^A = \langle \chi_j | \chi_i \rangle = \int_A \chi_j(\mathbf{r}) \chi_i(\mathbf{r}) d\mathbf{r} \quad (2-44)$$

which considers the real space distribution of χ_i and χ_j and their individual occupancies (v), weighted by their atomic overlap S_{ji}^A (being our AOM element), summed over all MO combinations. Note that in restricted HF and DFT, the occupations (v) will be equal to two.^[7]

2.3.2.4. FALDI Decomposition Development

For the purpose of the FALDI decomposition scheme, we make use of real-space distribution within QTAIM atomic basins, and FALDI is derived from the general DAFH function, $g_A(\mathbf{r})$. FALDI decomposes the total ED at any specified spatial coordinate into specific FALDI components.

$$\rho(\mathbf{r}) = \sum_i FALDI(\mathbf{r}) \quad (2-45)$$

Components of FALDI include: (i) *frag*-ED which describes the ED of a chemical fragment, (ii) *atom*-ED which describes the ED contribution of an atom, (iii) *loc*-ED which describes the ED localised to a specific atom, and (iv) *deloc*-ED which describes the ED that is delocalised

along an atom-pair. We can further break these components down in the remainder of this section.

As discussed previously, *atom*-ED describes the ED distributions in three dimensional space that is situated solely in one specific atomic basin, which correlates directly to our DAFH function, and thus can be described by $\rho(\mathbf{r}) = \sum_A^M g_A(\mathbf{r})$. *Frag*-ED is rather simple in retrospect, as it is simply the sum of atomic contributions that make up a specific fragment.

Although we can get valuable information from FALDI's *atom*- and *frag*-ED, FALDI allows us to dig deeper into the distribution of electrons throughout a system. This can be done with localisation and delocalisation indices. At this point it is important to distinguish between QTAIMs LIs and DIs, and of FALDIs.

- (a) QTAIM-defined LI gives a point count of the electrons localised to the specific atomic basin (λ_A), in which can be calculated by integrating $g_A(\mathbf{r})$ over its own atomic basin and can be expressed as the trace of the matrix product of its AOM with itself.

$$\lambda(A) = 2Tr(\mathbf{S}^A \mathbf{S}^A) \quad (2-46)$$

- (b) QTAIM-defined DI ($\delta_{A,B}$) gives a count of the electrons that are delocalised between two specified atomic basins, and can be expressed in terms the trace of the matrix product of two different AOM.

$$\delta(A, B) = 2Tr(\mathbf{S}^A \mathbf{S}^B + \mathbf{S}^B \mathbf{S}^A) \quad (2-47)$$

- (c) FALDI-defined LI ($\mathcal{L}_A(\mathbf{r})$) can be calculated in a similar way as the DAFH function in Eq. 43, however distributed in three-dimensional space. We can express FALDI-defined LI by the overlap of all 2-body combinations of MOs in real space weighted by the matrix product of its AOM with itself.

$$\mathcal{L}_A(\mathbf{r}) = 2 \sum_{ij}^{N/2} \chi_i^*(\mathbf{r}) \chi_j(\mathbf{r}) (\mathbf{S}^A \mathbf{S}^A)_{ji} \quad (2-48)$$

(d) FALDI-defined DI ($\mathcal{D}_{A,B}(\mathbf{r})$) is also distributed in three-dimensional space. We can express FALDI-defined DI by the overlap of all 2-body combinations of MOs weighted by the matrix product of two AOMs.

$$\mathcal{D}_{A,B}(\mathbf{r}) = 2 \sum_{ij}^{N/2} \chi_i^*(\mathbf{r}) \chi_j(\mathbf{r}) (\mathbf{S}^A \mathbf{S}^B + \mathbf{S}^B \mathbf{S}^A)_{ji} \quad (2-49)$$

Note that the benefit of FALDI-defined localisation- and delocalisation-indices are that they are distributed, as previously mentioned, in real three-dimensional space. This allows invaluable visualisation of the electron distribution within an atomic basin, $\mathcal{L}_A(\mathbf{r})$, and between two atomic basins, $\mathcal{D}_{A,B}(\mathbf{r})$.

2.4. Orbital Analysis

2.4.1. Molecular Orbitals

We can give the expression of an MO, and already have in Eq. 14, as a set of gaussian functions

$$\chi_j = \sum_{i=1}^N a_{ij} \varphi_i \quad (2-14)$$

whereby MO j is the sum of all basis functions i weighted by a coefficient a .

The electron density can thus be expressed as the orbital densities, which we have already defined in Eq. 33

$$\rho(\mathbf{r}) = \sum_i^{N_{MO}} v_i |\chi_i(\mathbf{r})|^2 \quad (2-33)$$

which describes the sum of the square of MO's at a specific point, weighted by its orbital occupation v_i , and because we always use DFT, this can be replaced to 2, as we assume double occupation.

2.4.2. Natural Bond Orbitals

Natural bond orbitals (NBO), developed by Weinhold are a form of mathematically derived orbitals, similarly to MO's, but limited by a criterion that the orbitals must be localised in a 1-centre or 2-centre region in the molecule.^[17] This results in NBO's that closely resemble Lewis-like bonds (and give the most accurate Lewis structure depiction of the wave function), whereby they force an electron pair to exist between a single bond for example. In its algorithm, it calculates the ED around the molecule and starts to fit the density in a Lewis-like fashion, and the remaining density being placed into Rydberg orbitals that remain orthonormal to the first orbitals. The highest percentage of the electron density that it can fit in this Lewis limit gives information to how accurate the Lewis structure is in depicting the system.

2.5. New Theoretical Developments

2.5.1. Cross-Section Decomposition of Electron Density

In chemistry, and more specifically synthetic chemistry, the physical properties of chemical bonding and interactions are to a large extent described by two atoms, but the problem arises in that the concept of multi-centred interactions have been known for at least 75 years. In QTAIM we observe a DB between all atoms that are involved in typical bonds, such as a C-C single bond, but also between atoms that we would not expect to be bonded. Cross-section decompositions^[4, 18-19] were introduced to decompose, quantify, and visualise the multi-centred nature of interactions; that is the individual components that contribute to the formation of a DB. This technique is imperative in explaining the natures of unusual bonds, as well as explaining the absence of DBs where we would otherwise expect them.

The cross-sections can decompose the *tot*-ED at a real space coordinate \mathbf{r} , be it a (3,-1) CP on a DB, into *loc*-ED and *deloc*-ED, and in which the *deloc*-ED can be further decomposed into individual components that contribute to the formation of DB. These individual components can be MOs, atom-pairs from FALDI, or NBOs, in which we name the MO-ED, FALDI-ED, and NBO-ED method, respectively.

Along with breaking down the *deloc*-ED into the components that contribute to its ED, we can also determine the nature of these interactions. By this, we mean whether they promote or impede the formation of a DB. By analysing the partial second derivative of the ED along the 2nd eigenvector (λ_2 -eigenvector), we can determine if the component concentrates density (negative partial second derivative), depletes (positive partial second derivative), or removing (negative ED), which are synonymous with bonding, nonbonding, and antibonding, respectively. In other words, concentrating components facilitate the formation of a DB, and depleting and removing components hinder the formation of a DB. It is important to note that these components' natures are not confined molecular wide; it may concentrate in one point in the system but deplete in another. We only measure its nature at \mathbf{r} in real space. We can then group each of the individual components according to their nature and visualise the *tot*-ED in two dimensional cross-sections, decomposed into the overall concentrating, depleting, and removing densities.

One thing to note is that in the case of MO-ED and NBO-ED, cross-section decomposition analysis decomposes the *deloc*-ED into concentrating and depleting density, whereas in the FALDI-ED method, the *deloc*-ED is further decomposed to include the removing density. The reason to why exclusively FALDI-ED recovers the removing/anti-bonding densities is because NBO and MO decompositions are based off of the first order ED, $\rho(\mathbf{r})$, whereas FALDI decomposition is based off of the pseudo-second order ED, pseudo- $\rho_2(\mathbf{r}_1, \mathbf{r}_2)$. So, more information is recovered for FALDI than from MO and NBO, and in turn we obtain a more fundamental and cleaner interpretation of the ED.

Thus, cross-section decompositions allow for the study of multi-centred interactions to identify the components that directly contribute to \mathbf{r} in real space of a system, and in turn to a DB, and thus understand the nature of these interactions more clearly. This method shows how

many interactions are not actually bicentric, but have a multitude of components that actually affect the presence/absence of a DB.

2.5.2. $CP(\mathbf{r})$ Function

We have previously discussed that, with regards to cross-section decompositions, we can decompose the *tot*-ED into concentrating, depleting, and for FALDI-ED, also removing densities at a point in space, \mathbf{r} , depending on the sign of the partial second derivative along the 2nd eigenvector (λ_2 -eigenvector). If the component is of a concentrating nature, then it indicates that the specific component *facilitates* the presence of a DB, and in turn the presence of a (3,–1) CP. If the component is of a depleting or removing nature, then it indicates that the specific component *hinders* the presence of a DB.

By grouping each individual component according to its nature, the *tot*-ED is a summation of all groupings

$$\rho_{tot}(\mathbf{r}) = \rho_{concentrating}(\mathbf{r}) + \rho_{depleting}(\mathbf{r}) + \rho_{removing}(\mathbf{r}) \quad (2-50)$$

Although we can classify the nature of a contributing component based on the partial second derivative as discussed above, and determine what facilitates or hinders the formation of a possible DB and (3,–1) CP, the presence/absence of a DB and (3,–1) CP is due solely on the gradient of the *tot*-ED, i.e. the first derivative of *tot*-ED, and its components. A CP in the ED is where the first derivative of the density at \mathbf{r} [$\partial\rho_{tot}(\mathbf{r})$] along λ_2 -eigenvector is zero.^[11] We can rewrite out Eq. 50 in terms of gradients.

$$\partial\rho_{tot}(\mathbf{r}) = \partial\rho_{concentrating}(\mathbf{r}) + \partial\rho_{depleting}(\mathbf{r}) + \partial\rho_{removing}(\mathbf{r}) \quad (2-51)$$

A clear back-and-forth between the conditions for a (3,–1) CP to be present becomes clear but becomes more complex to interpret; the gradient components must all add up to/be equal to zero at the (3,–1) CP, but the absolute gradient of the concentrating slopes must be larger than depleting about the (3,–1) CP. To make this interpretation easier, the $CP(\mathbf{r})$ function was

introduced by de Lange *et al*^[6] to detect the presence/absence of a DB between two atoms when measuring along λ_2 -eigenvector.

$$CP(\mathbf{r}) = -\text{sign}\left(\partial\rho_{\text{depleting}}(\mathbf{r})\right)\left[\partial\rho_{\text{concentrating}}(\mathbf{r}) + \partial\rho_{\text{depleting}}(\mathbf{r}) + \partial\rho_{\text{removing}}(\mathbf{r})\right] \quad (2-52)$$

which is simplified to

$$CP(\mathbf{r}) = -\text{sign}\left(\partial\rho_{\text{depleting}}(\mathbf{r})\right)\left(\partial\rho_{\text{tot}}(\mathbf{r})\right) \quad (2-53)$$

This $CP(\mathbf{r})$ function in principle expresses the gradient of the total density at \mathbf{r} but weighted by the sign of the gradient of depleting densities. This ensures that the $CP(\mathbf{r})$ function is negative in all regions of the scan except for regions that the sum of the $\partial\rho_{\text{concentrating}}(\mathbf{r})$ and $\partial\rho_{\text{removing}}(\mathbf{r})$ is larger in absolute value than that of $\partial\rho_{\text{depleting}}(\mathbf{r})$, and opposite in sign.

The $CP(\mathbf{r})$ function agrees with the definition of a CP, whereby at a CP, the first derivative density is zero. If the scan along λ_2 -eigenvector crosses *two* CPs, for example both the (3,-1) CP and ring CP, then the region on the $CP(\mathbf{r})$ between them are positive.

This function is an invaluable asset as it predicts DBs between any atom-pair participating in a real space formation of a DB, as seen with QTAIM. It has been shown to precisely predict the presence of any form of classical covalent bond, as well as intra-molecular hydrogen interactions in the form of X-H \cdots Y and so on. Therefore, this function would be of a great benefit in the study of unusual QTAIM bond paths, and also to study the *absence* of DB's where classical chemistry would expect one.

2.5.3. MO-DI

MO theory has been used extensively in the past decades in the study of chemical bonding, and because of this, it has been incorporated into many computational programs. MOs are well defined for small diatomic molecules, to which most of our understanding arises, however as

the number of atoms increase to form polyatomic molecules, our interpretation of MO theory becomes cloudy, leading to misinterpretations.

From MO theory, we understand that a constructive overlap between atomic orbitals (AO) leads to an accumulation of ED within the inter-nuclear space, and in turn we understand that this constructive overlap allows for larger delocalisation which we know to be a bonding mechanism.

QTAIM has also been used successfully in the efforts to explain chemical bonding, by making use of the topology of the ED distribution, and therefore avoiding MOs polyatomic interpretations.

With the MO-DI method, we look at how each MO contributes to QTAIM-defined DI, and how each MO combines with all other MOs, either constructively or destructively. From MO theory, we understand that a constructive overlap between AO leads to an accumulation of ED within the inter-nuclear space. This constructive overlap allows for larger delocalisation within/across the system which we know to be a bonding mechanism.

We can obtain the DI between atoms A & B by integrating each MO pair over both atomic basins, Eq. 54, whereby S_{ij}^A signifies a component of the AOM.

$$\delta(A, B) = 2 \left| - \sum_{ij} S_{ij}^A S_{ji}^B \right| \quad (2-54)$$

From Eq. 54, we can proceed to quantitatively determine the specific MO contribution to a specific DI. We can take Eq. 54 and modify it to represent a delocalised density matrix.

$$D_{ij}^{(A,B)} = 2 \left| -S_{ij}^A S_{ji}^B \right| \quad (2-55)$$

The sum of *all* AOM components then provides $\delta(A, B)$. If we were to examine the diagonal/trace of $D_{ij}^{(A,B)}$ matrix, whereby $D_{i=j}^{(A,B)}$, we would then recover the contribution that each MO makes independently to the DI(A,B). However if we examine the off-diagonal

components whereby $D_{i \neq j}^{(A,B)}$, then we recover the contribution that the orbital-pair makes to the $DI(A,B)$. If this value is positive, then it means that the orbital-pair contribute constructively, and therefore place density in the inter-nuclear space. If this value is negative, then it means that the orbital-pair depletes density from the inter-nuclear space. Finally, if we take the sum of the row/column, we obtain the net effect that the specific orbital has on the DI , taking into account all orbital-pair contributions. From this we can determine whether a specific MO is constructive or deconstructive in totality.

2.6. References

1. Bader, R.F.W. *Atoms in Molecules: A Quantum Theory*; Oxford University Press: Oxford, 1990.
2. de Lange, J.H.; Cukrowski, I. *J. Comput. Chem.* **2017**, *38*, 981-997.
3. Cukrowski, I.; van Niekerk, D.M.; de Lange, J.H. *Struct. Chem.* **2017**, *28*, 1429-1444.
4. de Lange, J.H.; van Niekerk, D.M.; Cukrowski, I. *J. Comput. Chem.* **2018**, *39*, 973-985.
5. de Lange, J.H.; Cukrowski, I. *J. Comput. Chem.* **2018**, *39*, 1517-1530.
6. de Lange, J.H.; van Niekerk, D.M.; Cukrowski, I. *J. Comput. Chem.* **2018**, *39*, 2283-2299.
7. Foresman, J.B.; Frisch, Æ. *Exploring Chemistry with Electronic Structure Methods*, 3rd ed., Gaussian Inc: Wallingford, 2015.
8. Koch, W.; Holthausen, M.C. *A chemist's guide to density functional theory*, 2nd ed., Wiley-VHC: Weinheim, 2001.
9. Cramer, C.J. *Essentials of Computational Chemistry*, 2nd ed., John Wiley & Sons: Chichester, 2004.
10. Feynman, R.P. *Phys. Rev.* **1939**, *56*, 340.
11. Matta, C.F.; Boyd, R.J. *The Quantum Theory of Atoms in Molecules*, Wiley-VCH: Weinheim, 2007.
12. Bader, R.F. *J. Phys. Chem. A* **1998**, *102*, 7314-7323.
13. Bader, R.F. *J. Phys. Chem. A* **2009**, *113*, 10391-10396.
14. Matta, C.F.; Hernández-Trujillo, J.; Tang, T.H.; Bader, R.F.W. *Chem. Eur. J.* **2003**, *9*, 1940-1951.
15. Ponec, R. *J. Math. Chem.* **1997**, *21*, 323-333.
16. Ponec, R. *J. Math. Chem.* **1998**, *23*, 85-103.
17. Weinhold, F.; Landis, C.R. *Chem. Educ. Res. Pract.* **2001**, *2*, 91-104.
18. Cukrowski, I.; de Lange, J.H.; Adeyinka, A.S.; Mangondo, P. *Comput. Theor. Chem.* **2015**, *1053*, 60-76.
19. de Lange, J.H.; van Niekerk, D.M.; Cukrowski, I. *Phys. Chem. Chem. Phys.* **2019**, *21*, 20988-20998.

Chapter 3

Molecular Orbitals Support Energy-Stabilizing 'Bonding' Nature of Bader's Bond Paths

Published in:

Journal of Physical Chemistry A **2020**, *124*, 5523-5533. DOI: 10.1021/acs.jpca.0c02234.

The Supplementary Information is provided in Appendix I

Molecular Orbitals Support Energy-Stabilizing ‘Bonding’ Nature of Bader’s Bond Paths

Ignacy Cukrowski,* Jurgens H. de Lange, Daniël M. E. van Niekerk and Thomas G. Bates

Department of Chemistry, Faculty of Natural and Agricultural Sciences, University of Pretoria, Lynnwood Road, Hatfield, Pretoria 0002, South Africa

*Correspondence to: Ignacy Cukrowski

E-mail: ignacy.cukrowski@up.ac.za

3.1. ABSTRACT

Our MO-based findings proved a bonding nature of each density bridge (DB, or a bond path with an associated critical point, CP) on a Bader’s molecular graph. A DB pin-points universal physical and net energy-lowering processes that might, but do not have to, lead to a chemical bond formation. Physical processes leading to electron density (ED) concentration in inter-nuclear regions of three distinctively different homo-polar H,H atom-pairs as well as classical C–C and C–H covalent bonds were found to be *exactly the same*. Notably, properties of individual MOs are inter-nuclear-region specific as they (i) either concentrate, deplete or do not contribute to ED at a CP and (ii) delocalise electron-pairs through either in- (positive) or out-of-phase (negative) interference. Importantly, dominance of a net ED concentration and positive e^- -pairs delocalisation made by a number of σ -bonding MOs is a common feature at a CP. This feature was found for the covalently-bonded atoms as well as homo-polar H,H atom-pairs investigated. The latter refer to a DB-free H,H atom-pair of the bay in the twisted biphenyl (Bph) and DB-linked H,H atom-pairs (i) in cubic Li_4H_4 , where each H-atom is involved in three highly repulsive interactions (over +80 kcal/mol) and (ii) involved in a weak attractive interaction when sterically clashing in the planar Bph.

3.2. INTRODUCTION

Chemistry is synonymous with the concept of chemical bonding that is being debated for decades with most approaches being solidly routed in two major ‘families’ of quantum mechanics (QM) methods. The first, wavefunction-based family encompasses applications of (i) molecular orbitals (MO),¹⁻⁴ valence bond (VB) theory,^{1,2,5,6} natural bond orbital (NBO)⁷⁻⁹ and natural orbitals for chemical valence (NOCV) within the ETS-NOCV¹⁰⁻¹³ energy decomposition scheme (ETS = extended transition state). The second, electron density (ED) based family (the quantum chemical topology (QCT) methods) incorporates the quantum theory of atoms in molecules (QTAIM),¹⁴⁻¹⁶ interacting quantum atoms (IQA),¹⁷⁻¹⁹ fractional occupation iterative Hirshfeld (FOHI),^{20,21} and fragment attributed molecular system energy change (FAMSEC).^{13,22-24} Most methods within orbital and electron density based approaches have been successfully applied in describing chemical bonding for many decades. Even though the two families have QM as a common denominator, their interpretations of chemical bonding might be drastically different. A typical, but not exclusive, example is a ubiquitous^{25,26} homopolar H,H atom-pair involved in a steric intra- and inter-molecular CH...HC contact in crowded molecular environments. To this effect, biphenyl (Bph) became an iconic subject of a nearly 3-decade long scientific debate.²⁵⁻⁴⁰ This is because (i) Bader’s bond path (BP)¹⁴ links *ortho*-H atoms that, according to the generally accepted view, are involved in a *steric repulsive interaction*^{27,30} in planar Bph and (ii) one could computationally investigate (dis)appearance of a BP on rotating two phenyl rings. Moreover, Bph is a prototype molecule in numerous studies and it features, as a molecular core, in 2.6% of all Cambridge Structural Database (CSD) structures.⁴¹

Notably, it is not the appearance of a BP between *ortho*-H-atoms involved in a steric contact but its (non)bonding interpretation that became a subject of a battle between the two camps. To avoid unnecessary repetitions, readers interested in historic development of this research debate are referred to most recent paper by Popelier.³⁹ Briefly, Bader’s notion of a bond path

representing an interaction of a bonding nature is generally supported/rejected by researches entrenched in the QCT/wavefunction-based interpretations. As a matter of fact, the dispute on chemical interpretation of a BP extended to other and classically ‘unexpected’ appearances of BPs, such as between He and C-atoms of adamantane,^{42–44} between noble gas atoms and noble gas and C atoms in endohedral fullerenes $\text{Ng}_2@C_{60}$ ($\text{Ng}=\text{He}-\text{Xe}$),⁴⁵ He, F, F^- dimers⁴⁶ or water dimers,⁴⁷ bay-type $\text{H}\cdots\text{H}$ interaction in *cis*-2-butene,^{9,13,48} or phenanthrene.^{25,40,49}

Our main aim is to put forth a chemical interpretation of BPs by investigating physical processes leading to the absence or presence of a BP. Our focus is on individual canonical MOs’ nature and contribution made to the electron density in specific inter-nuclear regions. Two classical covalent, C–C and C–H, bonds in Bph, the bay-type steric $\text{CH}\cdots\text{HC}$ contact in the planar Bph, the $\text{CH}\cdots\text{HC}$ inter-nuclear region without a BP in the twisted Bph, and finally the $\text{H}\cdots\text{H}$ interactions in a cubic form of LiH (Li_4H_4) will be investigated - Figure 1.

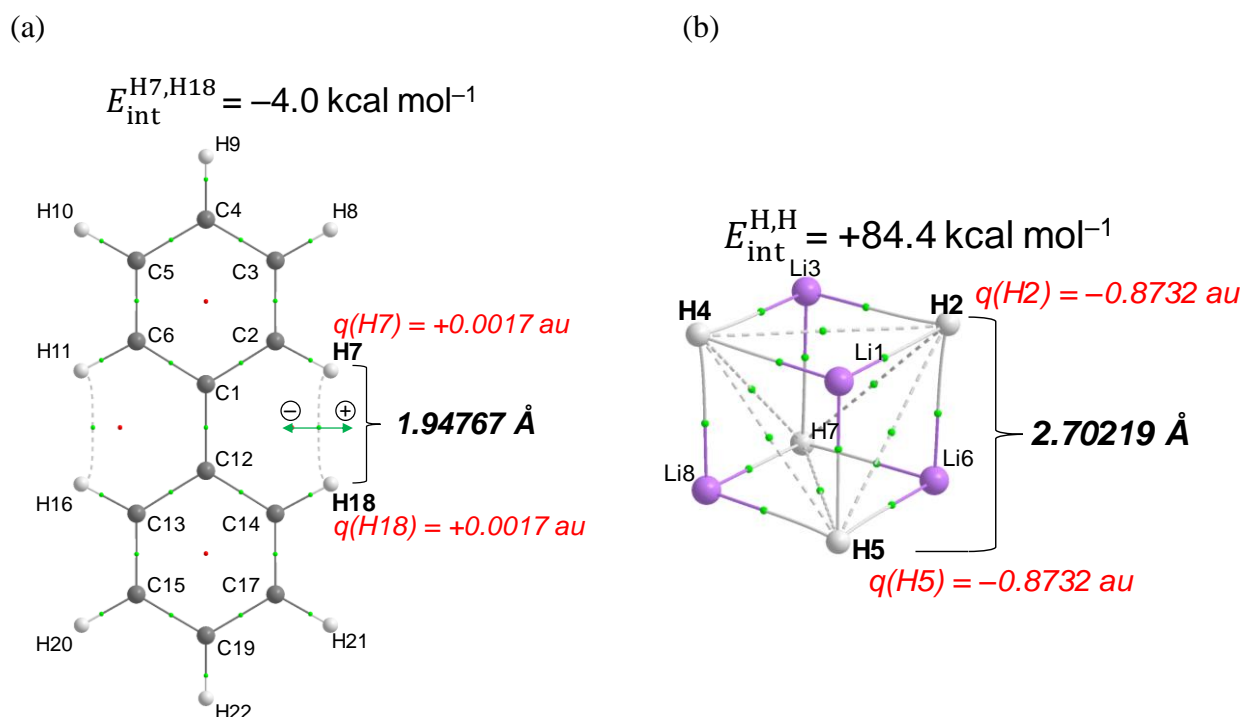


Figure 1. Molecular graphs of (a) planar biphenyl and (b) equilibrium structures of cubic Li_4H_4 calculated at the B3LYP–GD3/6-311++G(2pd,2df) level. The green and red dots represent (3,-1) and (3,+1) critical points, respectively.

Notably, we selected two distinctively different BP-linked homo-polar H,H atom-pairs. In the first instance, the H-atoms in the planar Bph are involved in a weak attractive interaction, have a small positive net atomic charge, $Q(\text{H})$, and overlap due to $d(\text{H,H}) \ll$ the sum of their van der Waals (vdW) radii. In the second case, the H-atoms in Li_4H_4 are involved in a very strong repulsive interaction, carry a large negative $Q(\text{H})$ and are well separated with $d(\text{H,H}) \gg$ the sum of H-atoms vdW radii. In the latter case and totally unexpectedly, six BPs originating from each H-atom, involving three Li,H and three H,H atom-pairs, are present – Figure 1b.

3.3. METHODS

3.3.1. Theoretical Background. We utilize the recently introduced MO-ED and MO-DI methods;⁵⁰ a brief description of our approach is detailed below while a full description of both methods is given in PART 1 of the Supporting Information, SI. Notably, the MO-ED method decomposes the total electron density at a specifically selected coordinate \mathbf{r}^* into contributions made by each orbital:

$$\rho(\mathbf{r}^*) = \sum_i^{N_{MO}} v_i |\chi_i(\mathbf{r}^*)|^2 \quad (1)$$

where χ_i is an MO with occupation v_i . \mathbf{r}^* is chosen to be a (3,-1) critical point (CP, or bond critical point) if present, or otherwise the coordinate of a minimum density point (MDP) along an inter-nuclear vector.

The decomposition is then followed along the eigenvector associated with the second eigenvalue of the Hessian matrix which we will refer to as the λ_2 -eigenvector. In most cases, the λ_2 -eigenvector is synonymous with a cross-section perpendicular to a given inter-nuclear vector. We then consider, for each MO, the partial directional second derivatives computed along the λ_2 -eigenvector. From that, each MO can be labelled as *concentrating* ED (negative second derivative), *depleting* ED (positive second derivative) or *non-contributing* to the ED (in the case of an MO node) at the selected \mathbf{r}^* . Typically, the nature of a selected MO varies at

different CPs/MDPs. MOs' contributions of the same fashion can then be grouped to provide a 'characterized' total density contribution of specific natures at \mathbf{r}^* :

$$\rho(\mathbf{r}^*) = \rho_{\text{concentrating}}(\mathbf{r}^*) + \rho_{\text{depleting}}(\mathbf{r}^*) + \rho_{\text{non-contributing}}(\mathbf{r}^*) \quad (2)$$

We also make use of recently-developed⁵¹ $CP(\mathbf{r})$ function to explain the presence of a bond path. This function accounts for the first derivatives computed on the total *concentrating*, *depleting* and *non-contributing* density terms in Eq. 2:

$$CP(\mathbf{r}) = -\text{sign}(\partial\rho_{\text{depleting}}(\mathbf{r})) \cdot [\partial\rho_{\text{concentrating}}(\mathbf{r}) + \partial\rho_{\text{depleting}}(\mathbf{r}) + \partial\rho_{\text{non-contributing}}(\mathbf{r})] \quad (3)$$

Specifically, the $CP(\mathbf{r})$ is positive in the vicinity of \mathbf{r} if the slope computed along the λ_2 -eigenvector on density provided by the MOs concentrating ED is greater and opposite in sign than the slope obtained for the MOs depleting ED. We have previously found⁵¹ that the $CP(\mathbf{r})$ will always be positive in the vicinity of a DB. For more details, please refer to Part 1 of the SI.

The MO-DI method, on the other hand, provides a MO-based decomposition of the QTAIM-defined delocalization index (DI). Such a matrix is obtained by first defining an atomic overlap matrix for an atom A with elements

$$S_{ij}^A = \int_A \sqrt{v_i} \sqrt{v_j} \chi_i^*(\mathbf{r}) \chi_j(\mathbf{r}) d\mathbf{r} \quad (4)$$

which satisfies $N(A) = \text{tr}(\mathbf{S}^A)$, where $N(A)$ is the total electronic population. A delocalized density matrix for atom-pair A,B can then be defined, with elements

$$D_{ij}^{(A,B)} = 2| -S_{ij}^A S_{ji}^B | \quad (5)$$

where all elements sum up to the QTAIM-defined DI(A,B). The $\mathbf{D}^{(A,B)}$ matrix provides information regarding the overlap and interference of MOs across two atomic basins. Diagonal elements, $D_{ii}^{(A,B)}$, provide each MO's contribution to the total number of electron pairs shared between A and B. This term results from mutual overlap of an MO across two atomic basins.

However, the off-diagonal elements, $D_{i \neq j}^{(A,B)}$, provide the extent to which an MO-pair either increases delocalized electron pairs (through constructive interference) or decreases delocalized electron pairs (through deconstructive interference). Therefore, the sum of any row or column of \mathbf{D}_{ij} gives the net contribution of an MO to the number of electron pairs shared between atoms A and B, after any MO-pair interference effects have been taken into account. An example of such a matrix as well as its interpretation are shown in Part 2 of the SI.

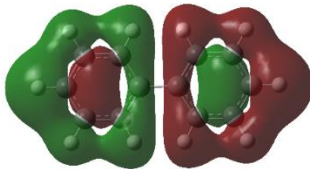
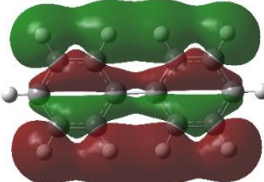
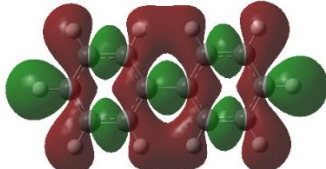
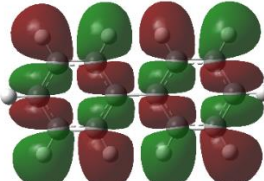
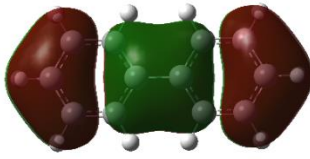
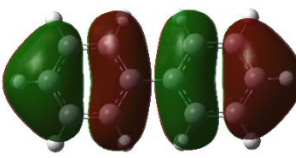
Finally, note that we prefer to use the density bridge (DB) term instead of BP as it perfectly describes the presence of a common topological property of electron density between any pair of atoms in a molecular environment.

3.3.2. Computational Details. All structures were computed in Gaussian 09, Rev. D⁵² using B3LYP with Grimme's D3 empirical dispersion⁵³ with 6-311++G(2df,2pd) in the gas phase; a full set of X,Y,Z coordinates of all molecules discussed in this work is provided in PART 2 in the SI. QTAIM molecular graphs were calculated using AIMAll v. 19.02.13.⁵⁴ Molecular orbital density data was obtained using in-house software.

3.4. RESULTS AND DISCUSSION

Both MO-ED and MO-DI methods⁵⁰ employ canonical, molecule-wide orbitals without any transformation. Moreover, no partitioning of molecules is required; hence, molecules' structural integrity is fully preserved, an approach not commonly adopted in previous MO-based studies. MOs relevant to this study are shown in Table 1 (a full set of MOs computed for the planar and twisted conformers of Bph are in PART 3 of the SI). Looking at the MO isosurfaces, they are remarkably alike in both Bph conformers. Unfortunately, the shape-similarity does not provide any clue as to why a DB is present (or absent) and hence does not provide any information on whether a MO *concentrates* or *depletes* density anywhere in 3D space occupied by a molecule.

Table 1. Selected top-views of MOs in planar Bph. Percentage contributions to ED at relevant BCPs and DI for interactions of interest are also shown.

Orbital	Isosurface	Interaction	% ED	% DI
χ_{24}		H7,H18	0% <i>non-contributing</i>	-6.16 %
		C1,C12	0% <i>non-contributing</i>	-0.41%
		C19,H22	19.9% <i>concentrating</i>	20.17%
χ_{29}		H7,H18	19.1% <i>concentrating</i>	33.13%
		C1,C12	0% <i>non-contributing</i>	0.13%
		C19,H22	8.3% <i>concentrating</i>	-0.01%
χ_{36}		H7,H18	19.1% <i>concentrating</i>	9.25%
		C1,C12	24.3% <i>concentrating</i>	15.45%
		C19,H22	8.3% <i>concentrating</i>	6.62%
χ_{37}		H7,H18	0% <i>non-contributing</i>	-10.10%
		C1,C12	0% <i>non-contributing</i>	-0.61%
		C19,H22	0% <i>non-contributing</i>	0.14%
χ_{38}		H7,H18	0% <i>non-contributing</i>	0.02%
		C1,C12	0% <i>depleting</i>	9.41%
		C19,H22	0% <i>depleting</i>	1.10%
χ_{41}		H7,H18	0% <i>non-contributing</i>	-0.02%
		C1,C12	0% <i>non-contributing</i>	-4.86%
		C19,H22	0% <i>depleting</i>	1.13%

One must realise that just a single set of canonical MOs is always computed for any polyatomic molecule and the molecule-specific electron density distribution is the result of combined individual MO's contributions. However, the ED distribution is not uniform throughout and each molecule has a specific set of covalent bonds and intramolecular, either attractive or repulsive, interactions. From this it follows that a molecule-wide MO cannot have an overall (non)bonding character. Clearly, each MO's nature, in terms of concentrating,

depleting or non-contributing to ED at a specific point \mathbf{r} in 3D space (such as a critical point on Bader's molecular graphs) can only be established by exploring an inter-nuclear region of an atom-pair of interest.

The second derivative of the ED is associated with electron concentration or depletion in the inter-nuclear region or, for that matter, any point in 3D space occupied by a molecule.¹⁴ We have established that the lowest energy MOs involving C_{1s} core electrons in Bph are (i) entirely C-atom-centred and (ii) non-contributing to ED at and in the vicinity of CPs of interest in this work, namely CP/MDP(H7,H18) in planar/twisted Bph and CP(C1,C12) and CP(C19,H22) in planar Bph.

3.4.1. MO-based picture of the C1–C12 and C19–H22 covalent bonds in the planar conformer. We investigate here the carbon-carbon linker (C1–C12) and one of the C–H bonds (C19–H22) as these atoms are not involved in any discernible non-covalent interaction – see Figure 2. A full set of results pertaining to CP(C1,C12) and CP(C19,H22) in the planar conformer is presented in Part 4 of the SI.

Importantly, regardless of the impact made by a local environment, the same and characteristic overall trends are observed for both covalent bonds, namely:

- 1) The directional second partial derivative (from now on called 2nd derivative) computed on the *total* ED is negative at both CPs(A,B) seen in Figures 2a,b. Naturally, the 2nd derivative is also negative in the vicinity of these CPs showing that ED became highly concentrated in the wider inter-nuclear regions. The trends observed in Figures 2a,b can be seen as a MO-ED signature of an overlap of atomic σ -orbitals that lead to the ED concentration, exactly as one would expect from covalent bonds' classical interpretation.
- 2) Traces of the 2nd derivative < 0 shown in Figures 2c,d are signatures of individual MOs that concentrate ED. Typically, only few MOs concentrate ED at a specific CP/MDP and examples for MOs with %-contributions to the total ED at a CP larger than 10% are shown in Figures 2c,d.

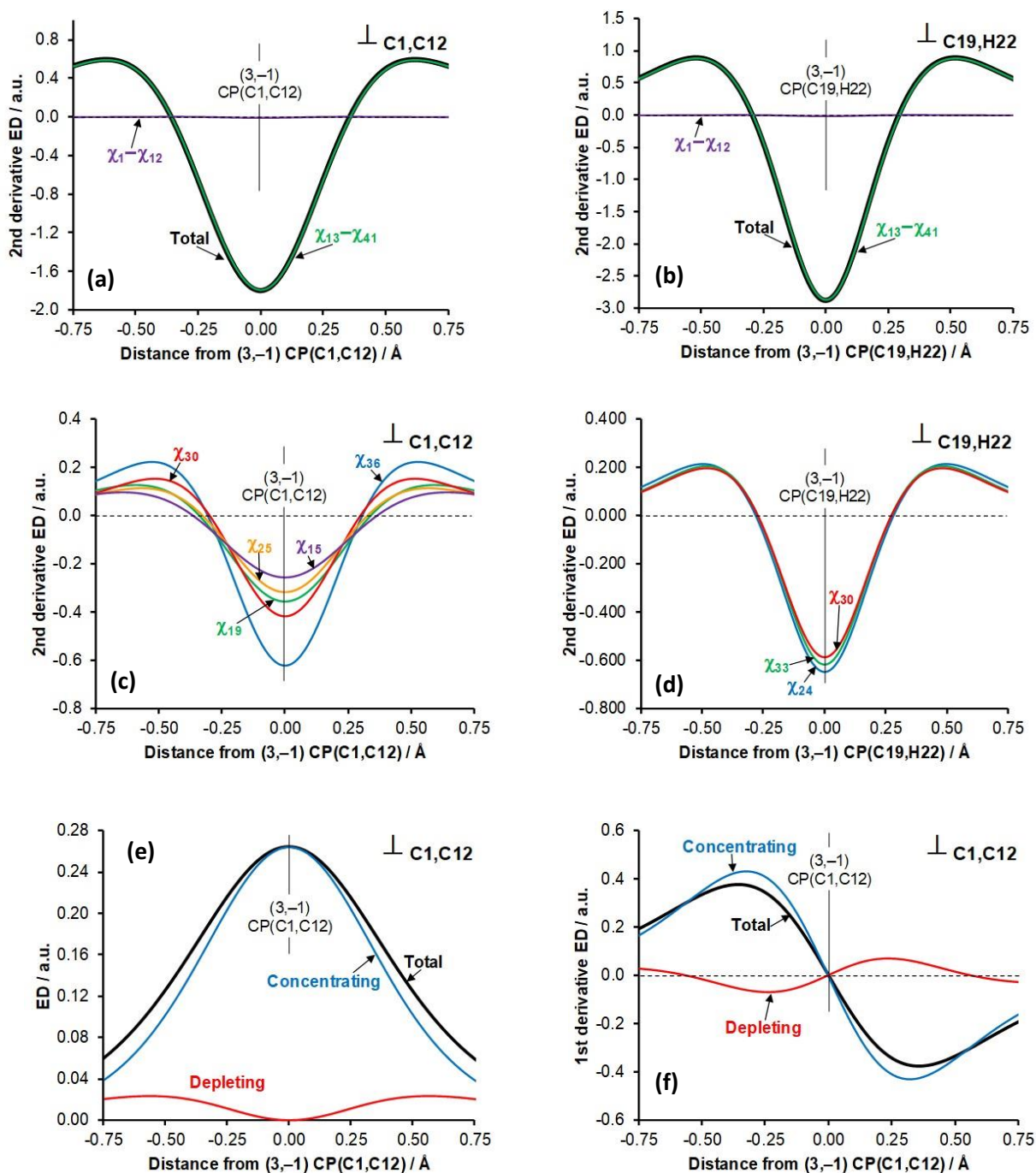


Figure 2. Cross-sections along the λ_2 -eigenvector in the C1,C12 and C19,H22 inter-nuclear regions. (a) to (d) – MO contributions to directional partial second derivative for C1,C12 or C19,H22, as indicated, and total ED (e) and directional partial first derivative (f) along the λ_2 -eigenvector, as selected individual MOs (a and b), grouped according to the contributions from the core ($\chi_1-\chi_{12}$, purple line) and valence ($\chi_{13}-\chi_{41}$, green line) MOs (c and d) or as the sum of all concentrating (blue) or depleting (red) MOs (e and f).

- 3) The overall combined contribution made by MOs 13-41 is of concentrating nature and the total ED peaks exactly at the relevant CP(A,B) – Figure 2e. There are also MOs that deplete ED in the vicinity of CPs, hence they are classified as such, but they are entirely non-contributing exactly at the CP's coordinates because $|\chi_i(\text{CP})|^2 = 0.0$. All these MOs are of π nature in the inter-nuclear region with a node at exactly the relevant CP as shown in Figure 2e.
- 4) The first derivative on the total ED is crossing at the coordinates of CPs(A,B), i.e., at the 0.0 value in Figure 2f.
- 5) The $CP(\mathbf{r})$ function (developed recently⁵¹ to explain the presence, or otherwise, of a DB) shows that the net slope of all concentrating MOs is greater in magnitude and opposite in sign than the net slope of all depleting MOs at a CP(A,B).

As seen from Figure 2 and Table S6, Figures S3 and S4, Part 4 in the SI, all occupied MOs that contribute to ED at CPs throughout a molecule do so differently in each inter-nuclear region, e.g., χ_{36} , in planar Bph, makes the largest contribution at CP(C1,C12) yet a very small contribution at CP(C19,H22), whereas χ_{24} contributes most at CP(C19,H22) but null at CP(C1,C12). Furthermore, the 2nd-derivative-defined nature of each MO's contribution (concentrating, depleting and non-contributing) is inter-nuclear region specific – see Table S6, Part 4 of the SI.

To fully understand the role played by each individual MO and quantify its participation in electron delocalization across two atomic basins, one can make a use of the MO-DI protocol (Tables S7-S9, Part 4 of the SI). It quantitatively accounts for positive or constructive (in-phase) and negative or destructive (out-of-phase) interference computed for each unique MO-pair. The net (or total) number of electron pairs delocalized (delocalization index, DI) between C1,C12 and C19,H22 atom-pairs is 1.06 and 0.97, respectively corresponding to a single covalent bond order. The MO-DI method also explains how the covalent bond order comes about, by calculating the overlap of each MO across two atomic basins as well as the interference with all other MOs. Investigation of specific MO-pairs using the MO-DI method

reveals useful insights and strong links to classical MO interpretations. For instance, the core $1s$ χ_1 and χ_2 orbitals contribute $1.0 e^-$ -pairs to $DI(C1,C12)$ as they completely overlap C1 and C12. However, due to their complete deconstructive interference with each other resulting in $-1.0 e^-$ -pairs, they do not make a net contribution to $DI(C1,C12)$ at all. This is an example of a typical bonding-antibonding MO-pair, in full agreement with a classical interpretation of these orbitals. This is a common pattern even among the valence orbitals, such as the χ_{38} and χ_{41} MO-pair with π character. χ_{38} and χ_{41} contribute a total of $0.14 e^-$ -pairs to $DI(C1,C12)$ through joint overlap over the C1/C12 atomic basins, but $-0.12 e^-$ -pairs are removed due to deconstructive interference with each other. Analysis of individual MO-pairs might be very tedious. However, analysing the combined contributions of *all* MOs proved to be the most insightful: the net $DI(C1,C12)$ of 1.06 is a result of 25 overlapping MOs, contributing $\sum_i D_{ii}^{(C1,C12)} = 2.82 e^-$ -pairs but with a net deconstructive interference of $\sum_{i \neq j} D_{i \neq j}^{(C1,C12)} = -1.76 e^-$ -pairs. This result can be re-stated using chemical jargon: the C–C bond has a maximum bond-order of ~ 3 , which is reduced to ~ 1 due to the presence of bonding-antibonding MO-pairs.

We also note here a strong relationship between our MO-ED and MO-DI results: all of the MOs that concentrate density to an inter-nuclear region also i) strongly overlap both atomic basins, and ii) interfere constructively with each other. This important observation shows that all MOs that concentrate density in an inter-nuclear region are of the same general nature (*i.e.* σ -symmetries) and contribute to the covalency of an interaction.

3.4.2. MO-based interpretation of absence and presence of a DB between H-atoms of a bay in Bph conformers. All the data and observations detailed above for classical covalent bonds paint a very strong picture of both the nature of MOs involved in the topological definition of a DB, as well as the nature and mechanism of electron delocalization across an interaction. This picture is in a full agreement with a general notion of covalent bonds

formation and their energy-minimising contribution to molecular energy. Hence, we decided to follow exactly the same protocol in investigating inter-nuclear regions between covalently non-bonded H7,H18 atom-pair in both Bph conformers – a full set of data is placed in Part 5 of the SI.

Looking at the MO isosurfaces, all contributing MOs are of a σ -fashion relative to the H \cdots H interaction in both conformers. Examples of cross-sections of MOs that concentrate ED, as identified by the 2nd derivative, are shown in Figures 3a,b. The shapes of traces are rather complex (due to congested molecular environment) and the number of concentrating and depleting MOs differs for both conformers. The trends obtained for the total ED revealed (Figures 3c,d) that there is no qualitative difference, as there is a region along the λ_2 -eigenvector (including coordinates of CP(H,H) and MDP(H,H)) where the 2nd-derivative < 0 . This shows that the overall and dominant effect is ED concentration in the inter-nuclear region that resulted in $\rho_{CP} = 0.01427$ a.u. (planar) and $\rho_{MDP} = 0.00529$ a.u. (twisted). Moreover, largely the same orbitals (χ_{23} , χ_{25} , χ_{29} , χ_{35} and χ_{36}) concentrate ED between H-atoms to a total of 72.9% and 61.6% in planar and twisted conformers, respectively.

The only significant difference is in the degree and the slope of MOs' contribution to each inter-nuclear region. We found that the overall degree of ED concentration, relative to depletion, is greater in planar (94.5%) than in twisted (71.3%) at respective points (CP and MDP). Individual MOs' contributions produced specific traces in the total ED (Figures 3c,d) that explain the difference in 1st derivatives (Figures 3e,f) and hence the presence of a DB(H7,H18) only in the planar Bph. Only in the planar Bph we see the trend (thick solid black line in Figure 3e) computed for the 1st derivative on the total ED crossing zero at the exact coordinates of CP(H,H) and the ring critical point (RCP). These critical points are classical topological features when atoms linked by a DB(A,B) form a ring on a molecular graph. The appearance/absence of these two critical points in Figures 3ef is synonymous with the presence/absence of a density bridge, here DB(H7,H18) in the planar Bph.

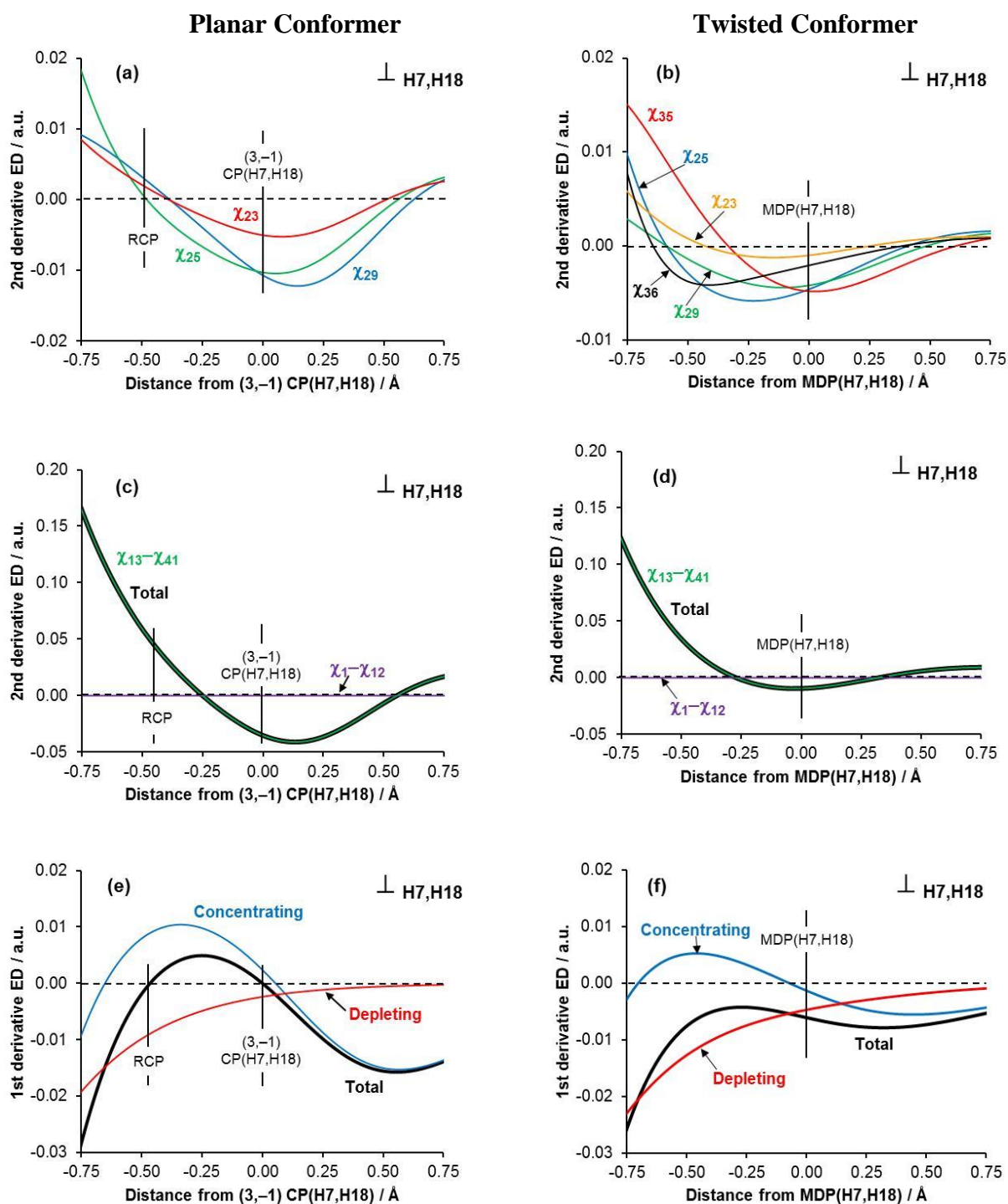


Figure 3 Decomposition of the directional partial second (a to d) and first (e and f) derivatives along the λ_2 -eigenvector in the H7,H18 inter-nuclear region in planar (left) and twisted (right) biphenyl, on selected individual MOs (a and b), grouped according to the contributions from the core ($\chi_1-\chi_{12}$, purple line) and valence ($\chi_{13}-\chi_{41}$, green line) MOs (c and d) or, for the first derivative, on the sum of all concentrating (blue) or depleting (red) MOs (e and f).

Decomposition of the trace of the total ED (Figures 3e,f) into the sums of concentrating and depleting MOs shows that the rate of change of concentrating MOs is greater than the rate of change of depleting MOs in planar Bph, while the opposite is true for twisted Bph. This single observation – as confirmed by the $CP(\mathbf{r})$ function⁵¹ and trends in 1st derivatives shown in Figures S5 and S6, Part 5 in the SI – is the only reason for the presence/absence of DB(H7,H18) in planar/twisted Bph.

To gain additional insight on the nature of the H...H interactions in terms of MOs, we used the MO-DI method – see Tables S11 and S12, Part 5 in the SI. They show a decomposition of the QTAIM-defined DI(H7,H18) of 0.031 and 0.011 e^- -pairs in the planar and twisted Bph, respectively, into contributions made by each MO. The MO-DI method takes into account the spatial overlap of an MO across both atomic basins (diagonal values, $\sum_i D_{ii}^{(H7,H18)}$) as well as the constructive or destructive interference of an MO with all remaining MOs (off-diagonal values, $\sum_{i \neq j} D_{ij}^{(H7,H18)}$).

As an example, let us consider χ_{29} in planar Bph – the MO that shows in-phase σ -symmetry for most H atoms and out-of-phase σ^* -symmetry for C–H bonds, Table 1. In case of the planar conformer, χ_{29} contributes net 0.010 e^- -pairs, *i.e.*, 33% of the DI(H7,H18). This is a result of spatial overlap (0.012 e^- -pairs) and overall interference with other MOs (it amounts to -0.002 e^- -pairs). Most significant constructive interference involves χ_{25} (in-phase σ -symmetry for H7,H18) which contributes an additional 0.009 e^- -pairs whereas most significant deconstructive interference involves χ_{37} (out-of-phase σ^* -symmetry for H7,H18) which reduces the total DI by -0.009 e^- pairs.

However, the most accurate picture of electron delocalization for the H7...H18 interactions can only be obtained by taking into account the overlap and interferences with all MOs. We note that the same general trend as what was observed for the C1–C12 bond, although to a much lesser degree, holds for the H7...H18 interaction in planar biphenyl. In total, MOs

overlapping both H7 and H18 contribute 0.064 delocalized e^- -pairs, but this gets reduced by -0.033 e^- -pairs as a result of destructive interferences. Very much the same holds true for the H7...H18 interaction in twisted biphenyl. Whereas spatially overlapping MOs contribute to DI(H7,H18) more or less the same, 0.060 e^- -pairs, the reduction of DI due to net destructive interferences (-0.049 e^- -pairs) is considerably greater than in the planar biphenyl. This clearly demonstrates that the in-phase MOs' overlap over the H...H interaction is relatively stronger than out-of-phase overlap in planar than twisted biphenyl. In chemical jargon terms, bonding-antibonding MO-pairs reduce the bond order less in planar than twisted biphenyl. Possibly the most important observation, however, is the same nature of MO-overlap as what was observed for the C1–C12 linker in planar Bph: all MOs that concentrate ED at the BCP/MDP(H7,H18) also i) interfere constructively with each other and ii) contribute to the DI in a net-positive fashion.

Taking all of the above results from the MO-ED and MO-DI decompositions into the account, it is abundantly clear that the interaction between H7 and H18 in planar or twisted biphenyl share two critical features. These features, which are also observed for covalent bonds, are: 1) a net concentration of ED in the interatomic region arising from multiple MOs of strictly σ -character and 2) a net delocalization of electron-pairs arising from MO-overlap. Furthermore, our results clearly demonstrate that (i) selecting just few MOs, even with dominant contributions, cannot sufficiently describe the H...H interactions of interest and (ii) it is only through the consideration of all occupied MOs that the topology of the total ED can be recovered and interpreted meaningfully. The only discernible difference between the H...H interactions in planar or twisted biphenyl is the presence of a density bridge. It arises purely from different rates of change of net concentrating relative to depleting MOs' contributions to the total ED, a fact that does not change the underlying nature of the interaction.

3.4.3. MO-based nature of the hydride H,H DBs in cubic Li₄H₄. Cubic Li₄H₄ is an interesting molecule as its molecular graph reveals six density bridges originating from each H-atom. Even more surprising is the presence of three DBs(HH) linking each H-atom with the remaining ones despite (i) $d(\text{HH}) \gg$ the sum of the vdW radii by 0.30 Å and (ii) each H-atom being involved in three large repulsive interactions with neighbouring H-atoms. The computed $E_{\text{int}}^{\text{H,H}} = +84.4 \text{ kcal mol}^{-1}$ is dominated by the classical electrostatic Coulomb energy term of $V_{\text{cl}}^{\text{H,H}} = +92.6 \text{ kcal mol}^{-1}$.

There are 2 groups of 4 doubly-occupied MOs: χ_1 – χ_4 are formed from $1s_{\text{Li}}$ whereas χ_5 – χ_8 from $1s_{\text{H}}$ orbitals – Figure 4. Each group of MOs consists of a single, symmetrical and in-phase MO as well as three degenerate orbitals of different symmetry combinations. Together, this set of 8 MOs describes 24 interactions, 12 Li–H, 6 Li···Li and 6 H···H, and interestingly, density bridges are present for all Li–H and H···H but Li···Li interactions.

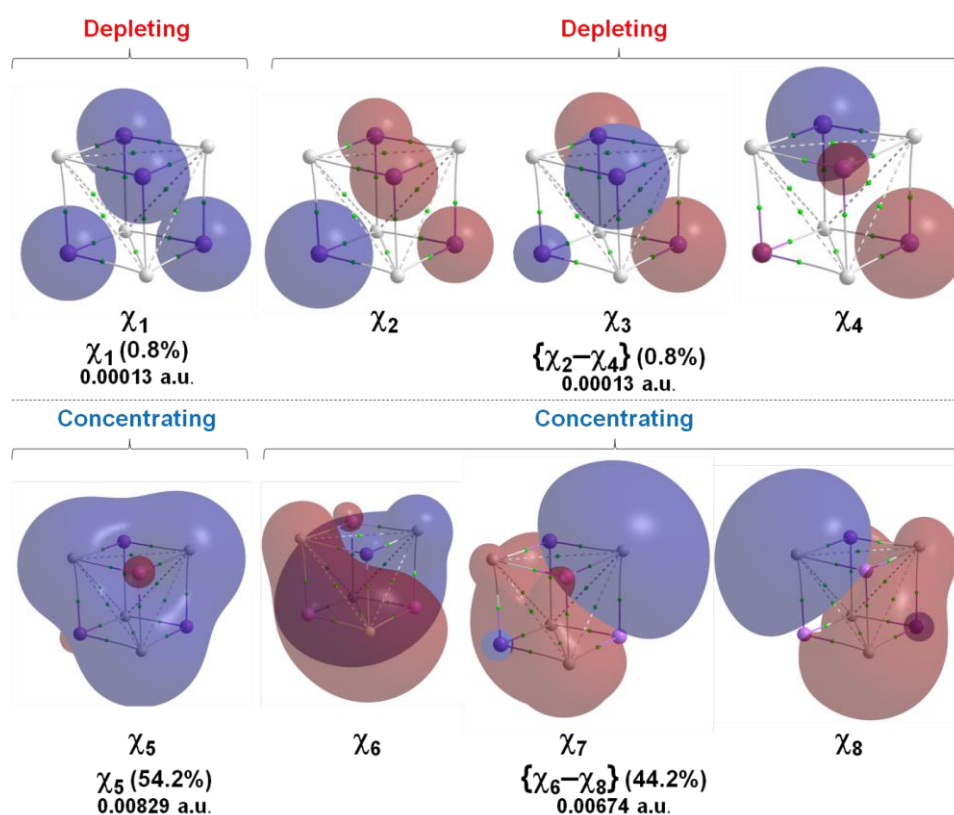


Figure 4. Shapes of the eight MOs in cubic Li₄H₄ (isovalue = 0.02 a.u.). The nature of each MOs contribution to a single H···H interaction, as defined by the sign of the 2nd-derivative, is shown.

We are particularly interested in explaining the presence of the DBs between hydride atoms and due to perfect symmetry of cubic Li_4H_4 , we will discuss the H2,H5 atom-pair as an example – a full set of relevant data is included in Part 6 in the SI. The 2nd derivative trends seen in Figure 5a reveal that concentrating in nature contributions to ED of 0.01530 a.u. at the CP(H2,H5) are made only by χ_5 – χ_8 MOs. This is because the 2nd derivative < 0 is observed at and in the vicinity of the CP(H2,H5). These orbitals contribute 98.3% to ED at this CP with 54.2% coming from χ_5 (Figure 5b). The remaining 1.7% of ED at the CP(H2,H5) comes from four MOs (χ_1 – χ_4) in a depleting fashion (Figure 5c) with χ_1 adding 0.8%.

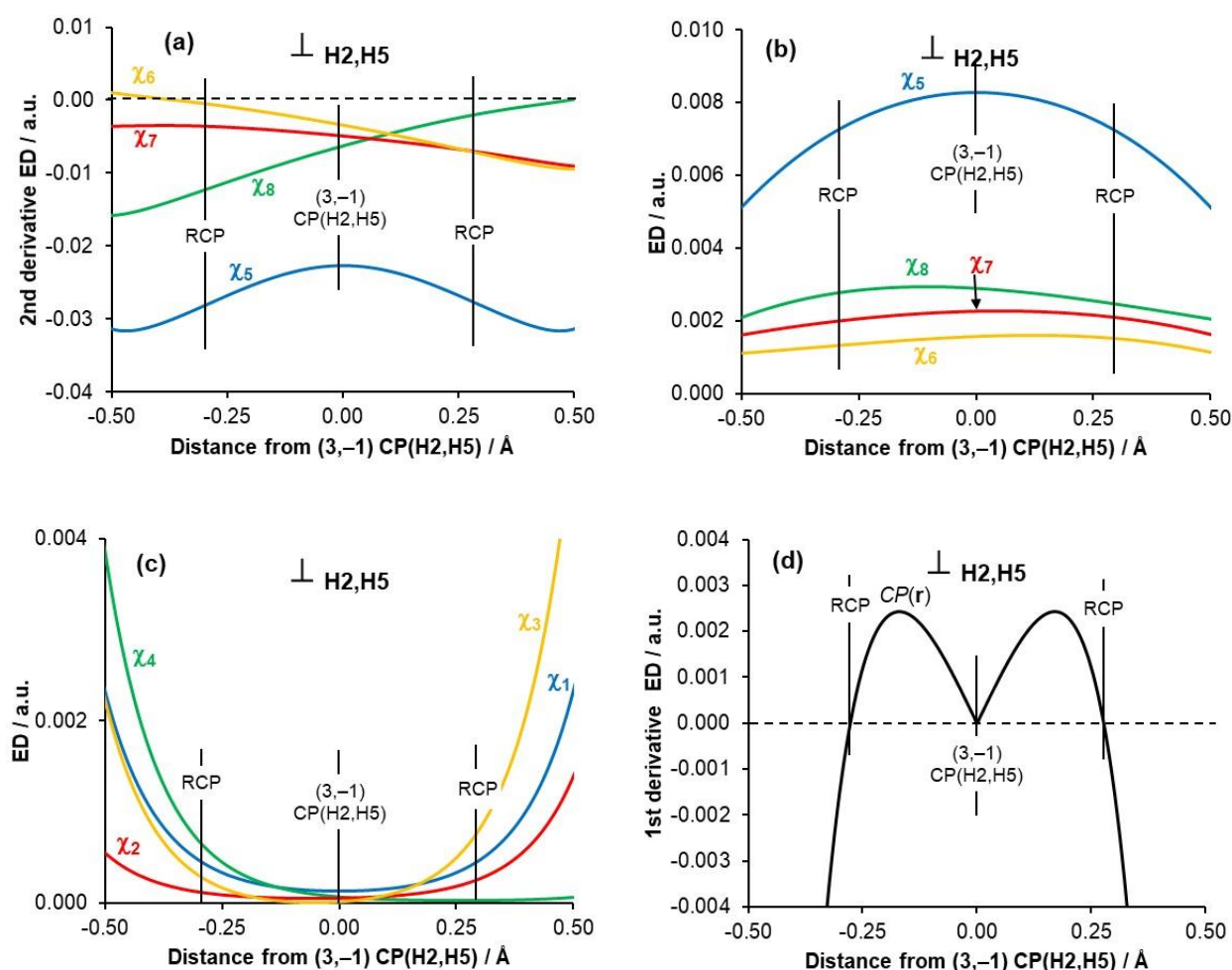


Figure 5. The partial directional 2nd-derivative (a), ED contributions made by higher-energy MOs (χ_5 – χ_8 , b) and lower-energy MOs (χ_1 – χ_4 , c) and the $CP(\mathbf{r})$ function (d) as cross-sections along the λ_2 -eigenvector for atom-pair H2,H5 in Li_4H_4 .

The three degenerate orbitals of different symmetry, (χ_2 - χ_4) and (χ_6 - χ_8), make combined identical contributions to ED at all three CP(H,H), namely 0.0013 and 0.0674 au, respectively. However, individual MO's contributions vary dramatically, *e.g.*, for χ_6 we obtained 0.0, 10.4 and 33.8 %-contributions to CP(H2,H4), CP(H2,H5) and CP(H4,H5), respectively – see Table S14 in Part 6 of the SI. As for the H...H interaction in planar Bph, the DBs between H-atoms in Li₄H₄ are present as a result of the greater slope of the total concentrating than depleting ED contributions made by MOs (Figure 5d).

The MO-DI results obtained for the representative H2...H5 interaction (Table S15, Part 6 of the SI) show that χ_1 localised on all four Li nuclei contributes negligibly to DI(H,H), through both overlap and constructive interference with other MOs. The DI(H2,H5) arises predominantly from the overlap of χ_5 (contributing 0.21 e^- -pairs) and the combined overlap of χ_6 - χ_8 (contributing a sum of 0.15 e^- -pairs) to a total of 0.36 e^- -pairs. However, χ_5 also interferes destructively with χ_6 - χ_8 and this reduces the total DI(H,H) by $-0.26 e^-$ -pairs. Hence, a small but not insignificant net total DI(H2,H5) = +0.09 e^- -pairs was obtained. This observation confirms the classical closed-shell nature of the H...H interactions as the χ_5 and χ_6 - χ_8 MOs form a seemingly bonding-antibonding pair, although in slight favour of net covalent character.

3.5. Conclusions

This work unambiguously shows that physical processes leading to appearance of density bridges (DBs) are exactly the same regardless of the strength and nature of interaction atoms are involved in. We report the MO-based interpretation of:

1. Classical C–C and C–H covalent bonds in the Bph. They represent very strong and overall attractive interactions due to dominant contribution coming from the exchange

correlation term (XC-term). In both cases, an electron-pair sharing (hence electron density concentration) in the inter-nuclear region takes place.

2. A steric CH \cdots HC contact in the non-equilibrium planar conformer of Bph. It is characterised by a weak and slightly attractive, due to dominance of the XC-term, interaction between homo-polar H-atoms.
3. A very large repulsive, due to dominance of electrostatic term, H \cdots H interaction in the *equilibrium structure* of cubic Li₄H₄. Remarkably, each H-atom is involved in three such repulsive, over +80 kcal mol⁻¹, interactions.

We have fully explained the appearance of DBs using the MO-ED and MO-DI protocols reported by us recently.

We used the directional second partial derivative (2nd-derivative) computed on the total electron density (ED) along the λ_2 -eigenvector crossing a critical, or minimum density, point (CP or MDP) on a Bader's molecular graph. The negative value of the 2nd-derivative was found for all interactions studied and it indicates a net concentration of electron density at and in the vicinity of CPs and MDP studied. In each case investigated, there are sets of MOs that (i) contribute either in concentrating or depleting fashion to the total ED or (ii) make no contribution at exactly the CP's coordinates. All MOs that concentrate ED in an inter-nuclear region also overlap both atomic basins and interfere constructively (in-phase) with other ED-concentrating MOs. Hence, they contribute in a positive fashion to the number of delocalized electron-pairs. Therefore, all MOs that contribute to the presence of a DB (through a concentration of ED) also contribute to the degree of covalency that is conveniently measured by a delocalisation index, DI(A,B).

Notably, the 2nd-derivative < 0 is a necessary (although not sufficient) condition for a DB to be present. For a DB to be present the rate of change of concentrating ED must be greater and opposite in sign than the rate of change of depleting ED along the λ_2 -eigenvector. Therefore,

the absence of a DB does not indicate the absence of concentrating MOs as it has been demonstrated for the H7,H18 atom-pair in the equilibrium (twisted) Bph.

All the above observations and conclusions are equally applicable to all and so diverse atom-pairs studied in this work. This leads us to the final conclusion regarding the MO's nature of DBs: *a DB indicates the presence of MOs that concentrate ED in an interatomic region and increase the degree of covalency of the relevant interaction, but the absence of a DB does not indicate the absence of such MOs.*

What is then the significance of a DB? Is there a universal attribute that could be used to describe the role played by a DB in a molecular system? It is well-known fact that the formation of covalent bonds (synonymous with ED sharing) decreases the energy of a molecular system, generally through orbital-expansion and regardless of a kinetic or potential energy driving force.⁵⁵ We have shown that this key property applies to MOs that contribute constructively to the formation of a DB. From the fact that processes leading to the appearance of any DB are the same, regardless of which atom-pair becomes linked by a DB, it follows that the energy-lowering effect must be applicable to all of them. In other words, formation of a specific set of DBs (in most cases they represent classical covalent bonds) exemplifies the manner in which a molecular system is distributing its density such that at a particular 3D placement of nuclei the electronic energy of the system is at its minimum.

One can also consider another scenario. The optimum geometry of a molecule is obtained from energy-optimisation protocols implemented in all major dedicated software packages. The resultant density distribution, incorporating density bridges as observed on Bader's molecular graphs, can be fully recovered from combined individual MO's contributions. Hence, the final set of MOs in an equilibrium structure represents lowest energy density distribution.

A DB has also been interpreted³³ as a '*privileged exchange channel*', which – according to some⁵⁶ – shows that a DB is present between two atoms as a result of the greatest exchange-

correlation stabilization out of multiple, competing ‘*exchange channels*’. Whilst this concept has been challenged recently,⁵⁷ some of us have previously shown⁵⁸ that the significant multi-centric character of many DBs makes the concept of ‘*privilege*’ quite hard to interpret and even more so to quantify. Upon the request of a reviewer, we can restate the concept of exchange channels in terms of MOs: an exchange channel can be seen as a product of the set of MOs that both concentrate ED and contribute to interatomic electron delocalization in a specific inter-nuclear region. We have shown that such a set of MOs will always be present if a DB is present. It is then tempting to also link the concept of ‘*privilege*’ with the relative slopes as per the $CP(\mathbf{r})$ function (see Eq. 3), but to do so will require careful consideration of a significant number of different and often highly controversial systems. We will be exploring these links in a future publication.

From all these final remarks it follows that a common attribute of a DB is its energy-minimising contribution to a molecular system. Also, by analogy to chemists’ understanding of covalent bonds, it is also clear that the presence of a DB is synonymous with a physical process of chemical bonding between two atoms that always stabilises a molecule. Bonding is a physical process that might, but does not have to, lead to the formation of a chemical bond as commonly understood by a chemist at large. Finally, bonding as a universal physical process can take place without being pin-pointed by the appearance of a DB. The H7,H18 atom-pair in a twisted conformer of Bph is an excellent example of such phenomenon. This work revealed that the only discernible difference between the H...H interactions in planar or twisted biphenyl arises purely from different rates of change of net concentrating relative to depleting MOs’ contributions to the total ED. The presence of a density bridge in the case of the planar conformer of Bph, does not change the fact that MOs delocalizing e^- -pairs and concentrating ED do dominate in both conformers.

It is our conviction that this work levels the ground for harmonious, cooperative and complementary research conducted by orbital- and electron density-based camps when, at least,

describing and characterising any possible interaction and chemical bond in all molecular structures is of interest.

Notes

The authors declare no competing financial interest.

3.6. ASSOCIATED CONTENT

3.6.1. Supporting Information

The Supporting Information is available free of charge at

Cartesian coordinates for all optimized molecules, **Part 1**. Theoretical background for the MO-ED and MO-DI methods, **Part 2**. Isosurfaces for all canonical MOs in planar and twisted Bph, **Part 3**. Complete characterization and decomposition of the ED at CP(C1,C12) and CP(C19,H22), tabulated and visualized; truncated as well as summarized tables of MO overlap and interferences for C1,C12 and C19,H22 atom-pairs, **Part 4**. Complete characterization and decomposition of the ED at CP(H7,H18) and MDP(H7,H18) in planar and twisted Bph, respectively, tabulated and visualized; truncated as well as summarized tables of MO overlap and interferences for H7,H18 atom-pair in planar and twisted Bph, **Part 5**. Complete characterization and decomposition of the ED at CP(H2,H4), CP(H2,H5) and CP(H4,H5) in Li₄H₄, tabulated and visualized; full table of MO overlap and interference for atom-pair H2,H5 in Li₄H₄, **Part 6**.

3.7. ACKNOWLEDGMENTS

The authors gratefully acknowledge the Centre for High Performance Computing (CHPC), South Africa, for providing computational resources to this research project and National Research Foundation of South Africa, Grant Number 105855, for financial support.

3.8. REFERENCES

- (1) *The Chemical Bond: Fundamental Aspects of Chemical Bonding*; Frenking, G., Shaik, S., Eds.; Wiley-VCH Verlag GmbH, & Co, KGaA, Weinheim, Germany, 2014.
- (2) *The Chemical Bond: Chemical Bonding Across the Periodic Table*; Frenking, G., Shaik, S., Eds.; Wiley-VCH Verlag GmbH & Co, KGaA, Weinheim, Germany, 2014.
- (3) Bickelhaupt, F. M.; Baerends, E. J. In *Reviews in Computational Chemistry*; Lipkowitz, K. B., Boyd, D. B. Eds.; VCH: New York, 2000; Vol. 15, Chapter 1.
- (4) Ziegler, T.; Rauk, A. Carbon monoxide, carbon monosulfide, molecular nitrogen, phosphorus trifluoride, and methyl isocyanide as sigma donors and pi acceptors. A theoretical study by the Hartree-Fock-Slater transition-state method. *Inorg. Chem.* **1979**, *18*, 1755–1759.
- (5) Wu, W.; Song, L.; Cao, Z.; Zhang, Q.; Shaik, S. Valence bond configuration interaction: a practical ab initio valence bond method that incorporates dynamic correlation, *J. Phys. Chem. A*, **2002**, *106*, 2721–2726.
- (6) Song, L.; Wu, W.; Zhang, Q.; Shaik, S. A practical valence bond method: a configuration interaction method approach with perturbation theoretic facility. *J. Comput. Chem.* **2004**, *25*, 472–478.
- (7) Weinhold, F.; Landis, C. R. *Valency and bonding. A natural bond orbital donor–acceptor perspective*; Cambridge University Press: Cambridge, U.K., 2005.
- (8) Weinhold, F. Rebuttal to the Bickelhaupt–Baerends case for steric repulsion causing the staggered conformation of ethane. *Angew. Chem. Int. Ed.* **2003**, *42*, 4188–4194.
- (9) Weinhold, F.; von Ragué Schleyer, P.; McKee, W. C. Bay-type H···H “bonding” in *cis*-2-butene and related species: QTAIM versus NBO description. *J. Comput. Chem.* **2014**, *35*, 1499–1508.
- (10) Mitoraj, M. P.; Michalak, A.; Ziegler, T. On the nature of the agostic bond between metal centers and β -hydrogen atoms in alkyl complexes. An analysis based on the extended transition state method and the natural orbitals for chemical valence scheme (ETS-NOCV). *Organometallics* **2009**, *28*, 3727–3733.
- (11) Mitoraj, M. P.; Michalak, A. σ -donor and π -acceptor properties of phosphorus ligands: An insight from the natural orbitals for chemical valence. *Inorg. Chem.* **2010**, *49*, 578–582.
- (12) Mitoraj, M. P.; Parafiniuk, M.; Srebro, M.; Handzlik, M.; Buczek, A. Michalak, A. Applications of the ETS-NOCV method in descriptions of chemical reactions. *J. Mol. Model.* **2011**, *17*, 2337–2352.

-
- (13) Cukrowski, I.; Sagan, F.; Mitoraj, M. P. On the stability of *cis*- and *trans*-2-butene isomers. An insight based on the FAMSEC, IQA, and ETS-NOCV schemes. *J. Comput. Chem.* **2016**, *37*, 2783–2798.
- (14) Bader, R. F. W. *Atoms in Molecules. A Quantum Theory*: Oxford University Press: Oxford, Great Britain, 1990.
- (15) Gillespie, R. J.; Popelier, P. L. A. *Chemical bonding and molecular Geometry. From Lewis to electron density*; Oxford University Press, Oxford, U.K., 2001.
- (16) Bader, R. F. W.; Fang, D.-C. Properties of atoms in molecules: caged atoms and the Ehrenfest force. *J. Chem. Theory Comput.* **2005**, *1*, 403–414.
- (17) Blanco, M. A.; Pendás, A. M.; Francisco, E. Interacting quantum atoms: a correlated energy decomposition scheme based on the quantum theory of atoms in molecules. *J. Chem. Theory Comput.* **2005**, *1*, 1096–1109.
- (18) Tiana, D.; Francisco, E.; Blanco, M. A.; Macchi, P.; Sironia, A.; Pendás, A. M. Restoring orbital thinking from real space descriptions: bonding in classical and non-classical transition metal carbonyls. *Phys. Chem. Chem. Phys.* **2011**, *13*, 5068–5077.
- (19) Pendás, A. M.; Blanco, M. A.; Francisco, E. Steric repulsions, rotation barriers, and stereoelectronic effects: a real space perspective. *J. Comput. Chem.* **2009**, *30*, 98–109.
- (20) Geldof, D.; Krishtal, A.; Blockhuys, F.; Van Alsenoy, C. An extension of the Hirshfeld method to open shell systems using fractional occupations. *J. Chem. Theory Comput.* **2011**, *7*, 1328–1335.
- (21) Geldof, D.; Krishtal, A.; Blockhuys, F.; Van Alsenoy, C. Quantum chemical study of self-doping PPV oligomers: spin distribution of the radical forms. *Theor. Chem. Acc.* **2012**, *131*, 1243.
- (22) Cukrowski, I. IQA-embedded fragment attributed molecular system energy change in exploring intramolecular interactions. *Comput. Theor. Chem.* **2015**, *1066*, 62–75.
- (23) Cukrowski, I.; van Niekerk, D. M. E.; de Lange, J. H. Exploring fundamental differences between red- and blue-shifted intramolecular hydrogen bonds using FAMSEC, FALDI, IQA and QTAIM. *Struct. Chem.* **2017**, *28*, 1429–1444.
- (24) Cukrowski, I. Reliability of HF/IQA, B3LYP/IQA, and MP2/IQA data in interpreting the nature and strength of interactions. *Phys. Chem. Chem. Phys.* **2019**, *21*, 10244–10260.
- (25) Matta, C. F.; Hernández-Trujillo, J.; Tang, T-H.; Bader, R. F. W. Hydrogen–hydrogen bonding: a stabilizing interaction in molecules and crystals. *Chem. Eur. J.* **2003**, *9*, 1940–1951.
- (26) Echeverría, J.; Aullón, G.; Danovich, D.; Shaik, S.; Alvarez, S. Dihydrogen contacts in alkanes are subtle but not faint. *Nature Chem.* **2011**, *3*, 323–330.

-
- (27) Cioslowski, J.; Mixon, S. T. Universality among topological properties of electron density associated with the hydrogen–hydrogen nonbonding interactions. *Can. J. Chem.*, **1992**, *70*, 443–449.
- (28) Poater, J.; Solà, M.; Bickelhaupt, F. M. Hydrogen–hydrogen bonding in planar biphenyl, predicted by atoms-in-molecules theory, does not exist. *Chem. Eur. J.* **2006**, *12*, 2889–2895.
- (29) Bader, R. F. W. Pauli repulsions exist only in the eye of the beholder. *Chem. Eur. J.* **2006**, *12*, 2896–2901.
- (30) Poater, J.; Solà, M.; Bickelhaupt, F. M. A model of the chemical bond must be rooted in quantum mechanics, provide insight, and possess predictive power. *Chem. Eur. J.* **2006**, *12*, 2902–2905.
- (31) Pacios, L. F.; Gómez, L. Conformational changes of the electrostatic potential of biphenyl: A theoretical study. *Chem. Phys. Lett.* **2006**, *432*, 414–420.
- (32) Hernández-Trujillo, J.; Matta, C. F. Hydrogen–hydrogen bonding in biphenyl revisited. *Struct. Chem.* **2007**, *18*, 849–857.
- (33) Pendás, A. M.; Francisco, E.; Blanco, M. A.; Gatti, C. Bond paths as privileged exchange channels. *Chem. Eur. J.* **2007**, *13*, 9362–9371.
- (34) Eskandari, K.; Van Alsenoy, C. Hydrogen–hydrogen interaction in planar biphenyl: A theoretical study based on the interacting quantum atoms and Hirschfeld atomic energy partitioning methods. *J. Comp. Chem.* **2014**, *35*, 1883–1889.
- (35) Jenkins, S.; Maza, J. R.; Xu, T.; Jiajun, D.; Kirk, S. R. Biphenyl: A stress tensor and vector-based perspective explored within the quantum theory of atoms in molecules. *Int. J. Quant. Chem.* **2015**, *115*, 1678–1690.
- (36) Jiajun, D.; Xu, Y.; Xu, T.; Momen, R.; Kirk, S. R.; Jenkins, S. The substituent effects on the biphenyl H···H bonding interactions subjected to torsion. *Chem. Phys. Lett.* **2016**, *651*, 251–256.
- (37) Li, J.; Huang, W.; Xu, T.; Kirk, S. R.; Jenkins, S. A vector-based representation of the chemical bond for the substituted torsion of biphenyl. *Chem. Phys. Lett.* **2018**, *702*, 32–37.
- (38) Jara-Cortés, J.; Hernández-Trujillo, J. Energetic analysis of conjugated hydrocarbons using the interacting quantum atoms method. *J. Comp. Chem.* **2018**, *39*, 1103–1111.
- (39) Popelier, P. L. A. Maxwell, P. I.; Thacker, J. C. R.; Alkorta, I. A relative energy gradient (REG) study of the planar and perpendicular torsional energy barriers in biphenyl. *Theoret. Chem. Acc.* **2019**, *138*, 12.

- (40) Hancock, R. D.; Nikolayenko, I. V. Do nonbonded H⁻-H interactions in phenanthrene stabilize it relative to anthracene? A possible resolution to this question and its implications for ligands such as 2,2'-bipyridyl. *J. Phys. Chem. A* **2012**, *116*, 8572–8583.
- (41) Bastiansen, O.; Samdal, S. Structure and barrier of internal rotation of biphenyl derivatives in the gaseous state: Part 4. Barrier of internal rotation in biphenyl, perdeuterated biphenyl and seven non-ortho-substituted halogen derivatives. *J. Mol. Struct.* **1985**, *128*, 115–125.
- (42) Haaland, A.; Shorokhov, J. D.; Tverdova, N. V. Topological analysis of electron densities: Is the presence of an atomic interaction line in an equilibrium geometry a sufficient condition for the existence of a chemical bond? *Chem.–Eur. J.* **2004**, *10*, 4416–4421.
- (43) Strenalyuk, T.; Haaland, A. Chemical bonding in the inclusion complex of He in adamantane (He@adam): The origin of the barrier to dissociation. *Chem.–Eur. J.* **2008**, *14*, 10223–10226.
- (44) von Hopffgarten, M.; Frenking, G. Chemical bonding in the inclusion complex of He in adamantane, He@adam: Antithesis and complement. *Chem.–Eur. J.* **2008**, *14*, 10227–10233.
- (45) Krapp, A.; Frenking, G. Is this a chemical bond? A theoretical study of Ng₂@C₆₀ (Ng=He, Ne, Ar, Kr, Xe). *Chem.–Eur. J.* **2007**, *13*, 8256–8270.
- (46) Weinhold, F. Natural bond critical point analysis: quantitative relationships between natural bond orbital-based and QTAIM-based topological descriptors of chemical bonding. *J. Comput. Chem.* **2012**, *33*, 2440–2449.
- (47) Cukrowski, I.; de Lange, J. H.; Adeyinka, A. S.; Mangondo, P. Evaluating common QTAIM and NCI interpretations of the electron density concentration through IQA interaction energies and 1D cross-sections of the electron and deformation density distributions. *Comput. Theor. Chem.* **2015**, *1053*, 60–76.
- (48) Matta, C. F.; Sadjadi, S-A.; Braden, D. A.; Frenking, G. The barrier to the methyl rotation in *cis*-2-butene and its isomerization energy to *trans*-2-butene, revisited. *J. Comput. Chem.* **2016**, *37*, 143–154.
- (49) Grimme, S.; Mück-Lichtenfeld, C.; Erker, G.; Kehr, G.; Wang, H.; Beckers, H.; Willner, H. When do interacting atoms form a chemical bond? Spectroscopic measurements and theoretical analyses of dideuteriophenanthrene. *Angew. Chem. Int. Ed.* **2009**, *48*, 2592–2595.

(50) de Lange, J. H.; van Niekerk, D. M. E.; Cukrowski, I. Quantifying individual (anti)bonding molecular orbitals' contributions to chemical bonding. *Phys. Chem. Chem. Phys.* **2019**, *21*, 20988–20998.

(51) de Lange, J. H.; van Niekerk, D. M. E.; Cukrowski, I. FALDI-based criterion for and the origin of an electron density bridge with an associated (3,-1) critical point on Bader's molecular graph, *J. Comp. Chem.* 2018, **39**, 2283–2299.

(52) Frisch, M. J.; Trucks, G. W.; Schlegel, H. B.; Scuseria, G. E.; Robb, M. A.; Cheeseman, J. R.; Scalmani, G.; Barone, V.; Mennucci, B.; Petersson, G. A. et al. *Gaussian 09*, Revision D.01; Gaussian, Inc.: Wallingford, CT, 2013.

(53) Grimme, S. Density functional theory with London dispersion corrections. *Wiley Interdiscip. Rev. Comput. Mol. Sci.* **2011**, *1*, 211–228.

(54) AIMAll (Version 19.02.13), Keith, T. A. TK Gristmill Software, Overland Park KS, USA, 2019 (aim.tkgristmill.com).

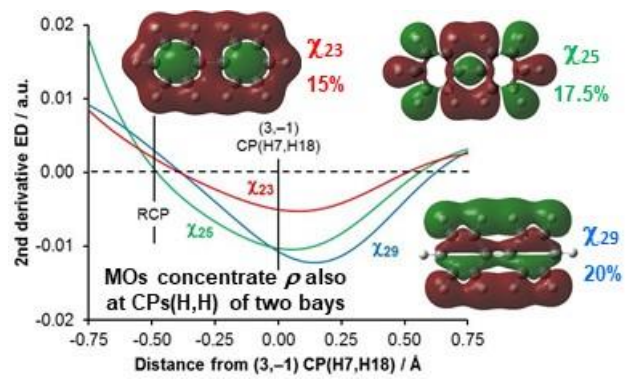
(55) Ruedenberg, K.; Schmidt, M. W. Physical understanding through variational reasoning: Electron sharing and covalent bonding. *J. Phys. Chem. A* **2009**, *113*, 1954–1968.

(56) Tognetti, V.; Joubert, L. On the physical role of exchange in the formation of an intramolecular bond path between two electronegative atoms. *J. Chem. Phys.* **2013**, *138*, 024102–024110.

(57) Jabłonski, M. On the uselessness of Bond Paths linking distant atoms and on the violation of the concept of privileged exchange channels, *ChemistryOpen* **2019**, *8*, 497–507.

(58) de Lange, J. H.; van Niekerk, D. M. E.; Cukrowski, I. FALDI-based decomposition of an atomic interaction line leads to 3D representation of the multicentre nature of interactions, *J. Comp. Chem.* **2018**, *39*, 973–985.

TOC Graphic



Chapter 4

The CH \cdots HC interaction in biphenyl is a delocalized, molecular wide and entirely non-classical interaction: results from FALDI analysis

Published in:

Journal of Computational Chemistry **2021**. DOI: 10.1002/jcc.26491.

The Supplementary Information is provided in Appendix II

The CH...HC interaction in biphenyl is a delocalized, molecular-wide and entirely non-classical interaction: results from FALDI analysis

Thomas G. Bates, Jurgens H. de Lange* and Ignacy Cukrowski*

Department of Chemistry, Faculty of Natural and Agricultural Sciences, University of Pretoria, Lynnwood Road, Hatfield, Pretoria 0002, South Africa

*Correspondence to: Ignacy Cukrowski
Jurgens de Lange:

E-mail: ignacy.cukrowski@up.ac.za
E-mail: jurgens.delange@up.ac.za

1. Abstract

In this study we aim to determine the origin of the electron density describing a CH...HC interaction in planar and twisted conformers of biphenyl. In order to achieve this, the fragment, atomic, localized, delocalized, intra- and inter-atomic (FALDI) decomposition scheme was utilized to decompose the density in the inter-nuclear region between the *ortho*-hydrogens in both conformers. Importantly, the structural integrity, hence also topological properties, were fully preserved as no ‘artificial’ partitioning of molecules was implemented. FALDI-based qualitative and quantitative analysis revealed that the majority of electron density arises from two, non-classical and non-local effects: strong overlap of *ortho* C–H σ -bonds, and long-range electron delocalization between the phenyl rings and *ortho* carbons and hydrogens. These effects resulted in a delocalized electron channel, i.e., a density bridge or a bond path in a QTAIM terminology, linking the H-atoms in the planar conformer. The same effects and phenomena are present in both conformers of biphenyl. We show that the CH...HC interaction is a molecular-wide event due to large and long-range electron delocalization, and caution against approaches that investigate CH...HC interactions without fully taking into account the remainder of the molecule.

2. Introduction

The wave-particle duality is one of the greatest sources of complexity in modern chemical structure theory. It imposes a holistic, non-local approach to the understanding of molecular structure in sharp contrast to the reductionist, atomistic dogma used by chemists. That said, wave-particle duality is somewhat accounted for in conceptual chemistry through the combination of a number of heuristics, including Lewis^[1] and resonance structures,^[2] ligand-field theory^[3] and construction of molecular orbitals (MOs) through symmetry-adapted atomic orbitals.^[4] On the other hand, modern computational approaches allow for the calculation of highly accurate *ab initio* electronic structures (incorporating the full effect of the wave-like nature of electrons), from simple Hartree-Fock MOs to multi-configurational, valence-bond resonance states.^[5]

The increased accuracy offered by quantum chemical computations comes at a cost however – that of more complex and difficult interpretation, especially in terms of general chemical concepts. A particularly controversial example is that of close H,H contacts in the planar conformer of biphenyl (Bph), which has been the subject of a raging debate for the last few decades.^[6–22] The H,H contacts serve as a good case study of the difficulty in reconciling atomistic chemistry with holistic quantum approaches. In a recent study^[23] on a purely MO-based description of the H,H contact in Bph, we have shown that i) MO isosurfaces provide very little information on the contact *or* any other bond in the molecule, ii) each MO contributes in a vastly different nature to every diatomic interaction, and iii) only through the combination of all MOs in a molecule can an interaction be characterized in any meaningful manner. Figure 1 shows how multiple MOs contribute to the electron density in the H,H inter-nuclear region and illustrates that two MOs, despite overlapping atoms in the same region, can contribute in opposite fashions. Importantly, we were able to show that, regardless of the presumed presence/absence of a chemical bond(ing), a physical process of bonding (arising from MO-overlaps and interferences) can describe the H,H contact in both conformers of Bph. Unfortunately, in using canonical MOs, we were not able to extract any meaningful chemical information in terms of which atoms, fragments or molecular

regions contribute to any of the interactions in the molecule. Therefore, an approach that can qualify and quantify the contributions made by different atoms and molecular fragments to a particular interaction of interest is highly desirable.

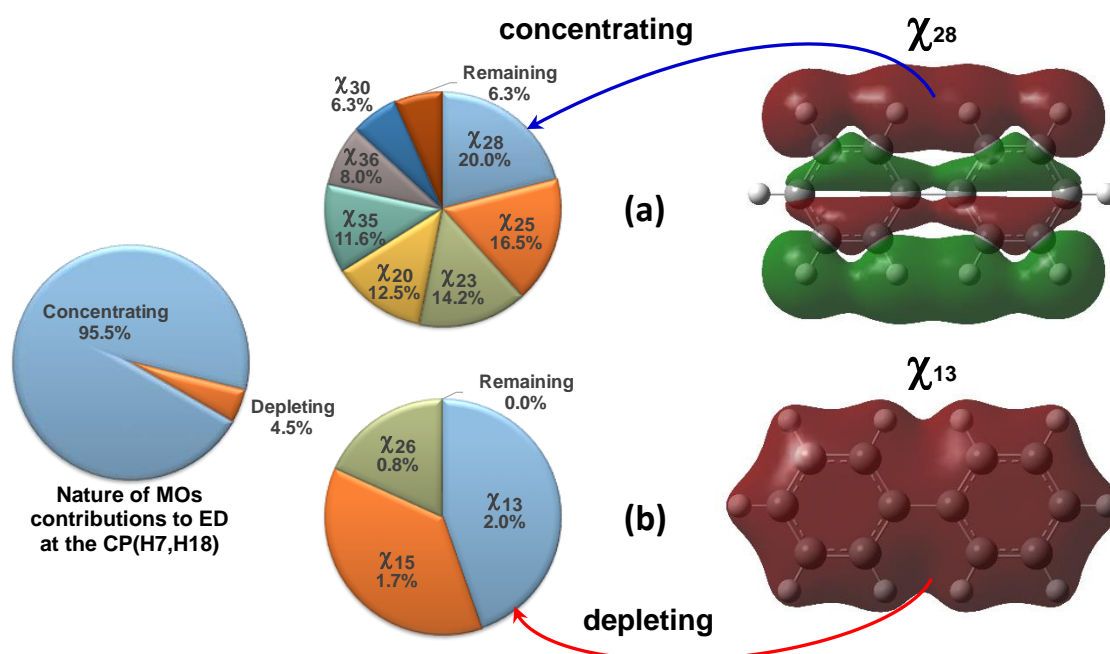


Figure 1. Decomposition of the electron density at the CP(H7,H18) in planar biphenyl into (a) concentrating density and (b) depleting density, as well as the decomposition of these densities into individual MOs contributions. Examples of MOs that make most significant contribution (either concentrate or deplete density at the CP(H7,H18) in planar biphenyl, χ_{28} and χ_{13} , respectively) are also shown.

A large number of post-wavefunction methods exist that can extract chemical information from the otherwise physical wavefunction. A concise list of these include the Natural Bond Orbitals (NBO) approach,^[24] the Extended Transition State coupled with Natural Orbitals for Chemical Valence (ETS-NOCV) decomposition scheme^[25] and the entire class of Quantum Chemical Topology methods^[26] (QCT, including the popular Quantum Theory of Atoms in Molecules,^[27] QTAIM). All of these approaches localize or decompose information within the wavefunction to provide some form of chemical interpretation. Unfortunately, the interpretations offered by these approaches are often widely different from each other as well as classical interpretations. In the case of the H,H contacts in biphenyl, as well as in a number of other systems,^[28–37] QTAIM and NBO in particular have offered polar opposite views^[6,10,11] despite using the same baseline

wavefunctions. Clearly, the quest for meaningful, chemical information from quantum mechanical data is far from solved.

In this work we take a slightly different approach to the problem of H,H contacts in Bph. We start with an axiom – that the H...H interaction exists in planar Bph, regardless of its nature (attractive or repulsive) or its energetic consequences (stabilizing or otherwise a molecule). We can further state, based on our MO-based evidence,^[23] that the H...H interaction also exists in the twisted (lowest-energy) conformer of Bph and that the interaction is built from the same constituents as present in the planar conformer. Then, instead of trying to evaluate whether the H...H interaction is a bond or a steric repulsion, or attempting to find the origin of the rotation barrier in Bph, we will only investigate the chemical characteristics of the interaction. Specifically, we aim to provide a qualitative and quantitative description of the electron density (ED) distribution in the H,H inter-nuclear region *in terms of* the influence of all atoms and/or molecular fragments. In doing so, we aim to sufficiently characterize the H...H interaction in chemical terms by embracing the molecular-wide nature of the quantum chemical electronic structure.

In order to meet our aims, we need to i) provide a complete mapping of the ED distribution in the H,H inter-nuclear region in terms of atoms and/or molecular fragments, and ii) characterise, quantify and organise each major contribution found in the region. To do so, we will utilise the Fragment, Atomic, Localized, Delocalized and Interatomic (FALDI)^[38–42] electron density decomposition scheme. FALDI is ideally suited for this task as it provides molecular-wide ED distributions in atomistic, chemically-intuitive terms. Moreover, qualitative and quantitative information from any atom, atom-pair or fragment can be gained at any coordinate in space and obtained information can be further grouped and organised to provide additional insight. We selected Bph as a case study as the approach proposed here is equally applicable to any intra- or intermolecular interaction and provides a qualitative and quantitative insight on how a molecular

system is spontaneously minimising its energy by redistributing ED and nuclei in the 3D space on, *e.g.*, a structural change from a twisted to a planar (non-equilibrium) structure.

3. Theoretical Background

Overview of the FALDI density decomposition scheme

Building upon concepts of the Domain Averaged Fermi Hole (DAFH) approach,^[43–45] FALDI calculates pseudo-2nd order contributions arising from (de)localized electrons within QTAIM-defined atomic basins. FALDI also commonly utilizes the Müller approximation^[46] as a reasonable alternative to the computationally-expensive full electron pair density matrix. A short description of FALDI's atom, atom-localized and interatomic-delocalized distributions for a restricted Hartree-Fock or Kohn-Sham wavefunction are given below, followed by an in-depth, for the first time, description of fragment-based density distributions.

The elements of an atomic overlap matrix (AOM),

$$S_{ij}^A = \int_{\Omega_A} \chi_i^*(\mathbf{r})\chi_j(\mathbf{r})d\mathbf{r} \quad (1)$$

where χ_i and χ_j are canonical MOs and the integral is over the volume of a QTAIM atomic basin, Ω_A , can be used to effectively calculate all FALDI density distributions. The density contribution at any coordinate \mathbf{r} in 3D space arising from the electrons found, on average, within Ω_A is known as an *atom*-ED distribution:

$$\mathbf{g}_A(\mathbf{r}) = 2 \sum_{ij} \chi_i^*(\mathbf{r})\chi_j(\mathbf{r})S_{ji}^A \quad (2)$$

The symbol $\mathbf{g}_A(\mathbf{r})$ arose from DAFH analysis, where it is usually further transformed through an isopycnic transformation and diagonalized. Integrating $\mathbf{g}_A(\mathbf{r})$ over the whole of molecular space provides the total number of electrons found, on average, within Ω_A , $\int \mathbf{g}_A(\mathbf{r})d\mathbf{r} = N(A)$. Note that $\mathbf{g}_A(\mathbf{r})$ is generally non-zero outside Ω_A , and *atom*-ED distributions therefore provide a molecular-wide distribution of the atomic electron population, $N(A)$.

FALDI can also provide real-space distributions of QTAIM-defined localization and delocalization indices (LI and DI, respectively). The density contribution to \mathbf{r} arising from electrons localized to Ω_A is known as a *loc*-ED distribution:

$$\mathcal{L}_A(\mathbf{r}) = 2 \sum_{ij}^{N_{\text{MO}}} \chi_i^*(\mathbf{r}) \chi_j(\mathbf{r}) (\mathbf{S}^A \mathbf{S}^A)_{ji} \quad (3)$$

where $\mathbf{S}^A \mathbf{S}^A$ is the matrix product of \mathbf{S}^A with itself so that $\text{LI}(A) = 2\text{Tr}(\mathbf{S}^A \mathbf{S}^A) = \int \mathcal{L}_A(\mathbf{r}) d\mathbf{r}$. $\mathcal{L}_A(\mathbf{r})$ is therefore a real-space distribution of $\text{LI}(A)$. Similarly, the density contribution at \mathbf{r} arising from electrons delocalized within two QTAIM basins, Ω_A and Ω_B , is known as a *deloc*-ED distribution:

$$\mathcal{D}_{A,B}(\mathbf{r}) = 2 \sum_{ij}^{N_{\text{MO}}} \chi_i^*(\mathbf{r}) \chi_j(\mathbf{r}) (\mathbf{S}^A \mathbf{S}^B + \mathbf{S}^B \mathbf{S}^A)_{ji} \quad (4)$$

where $\mathbf{S}^A \mathbf{S}^B + \mathbf{S}^B \mathbf{S}^A$ is used to ensure a symmetric matrix. Integration of $\mathcal{D}_{A,B}(\mathbf{r})$ over all molecular space yields the corresponding delocalization index, $\text{DI}(A, B) = 2\text{Tr}(\mathbf{S}^A \mathbf{S}^B + \mathbf{S}^B \mathbf{S}^A) = \int \mathcal{D}_{A,B}(\mathbf{r}) d\mathbf{r}$ – again showing that $\mathcal{D}_{A,B}(\mathbf{r})$ is the real-space distribution of $\text{DI}(A, B)$.

Some of us have noted^[42] before that, while QTAIM-defined LIs and DIs are physically exact, they can be chemically somewhat counterintuitive. Specifically, using Eqs. 3 and 4, we noted that $\mathcal{L}_A(\mathbf{r})$ is generally non-zero outside of Ω_A , suggesting that $\text{LI}(A)$ describes a portion of both core and valence electrons. We introduced^[42] the *localized-delocalized overlap* (LDO) algorithm, which alters each *loc*-ED in such a way as to remove any overlap, in an MO basis, with other *loc*-ED and *deloc*-ED distributions. The resulting distribution,

$$\mathcal{L}''_A(\mathbf{r}) = \sum_i^N n''_i^{\text{AA}} [\phi_i^{\text{AA}}(\mathbf{r})]^2 \quad (5)$$

where ϕ_i^{AA} is a natural density function composed of eigenvectors of $\mathbf{S}^A \mathbf{S}^A$ with modified occupation n''_i^{AA} , provides a distribution of electrons that can be exclusively found only in Ω_A . Integrating $\mathcal{L}''_A(\mathbf{r})$ over all molecular space provides a localization index, $\text{LI}_{\text{LDO}}(A)$ that describes

only core and non-bonded electrons, and is necessarily smaller than the corresponding QTAIM-defined localization index, LI_{QTAIM} . Correspondingly, each *deloc*-ED can be modified to produce a distribution $\mathcal{D}''_{A,B}(\mathbf{r})$ that counts all sources of delocalized electrons between Ω_A and Ω_B . More details can be found in ref. 40; however, for the remainder of this work, we will utilize the LDO algorithm. $LI(A)$, $DI(A,B)$ and corresponding *loc*- and *deloc*-ED distributions will henceforth refer to the exclusive (de)localized distributions modified by the LDO algorithm.

Putting all of the above together, FALDI therefore can decompose ED at any given coordinate \mathbf{r} into contributions from all atoms (*atom*-ED distributions),

$$\rho(\mathbf{r}) = \sum_A^M g_A(\mathbf{r}) \quad (6)$$

where M is the total number of atomic basins. Each *atom*-ED distribution, when calculated along a grid of points (such as a 1D cross-section or a 3D isosurface) provides a real-space distribution of the electrons that can be found within each atomic basin. Alternatively, FALDI can also decompose the density at \mathbf{r} in terms of intra-atomic localized (*loc*-ED) and inter-atomic delocalized (*deloc*-ED) distributions:

$$\rho(\mathbf{r}) = \sum_A^M \mathcal{L}_A(\mathbf{r}) + \sum_A^{M-1} \sum_{B=A+1}^M \mathcal{D}_{A,B}(\mathbf{r}) \quad (7)$$

Each *loc*-ED distribution maps the electrons exclusively localized to an atomic basin, and is generally limited to atomic core electrons and non-bonded electrons (such as strongly localized lone-pairs). Each inter-atomic *deloc*-ED distribution maps the electrons delocalized between two atomic basins, and includes covalently shared electrons as well as dispersion- and weakly-correlated electrons. Note that a *deloc*-ED distribution can be calculated for any atom-pair, regardless of their proximity in space or whether they are considered ‘bonded’.

The primary and novel use of FALDI in this work, however, is in terms of chemical fragments. Combining *loc*-ED and *deloc*-ED distributions defined for different atoms/atom-pairs allows for a number of fragment-based distributions defined below.

Fragment-related terms in FALDI analysis

All of the atom and atom-pair FALDI terms can be grouped together in order to provide a fragment-centric FALDI analysis. The resultant distributions and integrated terms can be identically interpreted as their atomic counterparts. A short definition of the fragment terms used in this paper follows.

Given two fragments, $\mathcal{F}1$ and $\mathcal{F}2$, the total density contribution of a fragment to any coordinate \mathbf{r} can be given by summation of FALDI *atom-ED* distributions:

$$g_{\mathcal{F}1}^{total}(\mathbf{r}) = \sum_A^{M_{\mathcal{F}1}} g_A(\mathbf{r}) \quad (8)$$

where $M_{\mathcal{F}1}$ is the number of atoms within $\mathcal{F}1$. Integration of Eq. 8 over all space occupied by a molecular system yields the total fragment electronic population, $N^{total}(\mathcal{F}1)$, and a 3D-isosurface of $g_{\mathcal{F}1}^{total}(\mathbf{r})$ yields a visualization of the total electronic contribution of $\mathcal{F}1$ to the molecule. $g_{\mathcal{F}1}^{total}(\mathbf{r})$ includes electrons localized to each fragment, as well as a contribution of electrons delocalized between $\mathcal{F}1$ and all other fragments/atoms.

Similarly, the atom-localized electronic contributions of each fragment,

$$\mathcal{L}_{\mathcal{F}1}(\mathbf{r}) = \sum_A^{M_{\mathcal{F}1}} \mathcal{L}_A(\mathbf{r}) \quad (9)$$

is the contribution at \mathbf{r} of electrons exclusively localized to each atom of the fragment. On its own, this term is not particularly informative, and includes the core and non-bonded electrons of each atom within the fragment. However, the intra-fragment delocalized electronic contribution,

$$\mathcal{D}_{\mathcal{F}1}^{intra}(\mathbf{r}) = \sum_A^{M_{\mathcal{F}1}-1} \sum_{B=A+1}^{M_{\mathcal{F}1}} \mathcal{D}_{A,B}(\mathbf{r}) \quad (10)$$

provides the contribution at \mathbf{r} of electrons delocalized between atoms of the same fragment, including covalently-shared and weakly-delocalized electrons. Eqs. 9 and 10 can be summed together to give the total intra-fragment electron distribution:

$$g_{\mathcal{F}1}^{intra}(\mathbf{r}) = \mathcal{L}_{\mathcal{F}1}(\mathbf{r}) + \mathcal{D}_{\mathcal{F}1}^{intra}(\mathbf{r}) \quad (11)$$

$g_{\mathcal{F}1}^{intra}(\mathbf{r})$ provides the contribution to \mathbf{r} from electrons localized to $\mathcal{F}1$, and includes both the atom-localized electrons and inter-atomic delocalized electrons among atom-pairs of the fragment. Integration of $g_{\mathcal{F}1}^{intra}(\mathbf{r})$ over all molecular space therefore yields the sum of LIs and DIs of the atoms of the fragment, which we will refer to as the total intra-fragment electron population, $N^{intra}(\mathcal{F}1) = \int g_{\mathcal{F}1}^{intra}(\mathbf{r})d\mathbf{r} = \sum_A \text{LI}(A) + \sum_{A,B} \text{DI}(A,B)$, where $A,B \in \mathcal{F}1$.

Inter-fragment delocalization can be calculated by considering *deloc*-ED distributions involving atom-pairs from two different fragments:

$$\mathcal{D}_{\mathcal{F}1,\mathcal{F}2}^{inter}(\mathbf{r}) = \sum_A^{M_{\mathcal{F}1}} \sum_B^{M_{\mathcal{F}2}} \mathcal{D}_{A,B}(\mathbf{r}) \quad (12)$$

$\mathcal{D}_{\mathcal{F}1,\mathcal{F}2}^{inter}(\mathbf{r})$ is a distribution of the electrons delocalized between two fragments, and integration over all space yields the inter-fragment delocalization index, $\text{DI}(\mathcal{F}1,\mathcal{F}2) = \int \mathcal{D}_{\mathcal{F}1,\mathcal{F}2}^{inter}(\mathbf{r}) d\mathbf{r} = \sum_{A,B} \text{DI}(A,B)$, where $A \in \mathcal{F}1$ and $B \in \mathcal{F}2$.

Finally, Eqs. 11 and 12 sum up to $g_{\mathcal{F}1}^{total}(\mathbf{r})$ (Eq 8),

$$g_{\mathcal{F}1}^{total}(\mathbf{r}) = g_{\mathcal{F}1}^{intra}(\mathbf{r}) + \sum_X^{\mathcal{M}} \frac{1}{2} \mathcal{D}_{\mathcal{F}1,\mathcal{F}X}^{inter}(\mathbf{r}) \quad (13)$$

where \mathcal{M} is the total number of fragments and if the orthodox (QTAIM) approach to atomic-basin overlap is used. In the case of the LDO approximation, as used in this work, $\mathcal{D}_{\mathcal{F}1,\mathcal{F}2}^{inter} \neq \mathcal{D}_{\mathcal{F}2,\mathcal{F}1}^{inter}$, and the terms need to be accounted for separately.

In this manuscript, we are primarily interested in the terms on the right-hand side of Eq. 13. $g_{\mathcal{F}1}^{intra}(\mathbf{r})$ is the fragment-equivalent of a *loc*-ED distribution, and is a useful measure of the contribution of a single fragment to a region of space. $\mathcal{D}_{\mathcal{F}1,\mathcal{F}2}^{inter}(\mathbf{r})$, on the other hand, is the fragment-equivalent of a *deloc*-ED distribution, and will be used to measure how the interaction between two fragments contributes to the ED in a region of space.

Cross-sections of FALDI terms

A number of cross-sections of inter-nuclear space is performed throughout this work, and we follow a similar approach as what we have used a number of times before.^[38–40] It involves the decomposition of the electron density at a specific coordinate \mathbf{r}^* and along a vector defined in terms of \mathbf{r}^* . Previously,^[47] the ED was decomposed at \mathbf{r}^* in terms of MO densities, which we referred to as the MO-ED method:

$$\rho(\mathbf{r}^*) = \sum_i^{N_{MO}} v_i |\chi_i(\mathbf{r}^*)|^2 \quad (14)$$

where χ_i is an MO with occupation v_i . In this work, we decompose the ED at \mathbf{r}^* in terms of the diatomic FALDI terms given in Eq. 7, which by analogy, we refer to as the FALDI-ED method. Alternatively, the density at \mathbf{r}^* can also be decomposed in terms of fragment contributions. The density is then given by the sum of intra- and inter-fragment delocalization contributions:

$$\rho(\mathbf{r}^*) = \sum_i^{\mathcal{M}} g_{\mathcal{F}_i}^{total}(\mathbf{r}^*) = \sum_i^{\mathcal{M}} g_{\mathcal{F}_i}^{intra}(\mathbf{r}^*) + \sum_i^{\mathcal{M}} \sum_X^{\mathcal{M}} \frac{1}{2} \mathcal{D}_{\mathcal{F}_i \mathcal{F}_X}^{inter}(\mathbf{r}^*) \quad (15)$$

The coordinate \mathbf{r}^* is usually a (3,−1) critical point (CP) in the total ED, or, in the absence of a CP, a minimum density point (MDP) defined as the coordinate with the lowest ED on an inter-nuclear vector. The eigenvector associated with the second eigenvalue of the Hessian matrix, originating at \mathbf{r}^* is determined and then followed for a pre-selected increment, after which the Hessian matrix is recalculated and a new eigenvector is found. This process is repeated for a set distance, typically 0.3–0.5 Å in one direction. The resulting path is generally referred to as the λ_2 -eigenvector, and (in most cases) resembles a cross-section of the inter-nuclear region of interest. A FALDI decomposition is done at each coordinate of the λ_2 -eigenvector.

We then consider, for each FALDI decomposition product at \mathbf{r}^* , the partial directional second derivative (henceforth referred to as simply 2nd derivative) computed along the λ_2 -eigenvector. From that, each FALDI product can be labelled as *concentrating* ED (negative 2nd derivative),

depleting ED (positive second derivative) or *removing* ED (when a FALDI product is negative) at the selected \mathbf{r}^* . The contributions of all FALDI products of the same nature can then be grouped to provide a ‘characterized’ total density contribution of specific natures at \mathbf{r}^* :

$$\rho(\mathbf{r}^*) = \rho_{\text{concentrating}}(\mathbf{r}^*) + \rho_{\text{depleting}}(\mathbf{r}^*) + \rho_{\text{removing}}(\mathbf{r}^*) \quad (16)$$

We also make use of recently-developed³⁹ $CP(\mathbf{r})$ function to explain the presence of a bond path. This function accounts for the first derivatives computed on the total *concentrating*, *depleting* and *removing* density terms in Eq. 16:

$$CP(\mathbf{r}) = -\text{sign}(\partial\rho_{\text{depleting}}(\mathbf{r})) \cdot [\partial\rho_{\text{concentrating}}(\mathbf{r}) + \partial\rho_{\text{depleting}}(\mathbf{r}) + \partial\rho_{\text{removing}}(\mathbf{r})] \quad (17)$$

Specifically, the $CP(\mathbf{r})$ is positive in the vicinity of \mathbf{r}^* if the slope of the FALDI products that concentrate ED is greater and opposite in sign than the slope of products that deplete ED. We have previously found³⁹ that the $CP(\mathbf{r})$ will always be positive in the vicinity of a density bridge, DB (commonly known as a bond path).

4. Computational Methods

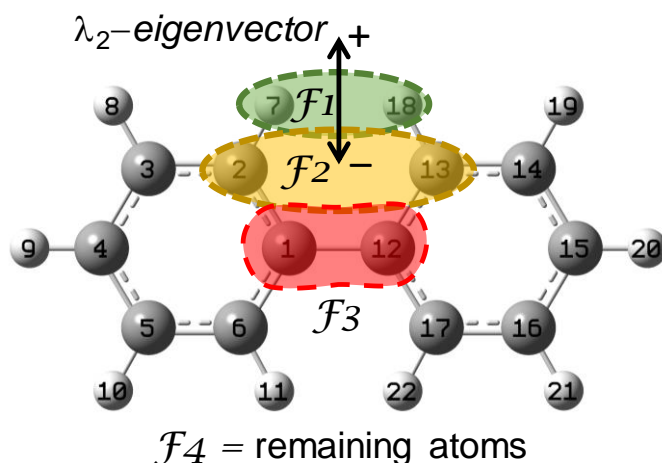
Both the planar and twisted conformers were optimised in Gaussian 09, Rev D.01^[48] using B3LYP with cc-pVDZ in the gas phase; a full set of coordinates for both conformations is provided in Part 1 in the SI. AIMAll v. 19.02.13.^[49] was used to gather QTAIM data, which was used in the calculation of FALDI electron density data using in-house software. Isosurfaces of FALDI products were visualized using VMD.^[50]

5. Results and Discussion

We are primarily interested in the origin of ED contributions in the inter-nuclear region of the CH...HC interaction in planar/twisted BPh. To achieve our goals, we will utilize the FALDI-ED method to investigate the ED along the λ_2 -eigenvector, originating from the CP(H7,H18) in planar Bph or the MDP(H7,H18) in twisted Bph, as shown in Scheme 1. We have used the exact same

approach before,^[23] but using an MO-based ED decomposition (the MO-ED method); below, results from the MO- and FALDI-ED methods will be briefly compared.

The decomposition products of the FALDI- and MO-ED methods are quite different. However, these products can be combined, based on the sign of their 2nd derivatives, into groups that *concentrate* or *deplete* ED at the CP/MDP of interest. The pseudo 2nd-order nature of FALDI decomposition also allows for a third group that *removes* ED. Despite the fundamental differences between MO theory and FALDI, decomposition of the ED yields strikingly similar results (see Figure 2) when the decomposition products are grouped as concentrating, depleting and removing.



Scheme 1. Definition of fragments for FALDI analysis. \mathcal{F}_1 : H7...H18, \mathcal{F}_2 : C2...C13, \mathcal{F}_3 : C1–C12 linker and \mathcal{F}_4 : combined fragment containing remainder of the molecule. The position and direction (+ and –) of the λ_2 -eigenvector used for cross-section analysis (crossing a CP and MDP in the planar and twisted Bph, respectively) is also shown.

This is very reassuring but should not be seen as entirely surprising because i) the same total ED was partitioned, ii) there can be only one physical process leading to a specific ED distribution among atoms of the same molecule and, hence iii) there must be a specific fraction of concentrating, depleting etc., density at any \mathbf{r} , regardless on how the quantified value was obtained. Data in Figure 2 serves as a brief comparison between the two methods; a full set of FALDI-ED cross-sections is compared with relevant MO-ED data in Part 2 of the SI.

Figure 2a shows the grouped 2nd-derivative ED contributions resulting from both MO- and FALDI-ED methods in planar Bph. The products from both MO and FALDI decompositions

contribute to a strong concentration of ED at CP(H7,H18), tempered by a few products that deplete ED. The components that remove ED exactly at the CP (in the case of FALDI-ED) make a negligible contribution to the 2nd-derivative. Therefore, the exact same topology of the total ED is recovered in both MO- and FALDI-ED decompositions, even though the constituent products are quantitatively somewhat different. The same is seen for the total ED itself, shown now for the twisted conformer in Figure 2b: both MO- and FALDI-ED methods reveal a larger contribution of concentrated ED than depleted ED, resulting in a slight concentration (shouldering) at MDP(H7,H18). Of course, the largest difference between the planar and twisted conformers is the lack of a DB connecting the H-atoms in the latter.

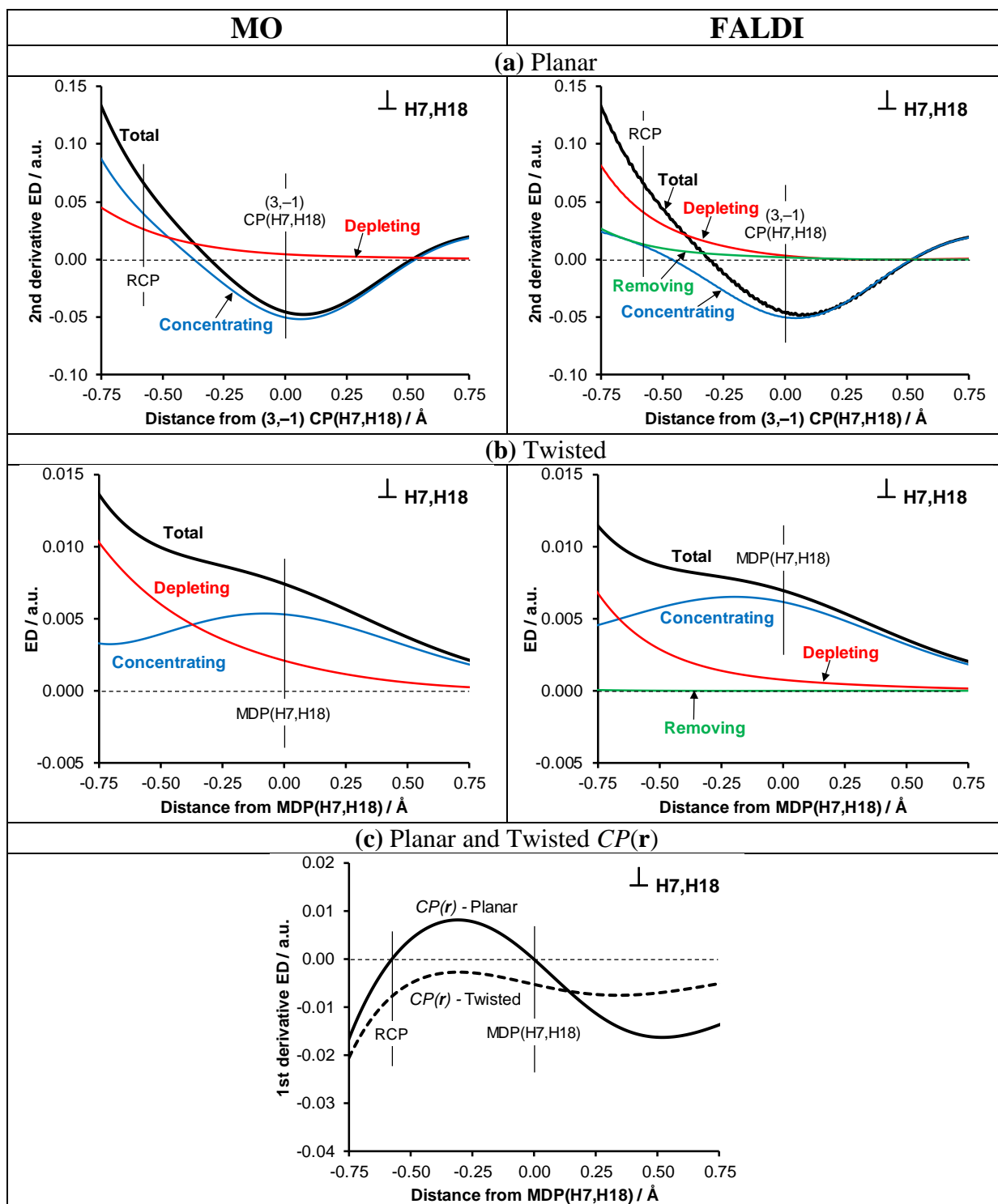


Figure 2. Decomposition of the 2nd derivative $\rho(\text{tot})$ in planar conformation (a), and of the Total-ED in twisted conformation (b) of both MO-ED and FALDI-ED along the 2nd eigenvector and crossing the CP(H7,H18) in the planar and MDP(H7,H18) in twisted, as well as showing the $CP(\mathbf{r})$ function in planar and twisted conformation for the MO-ED and FALDI-ED method (c).

As in our previous work,^[23] the presence/absence of a DB can be fully explained with the help of the $CP(\mathbf{r})$ function – Figure 2c. The $CP(\mathbf{r})$ function is positive in the vicinity of CP(H,H) in planar Bph, which shows that the slope of the concentrating ED products is greater and opposite in sign from the slope of the depleting and removing ED products – hence the presence of a DB.

The opposite is true in the case of the twisted conformer. Notably, the $CP(\mathbf{r})$ function is invariant to the decomposition – it is identical in both MO- and FALDI-ED methods.

Having established that FALDI can ‘reproduce’ trends generated by MOs, the next goal is to find the origin of the density, and as such we turn our attention to unique properties of the FALDI method.

FALDI Fragment analysis of planar and twisted biphenyl

There are 231 unique atom-pairs in Bph and all of them are analysed in order to gain necessary information. FALDI, however, allows for grouping of individual FALDI decomposition components into fragment-based indices and distributions. We will consider a fragment-based analysis first, in order to ease interpretation, before delving into specific atom-pair contributions in the next section.

There is a very large number of ways of defining fragments in a molecule. However, we have chosen a specific fragmentation scheme to maximize the insight gained towards answering our research question, whilst minimizing the number of terms to evaluate. Moreover, we found that alternative schemes yield similar interpretations – see Part 3 of the SI for details. The set of molecular fragments \mathcal{F}_n used in this work is shown in Scheme 1. To justify partitioning seen in Scheme 1 we note that fragments \mathcal{F}_1 , \mathcal{F}_2 and \mathcal{F}_3 were used previously to argue the nature of the H...H interaction^[13,20] based on QTAIM/IQA energetic terms. Fragment \mathcal{F}_4 represents the remaining 16 atoms of Bph not included in fragments \mathcal{F}_1 , \mathcal{F}_2 and \mathcal{F}_3 . Finally, it is important to

stress that the fragmentation scheme employed here does not result in cutting Bph into non-physical parts – FALDI-based partitioning fully preserves the molecule’s chemical integrity.

Due to the use of our LDO algorithm, *loc*-ED terms (which describe densities that are fully localized to a single atomic basin) do not contribute to either the CP(H,H) in planar or the MDP(H,H) in twisted Bph. Hence, this allows us to focus our interest only on contributions coming from *deloc*-ED terms (density delocalized between atomic basins). In terms of fragments, we will make use of: (i) intra-fragment delocalization, $\mathcal{D}_{\mathcal{F}_n}^{intra}(\mathbf{r})$, that quantifies the ED contribution at \mathbf{r} due to delocalization between each atom-pair within a selected fragment \mathcal{F}_n , and (ii) inter-fragment delocalization, $\mathcal{D}_{\mathcal{F}_n, \mathcal{F}_m}^{inter}(\mathbf{r})$, that describes the ED contribution at \mathbf{r} due to delocalization between each atom-pair (A,B) made of atoms belonging to different fragments, $A \in \mathcal{F}_n$ and $B \in \mathcal{F}_m$.

Cross-sections along the λ_2 -eigenvector for the H7,H18 region in planar Bph, as well as isosurfaces of the largest fragment contributions to the ED at CP(H7,H18), are shown in Figure 3. The largest contributor to the ED, by a large majority (58.6%), is the inter-fragment delocalization of fragments \mathcal{F}_1 and \mathcal{F}_2 . This describes the electrons delocalized between the *ortho*-carbons and *ortho*-hydrogens (*i.e.* C–H bonds) which results in a strong concentration of electrons at CP(H7,H18). The corresponding isosurface computed for $\mathcal{D}_{\mathcal{F}_1, \mathcal{F}_2}^{inter}(\mathbf{r})$ (see Figure 3d) reveals that the C–H electron delocalization forms a channel of delocalized density between the H-atoms. This observation confirms our previous speculation^[23] based on MOs – that the H \cdots H interaction is predominantly formed from the electron delocalization between two overlapping C–H bonds and fully justifies the use of the ‘CH \cdots HC’ notation to describe the contact. Moreover, two other fragment contributions also largely concentrate density in the H7,H18 region which, interestingly, highlights the significance of the effect that the rest of the molecule has on the bay region:

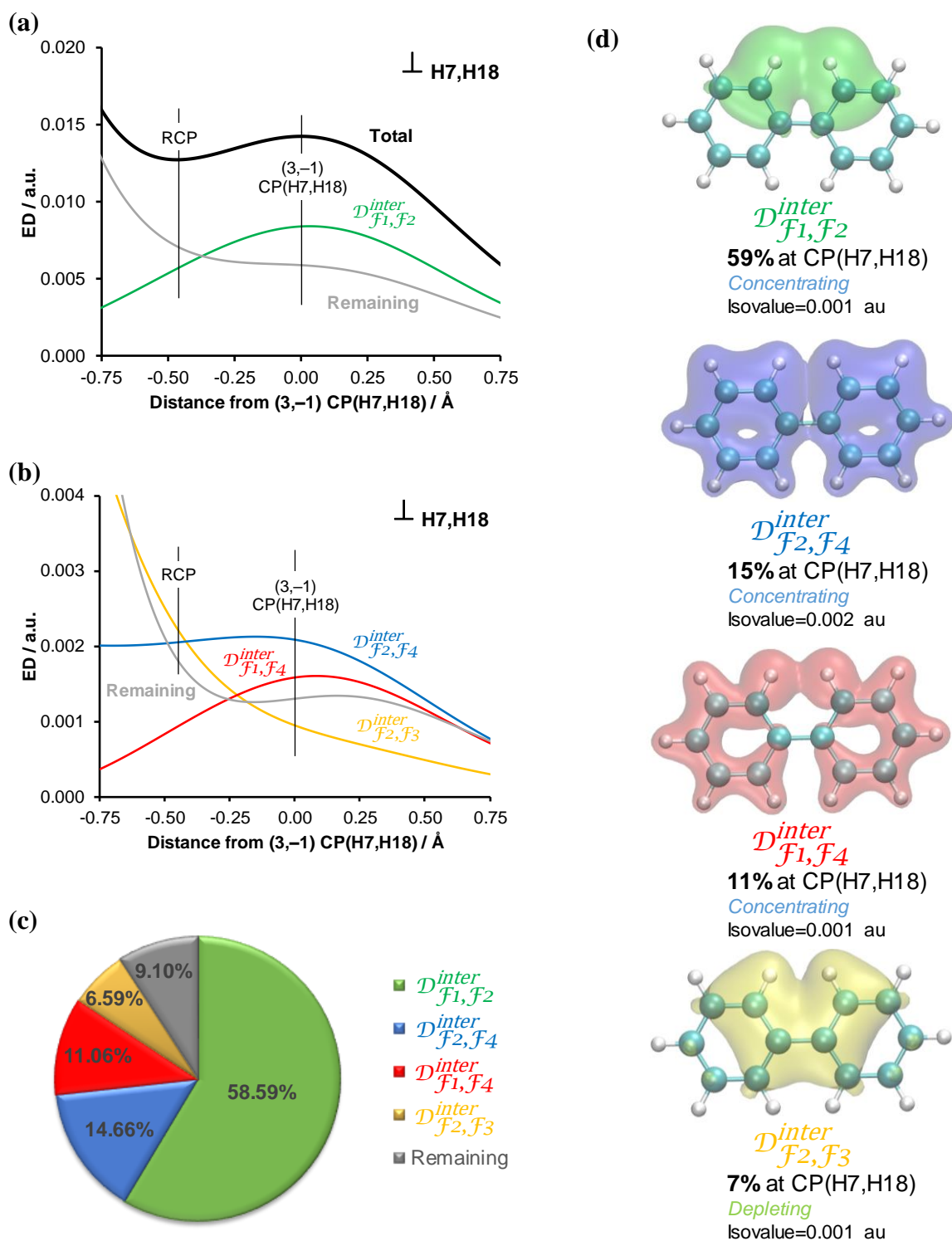


Figure 3. Decompositions showing (a) the leading and (b) remaining major FALDI fragment contributions to the ED of the CP(H7,H18) along the λ_2 -eigenvector in planar Bph. (c) provides the relative contributions to the ED at CP(H7,H18), and (d) isosurfaces of selected components.

the inter-fragment delocalization between fragments $\mathcal{F}2$ and $\mathcal{F}4$, and between $\mathcal{F}1$ and $\mathcal{F}4$ (15% and 11%, respectively). This observation signifies the importance and impact that the remainder

of the molecule (\mathcal{F}_4) has, as inherently both rings contribute a total of 26% to the density at CP(H7,H18) by interacting with H \cdots H, through $\mathcal{D}_{\mathcal{F}_1,\mathcal{F}_4}^{inter}(\mathbf{r})$, and with C \cdots C, through $\mathcal{D}_{\mathcal{F}_2,\mathcal{F}_4}^{inter}(\mathbf{r})$. The relevant isosurfaces (Figure 3d) again reveal that these FALDI terms, and hence essentially the entire molecule, contributes to the channel of delocalized density between the H-atoms of the bay. Clearly, the two aromatic rings delocalize ED to H- and C-atoms of the C–H fragments in the bay and in such a way promote the formation of the DB(H,H).

The only component that results in a significant depletion of density is the inter-fragment delocalization between \mathcal{F}_2 and \mathcal{F}_3 (6.6%) – the interaction between the *ortho*-carbons and the linker carbons. The isosurface of $\mathcal{D}_{\mathcal{F}_2,\mathcal{F}_3}^{inter}(\mathbf{r})$ is the only significant FALDI term that *does not* contribute to the delocalized electron channel between H-atoms. Interestingly, however, we found that the interaction between *ortho*-hydrogens and the linker carbons ($\mathcal{D}_{\mathcal{F}_1,\mathcal{F}_3}^{inter}(\mathbf{r})$), also concentrates ED at CP(H7,H18) – Figure 4a – although in an almost insignificant fashion (3.4 %).

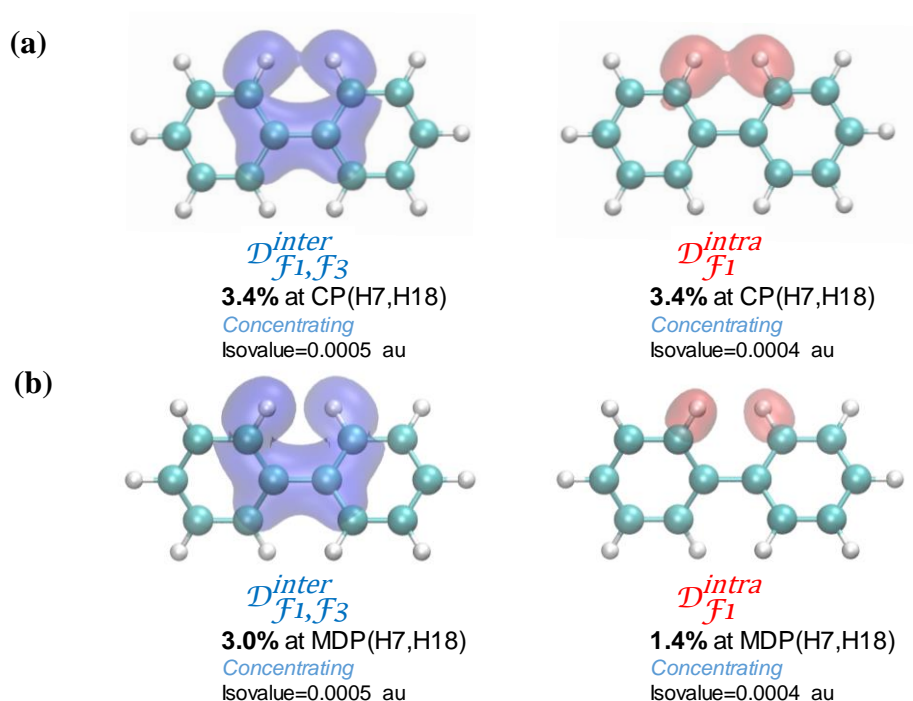


Figure 4. Isosurfaces of less significant, but noteworthy contributions in (a) planar and (b) twisted Bph.

In addition, the density directly shared by the H-atoms themselves ($\mathcal{D}_{\mathcal{F}_1}^{intra}(\mathbf{r})$) is concentrating and contributes to the delocalized electron channel, but also in minute manner (3.4 %, Figure 4a).

Finally, we note that all of the above observations pertains to σ - rather than π -delocalization, as no nodal surfaces are observed in the H,H inter-nuclear region for any of the FALDI isosurfaces.

From an electronic point of view, and taking into account the full range of molecular-wide electron delocalization as elucidated by FALDI, we note that a channel of delocalized electrons between H-atoms in planar Bph primarily originates from two quantum mechanical effects: i) coupling of two C–H σ -bonds and ii) σ -delocalization induced by the phenyl rings. On the other hand, delocalization between *ortho*- and linker-carbons inhibits the H...H electronic channel through a depletion at CP(H7,H18). The interplay of these effects results in a greater and opposite slope of the concentrating, relative to the depleting, FALDI products and ultimately results in an H,H DB (as confirmed by the $CP(\mathbf{r})$ function in Figure 2c).

Performing the same analysis for the H...H region in twisted Bph reveals that the same four components make up the majority of the density at MDP(H7,H18) – Figures 4b and 5. The same contributions that concentrate/deplete ED in planar Bph also concentrate/deplete ED in twisted Bph. This observation confirms^[23] that the CH...HC interaction is chemically identical and present in both conformers. In fact, the only discernible differences between the two compounds are the relative magnitudes of each component, as well as their relative slopes. In the twisted conformer, the interplay between the FALDI products results in a smaller slope of the concentrating products relative to the depleting products, resulting in the absence of a DB. Finally, looking at the traces computed for the major contributions (Figure 5a,b) we note that the most significant impact on the shape of the $CP(\mathbf{r})$ function (Figure 2c) and the absence of a DB in the twisted Bph is the delocalization between $\mathcal{F}2$ and $\mathcal{F}4$?. This is the only trace that does not have a bell shape as observed for $\mathcal{F}1, \mathcal{F}2$ (in planar and twisted Bph), $\mathcal{F}1, \mathcal{F}4$ (in both Bph conformers) and $\mathcal{F}2, \mathcal{F}4$ (only planar conformer).

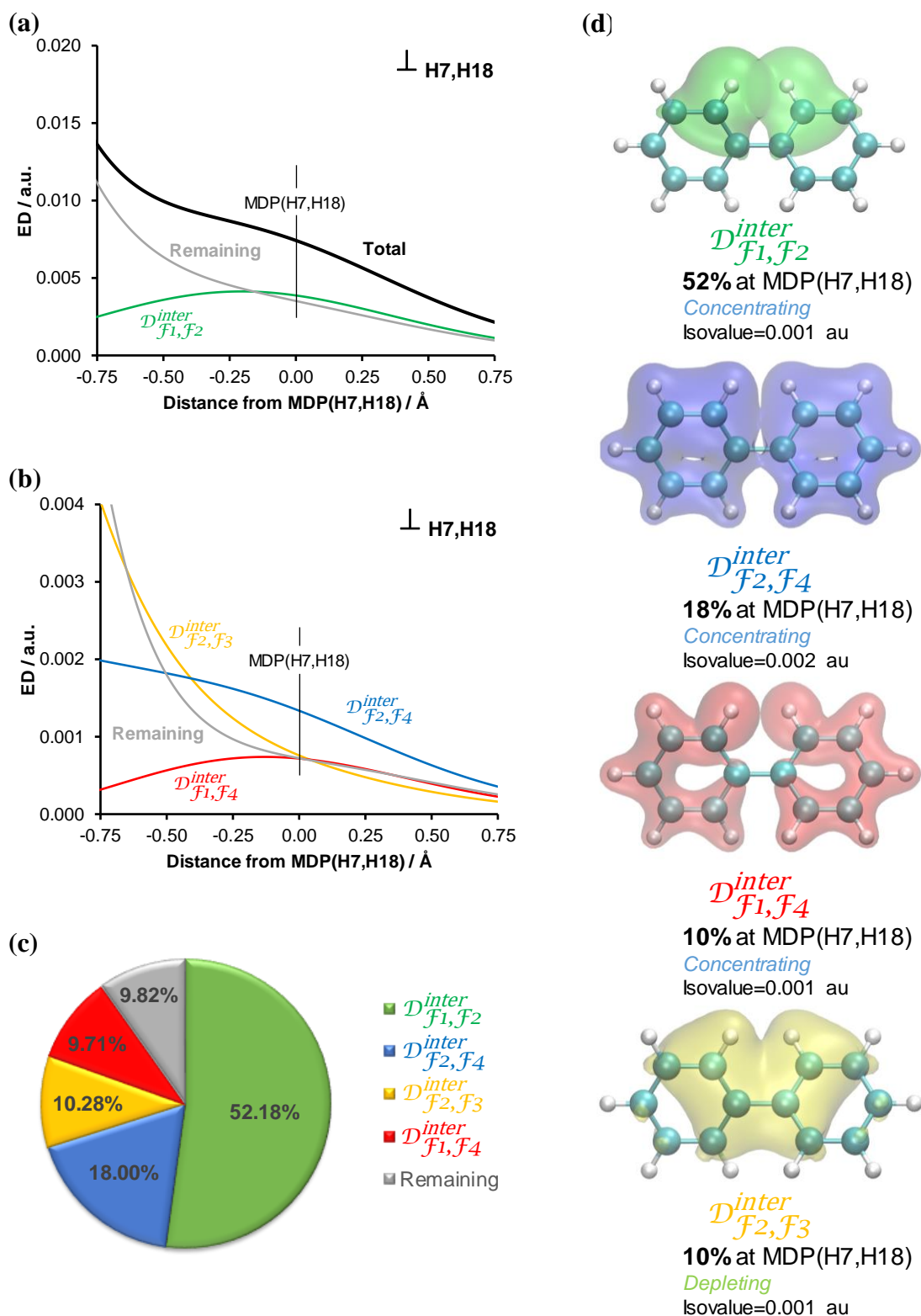


Figure 5. Decompositions showing (a) the leading and (b) remaining major FALDI fragment contributions to the ED of the MDP(H7,H18) along the λ_2 -eigenvector in twisted Bph. (c) provides the relative contributions to the ED at MDP(H7,H18), and (d) isosurfaces of selected components.

Note that the choice of isovalue for rendering the above-mentioned isosurfaces does not have an impact on our interpretation – the same molecular-wide trends are seen for larger isovalues as

well. In addition, the quantitative measures obtained from cross-section analysis is independent of the choice of isovalue for the isosurfaces. This fully confirms that the concentration of density associated with the CH \cdots HC interaction can be regarded as a molecular-wide event.

FALDI diatomic analysis of planar and twisted biphenyl

Whereas FALDI's fragment analysis reveals the largest trends in the electronic structure of a molecule, FALDI's atomic and atom-pair analysis allows one to further pin-point the origin of ED in a specific region.

Cross-section analyses along the λ_2 -eigenvector for the H7 \cdots H18 region in planar and twisted Bph reveal that there are nine significant contributors to the density at CP(H,H) and MDP(H,H) making up 77.5% and 73.9%, respectively. Isosurfaces of the most significant FALDI atom-pair contributions are shown in Table 1 and an extended set of significant contributions is placed in Table 2; a full set of FALDI atom-pair data is included in Part 4 of the SI.

Fragment analysis for planar Bph showed that there are four significant contributions. The largest contribution was the inter-fragment delocalization between $\mathcal{F}1$ and $\mathcal{F}2$ and based on the diatomic analysis, we see that this interaction is mostly made up from the bay-region atom-pairs C2,H7 and C13,H18. These two atom-pairs conjointly contribute 57.4% to the density at CP(H,H). We also see similarly to the fragment analysis, $\mathcal{D}_{\mathcal{F}1}^{intra}(\mathbf{r})$, that the H7 \cdots H18 atom pair makes a significant contribution, but relatively small compared to the bay-region C-H atom-pairs.

The fragment analysis also showed the importance of the rings and their interactions with the *ortho* C-H groups. Diatomic analysis shows that it is predominantly the *meta* carbons, C3 and C14, that delocalize density into the H,H inter-nuclear region. Specifically, C2-C3 and C13-C14 delocalizes and concentrates ED at CP(H7,H18) (8.2%), as do the long-range interactions C3 \cdots H7

Table 1. Isosurfaces of the most significant FALDI atom-pair contributions (Isovalue 0.001 a.u.) of concentrating, depleting, and removing nature to the electron density at the (3,-1) CP(H7,H18) and MDP(H7,H18) in **planar** and **twisted** biphenyl, respectively. We denoted 'sym' to represent that the atom-pair has a symmetrical interaction of the same contribution and nature.

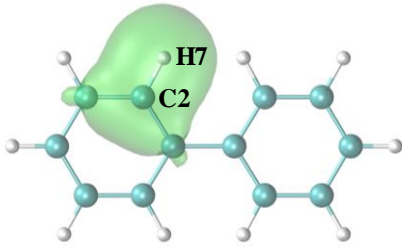
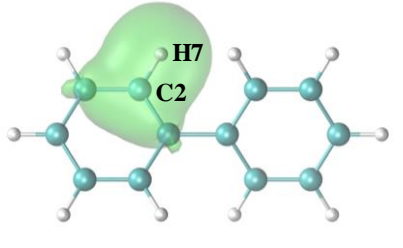
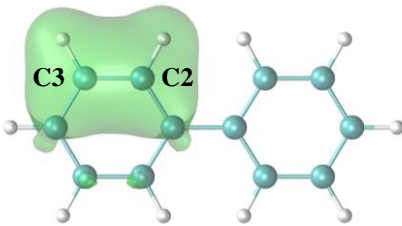
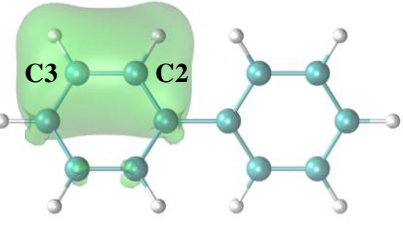
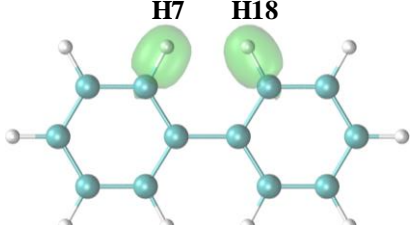
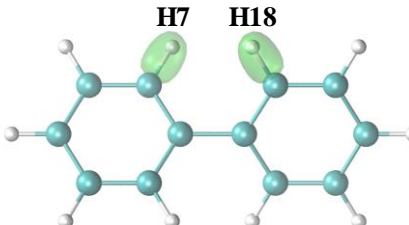
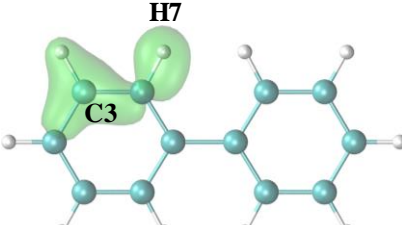
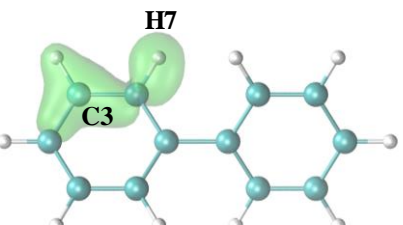
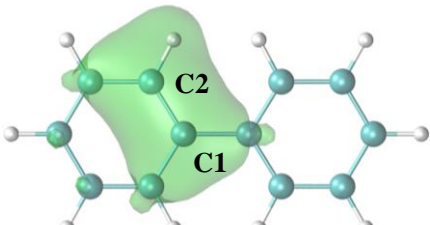
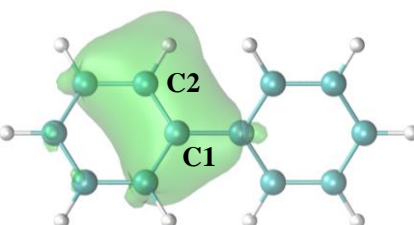
Planar	Twisted
Atom-pair; <i>deloc</i> -ED contribution a.u. / %-fraction, <i>nature</i>	
C2,H7; 0.004134 / 28.7	C2,H7; 0.001781 / 25.6
 <i>sym</i>	 <i>sym</i>
C2,C3; 0.000594 / 4.1, <i>conc</i>	C2,C3; 0.000337 / 4.8, <i>conc</i>
 <i>sym</i>	 <i>sym</i>
H7,H18; 0.000510 / 3.5, <i>conc</i>	H7,H18; 0.000103 / 1.5, <i>conc</i>
 <i>sym</i>	 <i>sym</i>
C3,H7; 0.000253 / 1.8, <i>conc</i>	C3,H7; 0.000110 / 1.6, <i>conc</i>
 <i>sym</i>	 <i>sym</i>
C1,C2; 0.000349 / 2.4, <i>deplet</i>	C1,C2; 0.000291 / 4.2, <i>deplet</i>
 <i>sym</i>	 <i>sym</i>

Table 2. Most notable FALDI-ED contributions and %-fractions to the (3,-1) CP(H7,H18) and MDP(H7,H18) in planar and twisted biphenyl, respectively, for concentrating, depleting, and removing density.

Atom-Pair	Planar	Twisted
	ED contribution a.u. / %-fraction	ED contribution a.u. / %-fraction
<i>Concentrating</i>		
<i>Total</i>	0.01372 / 95.1%	0.00617 / 88.6%
C2,H7 and C13,H18	0.00826 / 57.4%	0.00356 / 51.2%
C2,C3 and C13,C14	0.00118 / 8.2%	0.00068 / 9.6%
H7,H18	0.00051 / 3.5%	0.00010 / 1.5%
C14,H18 and C3,H7	0.00050 / 3.6%	0.00022 / 3.2%
<i>Remaining</i>	0.00325 / 22.5%	0.00161 / 23.1%
<i>Depleting</i>		
<i>Total</i>	0.00075 / 5.2%	0.00080 / 11.4%
C12,C13 and C1,C2	0.00070 / 4.8%	0.00058 / 8.4%
C2,C6 and C13,C17	-	0.00006 / 1.0%
<i>Remaining</i>	0.00005 / 0.4%	0.00015 / 2.1%
<i>Removing</i>		
<i>Total</i>	-0.000048 / -0.33%	-0.000003 / -0.1%
C2,C13	-0.000037 / -0.26%	-
<i>Remaining</i>	-0.000011 / -0.07%	-

and C14...H18 (3.6%). The remaining interactions of the ring (coming from the $\mathcal{F}4$ fragment) with the *ortho* C–H groups are all small individually, although they add up to a significant 14% of the ED at CP(H7,H18).

Analysis of atom-pairs in twisted Bph shows similar results and corroborates our previous statement regarding the similarity of the CH...HC interaction in both conformers. The only difference between planar and twisted conformers is the relative magnitude of each decomposition product. The contributions that is responsible for the majority of depleted ED at the H,H CP/MDP is that of atom-pairs C12,C13 and C1,C2 – the interaction between linker- and *ortho*-carbon atoms. Most notably, these atom-pairs contribute relatively more to the ED at MDP(H7,H18) in twisted Bph (8.4%) than at the CP(H7,H18) in planar Bph (4.8%).

Conclusion

Previously, an MO-based density decomposition was used^[23] successfully to unambiguously analyse the nature of the CH \cdots HC density bridge in Bph, and recovered that the MO constituents of the interaction are very similar to every other covalent bond in the molecule. However, the delocalized, molecular-wide nature of MOs makes any MO-based interpretation of the CH \cdots HC interaction quite difficult. We have shown in this work that FALDI analysis, both in terms of 3D isosurfaces and 1D cross-sections, can provide valuable insights regarding the origin and chemical character of the electron density forming the CH \cdots HC interaction.

It was found that the density in the H,H inter-nuclear region arose from two dominant effects: i) overlap of the electrons delocalized within the two *ortho* C–H σ -bonds, and ii) long-range delocalization of the phenyl rings with *ortho* carbon and hydrogen atoms. Both effects increase the σ -character^[23] of the CH \cdots HC interaction, and we suggest these effects as examples of non-classical, long-range σ -delocalization. The *meta* carbons, in particular, contribute more to the density of the CH \cdots HC interaction than the *para* carbons and hydrogens of the rings. In addition, both aforementioned effects resulted in the formation of a delocalized electron channel between the hydrogens (reminiscent of Pendás *et al*'s concept of privileged exchange channels^[14]), which was easily visualised by FALDI. Interestingly, the density delocalized between the *ortho* hydrogen atoms themselves were found to be an almost insignificant contribution. Finally, the density delocalized between the linker and *ortho* carbons *inhibits* the formation of the delocalized electron channel through a depletion of density in the H,H inter-nuclear region. We expect that the information that FALDI provides can be used to study the properties and tuneability of CH \cdots HC interactions in biphenyl as well as other systems.

The exact same effects described above were observed for the CH \cdots HC interaction in the twisted conformer of Bph as well, although to a lesser extent. We have found no evidence that the nature of the CH \cdots HC interaction is different in the two conformers – a delocalized electron

channel was observed in both conformers, and the same FALDI products gave rise to each. The absence of a density bridge in the twisted conformer was also elegantly explained through the $CP(\mathbf{r})$ function: in the twisted conformer, the rate of change of the FALDI products concentrating density in the H,H inter-nuclear region is lower than the rate of change of products depleting density.

In summary, our results clearly show that the CH \cdots HC interaction results from extreme, molecular-wide delocalization of electrons, and should be considered as entirely non-classical in origin. In particular, given how little the H-atoms themselves contribute to the H,H inter-nuclear region, we suggest that extreme care should be taken by any approach that seeks to study CH \cdots HC interactions locally and without considering the whole molecule. That said, the resultant density within the H,H inter-nuclear region appears the same as it does for any other covalent bond, regardless of its molecular-wide origin. This observation is fully in-line with other, energetic studies^[13,20] on the same molecule.

Finally, the highly delocalized nature of the CH \cdots HC interaction perhaps also hints at why consensus has not yet been reached by the scientific community regarding the cause of the rotation barrier in biphenyl. Regardless of the energetic nature of the CH \cdots HC interaction – whether attractive or repulsive, stabilizing or destabilizing – the density associated with the interaction is highly correlated with the rest of the molecule. Therefore, the CH \cdots HC interaction cannot be considered as the singular cause for the rotation barrier in biphenyl since the molecule as a whole forms part of the interaction. Afterall, a needle cannot be found if it forms a part of the haystack itself.

Conflicts of interest

The authors declare no conflict of interest.

Acknowledgments

The authors gratefully acknowledge the Centre for High Performance Computing (CHPC), South Africa, for providing computational resources to this research project and National Research Foundation of South Africa, Grant Number 105855, for financial support.

References

- [1] G. N. Lewis, *J. Am. Chem. Soc.* **1916**, *38*, 762–85.
- [2] L. Pauling, *The Nature of the Chemical Bond – An introduction to Modern Structural Chemistry*, Cornell University Press, New York, **1960**.
- [3] H. L. Schäfer, G. Gliemann, *Basic Principles of Ligand Field Theory*, Wiley-Interscience, New York, **1969**.
- [4] T. A. Albright, J. K. Burdett, M. Whangbo, *Orbital Interactions in Chemistry*, 2nd edition, John Wiley & Sons, New Jersey, **2013**.
- [5] I. N. Levine, *Quantum Chemistry*, 7th edition, Pearson Prentice Hall, New Jersey, **2014**.
- [6] C. F. Matta, J. Hernández-Trujillo, T-H. Tang, R. F. W. Bader, *Chem. Eur. J.* **2003**, *9*, 1940–1951.
- [7] J. Echeverría, G. Aullón, D. Danovich, S. Shaik, S. Alvarez, *Nature Chem.* **2011**, *3*, 323–330.
- [8] J. Cioslowski, S. T. Mixon, *Can. J. Chem.* **1992**, *70*, 443–449.
- [9] J. Poater, M. Solà, F. M. Bickelhaupt, *Chem. Eur. J.* **2006**, *12*, 2889–2895.
- [10] R. F. W. Bader, *Chem. Eur. J.* **2006**, *12*, 2896–2901.
- [11] J. Poater, M. Solà, F. M. Bickelhaupt, *Chem. Eur. J.* **2006**, *12*, 2902–2905.
- [12] L. F. Pacios, L. Gómez, *Chem. Phys. Lett.* **2006**, *432*, 414–420.
- [13] J. Hernández-Trujillo, C. F. Matta, *Struct. Chem.* **2007**, *18*, 849–857.
- [14] A. M. Pendás, E. Francisco, M. A. Blanco, C. Gatti, *Chem. Eur. J.* **2007**, *13*, 9362–9371.
- [15] K. Eskandari, C. Van Alsenoy, *J. Comp. Chem.* **2014**, *35*, 1883–1889.
- [16] S. Jenkins, J. R. Maza, T. Xu, D. Jiajun, S. R. Kirk, *Int. J. Quant. Chem.* **2015**, *115*, 1678–1690.
- [17] D. Jiajun, Y. Xu, T. Xu, R. Momen, S. R. Kirk, S. Jenkins, *Chem. Phys. Lett.* **2016**, *651*, 251–256.
- [18] J. Li, W. Huang, T. Xu, S. R. Kirk, S. Jenkins, *Chem. Phys. Lett.* **2018**, *702*, 32–37.
- [19] J. Jara-Cortés, J. Hernández-Trujillo, *J. Comp. Chem.* **2018**, *39*, 1103–1111.

- [20] P. L. A. Popelier, P. I. Maxwell, J. C. R. Thacker, I. Alkorta, *Theoret. Chem. Acc.* **2019**, *138*, 12–28.
- [21] R. D. Hancock, I. V. Nikolayenko, *J. Phys. Chem. A* **2012**, *116*, 8572–8583.
- [22] R. Laplaza, R. A. Boto, J. Contreras-Garcia, M. M. Montero-Campillo, *Phys. Chem. Chem. Phys.* **2020**, *22*, 21251–21256.
- [23] I. Cukrowski, J. H. de Lange, D. M. E. van Niekerk, T. G. Bates, *J. Phys. Chem. A* **2020**, *124*, 5523–5533.
- [24] F. Weinhold and C. R. Landis, *Valency and bonding. A natural bond orbital donor–acceptor perspective*; Cambridge University Press, Cambridge. **2005**.
- [25] M. P. Mitoraj, M. Parafiniuk, M. Srebro, M. Handzlik, A. Buczek, A. Michalak, *J. Mol. Model.* **2011**, *17*, 2337–2352.
- [26] P. L. A. Popelier, in *The Chemical Bond II. Structure and Bonding*, ed. D. Mingos, Springer, Cham, **2016**.
- [27] R. F. W. Bader, *Atoms in Molecules. A Quantum Theory*, Oxford University Press, Oxford, **1990**.
- [28] F. Weinhold, P. von Ragué Schleyer, W. C. McKee, *J. Comput. Chem.* **2014**, *35*, 1499–1508.
- [29] I. Cukrowski, F. Sagan, M. P. Mitoraj, *J. Comput. Chem.* **2016**, *37*, 2783–2798.
- [30] A. Haaland, J. D. Shorokhov, N. V. Tverdova, *Chem.–Eur. J.* **2004**, *10*, 4416–4421.
- [31] M. von Hopffgarten, G. Frenking, *Chem.–Eur. J.* **2008**, *14*, 10227–10233.
- [32] F. Weinhold, *J. Comput. Chem.* **2012**, *33*, 2440–2449.
- [33] I. Cukrowski, J. H. de Lange, A. S. Adeyinka, P. Mangondo, *Comput. Theor. Chem.* **2015**, *1053*, 60–76.
- [34] C. F. Matta, S-A. Sadjadi, D. A. Braden, G. Frenking, *J. Comput. Chem.* **2016**, *37*, 143–154.
- [35] S. Grimme, C. Mück-Lichtenfeld, G. Erker, G. Kehr, H. Wang, J. Beckers, H. Willner, *Angew. Chem. Int. Ed.* **2009**, *48*, 2592–2595.
- [36] J. Poater, F. M. Bickelhaupt, M. Solà, *J. Phys. Chem. A* **2007**, *111*, 5063–5070.
- [37] M. Jabłoński, *Chem. Phys. Lett.* **2020**, *759*, 137946–137651.
- [38] J. H. de Lange, I. Cukrowski, *J. Comp. Chem.* **2017**, *38*, 981–997.
- [39] I. Cukrowski, D. M. E. van Niekerk, J. H. de Lange, *Struct. Chem.* **2017**, *28*, 1429–1444.
- [40] J. H. de Lange, D. M. E. van Niekerk, I. Cukrowski, *J. Comp. Chem.* **2018**, *39*, 973–985.
- [41] J. H. de Lange, D. M. E. van Niekerk, I. Cukrowski, *J. Comp. Chem.* **2018**, *39*, 2283–299.
- [42] J. H. de Lange, I. Cukrowski, *J. Comp. Chem.* **2018**, *39*, 1517–1530.
- [43] R. Ponec, *J. Math. Chem.* **1997**, *21*, 323–333.

- [44] R. Ponec, *J. Math. Chem.* **1998**, *23*, 85–103.
- [45] P. Bultinck, D. L. Cooper, R. Ponec, *J. Phys. Chem. A* **2010**, *114*, 8754–8763.
- [46] A. Müller, *Phys. Lett. A* **1984**, *105*, 446–452.
- [47] J. H. de Lange, D. M. E. van Niekerk, I. Cukrowski, *Phys. Chem. Chem. Phys.* **2019**, *21*, 20988–20998.
- [48] M. Frisch, G. Trucks, H. Schlegel, G. Scuseria, M. Robb, J. Cheeseman, G. Scalmani, V. Barone, B. Mennucci, G. Petersson, H. Nakatsuji, X. Li, M. Caricato, A. Marenich, J. Bloino, B. Janesko, R. Gomperts, B. Mennucci, H. Hratchian, J. Ortiz, A. Izmaylov, J. Sonnenberg, D. Williams-Young, F. Ding, F. Lipparini, F. Egidi, J. Goings, B. Peng, A. Petrone, T. Henderson, D. Ranasinghe, V. Zakrzewski, J. Gao, N. Rega, G. Zheng, W. Liang, M. Hada, M. Ehara, K. Toyota, R. Fukuda, J. Hasegawa, M. Ishida, T. Nakajima, Y. Honda, O. Kitao, H. Nakai, T. Vreven, K. Throssell, J. J. Montgomery, J. Peralta, F. Ogliaro, M. Bearpark, J. Heyd, E. Brothers, K. Kudin, V. Staroverov, T. Keith, R. Kobayashi, J. Normand, K. Raghavachari, A. Rendell, J. Burant, S. Iyengar, J. Tomasi, M. Cossi, J. Millam, M. Klene, C. Adamo, R. Cammi, J. Ochterski, R. Martin, K. Morokuma, O. Farkas, J. Foresman, D. Fox, Gaussian, Inc., Wallingford CT, **2009**.
- [49] AIMAll (Version 19.02.13), Keith, T. A. TK Gristmill Software, Overland Park KS, USA, **2019** (aim.tkgristmill.com).
- [50] W. Humphrey, A. Dalke, K. Schulten, *J. Molec. Graphics* **1996**, *14*, 33–38.

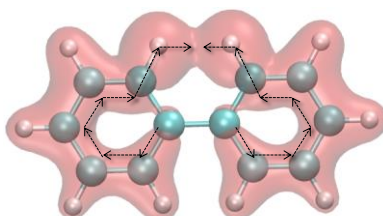
TOC

GRAPHICAL ABSTRACT

THOMAS G. BATES, JURGENS H. DE LANGE AND IGNACY CUKROWSKI

The CH...HC interaction in biphenyl is a delocalized, molecular-wide and entirely non-classical interaction: results from FALDI analysis

**CH...HC interaction welcomes
electrons from *all* atoms!**



The FALDI scheme is used to show that the majority of atoms in biphenyl contribute electron density to the H,H inter-nuclear region to form a channel of delocalized density, *i.e.*, the Bader's bond path. This illustrates how a molecular system, here a planar biphenyl, is minimising its energy when being disturbed from its equilibrium twisted structure.

Chapter 5

NBOs Support MO and FALDI based 'Bonding' Description of CH \cdots HC Bond Paths in Planar Biphenyl

Prepared for submission to:

Journal of Computational Chemistry **2020**.

The Supplementary Information is provided in Appendix III

NBOs Support MO and FALDI based ‘Bonding’ Description of CH \cdots HC Bond Paths in Planar Biphenyl

Thomas G. Bates, Ignacy Cukrowski and Jurgens H. de Lange*

*Department of Chemistry, Faculty of Natural and Agricultural Sciences, University of Pretoria,
Lynnwood Road, Hatfield, Pretoria 0002, South Africa*

*Correspondence to: Jurgens de Lange:

E-mail: jurgens.delange@up.ac.za

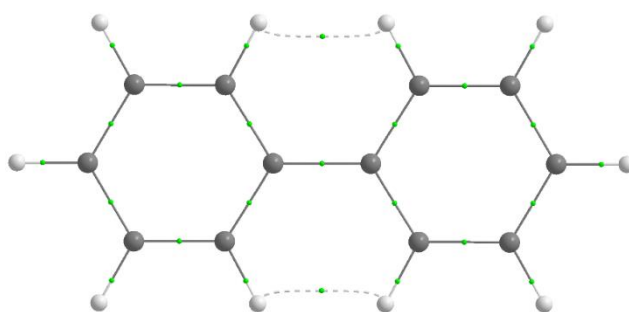
5.1. Abstract

Just as molecular orbitals (MOs) and Fragment, Atomic, Localised, Delocalised, and Interatomic (FALDI) support the ‘bonding’ description of the density bridges (DB), otherwise known as bond paths, between the *ortho*-hydrogens in the planar conformation of biphenyl, so too do natural bond orbitals (NBOs). By decomposing the density along λ_2 -eigenvector from the bond critical point between the *ortho*-hydrogens, NBOs show that the density is overwhelmingly concentrating (i.e. energy-minimising) in both conformers. NBO results are generally in line with the FALDI interpretation – that the major mechanism of this bonding interaction is due to a C-H \cdots H-C, 4-centred effect. What can be concluded from this NBO-based decomposition, as well as from MO and FALDI analysis, is that the interpretation of a DB is the same whether the density is decomposed into MOs, FALDI-components, or NBOs. However, this study also shows that NBOs are not suited to study weak, non-covalent interactions since they do not show the true extent of delocalisation within a molecule.

5.2. Introduction

Amongst the many scientific debates, one that is in essence due to the lack of a concise definition of a chemical bond is one that has spanned almost three decades, about the nature of a specific intra-molecular hydrogen-hydrogen interaction. In systems such as the planar conformation of biphenyl (Bph, Scheme 1), QTAIM^[1] designates a density bridge (DB, otherwise referred to as a bond path) between the two *ortho*-hydrogen pairs. This DB causes problems in the classical notion of bonding.

A DB in QTAIM depicts a line of maximum density between two atoms, resembling conventional Lewis-structures, which is why QTAIM became a very powerful and prominent tool as a computational technique – QTAIM recovers, from the electron density topology, our classical chemical concepts. The fact that QTAIM depicts a DB between these hydrogens though, first observed by Cioslowski and Mixon,^[2] has triggered a back and forth of analysis leading to the division on the nature of this interaction. A wide spectrum of tools and methods have been used to investigate this problem, either concluding that the DB signals a bonding interaction, or concluding that the conventional classical view still stands and that these *ortho*-hydrogens are part of a steric clash.



Scheme 1. Molecular graph of planar biphenyl

From this back and forth, rebuttal and counter-rebuttal, we see a common trend arise. Most arguments can be grouped into two families of methods: (i) orbital-based methods, and (ii) density-based methods. From these groups, two different conclusions are drawn about the nature of this CH \cdots HC interaction – orbital-based methods generally conclude a steric clash,

whilst density-based methods conclude a bonding/attractive interaction. This causes a problem because the underlying wavefunction and physics is the same; however, the method of analysis seems to be the isolating issue, or perhaps rather the interpretation of the analysis. Poater *et al*^[3] for example used energy decomposition analysis (EDA) to show that the *ortho*-hydrogens in planar Bph have a maximum in Pauli repulsion, resulting in the increased energy of the system compared to equilibrium (twisted) Bph. Another example of an orbital-based method that concluded a non-bonding nature for CH \cdots HC is that from the natural bond orbital (NBO) analysis of *cis*-2-butene by Weinhold *et al*.^[4] This showed an “overwhelmingly repulsive net character” of these CH \cdots HC interactions, in line with the classical interpretation of such interactions. They concluded this because, although there are some donor-acceptor (bond-antibond) interactions which are stabilising, the steric donor-donor interactions overshadowed the former.

Contrarywise, Pendás *et al*^[5] showed using interacting quantum atoms (IQA)^[6] how DBs in QTAIM indicate “privileged exchange channels”; in other words, they indicate important channels of exchange-correlation that subsequently decrease the energy of the molecular system. Furthermore, Eskandari *et al*^[7] also used IQA to indicate that the energy components in planar Bph show a net *attractive* interaction between Bph’s *ortho*-hydrogens. In a more recent study, Popelier *et al*^[8] used their newly proposed relative energy gradient (REG) method using IQA contributions to conclude that there is indeed a destabilisation due to the *ortho*-hydrogens, however it is reduced by the formation of a weak covalent bond.

There is a clear division in the overall consensus of the nature of this interaction, albeit the wavefunction and physics is identical. As such, we aim to reconcile these methods to point to one distinct and clear interpretation. To do this, we used cross-section analysis^[9-11] in which the electron density (ED) at a chosen point \mathbf{r} is decomposed into individual contributors. When this is scanned along λ_2 -eigenvector, upon examining the directional second partial derivative

(2nd-derivative), one can determine which components concentrate the density at \mathbf{r} (negative 2nd-derivative), and which deplete the density (positive 2nd-derivative). This allows for unambiguous analysis of the density and the use of different decomposition methods for interpretation.

The first study that we embarked on involved decomposing the electron density along λ_2 -eigenvector, crossing the bond critical, and minimum density, point (BCP and MDP) between the *ortho*-hydrogens, in planar and twisted Bph, respectively, into its molecular orbital (MO) contributions.^[12] What this study revealed was that a large number of MOs contributed in tandem to this DB, rather than one or two dominant contributions. Upon conducting cross-sections of classical covalent bonds in the molecule, it was found that the MO contributions of the CH \cdots HC interaction are very similar to the classical covalent bonds, showing us that the interaction has a degree of covalency, rather than steric repulsion. Nevertheless, the delocalised, molecular wide nature of MOs makes it difficult to interpret a deeper chemical meaning about this H,H contact. The second study made use of FALDI,^[10, 13-16] whereby the same electron density as above was decomposed into FALDI components.^[17] Much like the MO study, a large number of FALDI components contribute to the DB of the H,H contact, however two major interactions stand out, namely the two *ortho* C-H bonds. Moreover, FALDI decomposition analysis showed the importance of the long-range delocalisation of the remainder of phenyl rings in conjunction with the *ortho* C-H σ -bonds. These results show that the CH \cdots HC interaction results from a large, molecular-wide delocalisation of electrons.

Conjointly, both the MO and FALDI study revealed that the same effects that make up the density within the H,H contact in planar, are also present in the twisted conformation. The presence of a DB exclusively in the planar conformation, however, is explained by the $CP(\mathbf{r})$ function. Both MOs and FALDI show that a DB exists because slopes of the concentrating MOs/FALDI components are larger and opposite in sign than the slopes of the depleting

components, ensuring that the $CP(\mathbf{r})$ function is only positive in these regions, specifically around the BCP. This is not the case for the twisted conformation.

In this chapter, we will use cross-section analysis to decompose the total electron density of the $CH\cdots HC$ interaction into NBO contributions. Due to the rising popularity of NBOs, and that it has previously been used in the debate about the nature of intra-molecular hydrogen-hydrogen interactions, it is imperative to analyse the electron density from an NBO perspective. Since NBOs force a Lewis-bond picture, one can directly compare the findings with the FALDI-based decomposition conducted in the previous chapter.

5.3. Theoretical Background

We utilise cross-section analysis,^[9-11] in which we decompose the total electron density at position \mathbf{r} into contributions made by natural bond orbitals (NBOs):

$$\rho(\mathbf{r}) = \sum_i^{N_{NBO}} v_i |\chi_i(\mathbf{r})|^2 \quad (5-1)$$

where χ_i is an NBO with occupation v_i . Note that the wavefunctions in NBOs are forced to represent Lewis-like connections, and as such, the majority of NBOs will have an occupation of 2. Since we decompose the total electron density from NBOs, we can subsequently name this method NBO-ED. The position \mathbf{r} in this study on Bph is the bond critical point (BCP) of $H\cdots H$ if present, otherwise the minimum density point (MDP) was used. In this case, the BCP(H,H) is used in planar Bph, and MDP(H,H) is used in twisted Bph.

When the total electron density is decomposed along λ_2 -eigenvector from the position \mathbf{r} , the nature of the total electron density can be determined from the directional second partial derivative (2^{nd} -derivative); the density can be concentrating (i.e. a negative region around BCP/MDP) or depleting (i.e. no negative region). As mentioned above, this total density can be decomposed into its NBO contributions, i.e. into the contributions from all 230 NBOs. The same process is used to determine the nature of each contribution, and as such when the

contributions are grouped and summed according to their nature, one gets the total *concentrating* and total *depleting* contribution to the total electron density as

$$\rho_{tot}(\mathbf{r}) = \rho_{concentrating}(\mathbf{r}) + \rho_{depleting}(\mathbf{r}) \quad (5-2)$$

Although the nature of the contribution is determined by the 2nd-derivative, the absence/presence of a DB is determined by the gradients (1st-derivative) of the contributions. It is well known that a CP in the electron density is defined as a point in space where the gradient of the density is equal to zero,^[1] and so equation 5-2 becomes

$$\partial\rho_{tot}(\mathbf{r}) = \partial\rho_{concentrating}(\mathbf{r}) + \partial\rho_{depleting}(\mathbf{r}) \quad (5-3)$$

At the same time however, the absolute concentrating gradient needs to be larger and opposite in sign than the depleting gradient. To make analysis easier, the $CP(\mathbf{r})$ function is used

$$CP(\mathbf{r}) = -sign\left(\partial\rho_{depleting}(\mathbf{r})\right)\left(\partial\rho_{tot}(\mathbf{r})\right) \quad (5-4)$$

This function expresses the gradient of the total electron density but weighted by the sign of the depleting density gradient. This guarantees that the $CP(\mathbf{r})$ function is negative in all regions, excluding the region where the absolute concentrating density gradient is larger and opposite in sign to the absolute depleting density gradient.

5.4. Computational Methods

Both the planar and twisted conformations of Bph were optimised in Gaussian 09, Rev. D.01^[18] using restricted B3LYP with cc-pVDZ basis set in gas phase. The cartesian coordinates are given in Part 1 of Appendix III. The NBO populations^[19] were then calculated from these optimised structures under the same conditions stated above. QTAIM data was obtained using AIMAll v. 19.02.13.^[20] to be used in the aid of the calculation of NBO density data along λ_2 -eigenvector of the BCP(H7,H18) and MDP(H7,H18) for planar and twisted Bph, respectively, obtained using in-house software. All NBO isosurfaces were obtained using Gaussian 09, Rev. D.01.

5.5. Results and Discussion

As previously discussed in the introduction, we want to investigate how an NBO decomposition compares to MO- and FALDI-based decompositions. Previously we showed that the decomposition of the total electron density into FALDI components gives the same overall picture as the decomposition into MO components.^[17] FALDI however allows for a far better analysis as it has a higher resolution (231 atom-pairs compared to 41 MOs). This allows one to pinpoint the origin of the density at \mathbf{r} , as well as identify the contributions in chemically intuitive terms, i.e. atom-pairs. In this study, the decomposition of the electron density between the H,H contact into its NBO components will be compared to the FALDI-based decomposition. It is important to note here, that the FALDI cross-sections were compared to MO cross-sections, and found to be qualitatively identical in shape and nature and reveal much of the same information.^[17] Hence, the comparison of NBO-based decomposition to that of FALDI is a comparison with MO-based decomposition as well.

To start with, one can look at the comparison of the total electron density decompositions, shown in Figure 1. These cross-sections compare the NBO-based decomposition to the FALDI-based decomposition, whereby the total density (black line) was decomposed into the total concentrating density (blue line) and total depleting density (red line). Although quantitatively different, one can see that the overall trend is identical for NBO-based decomposition as for the FALDI-based decomposition. Figure 1a shows the grouped 2nd-derivative ED contributions, comparing the NBO-based decomposition to that of FALDI-based decomposition. These show that both the FALDI and NBO components contribute to a large concentration of the electron density between the *ortho*-hydrogens in the planar conformer. This indicates an accumulation of density into its inter-nuclear region which is not what one would expect for a steric clash. However, although the same trend is shown for both methods (i.e. concentration of density), NBO analysis does not provide the same topology of the total

electron density as FALDI analysis, and in turn MO analysis. One can see this from where the total density starts at -0.75 \AA , and from the topology of the density around the ring critical point (RCP). This causes a problem because the density from NBO analysis becomes incomparable to other methods. The same problem is recovered for the total electron density itself, shown for the twisted conformer in Figure 1b: the total density starts a lot higher at -0.75 \AA in the NBO analysis. Nonetheless, both methods show a larger contribution of concentrated density than depleting density, as well as a slight concentration of total density (shouldering) around the MDP. The same accumulation of density that was observed for the 2nd-derivative total density in planar was found for the twisted conformation as well (full cross-section comparisons are given in Part 2 of Appendix III).

This calls to question why only the planar conformation exhibits a DB and the twisted doesn't – this is explained by Figure 1c. This shows the $CP(\mathbf{r})$ function for both conformations, comparing the $CP(\mathbf{r})$ functions from the NBO contributions and the FALDI contributions. In the planar conformation the $CP(\mathbf{r})$ function is positive in the vicinity of the BCP between the *ortho*-hydrogens, and negative in the vicinity of the MDP in the twisted conformation. This means that the slope of the concentrating density is greater and opposite in sign than the slope of the depleting density (and removing density in the case of FALDI) in the planar conformation, forming the DB. The opposite is true in the case of the twisted conformer; the slope of the concentrating density is not greater and opposite in sign than the slope of the depleting density, even though the absolute value is much larger.

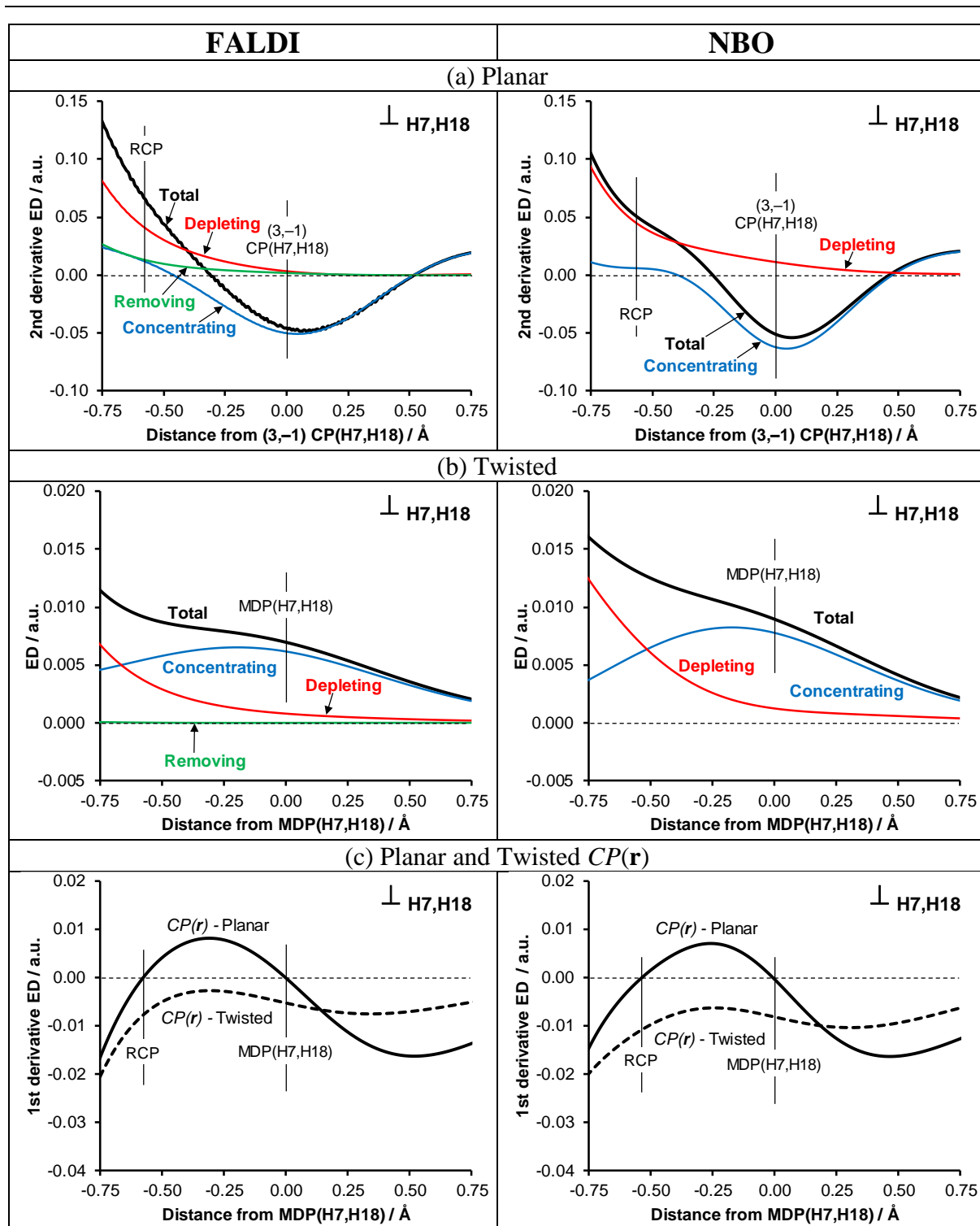
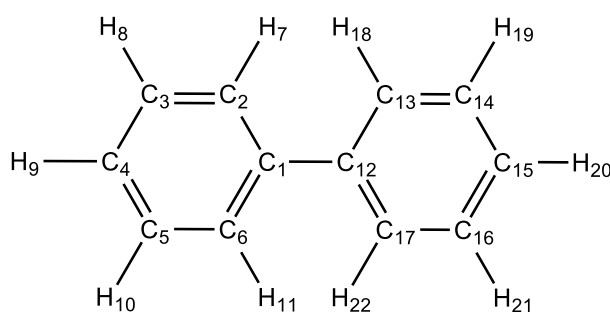


Figure 1. Cross-section comparison between FALDI-ED (left) and NBO-ED (right) analysis along λ_2 -eigenvector, crossing the BCP(H7,H18) and MDP(H7,H18) where applicable in planar and twisted biphenyl, respectively. (a) shows the decomposition of the partial second derivative of the total density in planar conformation, (b) shows the decomposition of total density in twisted conformation, and (c) shows the $CP(r)$ function for both planar and twisted conformations.

Now that it is shown that NBOs do in fact reproduce the same qualitative results as with FALDI-based decompositions in that they too predict an overall concentrating, i.e. energy-lowering nature of the H,H contact in planar Bph, the question now arises to which NBOs significantly contribute to the density. This information is provided in Table 1, providing the major NBOs that contribute to the concentrating and depleting density at the BCP and MDP in planar and twisted Bph, respectively. Furthermore, the atom(-pair) corresponding to each NBO is provided with its associated electron density contribution (a.u.) and its %-fraction. Because NBOs result in Lewis-like connections and FALDI decomposes density into atom-pair contributions, we should be able to directly compare the current results from NBO analysis with our previous study.^[17] Atom-numbering is provided in Scheme 2 below.



Scheme 2. Atom numbering of biphenyl

Table 1. Electron density contribution (a.u.) with its corresponding %-fraction for the major NBOs contributing to concentrating and depleting density at the BCP(H7,H18) in planar and MDP(H7,H18) in twisted biphenyl. For each NBO is also the given atom, or atom-pair that it describes and the corresponding type of NBO (e.g. bonding or Rydberg).

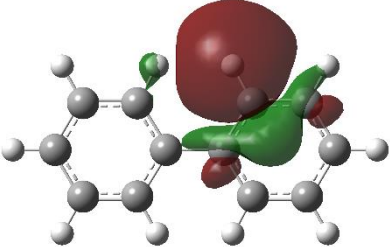
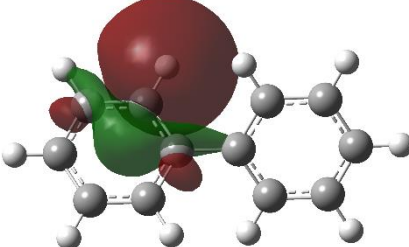
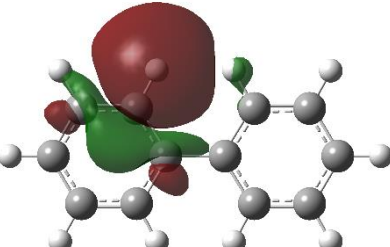
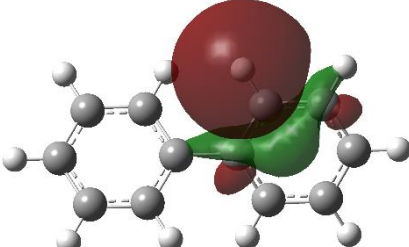
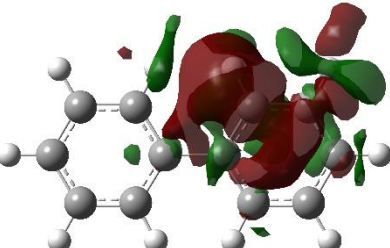
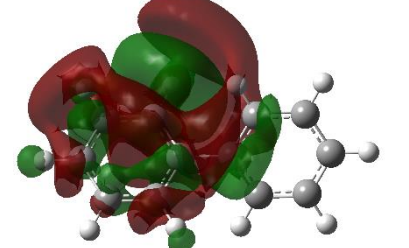
Planar		
Concentrating		
NBO	Orbital-Type / Atom(-Pair)	ED contribution a.u. / %-fraction
28	σ -Bonding / C13,H18	0.00620 / 42.4
29	σ -Bonding / C2,H7	0.00620 / 42.4
185	Rydberg / C13	0.00087 / 6.0
<i>Remaining</i>	–	<i>0.00023 / 1.6</i>
<i>Total</i>	–	<i>0.01351 / 92.4</i>
Depleting		
NBO	Orbital-Type / Atom(-Pair)	ED contribution a.u. / %-fraction
15	σ -Bonding / C2,C3	0.00034 / 2.3
16	σ -Bonding / C13,C14	0.00033 / 2.3
22	σ -Bonding / C1,C6	0.00011 / 0.8
21	σ -Bonding / C12,C17	0.00011 / 0.8
<i>Remaining</i>	–	<i>0.00022 / 1.5</i>
<i>Total</i>	–	<i>0.00112 / 7.6</i>
Twisted		
Concentrating		
NBO	Orbital-Type / Atom(-Pair)	ED contribution a.u. / %-fraction
35	σ -Bonding / C2,H7	0.00265 / 29.5
32	σ -Bonding / C13,H18	0.00265 / 29.5
109	Rydberg / C2	0.00227 / 25.2
37	π -Bonding / C2,C3	0.00016 / 1.8
<i>Remaining</i>	–	<i>0.00007 / 0.8</i>
<i>Total</i>	–	<i>0.00780 / 86.7</i>
Depleting		
NBO	Orbital-Type / Atom(-Pair)	ED contribution a.u. / %-fraction
41	π -Bonding / C12,C13	0.00035 / 3.9
14	σ -Bonding / C2,C3	0.00016 / 1.8
16	σ -Bonding / C13,C14	0.00016 / 1.8
21	σ -Bonding / C12,C17	0.00010 / 1.2
<i>Remaining</i>	–	<i>0.00041 / 4.6</i>
<i>Total</i>	–	<i>0.00119 / 13.3</i>

When looking at the individual NBOs that contribute to the density, two NBOs stand out jointly contributing 84.8% in the planar conformation, and 59.0% in twisted, namely the two covalent *ortho* C-H bonds of the bay-region (C2,H7 & C13,H18). The isosurfaces of these two NBOs, as well as the third largest contributor for both conformations, are shown in Table 2. The remainder of the NBO isosurfaces for all major contributions are given in Part 3 of Appendix III. This is qualitatively comparable to the decomposition into FALDI components, which also revealed that the largest contributions were from the covalent *ortho* C-H bonds. Notably, and again in line with our FALDI decomposition results, these NBOs are of σ -character.

Quantitatively however, the NBO-based decomposition causes some problems. Both decompositions into MO components and FALDI components revealed that this H,H contact is due to extreme delocalisation throughout the molecule. Many MOs and atom-pairs contribute in conjunction to place the density in the inter-nuclear region of the *ortho*-hydrogens, however decomposition into NBO components suggests a localised view of the density. This cannot be the case.

The reason to why NBOs give this extreme localised view is due to NBO formalism, whereby the NBOs will be described as one atom-pair, though as one can see from their isosurfaces, they are far more delocalised than one would expect, covering more than just those two atoms. This is why they account for so much of the density. This is a fault with the NBO method. Furthermore, the Rydberg orbitals that contribute a significant amount, 6.0% in planar and 25.2% in twisted, represent atoms C13 and C2, respectively. By taking a look at these isosurfaces, one can see why they contribute such a large amount – they have a large delocalisation which is near impossible to interpret, however the NBO method still represents these NBOs as single atom contributions.

Table 2. Isosurfaces of the most significant (above 5% contribution) NBO contributions (Isovalue 0.02 a.u.) at the (3,-1) CP(H7,H18) and MDP(H7,H18) in **planar** and **twisted** biphenyl, respectively.

Planar	Twisted
NBO; ED contribution a.u. / %-fraction, <i>nature</i>	
NBO 28; 0.00620 / 42.4, <i>conc</i>	NBO 35; 0.00265 / 29.5, <i>conc</i>
	
NBO 29; 0.00620 / 42.4, <i>conc</i>	NBO 32; 0.00265 / 29.5, <i>conc</i>
	
NBO 185; 0.00087 / 6.0, <i>conc</i>	NBO 109; 0.00227 / 25.2, <i>conc</i>
	

Apart from the NBO- and FALDI-based decompositions being in agreement with regards to the two largest interactions, past that they deviate. For example, in planar Bph NBOs 15 and 16 representing C2,C3 and C13,C14, respectively, are depleting in NBO analysis, but in FALDI analysis they are concentrating. This specific problem can be seen for both conformations. This is not the only issue however with NBO analysis. In FALDI analysis we see direct symmetry in the major interactions in both planar and twisted conformers, i.e. if C1,C2 was concentrating, then C12,C13 would also be concentrating with identical (or near identical) electron density contribution. This is not the case with NBO-based decomposition, as can be seen in the depleting density for the twisted conformation; C12,C13 is depleting but the symmetrical C1,C2 is not picked up.

5.6. Conclusions

The main principle of the work presented in this chapter is to validate the work previously conducted from the decomposition of electron density into MO and FALDI contributions. Although historically in this scientific debate, an orbital based method has generally concluded that the interaction between the *ortho*-hydrogens in planar Bph (and other similar systems) is of a steric clash – this is clearly not the case. This chapter followed the same analysis as the previous two studies,^[12, 17] by decomposing the density at the BCP and MDP of the H,H contact in planar and twisted Bph, respectively. The previous studies involved decomposing the densities into MO contributions and FALDI contributions, and this study decomposes the density into NBO contributions.

When compared to FALDI-based decomposition, one can see that the total electron density decompositions into NBO contributions reveals that the overall trends are the same; there is an accumulation (i.e. concentration) of density around the BCP and the MDP of both conformers. Along with this, the cross-section analysis revealed that both FALDI- and NBO-based decompositions show that the absence of a DB in the twisted conformation is due to the slopes of the concentrating density not being greater and opposite in sign than the slope of the depleting density. On top of this, NBO analysis found that the two largest contributions to the density at both the BCP and MDP are due to the covalent *ortho* C-H bonds of the bay-region, in line with the results from FALDI, further confirming that this is a CH \cdots HC interaction rather than purely an H \cdots H interaction.

Although NBO analysis revealed much of the same information as FALDI analysis, it still falls short in comparison. Both MO and FALDI analysis are directly comparable in that they have an identical topology of the total electron density, whereby from Figure 1 we see that this NBO analysis deviates largely (although follows the same trend). Furthermore, both of the previous studies unveiled that this interaction is due to large molecular wide delocalisation –

there is a large interplay from all components to form this density between the *ortho*-hydrogens. NBO on the other hand gives a very localised view of this interaction, making the assumption that $\pm 85\%$ of the density is due to just two covalent bonds. The remaining contributing NBOs deviate from the findings from FALDI analysis, in which the nature (concentrating or depleting) of the NBOs do not match up with the corresponding atom-pair contributions from FALDI. On top of that, symmetrical NBOs are not always unveiled; in FALDI-based decomposition, even for the smallest contributions, you can find the symmetrical atom-pair of near-identical contribution and nature. This inconsistency in NBOs can be chalked up to the fact that the wavefunctions in NBO calculations are manipulated and forced to represent conventional Lewis-structures, and with highly delocalised systems such as with Bph, the accuracy seems to drop as we have smaller, non-covalent interactions.

This brings us to the conclusion that although NBO analysis shows similar trends as FALDI analysis, NBOs are not suited to study weak, non-covalent interactions, since they do not accurately detect the extent of delocalisations in the molecule.

5.7. References

1. Bader, R.F.W. *Atoms in Molecules: A Quantum Theory*; Oxford University Press: Oxford, 1990.
2. Cioslowski, J.; Mixon, S.T. *Can. J. Chem.* **1992**, *70*, 443-449.
3. Poater, J.; Solà, M.; Bickelhaupt, F.M. *Chem. Eur. J.* **2006**, *12*, 2889-2895.
4. Weinhold, F.; Schleyer, P.v.R.; McKee, W.C. *J. Comput. Chem.* **2014**, *35*, 1499-1508.
5. Pendás, A.M.; Francisco, E.; Blanco, M.A.; Gatti, C. *Chem. Eur. J.* **2007**, *13*, 9362-9371.
6. Blanco, M.A.; Martín Pendás, A.; Francisco, E. *J. Chem. Theory Comput.* **2005**, *1*, 1096-1109.
7. Eskandari, K.; Van Alsenoy, C. *J. Comput. Chem.* **2014**, *35*, 1883-1889.
8. Popelier, P.L.; Maxwell, P.I.; Thacker, J.C.; Alkorta, I. *Theor. Chem. Acc.* **2019**, *138*, 12.
9. Cukrowski, I.; de Lange, J.H.; Adeyinka, A.S.; Mangondo, P. *Comput. Theor. Chem.* **2015**, *1053*, 60-76.
10. de Lange, J.H.; van Niekerk, D.M.; Cukrowski, I. *J. Comput. Chem.* **2018**, *39*, 973-985.
11. de Lange, J.H.; van Niekerk, D.M.; Cukrowski, I. *Phys. Chem. Chem. Phys.* **2019**, *21*, 20988-20998.
12. Cukrowski, I.; de Lange, J.H.; van Niekerk, D.M.; Bates, T.G. *J. Phys. Chem. A* **2020**, *124*, 5523-5533.
13. de Lange, J.H.; Cukrowski, I. *J. Comput. Chem.* **2017**, *38*, 981-997.
14. Cukrowski, I.; van Niekerk, D.M.; de Lange, J.H. *Struct. Chem.* **2017**, *28*, 1429-1444.
15. de Lange, J.H.; Cukrowski, I. *J. Comput. Chem.* **2018**, *39*, 1517-1530.
16. de Lange, J.H.; van Niekerk, D.M.; Cukrowski, I. *J. Comput. Chem.* **2018**, *39*, 2283-2299.
17. Bates, T.G.; de Lange, J.H.; Cukrowski, I. *Submitted to Phys. Chem. Chem. Phys.* **2020**.
18. M. Frisch, G. Trucks, H. Schlegel, G. Scuseria, M. Robb, J. Cheeseman, G. Scalmani, V. Barone, B. Mennucci, G. Petersson, H. Nakatsuji, X. Li, M. Caricato, A. Marenich, J. Bloino, B. Janesko, R. Gomperts, B. Mennucci, H. Hratchian, J. Ortiz, A. Izmaylov, J. Sonnenberg, D. Williams-Young, F. Ding, F. Lipparini, F. Egidi, J. Goings, B. Peng, A. Petrone, T. Henderson, D. Ranasinghe, V. Zakrzewski, J. Gao, N. Rega, G. Zheng, W. Liang, M. Hada, M. Ehara, K. Toyota, R. Fukuda, J. Hasegawa, M. Ishida, T. Nakajima, Y. Honda, O. Kitao, H. Nakai, T. Vreven, K. Throssell, J. J. Montgomery, J. Peralta, F. Ogliaro, M. Bearpark, J. Heyd, E. Brothers, K. Kudin, V. Staroverov, T. Keith, R. Kobayashi, J. Normand, K. Raghavachari, A. Rendell, J. Burant, S. Iyengar, J. Tomasi,

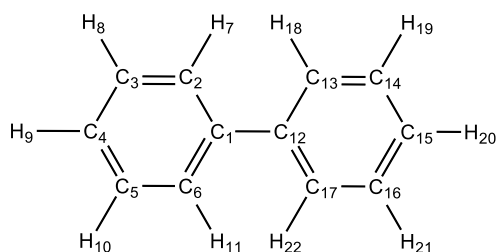
- M. Cossi, J. Millam, M. Klene, C. Adamo, R. Cammi, J. Ochterski, R. Martin, K. Morokuma, O. Farkas, J. Foresman, D. Fox, Gaussian, Inc., Wallingford CT, **2009**.
19. Glendening, E.D.; Landis, C.R.; Weinhold, F. *Wiley Interdiscip. Rev. Comput. Mol. Sci.* **2012**, 2, 1-42.
20. AIMAll (Version 19.02.13), Keith, T. A. TK Gristmill Software, Overland Park KS, USA, **2019** (aim.tkgristmill.com).

Chapter 6

Conclusions

6.1. Summary

This dissertation takes on an unambiguous analysis of the density between *ortho*-hydrogens in planar biphenyl (Bph) that has been a topic of debate for almost three decades. This debate has not been about whether the density exists between the CH \cdots HC interaction, but rather questioning the nature of this interaction. It is known that the equilibrium structure of Bph is ‘twisted’ with a dihedral angle (ϕ) of $\pm 42^\circ$ between the two rings and has a rotational barrier of 2.1 kcal.mol $^{-1}$ between the twisted conformation and its planar transition state ($\phi=0^\circ$). If we looked at this molecule through the lens of classical chemistry, it would be reasoned that the *ortho*-hydrogens take part in a steric clash in planar Bph (H7,H18 in Scheme 1), which causes the molecule to become twisted. This is in essence the argument made by one side of the debate. The other side argues that these hydrogens are actually stabilising in planar Bph, and agrees with the QTAIM^[1] position, that a density bridge (DB, referred to as a bond path, BP, in the scopes of QTAIM) exists between *ortho*-hydrogens, and that it represents a bonding process that stabilises the planar conformation.



Scheme 1. Atom numbering of biphenyl

A pivotal aspect of this research is that there has been a divide about the nature of the DB in planar Bph. As mentioned prior to this chapter, the studies done thus far can be grouped into orbital- and density-based studies, the former suggesting a non-bonding, steric clash, and the latter suggesting a bonding or at the very least, a stabilising interaction. This research joined the debate by primarily making use of the in-house developed *cross-section decomposition* analysis to decompose the densities at the CH \cdots HC bond critical, or minimal density, point (BCP or MDP) in the planar and twisted conformation of Bph, respectively. Of the four aims

presented in Chapter 1, cross-section analysis was able to achieve each goal, perhaps most significantly that the orbital- and density-based analyses can be reconciled.

The results were divided into three parts: cross-section analysis of the decomposition of electron density (ED) into (i) molecular orbital (MO) contributions, (ii) FALDI contributions, and (iii) natural bond orbital (NBO) contributions. Each chapter follows on from the previous, creating somewhat of a story, further elaborating on the nature and origins of the density within the H,H contact.

To briefly recap, the cross-section analysis decomposes the total ED along the λ_2 -eigenvector, crossing the BCP(H,H) or MDP(H,H). The decomposition reveals the individual contributors to the density, and from the directional second partial derivative (2^{nd} -derivative), one can determine their nature. The classification is as follows:

1. If the 2^{nd} -derivative ED < 0 around the BCP(H,H)/MDP(H,H), then the contributor is *concentrating*.
2. If the 2^{nd} -derivative ED > 0 around the BCP(H,H)/MDP(H,H), then the contributor is *depleting*.
3. In the case of FALDI-ED only, a third nature is defined, whereby if the ED at the BCP(H,H)/MDP(H,H) is negative, then the contributor is *removing*.
4. If the contribution at the BCP(H,H)/MDP(H,H) is negligible, then the contributor is *non-contributing*.

In the first results-chapter, Chapter 3, the MO-ED (cross-section decomposition of the ED into MO contributions) and MO-DI methods were applied.^[2] Within this study, three cases were analysed: (i) classical C-C and C-H covalent interactions, (ii) ‘steric’ CH \cdots HC interaction in the planar and twisted conformations of Bph and (ii) ‘steric’ H \cdots H interactions in the cubic Li₄H₄ structure. In all three cases, it was seen in the cross-section analysis that the ED at the BCP(H,H) and MDP(H,H) were made up of a multitude of MOs spanning the whole molecule,

rather than a single major contributing MO. On top of this, the total density in all three cases (planar and twisted Bph alike) has a negative 2nd-derivative around the BCP(H,H) and MDP(H,H). However, this causes a problem in that the twisted conformer of Bph does not exhibit a BP, only planar does. Therefore, a closer look was taken into the rates of change (1st-derivative) of the ED by making use of the $CP(\mathbf{r})$ function. In the case of the classical C-C and C-H covalent bonds, the $CP(\mathbf{r})$ function has a positive region around the BCPs, predicting that a DB is present between the two atoms (which we know are covalently bonded). This means that the slopes of the concentrating components are larger and opposite in sign than the slopes of the depleting and removing components. In the case of planar and twisted Bph however, only planar has this positive region. This leads to a major conclusion of this work and the achievement of our first aim:

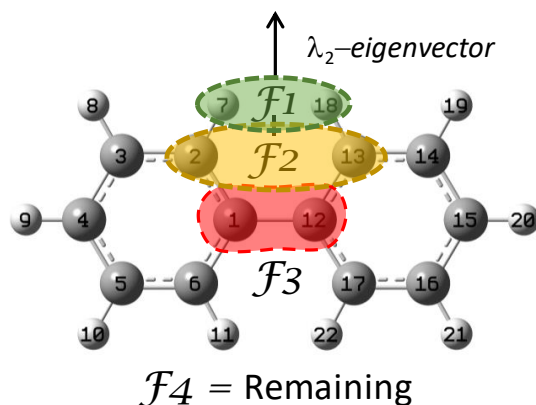
Although the 2nd-derivative must be negative around the BCP(H,H) or MDP(H,H) for a DB to be present, another deciding factor is apparent; the rates of change of the concentrating components must be greater and opposite in sign than the depleting component.

This MO-based analysis was furthered by utilising the MO-DI method. Similarly to how the density at the BCP(H,H) or MDP(H,H) was decomposed into individual MO contributions, the MO-DI method decomposes the QTAIM delocalisation index (DI) into MO contributions. From this, one can determine the extent each MO contributes electron pairs to the DI, and also how the MOs interact together. Some MOs interfere constructively, increasing the delocalised electron pairs within the overlapped atomic basins, whereas others interfere destructively, decreasing the delocalised electron pairs – this resembles concept of bonding and antibonding in MO theory. From the joint analysis of MO-ED and MO-DI, it was seen that all the MOs that contribute concentrating density to the DB also interfere constructively with the other

concentrating MOs, increasing the degree of covalency of the interaction. This was seen likewise with both the classical covalent bonds, and the CH \cdots HC interaction in planar Bph.

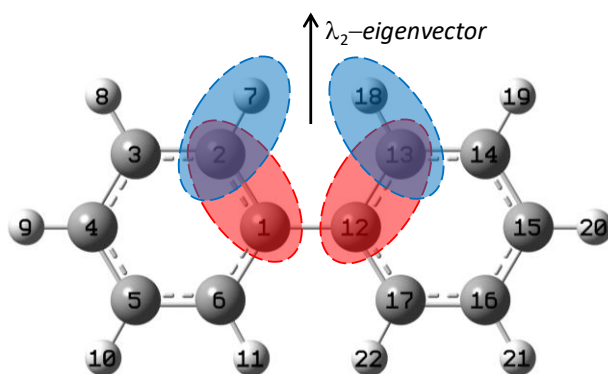
In the second results-chapter, Chapter 4, cross-section decomposition of the ED was conducted, whereby in this case, the density was decomposed into FALDI components.^[3] There are two aspects of this study, that work hand-in-hand: (i) FALDI fragment analysis and (ii) FALDI diatomic analysis. Before addressing the fragment analysis, the diatomic analysis will be expanded upon first.

There are 41 MOs in Bph, and so the MO-ED method decomposes the density into 41 individual MO contributions. However, the FALDI-ED method can decompose the ED into atom-pair contributions, of which there are 231 atom-pairs in Bph. Not only does this provide a higher resolution into the effects at play at the BCP(H,H)/MDP(H,H), but we also obtain contributions in more chemically intuitive terms, i.e. atom-pairs compared to molecular wide delocalised MOs. The fragment analysis on the other hand allows one to form fragments of ones choosing within the molecule and determine the degree of contribution and nature of its contribution to the density measured. This analysis looks at both intra-fragment contributions (contributions made to the density due to each atom-pair delocalisation within the fragment) and inter-fragment contributions (contributions made to the density due to each atom-pair *between* two fragments). This highlights an advantage of FALDI, as previously one would need to fragment the molecule into arbitrary, unchemical radical states (physically remove parts of the molecule), however FALDI maintains the molecular and electronic integrity of the molecule.



Scheme 2. Definition of fragments for FALDI analysis. \mathcal{F}_1 : H7...H18, \mathcal{F}_2 : C2...C13, \mathcal{F}_3 : C1–C12 linker and \mathcal{F}_4 : combined fragment containing remainder of the molecule. The position and direction of the λ_2 -eigenvector used for cross-section analysis is also shown.

In Scheme 2 above, one can see how Bph was fragmented in both conformers. This analysis provided similar results for both planar and twisted conformations, whereby the inter-fragment delocalisation between \mathcal{F}_1 and \mathcal{F}_2 , consisting of the two *ortho*-hydrogens and *ortho*-carbons in the bay-region, contributed the largest amount of density, of a concentrating nature, to the BCP(H,H) and MDP(H,H). We found that the largest depleting fragment contribution to the aforementioned density was the inter-fragment delocalisation of \mathcal{F}_2 and \mathcal{F}_3 .



Scheme 3. Illustration of the major atom-pair contributions. Atom-pairs in blue demarcate the concentrating atom-pairs contributing the most to both the intra-fragment delocalisation \mathcal{F}_1 and to the density at CP(H,H) and MDP(H,H). Atom-pairs in red demarcate the depleting atom-pairs contributing the most to the inter-fragment delocalisation between $\mathcal{F}_1, \mathcal{F}_2$ and to the density at CP(H,H) and MDP(H,H).

Upon analysing the diatomic interactions, we obtain a deeper explanation into the fragment analysis and determined the atom-pair origin of the density at the BCP(H,H) and MDP(H,H).

As mentioned above, the inter-fragment delocalisation between \mathcal{F}_1 and \mathcal{F}_2 contributed the vast

majority of density, and by inspecting the atom-pair contributions we found that the two covalent *ortho* C-H bonds (illustrated in blue in Scheme 3) donates more than half of the density to BCP(H,H) and MDP(H,H) in both planar and twisted Bph, in-line with the fragment analysis. One might have assumed that H7,H18 would have been the main contributor, but this atom-pair contributed only 3.5% in planar and 1.5% and twisted. The largest depleting density was from the inter-fragment delocalisation of $\mathcal{F}2$ and $\mathcal{F}3$, and the largest contributing atom-pairs responsible for this are due to the relatively small contributions (in comparison to the two *ortho* C-H atom-pairs) of C1,C2 and C12,C13 atom-pairs in both conformers (illustrated in red in Scheme 3). This insight is first of its kind and leads to the achievement of our second aim:

Although one would have assumed that the origin of the density at BCP(H,H) and MDP(H,H) would have been from H7,H18, it is rather due to a channel of density formed from the large delocalisation of density throughout the molecule, with the largest contributions being from the delocalisation of the two covalent C-H bonds in the bay-region.

Outside of looking at the individual contributors, the overall cross-sections were compared to that of MO-ED. This comparison without a doubt shows that qualitatively, FALDI-ED and MO-ED describe the density at BCP(H,H) and MDP(H,H) in the same way: (i) they both show an overall concentrating nature of the total density along the λ_2 -eigenvector, (ii) the concentrating density overshadows the depleting density, and (iii) the rates of change of the concentrating density is indeed larger and opposite in sign than the depleting density, causing only the planar conformer to have a DB linking the *ortho*-hydrogens. Furthermore, the two analyses show that the density is due to a vast delocalisation throughout the molecule, as shown from the numerous MOs and atom-pairs that contribute to the density within the H,H contact.

The third, and final results-chapter, Chapter 5, follows on and concludes the cross-section decomposition investigations by using this technique to decompose the ED within the H,H

contact into NBO contributions. The cross-sections of the total ED decomposition were compared with those obtained from FALDI, and overall, they produce similar results, just as FALDI-ED had done with MO-ED, in that both conformations have an accumulation/concentration of density around the BCP(H,H) and MDP(H,H). On top of that, NBO decomposition also produced somewhat similar results to FALDI, whereby in both conformers the *ortho* C-H bonds in the bay-region contribute the largest amount of concentrating density to the BCP(H,H) and MDP(H,H). However, NBOs had its setbacks due to the wavefunctions being transformed to resemble, as much as possible, Lewis-like bonds. This caused a reduction in resolution in which symmetrical NBOs (NBOs depicting symmetrical atom-pairs) were not always detected with an equal donation of density. On top of this, NBO-ED did not always produce the same results as FALDI-ED did in terms of the nature of identical contributions. Finally, although NBOs showed that the two *ortho* C-H bonds contributed the majority of density to the CP(H,H) and MDP(H,H), NBOs give a highly localised view of this density, whereas FALDI and MO analysis shows that the density is due to molecular wide delocalisation.

Overall, taking into account all three analyses on the density at the BCP(H,H) and MDP(H,H) in the planar and twisted conformation, respectively, from different viewpoints (MOs, FALDI density, and NBOs), we achieved the last two aims set out in Chapter 1:

From the three analyses on the measured densities in planar and twisted Bph, we see that the density in both conformations is concentrating. This suggests that even though the density delocalised between the two ortho-hydrogens is small, a weak covalent bond is formed.

which leads to the following

Although prior to this work, orbital- and density-based methods were at odds about the overall nature of the ortho-hydrogens, this work

reconciles the two families, as both our orbital-based analyses (MOs and NBOs) show the same overall picture as our density-based analysis (FALDI) – no matter where the density comes from, it remains the same and all point to a concentrating DB in planar Bph.

From the analyses of all three density methods, my judgement would be that FALDI-ED is best suited for density decomposition analysis. Not only does it provide a higher resolution in regard to the contributions to a measured density, it provides the contributions in chemically intuitive terms. One can determine the origin as well as the nature of the density in terms of molecular fragments and atomic pairwise contributions. Previously, a common method of fragmenting the molecule would have been done by cutting the molecule into arbitrary, unchemical radical states. Poater *et al.*^[4] had done this by ‘cutting’ off the *ortho*-hydrogens, converting Bph into a tetra-radical molecule, but the question arises as to whether this would still represent Bph, or would the electronic environment change too much? This wasn’t directly addressed in these studies; however, it highlights another advantage of FALDI that was utilised in Chapter 4 – FALDI allows for the fragmentation of a molecule, whilst keeping the molecular and electronic integrity intact.

Throughout these studies, a common trend occurs – DBs are not signals of *privileged* exchange channels as defined by Pendás *et al.*^[5] MO-, FALDI- and NBO-ED all show that a collaboration of multiple interactions leads to the formation of DBs rather than just one exchange channel. This was similarly concluded by de Lange *et al.*^[6]

The presence of a DB is generally thought to coincide with the idea of stabilisation of the molecule. Popelier *et al.*^[7] noted that DBs are an energy lowering phenomenon, in which the electrons configure themselves in such a way to bring the molecule to its lowest energy state. However, we should try to disregard the notion of a chemical *bond*. This noun presumes that a chemical bond is a real, physical object within a molecule. Rather, we should replace this term

with the concept of *bonding* between two or more atoms, as this represents a process of stabilisation and energy lowering in a system.^[8] This work leads us to the conclusion that the CH \cdots HC interaction in the planar conformer of Bph is *bonding*, with MOs, FALDI and NBOs to back this up. These *ortho*-hydrogens do in fact have a DB linking them, leading to a weak covalent interaction, and this is largely due to the densities from both C-H atom-pairs in the bay-region forming an ED channel between the hydrogens.

6.2. Future Work

Whilst this dissertation primarily covers a density argument supporting the notion of a bonding process between the *ortho*-hydrogens in planar Bph, there is a lot of work that could still be done surrounding this topic.

One focus point would be to study the energetics of planar and twisted Bph. With the use of FAMSEC^[9] one can fragment the molecule (whilst keeping the integrity of the molecule intact) and determine which fragments are stabilised/destabilised, as well as look at atom-pair stabilities. This would shed light into why the equilibrium conformation is twisted and identify the cause of destabilisation within the planar conformer. It has been argued by Matta *et al.*^[10] as well as others^[7, 11-12] that the CH \cdots HC interaction is actually stabilising, but if the CH \cdots HC interaction is not the cause of the destabilisation, then FAMSEC could shed light on the real source.

Another promising study would be the analysis of the substituent effects on Bph. By adding substituents in varying positions of Bph, one can look at how meta-directing and ortho/para-directing groups effect (i) the density between the *ortho*-hydrogens, (ii) the overall stability of the molecule, (iii) the dihedral angle between the two rings and (iv) the rotation barrier between planar and the twisted substituted-Bph. One could also incorporate artificial intelligence/machine learning to aid in this analysis.

6.3. References

1. Bader, R.F.W. *Atoms in Molecules: A Quantum Theory*; Oxford University Press: Oxford, 1990.
2. Cukrowski, I.; de Lange, J.H.; van Niekerk, D.M.; Bates, T.G. *J. Phys. Chem. A* **2020**, *124*, 5523-5533.
3. Bates, T.G.; de Lange, J.H.; Cukrowski, I. *Submitted to Phys. Chem. Chem. Phys.* **2020**.
4. Poater, J.; Solà, M.; Bickelhaupt, F.M. *Chem. Eur. J.* **2006**, *12*, 2889-2895.
5. Pendás, A.M.; Francisco, E.; Blanco, M.A.; Gatti, C. *Chem. Eur. J.* **2007**, *13*, 9362-9371.
6. de Lange, J.H.; van Niekerk, D.M.; Cukrowski, I. *J. Comput. Chem.* **2018**, *39*, 2283-2299.
7. Popelier, P.L.; Maxwell, P.I.; Thacker, J.C.; Alkorta, I. *Theor. Chem. Acc.* **2019**, *138*, 12.
8. Bader, R.F.W. *J. Phys. Chem. A* **1998**, *102*, 7314-7323.
9. Cukrowski, I.; Sagan, F.; Mitoraj, M.P. *J. Comput. Chem.* **2016**, *37*, 2783-2798.
10. Matta, C.F.; Hernández-Trujillo, J.; Tang, T.H.; Bader, R.F.W. *Chem. Eur. J.* **2003**, *9*, 1940-1951.
11. Hernández-Trujillo, J.; Matta, C.F. *Struct. Chem.* **2007**, *18*, 849-857.
12. Eskandari, K.; Van Alsenoy, C. *J. Comput. Chem.* **2014**, *35*, 1883-1889.

Appendix I

Molecular Orbitals Support Energy-Stabilizing 'Bonding' Nature of Bader's Bond Paths

Published in:

Journal of Physical Chemistry A **2020**, *124*, 5523-5533. DOI: 10.1021/acs.jpca.0c02234.

Supplementary Information

Molecular Orbitals Support Energy-Stabilizing ‘Bonding’ Nature of Bader’s Bond Paths

Ignacy Cukrowski,* Jurgens H. de Lange, Daniël M. E. van Niekerk and Thomas G. Bates

*Department of Chemistry, Faculty of Natural and Agricultural Sciences, University of Pretoria,
Lynnwood Road, Hatfield, Pretoria 0002, South Africa*

Supporting Information

*Correspondence to: Ignacy Cukrowski

E-mail: ignacy.cukrowski@up.ac.za

Content	Page
Part 1. Theoretical background	
The MO-ED method	137
The MO-DI method	142
Part 2. Cartesian coordinates of molecules studied	
Planar biphenyl	146
Twisted biphenyl	147
Li ₄ H ₄	148
Part 3. Canonical molecular orbitals in biphenyl	
Planar biphenyl	149
Twisted biphenyl	156
Part 4. Data pertaining to covalent bonds in biphenyl	
MO-ED and MO-DI data	163
Decomposition of the total-ED at CP(C1,C12) and CP(C19,H22)	168
Part 5. Data pertaining to CP/MDP(H7,H18) in the planar/twisted biphenyl	
MO-ED and MO-DI data	170
Decomposition of the total-ED at relevant CP/MDP(H7,H18)	175
Part 6. Data pertaining to H ···H density bridges in Li₄H₄	
MO-ED and MO-DI data	177
Decomposition of the total-ED at the CP(H2,H5)	180

Part 1

A theoretical background

The MO-ED Method

The MO-ED method seeks to describe the total electron density, as well as its topology, in terms of molecular orbital density contributions. Specifically, we aim here to describe the presence of a density bridge, with its associated critical point, in terms of MO densities. To do so we will first review some preceding topics related to the topology of the electron density.

The topology of the electron density

Within the field of Quantum Chemical Topology (QCT), a critical point (CP) in the electron density (ED) at a coordinate \mathbf{r}_c is a local maximum, minimum or a saddle point where the first derivative (and each of its three components) vanishes:

$$\nabla\rho(\mathbf{r}_c) = \mathbf{i}\frac{\partial\rho}{\partial x} + \mathbf{j}\frac{\partial\rho}{\partial y} + \mathbf{k}\frac{\partial\rho}{\partial z} = 0 \quad (1)$$

Each CP is a local maximum or minimum along each of the three principle axes corresponding to maximum curvature. The type of CP can be determined by evaluating components of the Hessian matrix, which describe the partial second derivatives of the ED at \mathbf{r}_c :

$$\mathbf{A}(\mathbf{r}_c) = \begin{pmatrix} \frac{\partial^2\rho}{\partial x^2} & \frac{\partial^2\rho}{\partial x\partial y} & \frac{\partial^2\rho}{\partial x\partial z} \\ \frac{\partial^2\rho}{\partial y\partial x} & \frac{\partial^2\rho}{\partial y^2} & \frac{\partial^2\rho}{\partial y\partial z} \\ \frac{\partial^2\rho}{\partial z\partial x} & \frac{\partial^2\rho}{\partial z\partial y} & \frac{\partial^2\rho}{\partial z^2} \end{pmatrix} \quad (2)$$

The Hessian matrix can be diagonalized to give three curvatures along the principle axes at \mathbf{r}_c , yielding three eigenvalues, λ_1 , λ_2 and λ_3 , and associated eigenvectors. The sign of each eigenvalue reveals whether \mathbf{r}_c is a local minimum or maximum along the associated eigenvector, where positive and negative eigenvalues relate to local minima and maxima, respectively.

Each CP can be classified according to its partial first and second derivatives, and is given a rank, ω , and signature, σ . The rank determines the number of non-zero curvatures (eigenvalues of the Hessian matrix). In other words, a rank of (+3) indicates that a CP is a local maximum or minimum in all three principle axes. The signature is the algebraic sum of the signs of the eigenvalues, and a signature of (−1) indicates that \mathbf{r}_c is a local minimum in one axis but a local maximum in the remaining two axes (+1 −1 −1 = −1). While many CPs of rank 1 and 2 exist in

any ED distribution, only a number of CPs of rank 3 will exist, subject to the Poincaré-Hopf relationship,¹ and rank 3 CPs are therefore of particular use in QCT.

The topology of the ED is generally dominated by the electrostatic attractive force between nuclei and electrons, and as such, every nuclear coordinate is marked by a (+3,-3) CP – a local maximum in all three principle axes. (+3,-1) CPs are often found between pairs of nuclei and are known as bond critical points (BCPs). CPs found within a ring of nuclei are (+3,+1) CPs, known as ring critical points (RCPs), and a CP enclosed by a number of ring critical points is always a (+3,+3) CP, known as a cage critical point (CCP).

QCT has revealed a peculiar property regarding the ED distribution between nuclei. A BCP is always observed at the interface between two zero-flux surfaces outside of the limit at infinity, *i.e.* interatomic zero-flux surfaces. Two gradient vectors originate at each of the enclosed nuclei and terminate at the BCP. The path defined by these two vectors is known as a density bridge (DB, also known as a *bond path* or a *line path*²). The ED is at a local maximum perpendicular to the DB at each and every coordinate of the DB. A DB is a remarkable yet still misunderstood property of the ED. The collection of DBs gives rise to a *molecular graph*, which defines QTAIM-based atomic connectivity.

Two of the eigenvalues of the Hessian matrix (λ_1 and λ_2) will be negative at each and every coordinate of a DB, indicating a negative partial second derivative along the principle vectors perpendicular to the DB itself. A negative partial second derivative at \mathbf{r} , $\frac{\partial^2 \rho(\mathbf{r})}{\partial \mathbf{r}^2}$, can be seen as a measure of local *concentration* of the ED, in that the ED at \mathbf{r} is greater than the average of its neighbouring coordinates along a specific vector.⁷ Along the DB, the third eigenvalue of the Hessian matrix (λ_3) will always be positive, indicating a local *depletion* of ED. Generally, at a given coordinate \mathbf{r} along an internuclear vector and as long the two nuclei are not part of a cage, $\lambda_1 < 0$ and $\lambda_3 > 0$. The sign of the remaining eigenvalue, λ_2 , then generally determines whether ED is concentrated at \mathbf{r} relative to its neighbouring environment, thereby forming an DB if a CP is present, or whether the ED is depleted. Such concentrations and depletions have been used extensively by both QTAIM and other QCT techniques, such as the Noncovalent Interactions (NCI) technique,^{3,4} to indicate ‘*attractive*’ or ‘*repulsive*’ interactions. However, some of us previously showed⁵ that measures of ED concentration utilising λ_2 is only relative to the local environment where it is measured.

Cross-sections along λ_2 -eigenvector

As stated above, the presence of a DB can be fully determined in most circumstances from investigation of i) the partial directional first derivative and ii) the sign of the partial directional second derivative of the ED along the eigenvector associated with the λ_2 eigenvalue of the Hessian matrix. We will henceforth refer to this eigenvector simply as the λ_2 -eigenvector. We have previously noted^{5,6} that the ED distribution, as well as decompositions of the ED, of cross-sections along this vector can provide tremendous information regarding *why* a DB for a particular chemical interaction is present or not. Specifically, the overall concentration or depletion of ED along the λ_2 -eigenvector provides valuable information regarding the character of the interaction, and the individual concentration or depletion of ED decomposition products can provide insight into the underlying mechanics. Cross-sections along one of the other principle axes, *i.e.* λ_1 - or λ_3 -eigenvectors, can provide useful information regarding the ED concentration/depletion relative to different interatomic interactions.

Decomposition of ED and its topology in terms of MO densities

The ED can easily be decomposed in terms of canonical or natural molecular orbitals (MOs),

$$\rho(\mathbf{r}) = \sum_i^{N_{MO}} v_i |\chi_i(\mathbf{r})|^2 \quad (3)$$

where χ_i is an MO with occupation v_i . The coordinate \mathbf{r} can be varied (specifically, in this case, along the λ_2 -eigenvector) in order to measure the orbital contributions to the ED in a region of real-space, as well as then calculate partial directional first and second derivatives.

It is useful to define a consistent and universal coordinate, \mathbf{r}^* , which can be used to quantify an orbital's ED contribution to any internuclear region in a transferable fashion. While there are potentially multiple different approaches to define such an \mathbf{r}^* , we have decided to use the topology of the ED as a general guide. If a (3,-1) CP is present, then we define $\mathbf{r}^* = \mathbf{r}_c$, the coordinate of the CP. If a (3,-1) CP is not present, then we set \mathbf{r}^* to be the position of the minimum density point (MDP)¹⁵, which is defined as the coordinate on an internuclear vector where the ED is at a minimum. The MDP is well-defined for any given atom-pair, and the MDP and BCP often coincides to the same coordinate unless the corresponding DB is particularly bent.

Next, we consider the partial directional second derivatives along the λ_2 -eigenvector of each MO density as measured at \mathbf{r}^* , $\frac{\partial^2 v_i |\chi_i(\mathbf{r}^*)|^2}{\partial \lambda^2}$. We can label each MO as concentrating ED (negative second derivative), depleting ED (positive second derivative), non-contributing to the ED (in the case of an MO node) or removing ED (in the case of negative occupations in multi-reference

wavefunctions). The ED at \mathbf{r}^* can then be defined in terms of MO components with different characters:

$$\begin{aligned} \rho(\mathbf{r}^*) &= \rho_{\text{concentrating}}(\mathbf{r}^*) + \rho_{\text{depleting}}(\mathbf{r}^*) + \rho_{\text{non-contributing}}(\mathbf{r}^*) \\ &+ \rho_{\text{removing}}(\mathbf{r}^*) \end{aligned} \quad (4)$$

Each individual MO's character is therefore defined relative to a specific internuclear region, as opposed to a "net" character given based on inspection of molecular-wide isosurface or interference patterns of atomic orbitals.

The CP(r) function as a criteria for the presence of a DB

Using the above information regarding the decomposition of the ED distribution (Eq. 4), a similar decomposition can be performed for the partial directional first and second derivatives along the λ_2 -eigenvector, as shown for the first derivative:

$$\begin{aligned} \partial\rho(\mathbf{r}^*) &= \partial\rho_{\text{concentrating}}(\mathbf{r}^*) + \partial\rho_{\text{depleting}}(\mathbf{r}^*) + \partial\rho_{\text{non-contributing}}(\mathbf{r}^*) \\ &+ \partial\rho_{\text{removing}}(\mathbf{r}^*) \end{aligned} \quad (5)$$

For a DB to be present, Eq. 5 should be zero at some coordinate (specifically at a CP(3,-1)) somewhere on the λ_2 -eigenvector. Naturally, this means that $\partial\rho(\mathbf{r})$ will approach zero in the vicinity of a CP or MDP; the net sign of $\partial\rho(\mathbf{r})$ is, however, numerically dependent and irrelevant for the following discussion. That means that individual terms in Eq. 5 will sum up to zero, or their sum will approach zero in the vicinity of a CP or MDP. $\partial\rho_{\text{non-contributing}}(\mathbf{r}^*)$ will always be zero (or numerically so), and, in the interest of simplicity, we can ignore $\partial\rho_{\text{removing}}(\mathbf{r}^*)$ as we are not dealing with any multi-determinant wavefunctions in this work. That leaves the interplay between the slopes of MOs that concentrate or deplete ED ($\partial\rho_{\text{concentrating}}(\mathbf{r}^*) + \partial\rho_{\text{depleting}}(\mathbf{r}^*)$) that will determine whether $\partial\rho(\mathbf{r})$ crosses zero. The two possibilities which will lead to the formation of a DB is if i) both the slopes of concentrating and depleting contributions at \mathbf{r}^* are zero, or ii) the slopes of concentrating and depleting contributions at \mathbf{r}^* are equal, but opposite in sign. We already know that the signs of the partial second derivatives along the λ_2 -eigenvector for the concentrating and depleting contributions are negative and positive, respectively, and for a DB to be present, the partial second derivative of the total ED is also negative ($\lambda_2 < 0$). Therefore, in the vicinity of a (3,-1) CP, the absolute gradient of the concentrating contributions will be greater than the absolute gradient of the depleting contributions, leading to the following conditions:

$|\partial\rho_{\text{concentrating}}(\mathbf{r}^*)| > |\partial\rho_{\text{depleting}}(\mathbf{r}^*)|$, in the vicinity of a (3,-1) CP

$|\partial\rho_{\text{concentrating}}(\mathbf{r}^*)| < |\partial\rho_{\text{depleting}}(\mathbf{r}^*)|$, outside the vicinity of a (3,-1), and

$|\partial\rho_{\text{concentrating}}(\mathbf{r}^*)| - |\partial\rho_{\text{depleting}}(\mathbf{r}^*)| = 0$, at a (3,-1) CP

The second condition will hold for most interactions of interest, regardless of whether a DB is present or not. If a DB is not present, then the first and third condition will not be met. If a (3,+1) CP is present, then the first condition will not be met. In order to evaluate the interplay of these effects, we have proposed a function for detecting DBs when measured along the λ_2 -eigenvector:

$$CP(\mathbf{r}) = -\text{sign}(\partial\rho_{\text{depleting}}(\mathbf{r})) \cdot [\partial\rho_{\text{concentrating}}(\mathbf{r}) + \partial\rho_{\text{depleting}}(\mathbf{r}) + \partial\rho_{\text{removing}}(\mathbf{r})] \quad (6)$$

The $CP(\mathbf{r})$ function simply returns the slope of the total ED (Eq. 5), but modified by the sign of the net slope of the nonbonding contributions. The $CP(\mathbf{r})$ function will therefore also be equal to 0 at \mathbf{r}^* , if a DB is present. However, in the *vicinity* of a DB, a region along the λ_2 -eigenvector will always exist where $CP(\mathbf{r})$ is positive, in one or both directions, whereas $CP(\mathbf{r})$ will always be negative if a BCP is absent.

The physical interpretation of the $CP(\mathbf{r})$ function is simple: a DB will exist only if the combined slope of all MOs that concentrate ED in an inter-nuclear region is greater and opposite in sign than the combined slope of all MOs that deplete ED.

The MO-DI Method

The MO-DI method describes the QTAIM-defined delocalization index in terms of MO contributions to the pair-density. We will first review the basic concepts of how delocalization indices are calculated within QTAIM.

The integration of the overlap between all MO pairs over a QTAIM-defined atomic domain, $\Omega(A)$, can be written as a matrix associated with atom A, \mathbf{S}^A , and is known as an *atomic overlap matrix* (AOM).¹ The elements of an N_{MO} by N_{MO} atomic overlap matrix,

$$S_{ij}^A = \sum_{ij} \int_A \sqrt{v_i} \sqrt{v_j} \chi_i^*(\mathbf{r}) \chi_j(\mathbf{r}) d\mathbf{r} \quad (7)$$

provide information on how each MO (diagonal elements) or a MO-pair (off-diagonal elements) contribute to the ED distribution of atom A. The atomic population (the average number of electrons found in the atomic basin) is therefore simply the sum of diagonal elements of the AOM:

$$N(A) = tr(\mathbf{S}^A) \quad (8)$$

The off-diagonal elements of each AOM, however, provide valuable information regarding the 2nd-order density distribution across the atom, *i.e.* how MOs interfere (de)constructively within $\Omega(A)$.^{8,9} Such information can be used to indicate the degree of localization or delocalization of electrons within the atomic basin. Specifically, by integrating the pair density across two domains simultaneously, the total electron delocalization between electrons in each basin can be calculated:

$$\begin{aligned} \delta(A,B) &= 2 \left| - \sum_{ij} \int_A d\mathbf{r}_1 \int_B d\mathbf{r}_2 v_i v_j \{ \chi_i^*(\mathbf{r}_1) \chi_j(\mathbf{r}_1) \chi_j^*(\mathbf{r}_2) \chi_i(\mathbf{r}_2) \} \right| \\ &= 2 \left| - \sum_{ij} S_{ij}^A S_{ji}^B \right| \end{aligned} \quad (9)$$

where we have used the definition for the elements of the AOM from Eq. 7. $\delta(A,B)$ is known as the delocalization index (DI)^{10,11} for atom pair A,B. In single-determinant wavefunctions, it is often calculated by only considering spin-orbitals between parallel spin electrons, in order to calculate only the delocalization arising from Fermi correlation. Finally, note that the integrations can be swapped ($d\mathbf{r}_1$ over $\Omega(B)$, $d\mathbf{r}_2$ over $\Omega(A)$) which will give the equivalent number of

electrons, indicating that the number of electrons found on average in $\Omega(A)$ but delocalized into $\Omega(B)$ is the same as the number of electrons found on average in $\Omega(B)$ but delocalized into $\Omega(A)$; hence, the factor of 2 in Eq. 9.

Since Eq. 9 is written in terms of MOs, it is easy to recover the contribution of each MO and MO-pair to the total DI. A delocalized density matrix can be easily defined in terms of AOM elements:

$$D_{ij}^{(A,B)} = 2|-S_{ij}^A S_{ji}^B| \quad (10)$$

Diagonal elements of this matrix, $D_{ii}^{(A,B)}$, provides the contributions of each MO's contribution to the total number of electron pairs shared between A and B. However, the off-diagonal elements, $D_{i \neq j}^{(A,B)}$, provides the extent to which an MO-pair increases delocalized electron pairs (through constructive interference) or decreases delocalized electron pairs (through destructive interference). Therefore, the sum of any row or column of \mathbf{D}_{ij} gives the net contribution of an MO to the number of electron pairs shared between atoms A and B, after any MO-pair interference effects have been taken into account.

MO	MO 1	MO 2	MO 3	MO 4	MO 5	MO 6	MO 7
MO 1	1.00	-1.00	0.00	0.00	0.00	0.00	0.00
MO 2	-1.00	1.00	0.00	0.00	0.00	0.00	0.00
MO 3	0.00	0.00	1.00	-0.27	0.00	0.00	0.00
MO 4	0.00	0.00	-0.27	1.00	-0.71	0.00	0.00
MO 5	0.00	0.00	0.00	-0.71	1.00	0.00	0.00
MO 6	0.00	0.00	0.00	0.00	0.00	1.00	0.00
MO 7	0.00	0.00	0.00	0.00	0.00	0.00	1.00
<i>Sum</i>	0.00	0.00	0.73	0.02	0.29	1.00	1.00
<i>Percentage</i>	0%	0%	24%	1%	10%	33%	33%

Figure S1. Delocalized matrix for N_2 , as calculated at HF/6-311++G(2df,2pd) level.

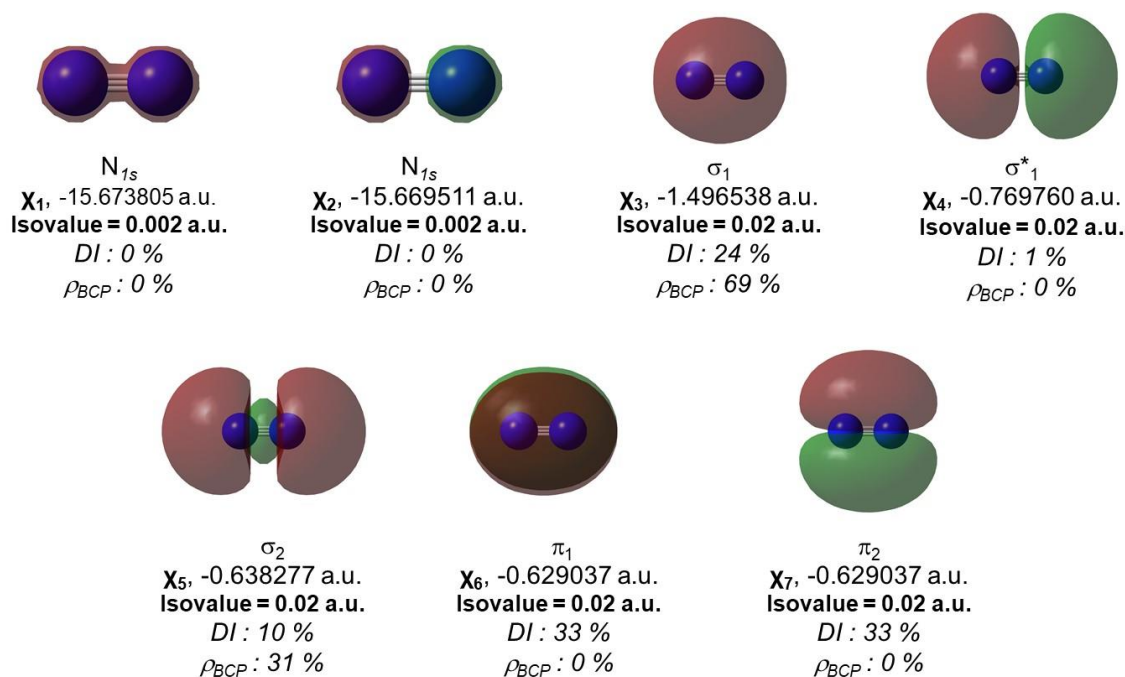


Figure S2. 3D-isosurfaces of MOs of N_2 at the HF/6-311++g(2df,2pd) level. Percentage contributions to the $DI(N,N)$ as well as to the electron density at the (3,-1) CP(N,N) are also shown.

For instance, consider the MOs in N_2 , as calculated by HF/6-311++G(2df,2pd), shown in Figure S2. The delocalized matrix \mathbf{D} is shown above, in Figure S1. The core $1s_N$ orbitals form a bonding and antibonding pair, χ_1 and χ_2 . Both MOs contribute 1 electron pair to the total DI ($D_{11}^{(A,B)} = D_{22}^{(A,B)} = 1.0$). However, the two orbitals are out-of-phase with each other, and interferes destructively so that $D_{12}^{(A,B)} = D_{21}^{(A,B)} = -1.0$. Therefore, the net contribution of MOs 1 and 2 is 0 electron pairs each, showing a classical bonding-antibonding pair. However, χ_3 – a σ -bonding MO – also contributes 1.0 electron pairs to the total DI, but interferes only weakly with χ_4 – a σ -antibonding MO. The net contribution of χ_3 is then 0.72 electron pairs. Finally, χ_4 interferes destructively with both χ_3 and χ_5 (the second σ -bonding MO), thereby bringing its net contribution down to only 0.02 electron pairs.

References

1. R. F. Bader. In *Atoms in molecules*; Wiley Online Library, **1990**.
2. S. Shahbazian. *Chem. Eur. J.* **2018**, doi: 10.1002/chem.201705163.
3. J. Contreras-García; E. R. Johnson; S. Keinan; R. Chaudret; J.-P. Piquemal; D. N. Beratan; W. Yang. *J. Chem. Theory Comput.* **2011**, 7, 625-632.
4. A. Otero-de-la-Roza; E. R. Johnson; J. Contreras-García. *PCCP* **2012**, 14, 12165-12172.

Appendix I

5. I. Cukrowski; J. H. de Lange; A. S. Adeyinka; P. Mangondo. *Comput. Theor. Chem.* **2015**, 1053, 60-76.
6. J. H. de Lange; D. M. van Niekerk; I. Cukrowski. *J. Comput. Chem.* **2018**, 39, 973-985.
7. J. H. Lange; I. Cukrowski. *J. Comput. Chem.* **2017**, 38, 981-997.
8. R. F. Bader. *Monatshefte für Chemie/Chemical Monthly* **2005**, 136, 819-854.
9. F. Cortés-Guzmán; R. F. Bader. *Coord. Chem. Rev.* **2005**, 249, 633-662.
10. R. F. Bader; M. E. Stephens. *J. Am. Chem. Soc.* **1975**, 97, 7391-7399.
11. R. Daudel; R. Bader; M. Stephens; D. Borrett. *Can. J. Chem.* **1974**, 52, 1310-1320.

End of Part 1

Part 2. Cartesian coordinates of molecules studied**Table S1.** Cartesian coordinates of planar biphenyl at the B3LYP/6-311++g(2df,2pd)/GD3 level.

Atom	X	Y	Z
C1	0.000000	0.745401	0.000000
C2	1.194303	1.480695	0.000000
C3	1.196327	2.868658	0.000000
C4	0.000000	3.575187	0.000000
C5	-1.196327	2.868658	0.000000
C6	-1.194303	1.480695	0.000000
H7	2.147022	0.973835	0.000000
H8	2.139620	3.398460	0.000000
H9	0.000000	4.656587	0.000000
H10	-2.139620	3.398460	0.000000
H11	-2.147022	0.973835	0.000000
C12	0.000000	-0.745401	0.000000
C13	-1.194303	-1.480695	0.000000
C14	1.194303	-1.480695	0.000000
C15	-1.196327	-2.868658	0.000000
H16	-2.147022	-0.973835	0.000000
C17	1.196327	-2.868658	0.000000
H18	2.147022	-0.973835	0.000000
C19	0.000000	-3.575187	0.000000
H20	-2.139620	-3.398460	0.000000
H21	2.139620	-3.398460	0.000000
H22	0.000000	-4.656587	0.000000

Appendix I

Table S2. Cartesian coordinates of twisted biphenyl at the B3LYP/6-311++g(2df,2pd)/GD3 level.

Atom	X	Y	Z
C1	0.000000	0.740639	0.000000
C2	1.125949	1.459671	0.416302
C3	1.126421	2.848508	0.416623
C4	0.000000	3.549616	0.000000
C5	-1.126421	2.848508	-0.416623
C6	-1.125949	1.459671	-0.416302
H7	1.999325	0.924884	0.764579
H8	2.005079	3.383880	0.751032
H9	0.000000	4.631157	0.000000
H10	-2.005079	3.383880	-0.751032
H11	-1.999325	0.924884	-0.764579
C12	0.000000	-0.740639	0.000000
C13	-1.125949	-1.459671	0.416302
C14	1.125949	-1.459671	-0.416302
C15	-1.126421	-2.848508	0.416623
H16	-1.999325	-0.924884	0.764579
C17	1.126421	-2.848508	-0.416623
H18	1.999325	-0.924884	-0.764579
C19	0.000000	-3.549616	0.000000
H20	-2.005079	-3.383880	0.751032
H21	2.005079	-3.383880	-0.751032
H22	0.000000	-4.631157	0.000000

Appendix I

Table S3. Cartesian coordinates of cubic Li₄H₄ at the B3LYP/6-311++g(2df,2pd)/GD3 level.

Atom	X	Y	Z
Li1	-1.118656	-0.942737	-0.365387
H2	-1.449309	0.667838	0.437822
Li3	-0.189314	1.309120	-0.723882
H4	0.013932	-0.265758	-1.633203
H5	0.207746	-1.436650	0.794396
Li6	-0.012695	0.242165	1.488227
H7	1.227625	1.034573	0.400985
Li8	1.320666	-0.608549	-0.398958

End of Part 2

Part 3 – Canonical molecular orbitals in biphenyl

Table S4. Full list of MOs in the planar Bph; isovalue = 0.01 a.u.

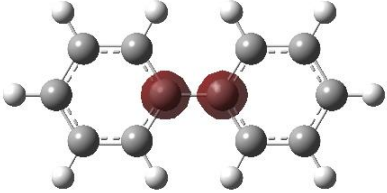

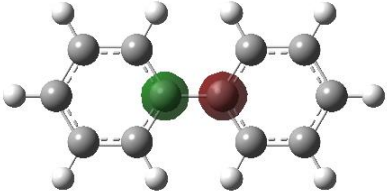

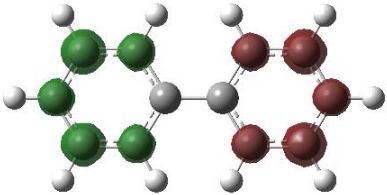
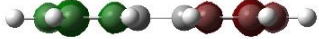
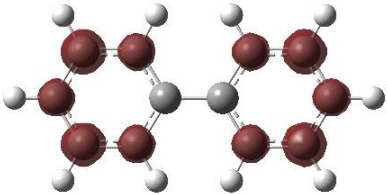
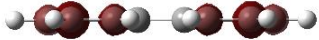
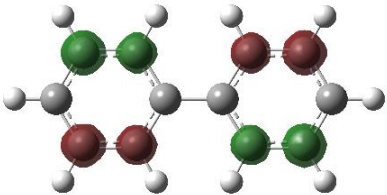
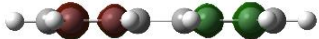
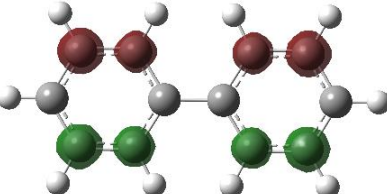
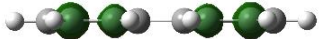
MO	Top View	Side View
χ_1		
χ_2		
χ_3		
χ_4		
χ_5		
χ_6		

Table S4 continues – planar Bph.

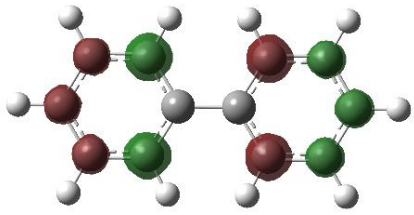
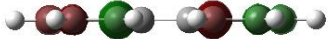
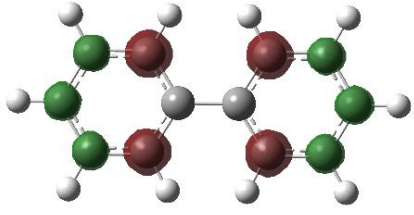
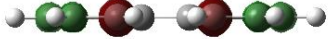
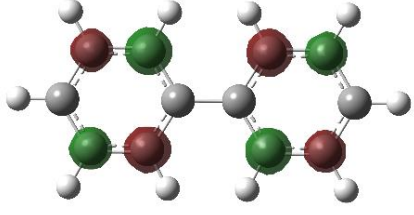
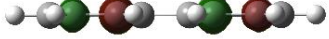
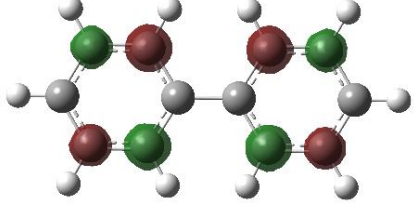
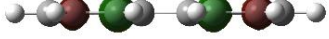
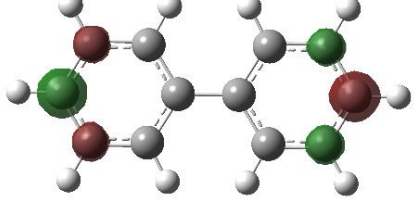
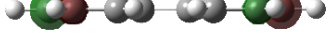
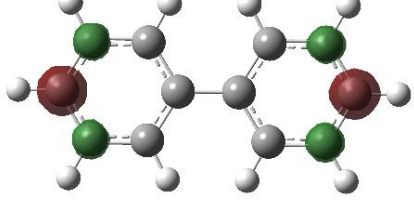

χ_7		
χ_8		
χ_9		
χ_{10}		
χ_{11}		
χ_{12}		

Table S4 continues – planar Bph.

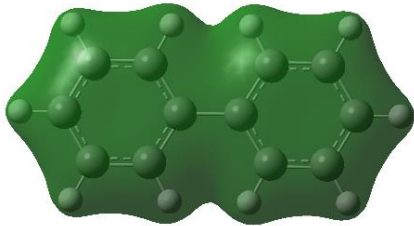
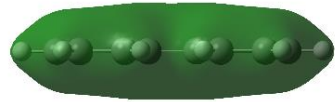
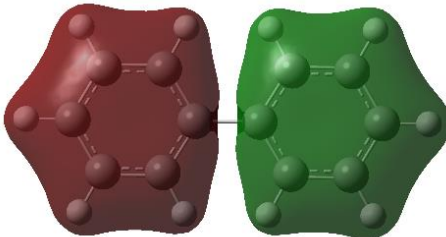
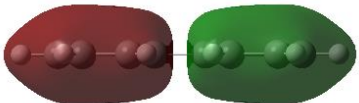
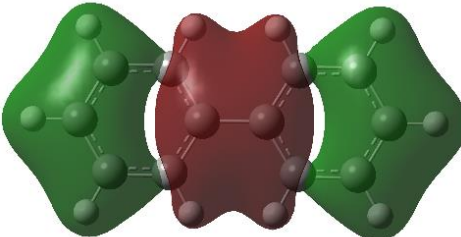
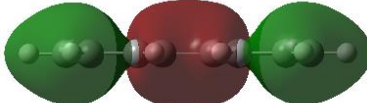
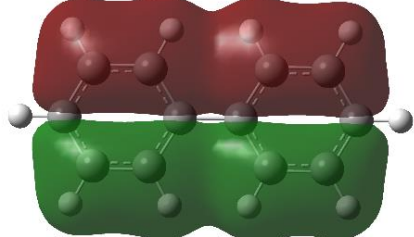
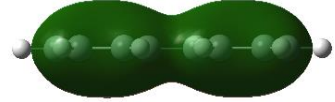
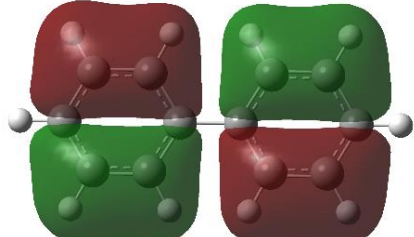
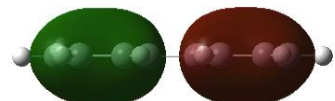
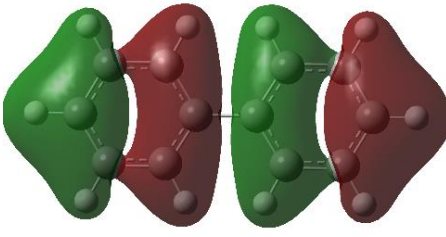
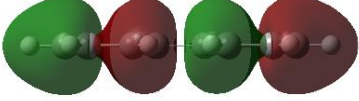
χ_{13}		
χ_{14}		
χ_{15}		
χ_{16}		
χ_{17}		
χ_{18}		

Table S4 continues – planar Bph.

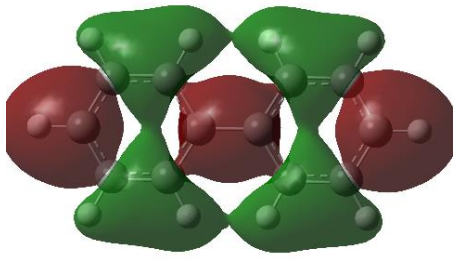
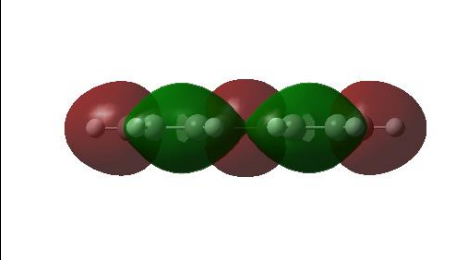
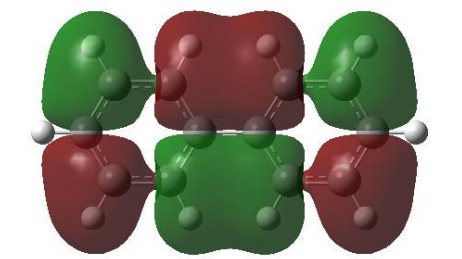
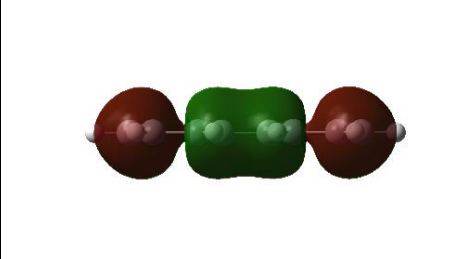
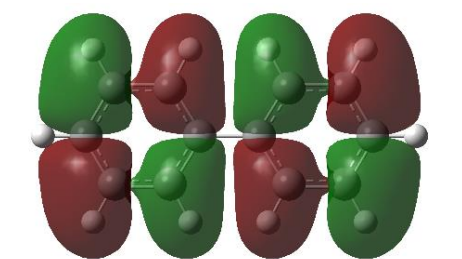
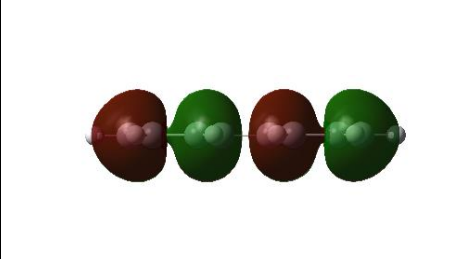
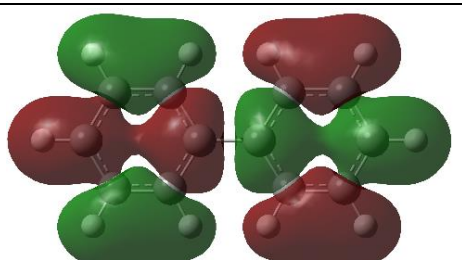
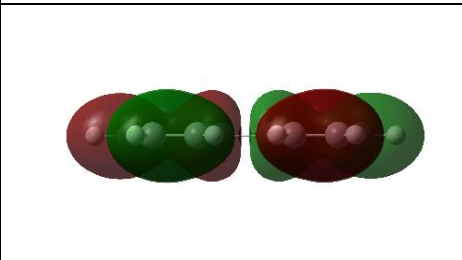
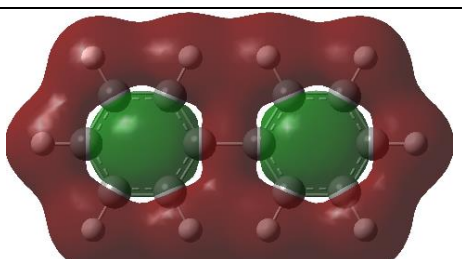
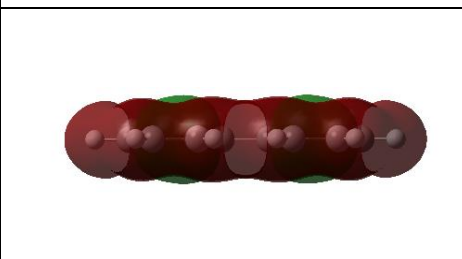
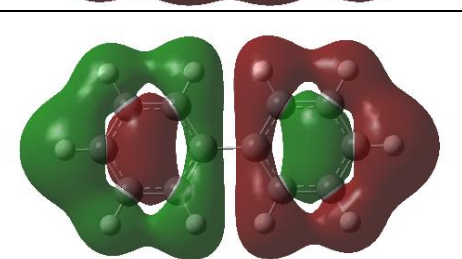
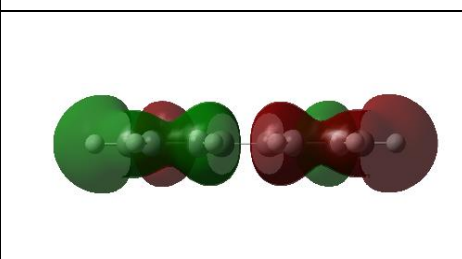
χ_{19}		
χ_{20}		
χ_{21}		
χ_{22}		
χ_{23}		
χ_{24}		

Table S4 continues – planar Bph.

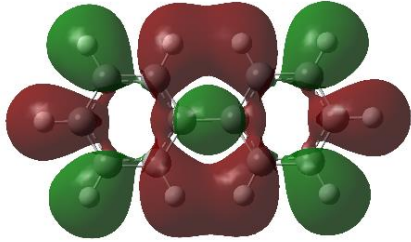

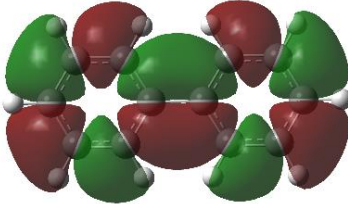
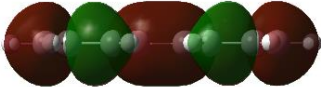
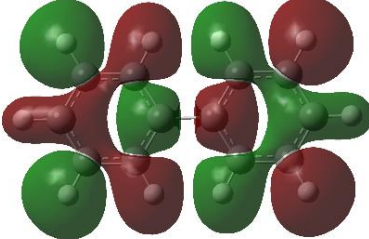
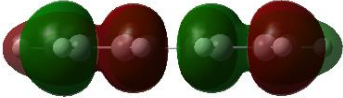
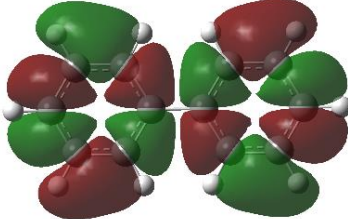
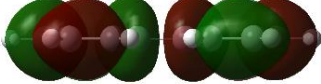
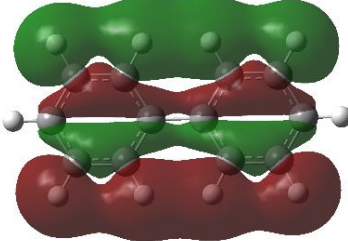

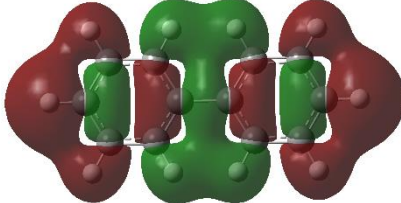
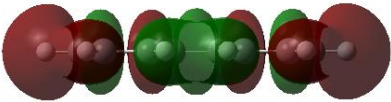
χ_{25}		
χ_{26}		
χ_{27}		
χ_{28}		
χ_{29}		
χ_{30}		

Table S4 continues – planar Bph.

χ_{31}		
χ_{32}		
χ_{33}		
χ_{34}		
χ_{35}		
χ_{36}		

Table S4 continues – planar Bph.

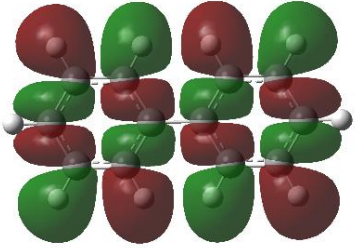

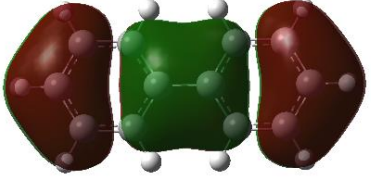
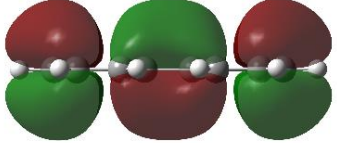
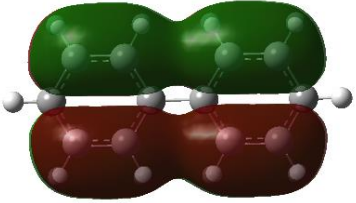
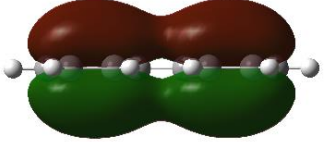
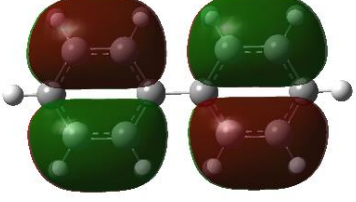
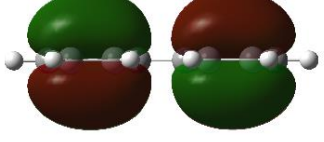
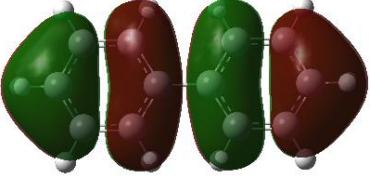
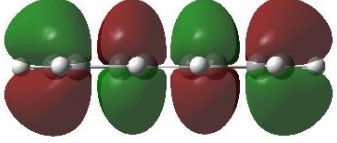
χ_{37}	 A 3D molecular orbital visualization showing a 4x4 grid of lobes. The lobes are colored red and green, arranged in a checkerboard pattern. Each lobe is centered on a carbon atom of a benzene ring.	 A 3D molecular orbital visualization showing four lobes in a row. The lobes are colored red and green, alternating in color. Each lobe is centered on a carbon atom of a benzene ring.
χ_{38}	 A 3D molecular orbital visualization showing three lobes. The central lobe is green and the two side lobes are red. Each lobe is centered on a carbon atom of a benzene ring.	 A 3D molecular orbital visualization showing three lobes in a row. The central lobe is green and the two side lobes are red. Each lobe is centered on a carbon atom of a benzene ring.
χ_{39}	 A 3D molecular orbital visualization showing two lobes. The top lobe is green and the bottom lobe is red. Each lobe is centered on a carbon atom of a benzene ring.	 A 3D molecular orbital visualization showing two lobes in a row. The left lobe is red and the right lobe is green. Each lobe is centered on a carbon atom of a benzene ring.
χ_{40}	 A 3D molecular orbital visualization showing two lobes. The left lobe is red and the right lobe is green. Each lobe is centered on a carbon atom of a benzene ring.	 A 3D molecular orbital visualization showing two lobes in a row. The left lobe is green and the right lobe is red. Each lobe is centered on a carbon atom of a benzene ring.
χ_{41}	 A 3D molecular orbital visualization showing four lobes. The central two lobes are green and the two side lobes are red. Each lobe is centered on a carbon atom of a benzene ring.	 A 3D molecular orbital visualization showing four lobes in a row. The lobes are colored red and green, alternating in color. Each lobe is centered on a carbon atom of a benzene ring.

Table S5. Full list of MOs in the twisted Bph; isovalue = 0.01 a.u.

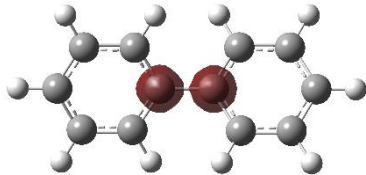
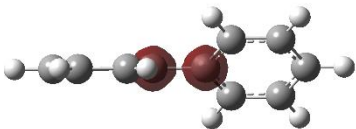
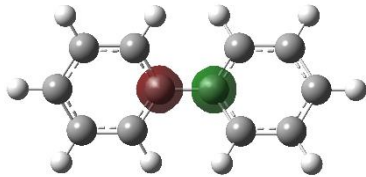
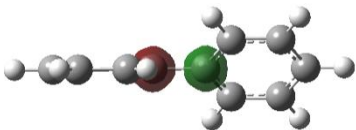
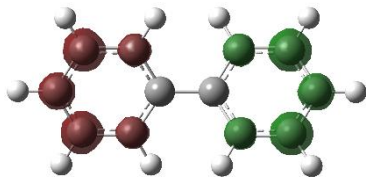
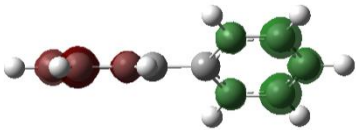
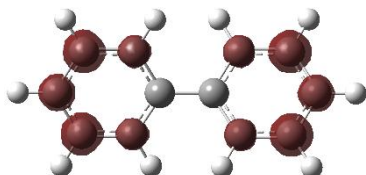
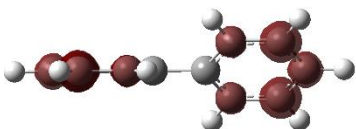
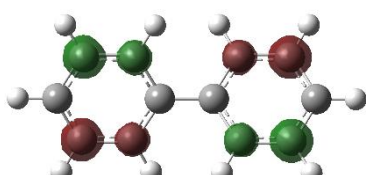
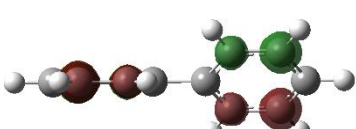
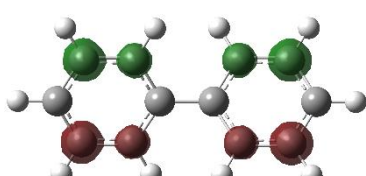
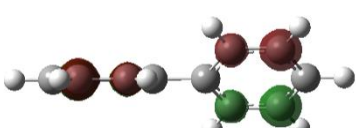
MO	Top View	Side View
χ_1		
χ_2		
χ_3		
χ_4		
χ_5		
χ_6		

Table S5 continues – twisted Bph.

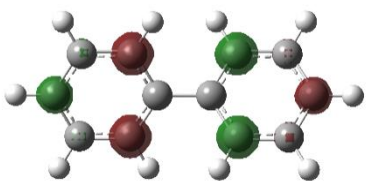
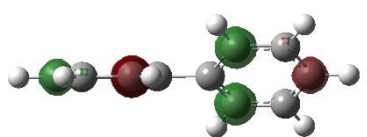
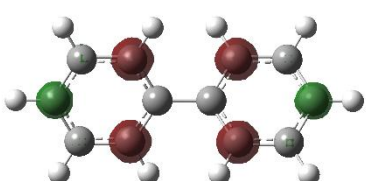
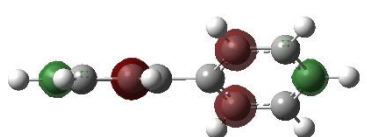
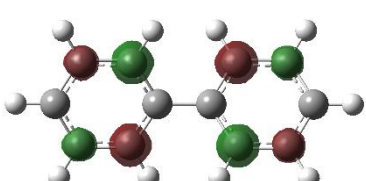
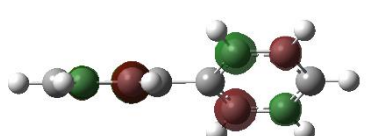
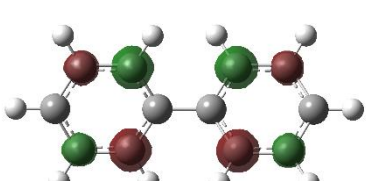
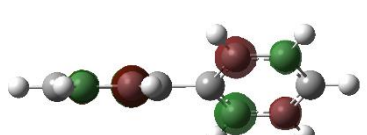
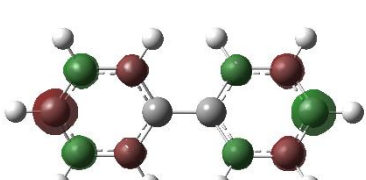
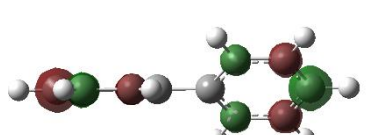
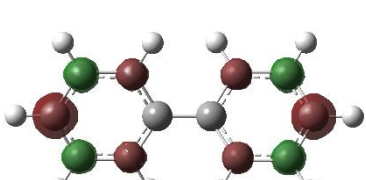
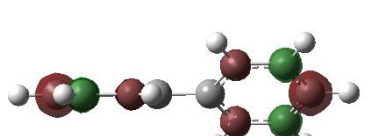
χ_7		
χ_8		
χ_9		
χ_{10}		
χ_{11}		
χ_{12}		

Table S5 continues – twisted Bph.

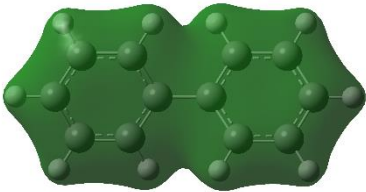
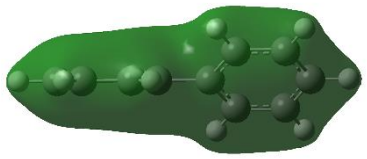
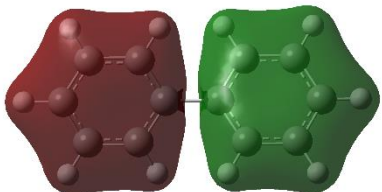
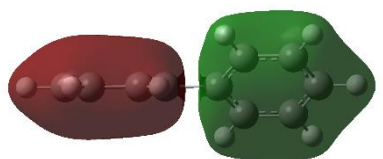
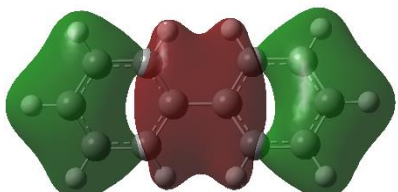
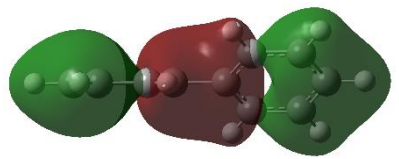
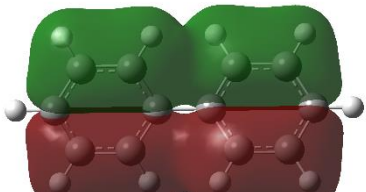
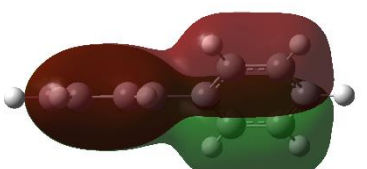
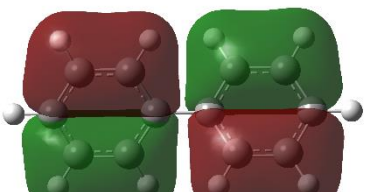
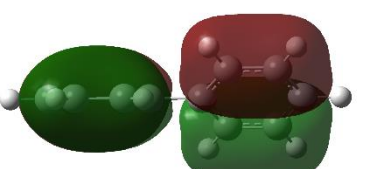
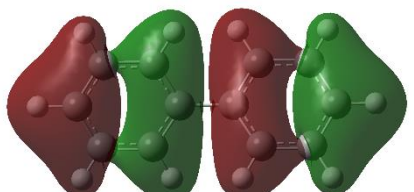
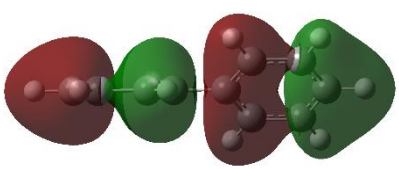
χ_{13}		
χ_{14}		
χ_{15}		
χ_{16}		
χ_{17}		
χ_{18}		

Table S5 continues – twisted Bph.

χ_{19}		
χ_{20}		
χ_{21}		
χ_{22}		
χ_{23}		
χ_{24}		

Table S5 continues – twisted Bph.

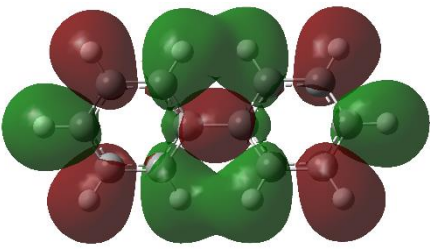
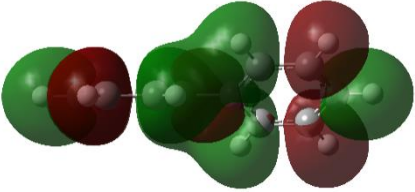
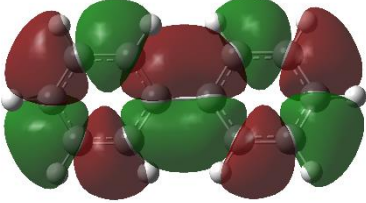
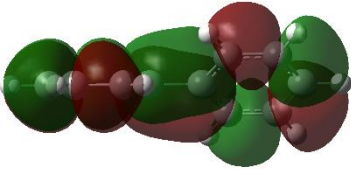
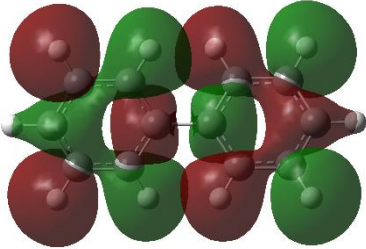
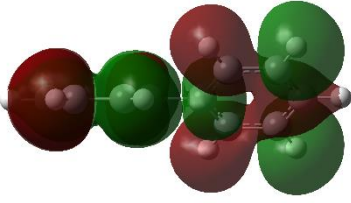
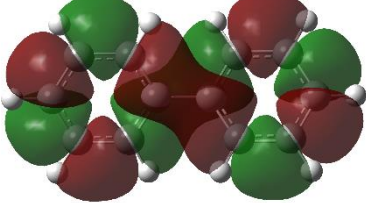
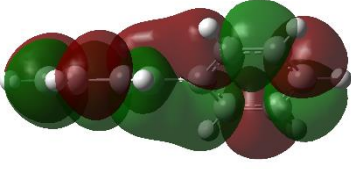
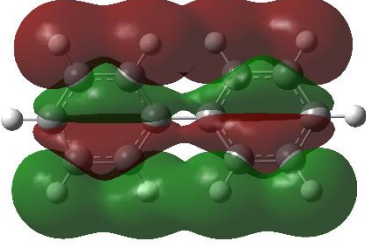
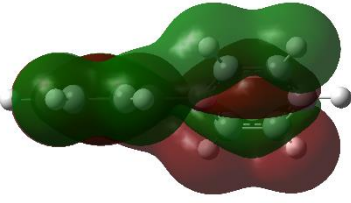
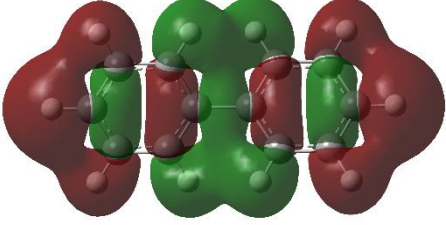
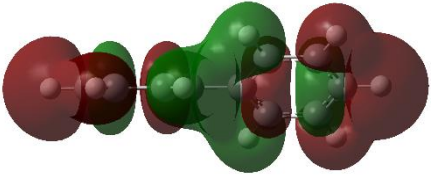
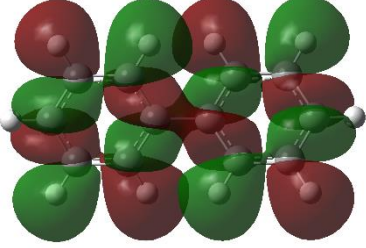
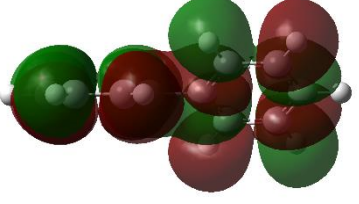
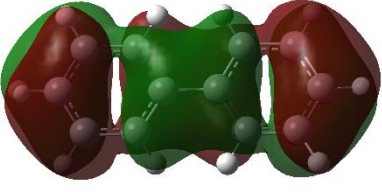
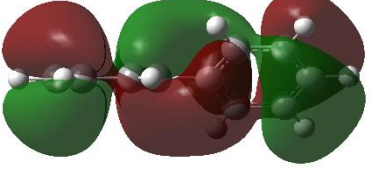
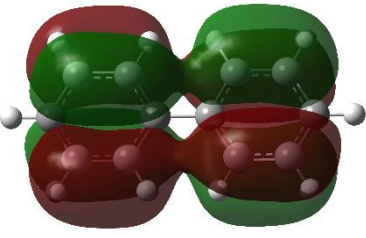
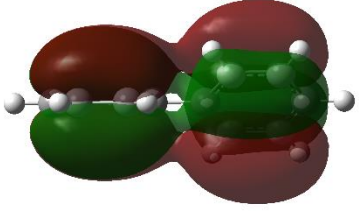
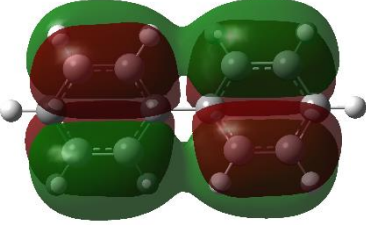
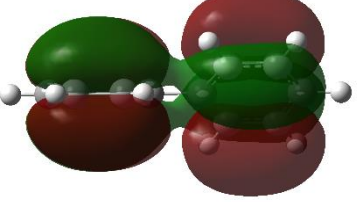
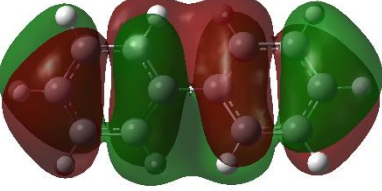
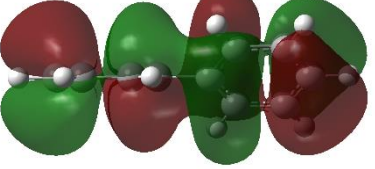
χ_{25}		
χ_{26}		
χ_{27}		
χ_{28}		
χ_{29}		
χ_{30}		

Table S5 continues – twisted Bph.

χ_{31}		
χ_{32}		
χ_{33}		
χ_{34}		
χ_{35}		
χ_{36}		

Table S5 continues – twisted Bph.

χ_{37}		
χ_{38}		
χ_{39}		
χ_{40}		
χ_{41}		

End of Part 3

Part 4 – Data pertaining to covalent bonds in biphenyl

Table S6. MO-ED data at (3,-1) CP(C1,C12) & CP(C19,H22) in the planar Bph.

MO	Energy (a.u.)	C1,C12		C19,H22	
		ED contribution (a.u.) / %-fraction	Classification based on 2nd derivative sign (λ_2)	ED contribution (a.u.) / %-fraction	Classification based on 2nd derivative sign (λ_2)
χ_1	-10.19173	0.00010 / 0.0%	<i>concentrating</i>	0.00000 / 0.0%	<i>non-contributing</i>
χ_2	-10.19145	0.00000 / 0.0%	<i>non-contributing</i>	0.00000 / 0.0%	<i>non-contributing</i>
χ_3	-10.17726	0.00000 / 0.0%	<i>non-contributing</i>	0.00000 / 0.0%	<i>non-contributing</i>
χ_4	-10.17724	0.00000 / 0.0%	<i>non-contributing</i>	0.00000 / 0.0%	<i>non-contributing</i>
χ_5	-10.17720	0.00000 / 0.0%	<i>non-contributing</i>	0.00000 / 0.0%	<i>non-contributing</i>
χ_6	-10.17718	0.00000 / 0.0%	<i>non-contributing</i>	0.00000 / 0.0%	<i>non-contributing</i>
χ_7	-10.17658	0.00000 / 0.0%	<i>non-contributing</i>	0.00000 / 0.0%	<i>non-contributing</i>
χ_8	-10.17657	0.00000 / 0.0%	<i>non-contributing</i>	0.00000 / 0.0%	<i>non-contributing</i>
χ_9	-10.17653	0.00000 / 0.0%	<i>non-contributing</i>	0.00000 / 0.0%	<i>non-contributing</i>
χ_{10}	-10.17652	0.00000 / 0.0%	<i>non-contributing</i>	0.00000 / 0.0%	<i>non-contributing</i>
χ_{11}	-10.17586	0.00000 / 0.0%	<i>non-contributing</i>	0.00005 / 0.0%	<i>concentrating</i>
χ_{12}	-10.17586	0.00000 / 0.0%	<i>non-contributing</i>	0.00005 / 0.0%	<i>concentrating</i>
χ_{13}	-0.87581	0.01896 / 7.2%	<i>concentrating</i>	0.00150 / 0.5%	<i>concentrating</i>
χ_{14}	-0.85459	0.00000 / 0.0%	<i>non-contributing</i>	0.00357 / 1.2%	<i>concentrating</i>
χ_{15}	-0.78384	0.03774 / 14.3%	<i>concentrating</i>	0.00980 / 3.3%	<i>concentrating</i>
χ_{16}	-0.75827	0.00000 / 0.0%	<i>non-contributing</i>	0.00000 / 0.0%	<i>non-contributing</i>
χ_{17}	-0.74841	0.00000 / 0.0%	<i>non-contributing</i>	0.00000 / 0.0%	<i>non-contributing</i>
χ_{18}	-0.72791	0.00000 / 0.0%	<i>non-contributing</i>	0.01662 / 5.7%	<i>concentrating</i>
χ_{19}	-0.63238	0.04513 / 17.1%	<i>concentrating</i>	0.02476 / 8.5%	<i>concentrating</i>
χ_{20}	-0.62793	0.00000 / 0.0%	<i>non-contributing</i>	0.00000 / 0.0%	<i>non-contributing</i>
χ_{21}	-0.59212	0.00000 / 0.0%	<i>non-contributing</i>	0.00000 / 0.0%	<i>non-contributing</i>
χ_{22}	-0.58592	0.00000 / 0.0%	<i>non-contributing</i>	0.01386 / 4.7%	<i>concentrating</i>
χ_{23}	-0.54310	0.01894 / 7.2%	<i>concentrating</i>	0.01360 / 4.6%	<i>concentrating</i>
χ_{24}	-0.50360	0.00000 / 0.0%	<i>non-contributing</i>	0.05810 / 19.9%	<i>concentrating</i>
χ_{25}	-0.48074	0.03774 / 14.3%	<i>concentrating</i>	0.02312 / 7.9%	<i>concentrating</i>
χ_{26}	-0.47350	0.00000 / 0.0%	<i>non-contributing</i>	0.00000 / 0.0%	<i>non-contributing</i>
χ_{27}	-0.44376	0.00000 / 0.0%	<i>non-contributing</i>	0.00263 / 0.9%	<i>concentrating</i>
χ_{28}	-0.43615	0.00000 / 0.0%	<i>non-contributing</i>	0.00000 / 0.0%	<i>non-contributing</i>
χ_{29}	-0.43567	0.00000 / 0.0%	<i>non-contributing</i>	0.00000 / 0.0%	<i>non-contributing</i>
χ_{30}	-0.43051	0.04133 / 15.6%	<i>concentrating</i>	0.04914 / 16.8%	<i>concentrating</i>

Table S6 continues.

MO	Energy (a.u.)	C1,C12		C19,H22	
		ED contribution (a.u.) / %-fraction	Classification based on 2nd derivative sign (λ_2)	ED contribution (a.u.) / %-fraction	Classification based on 2nd derivative sign (λ_2)
χ_{31}	-0.41671	0.00000 / 0.0%	<i>non-contributing</i>	0.00000 / 0.0%	<i>non-contributing</i>
χ_{32}	-0.39513	0.00000 / 0.0%	<i>depleting</i>	0.00000 / 0.0%	<i>depleting</i>
χ_{33}	-0.36916	0.00000 / 0.0%	<i>non-contributing</i>	0.05161 / 17.6%	<i>concentrating</i>
χ_{34}	-0.36616	0.00000 / 0.0%	<i>non-contributing</i>	0.00000 / 0.0%	<i>depleting</i>
χ_{35}	-0.36285	0.00000 / 0.0%	<i>non-contributing</i>	0.00000 / 0.0%	<i>non-contributing</i>
χ_{36}	-0.34790	0.06432 / 24.3%	<i>concentrating</i>	0.02425 / 8.3%	<i>concentrating</i>
χ_{37}	-0.33466	0.00000 / 0.0%	<i>non-contributing</i>	0.00000 / 0.0%	<i>non-contributing</i>
χ_{38}	-0.29363	0.00000 / 0.0%	<i>depleting</i>	0.00000 / 0.0%	<i>depleting</i>
χ_{39}	-0.26531	0.00000 / 0.0%	<i>non-contributing</i>	0.00000 / 0.0%	<i>non-contributing</i>
χ_{40}	-0.25903	0.00000 / 0.0%	<i>non-contributing</i>	0.00000 / 0.0%	<i>non-contributing</i>
χ_{41}	-0.23027	0.00000 / 0.0%	<i>non-contributing</i>	0.00000 / 0.0%	<i>depleting</i>

Appendix I

Table S7. MO-DI data (in e^- -pairs) for covalent bond C1–C12 in the planar Bph.

MO	1–21 ^a	22	23	24	25	26	27	28	29	30	31	32	33	34	35	36	37	38	39	40	41
1–21	0.38 ^a	-0.02	0.00	-0.01	0.05	0.02	-0.01	-0.01	0.00	0.00	0.00	0.00	-0.01	0.00	0.01	0.02	-0.01	0.00	0.00	0.00	0.00
22	-0.02	0.02	0.00	0.00	0.00	0.00	0.01	0.00	0.00	-0.01	0.00	0.00	0.00	0.00	0.00	0.00	0.00	0.00	0.00	0.00	0.00
23	0.00	0.00	0.02	0.00	0.01	0.00	0.00	0.00	0.00	0.03	0.00	0.00	0.00	0.00	0.00	0.03	0.00	0.00	0.00	0.00	0.00
24	-0.01	0.00	0.00	0.00	0.00	0.00	0.00	0.00	0.00	0.00	0.00	0.00	0.00	0.00	0.00	0.00	0.00	0.00	0.00	0.00	0.00
25	0.05	0.00	0.01	0.00	0.01	0.00	0.00	0.00	0.00	0.01	0.00	0.00	0.00	0.00	0.00	0.02	0.00	0.00	0.00	0.00	0.00
26	0.02	0.00	0.00	0.00	0.00	0.03	0.00	-0.02	0.00	0.00	0.00	0.00	0.00	0.00	0.02	0.00	-0.02	0.00	0.00	0.00	0.00
27	-0.01	0.01	0.00	0.00	0.00	0.00	0.01	0.00	0.00	0.00	0.00	0.00	0.00	0.00	0.00	0.00	0.00	0.00	0.00	0.00	0.00
28	-0.01	0.00	0.00	0.00	0.00	-0.02	0.00	0.03	-0.01	0.00	0.00	0.00	0.00	0.00	-0.01	0.00	0.02	0.00	0.00	0.00	0.00
29	0.00	0.00	0.00	0.00	0.00	0.00	0.00	-0.01	0.00	0.00	0.00	0.00	0.00	0.00	0.00	0.00	-0.01	0.00	0.00	0.00	0.00
30	0.00	-0.01	0.03	0.00	0.01	0.00	0.00	0.00	0.00	0.05	0.00	0.00	0.00	0.00	0.00	0.05	0.00	0.00	0.00	0.00	0.00
31	0.00	0.00	0.00	0.00	0.00	0.00	0.00	0.00	0.00	0.00	0.00	0.00	0.00	0.00	0.00	0.00	0.00	0.00	0.00	0.00	0.00
32	0.00	0.00	0.00	0.00	0.00	0.00	0.00	0.00	0.00	0.00	0.00	0.11	0.00	-0.02	0.00	0.00	0.00	0.09	0.00	0.00	-0.07
33	-0.01	0.00	0.00	0.00	0.00	0.00	0.00	0.00	0.00	0.00	0.00	0.00	0.00	0.00	0.00	0.00	0.00	0.00	0.00	0.00	0.00
34	0.00	0.00	0.00	0.00	0.00	0.00	0.00	0.00	0.00	0.00	0.00	-0.02	0.00	0.01	0.00	0.00	0.00	-0.02	0.00	0.00	0.02
35	0.01	0.00	0.00	0.00	0.00	0.02	0.00	-0.01	0.00	0.00	0.00	0.00	0.00	0.00	0.01	0.00	-0.01	0.00	0.00	0.00	0.00
36	0.02	0.00	0.03	0.00	0.02	0.00	0.00	0.00	0.00	0.05	0.00	0.00	0.00	0.00	0.00	0.05	0.00	0.00	0.00	0.00	0.00
37	-0.01	0.00	0.00	0.00	0.00	-0.02	0.00	0.02	-0.01	0.00	0.00	0.00	0.00	0.00	-0.01	0.00	0.02	0.00	0.00	0.00	0.00
38	0.00	0.00	0.00	0.00	0.00	0.00	0.00	0.00	0.00	0.00	0.00	0.09	0.00	-0.02	0.00	0.00	0.00	0.08	0.00	0.00	-0.06
39	0.00	0.00	0.00	0.00	0.00	0.00	0.00	0.00	0.00	0.00	0.00	0.00	0.00	0.00	0.00	0.00	0.00	0.00	0.00	0.00	0.00
40	0.00	0.00	0.00	0.00	0.00	0.00	0.00	0.00	0.00	0.00	0.00	0.00	0.00	0.00	0.00	0.00	0.00	0.00	0.00	0.00	0.00
41	0.00	0.00	0.00	0.00	0.00	0.00	0.00	0.00	0.00	0.00	0.00	-0.07	0.00	0.02	0.00	0.00	0.00	-0.06	0.00	0.00	0.06
Diagonal	2.30 ^a	0.02	0.02	0.00	0.01	0.03	0.01	0.03	0.00	0.05	0.00	0.11	0.00	0.01	0.01	0.05	0.02	0.08	0.00	0.00	0.06
Off-Diagonal	-1.87 ^a	-0.03	0.06	0.00	0.09	-0.01	0.00	-0.03	0.00	0.08	0.00	0.00	-0.01	-0.02	0.00	0.11	-0.03	0.01	0.00	0.00	-0.11
Total	0.43	0.00	0.08	0.00	0.11	0.02	0.00	-0.01	0.00	0.13	0.00	0.10	-0.01	-0.01	0.01	0.16	-0.01	0.10	0.00	0.00	-0.05

^a MOs 1–21 were combined for the sake of brevity. The contributions made by diagonal elements of these MOs equal 2.30, whereas off-diagonal terms of only these MOs equal -1.92 to give a net contribution of 0.38. Interference with the remaining MOs (MOs 22–41) gives a positive, off-diagonal contribution of +0.05, so that the total contribution of MOs 1–21 equals 0.43.

Appendix I

Table S8. MO-DI data (in e^- -pairs) for covalent bond C19–H22 in planar Bph.

MO	1–21 ^a	22	23	24	25	26	27	28	29	30	31	32	33	34	35	36	37	38	39	40	41
1–21	0.13 ^a	0.02	0.00	0.02	0.02	0.00	0.01	0.00	0.00	0.00	0.00	0.00	0.00	0.00	0.00	0.00	0.00	0.00	0.00	0.00	0.00
22	0.02	0.00	0.00	0.01	0.00	0.00	0.00	0.00	0.00	0.00	0.00	0.00	0.00	0.00	0.00	0.00	0.00	0.00	0.00	0.00	0.00
23	0.00	0.00	0.00	0.01	0.00	0.00	0.00	0.00	0.00	0.01	0.00	0.00	0.01	0.00	0.00	0.00	0.00	0.00	0.00	0.00	0.00
24	0.02	0.01	0.01	0.05	0.01	0.00	0.00	0.00	0.00	0.04	0.00	0.00	0.04	0.00	0.00	0.02	0.00	0.00	0.00	0.00	0.00
25	0.02	0.00	0.00	0.01	0.01	0.00	0.00	0.00	0.00	0.01	0.00	0.00	0.01	0.00	0.00	0.00	0.00	0.00	0.00	0.00	0.00
26	0.00	0.00	0.00	0.00	0.00	0.00	0.00	0.00	0.00	0.00	0.00	0.00	0.00	0.00	0.00	0.00	0.00	0.00	0.00	0.00	0.00
27	0.01	0.00	0.00	0.00	0.00	0.00	0.00	0.00	0.00	0.00	0.00	0.00	0.00	0.00	0.00	0.00	0.00	0.00	0.00	0.00	0.00
28	0.00	0.00	0.00	0.00	0.00	0.00	0.00	0.00	0.00	0.00	0.00	0.00	0.00	0.00	0.00	0.00	0.00	0.00	0.00	0.00	0.00
29	0.00	0.00	0.00	0.00	0.00	0.00	0.00	0.00	0.00	0.00	0.00	0.00	0.00	0.00	0.00	0.00	0.00	0.00	0.00	0.00	0.00
30	0.00	0.00	0.01	0.04	0.01	0.00	0.00	0.00	0.00	0.04	0.00	0.00	0.04	0.00	0.00	0.02	0.00	0.00	0.00	0.00	0.00
31	0.00	0.00	0.00	0.00	0.00	0.00	0.00	0.00	0.00	0.00	0.00	0.00	0.00	0.00	0.00	0.00	0.00	0.00	0.00	0.00	0.00
32	0.00	0.00	0.00	0.00	0.00	0.00	0.00	0.00	0.00	0.00	0.00	0.00	0.00	0.00	0.00	0.00	0.00	0.00	0.00	0.00	0.00
33	0.00	0.00	0.01	0.04	0.01	0.00	0.00	0.00	0.00	0.04	0.00	0.00	0.04	0.00	0.00	0.02	0.00	0.00	0.00	0.00	0.00
34	0.00	0.00	0.00	0.00	0.00	0.00	0.00	0.00	0.00	0.00	0.00	0.00	0.00	0.00	0.00	0.00	0.00	0.00	0.00	0.00	0.00
35	0.00	0.00	0.00	0.00	0.00	0.00	0.00	0.00	0.00	0.00	0.00	0.00	0.00	0.00	0.00	0.00	0.00	0.00	0.00	0.00	0.00
36	0.00	0.00	0.00	0.02	0.00	0.00	0.00	0.00	0.00	0.02	0.00	0.00	0.02	0.00	0.00	0.01	0.00	0.00	0.00	0.00	0.00
37	0.00	0.00	0.00	0.00	0.00	0.00	0.00	0.00	0.00	0.00	0.00	0.00	0.00	0.00	0.00	0.00	0.00	0.00	0.00	0.00	0.00
38	0.00	0.00	0.00	0.00	0.00	0.00	0.00	0.00	0.00	0.00	0.00	0.00	0.00	0.00	0.00	0.00	0.00	0.00	0.00	0.00	0.00
39	0.00	0.00	0.00	0.00	0.00	0.00	0.00	0.00	0.00	0.00	0.00	0.00	0.00	0.00	0.00	0.00	0.00	0.00	0.00	0.00	0.00
40	0.00	0.00	0.00	0.00	0.00	0.00	0.00	0.00	0.00	0.00	0.00	0.00	0.00	0.00	0.00	0.00	0.00	0.00	0.00	0.00	0.00
41	0.00	0.00	0.00	0.00	0.00	0.00	0.00	0.00	0.00	0.00	0.00	0.00	0.00	0.00	0.00	0.00	0.00	0.00	0.00	0.00	0.00
Diagonal	0.03 ^a	0.00	0.00	0.05	0.01	0.00	0.00	0.00	0.00	0.04	0.00	0.00	0.04	0.00	0.00	0.01	0.00	0.00	0.00	0.00	0.00
Off-Diagonal	0.17 ^a	0.04	0.05	0.15	0.06	0.00	0.00	0.00	0.00	0.11	0.00	0.00	0.11	0.00	0.00	0.06	0.00	0.01	0.00	0.00	0.01
Total	0.20 ^a	0.04	0.05	0.19	0.07	0.00	0.01	0.00	0.00	0.16	0.00	0.00	0.15	0.01	0.00	0.06	0.00	0.01	0.00	0.00	0.01

^a MOs 1–21 were combined for the sake of brevity. The contributions made by diagonal elements of these MOs equal 0.03, whereas off-diagonal terms of only these MOs equal +0.1 to give a net contribution of 0.13. Interference with the remaining MOs (MOs 22–41) gives a positive, off-diagonal contribution of +0.04, so that the total contribution of MOs 1–21 equals 0.20.

Table S9. Summary of MO-ED & MO-DI data, for covalent bonds C1,C12 & C19,H22 in planar BPh

Classification based on λ_2	C1,C12		C19,H22	
	Number of MOs	Contribution to $\rho(\text{CP})^a$	Number of MOs	Contribution to $\rho(\text{CP})^a$
<i>Concentrating</i>	8	0.264	15	0.293
<i>Depleting</i>	2	0.000	4	0.000
<i>Non-contributing</i>	31	0.000	22	0.000
Delocalization	Contribution to DI^b		Contribution to DI^b	
<i>Overlapping</i>	2.82		0.19	
<i>Interference</i>	-1.76		0.77	
<i>Net DI</i>	1.06		0.97	

^a in a.u.; ^b in e^- -pairs.

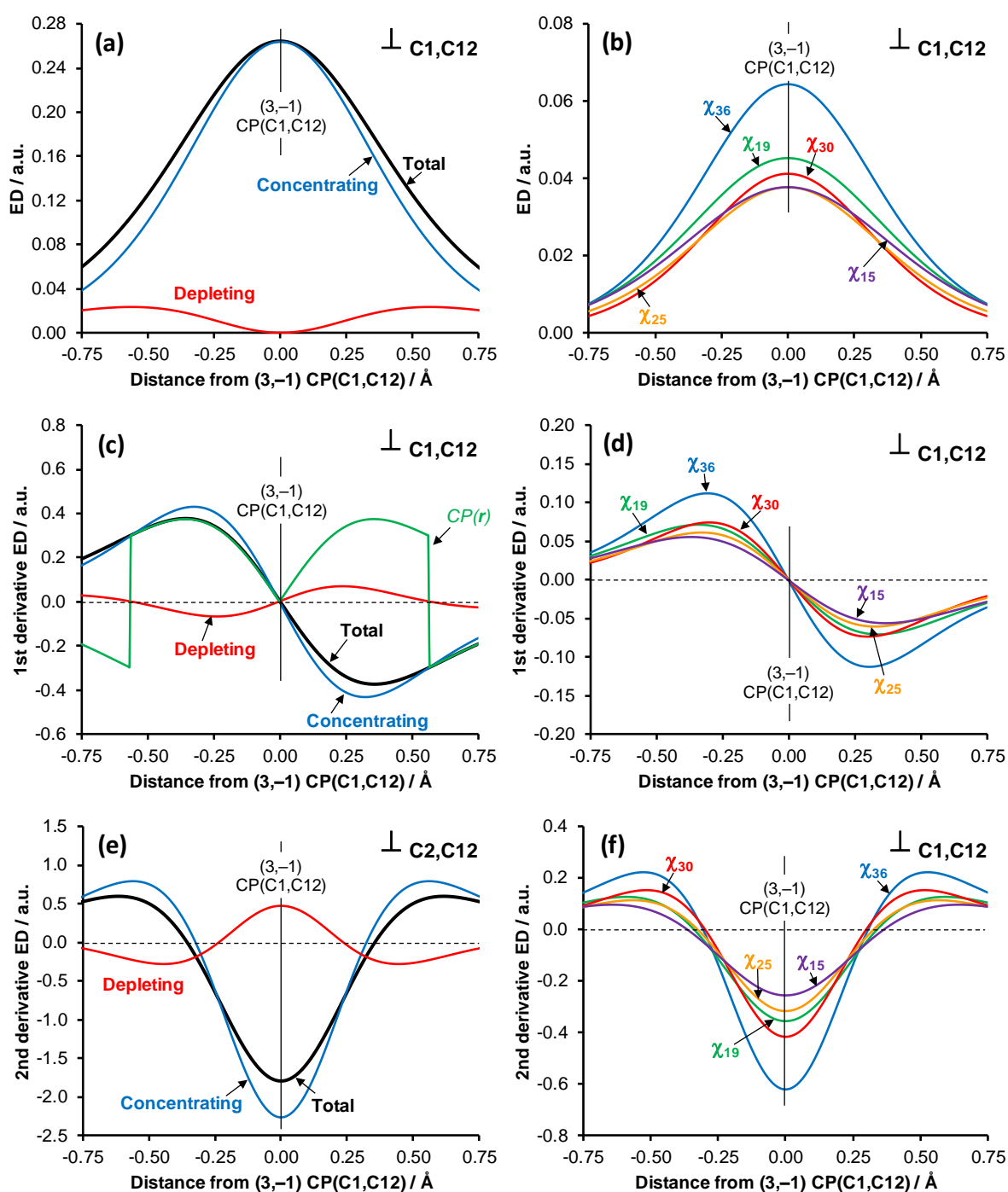


Figure S3. Decomposition of the total-ED (a), first derivative (c) and directional second partial derivatives (e) along the λ_2 -eigenvector in the C1,C12 inter-nuclear region in planar biphenyl, as well as the subsequent decomposition of the concentrating density into the largest MO contributions (b,d,f)

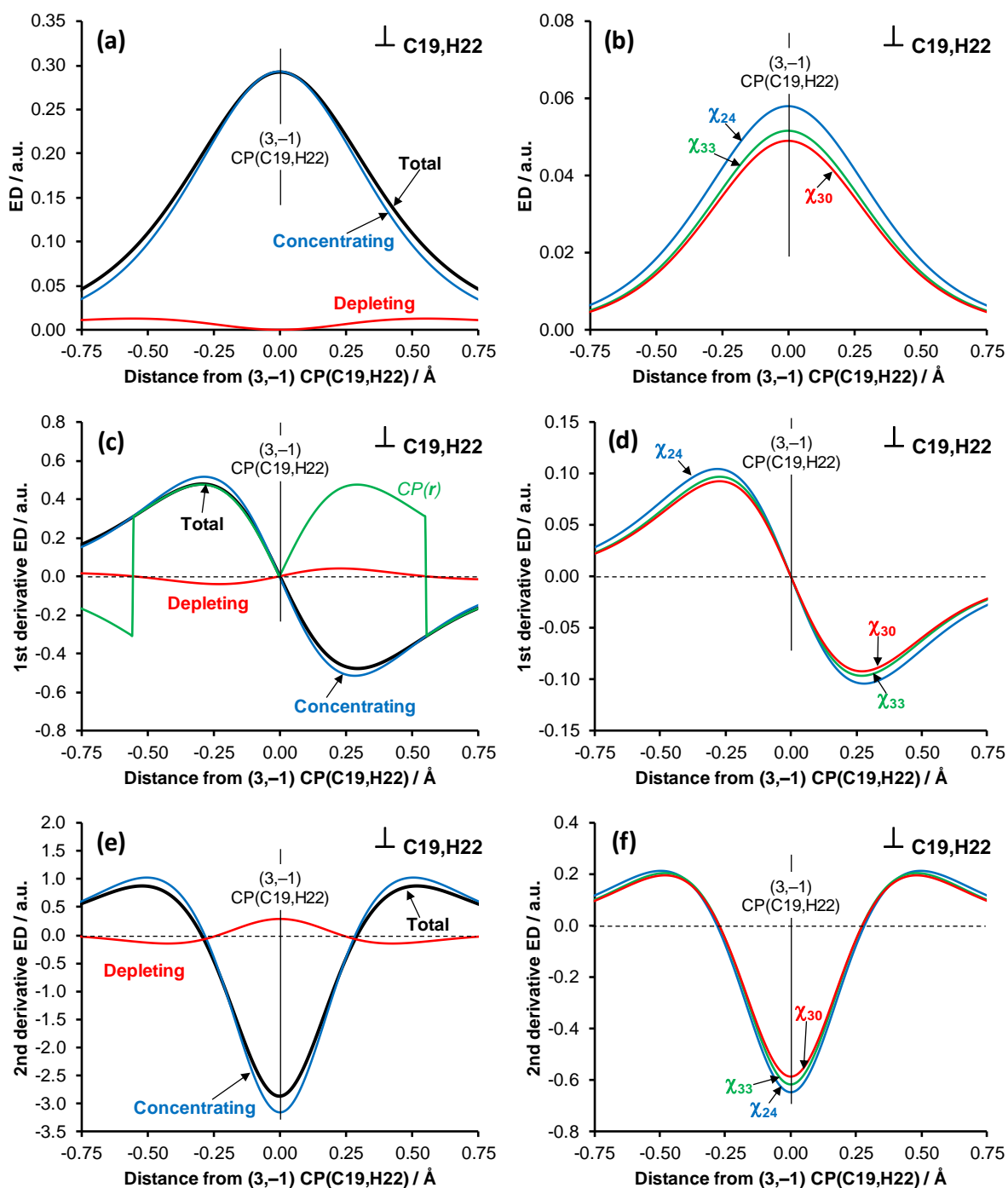


Figure S4. Decomposition of the total-ED (a), first derivative (c) and directional second partial derivatives (e) along the λ_2 -eigenvector in the C19,H22 inter-nuclear region in planar biphenyl, as well as the subsequent decomposition of the concentrating density into the largest MO contributions (b,d,f)

End of Part 4

Part 5 – Data pertaining to CP/MDP(H7,H18) in the planar/twisted biphenyl

Table S10. MO-ED data at (3,-1) CP(H7,H18) in planar and at MDP(H7,H18) in twisted Bph.

MO	Energy (a.u.)	Planar		Twisted	
		ED contribution (a.u.) / %-fraction	Classification based on 2nd derivative sign (λ_2)	ED contribution (a.u.) / %-fraction	Classification based on 2nd derivative sign (λ_2)
χ_1	-10.19173	0.00000 / 0.0%	<i>non-contributing</i>	0.00000 / 0.0%	<i>non-contributing</i>
χ_2	-10.19145	0.00000 / 0.0%	<i>non-contributing</i>	0.00000 / 0.0%	<i>non-contributing</i>
χ_3	-10.17726	0.00000 / 0.0%	<i>non-contributing</i>	0.00000 / 0.0%	<i>non-contributing</i>
χ_4	-10.17724	0.00000 / 0.0%	<i>non-contributing</i>	0.00000 / 0.0%	<i>non-contributing</i>
χ_5	-10.17720	0.00000 / 0.0%	<i>non-contributing</i>	0.00000 / 0.0%	<i>non-contributing</i>
χ_6	-10.17718	0.00000 / 0.0%	<i>non-contributing</i>	0.00000 / 0.0%	<i>non-contributing</i>
χ_7	-10.17658	0.00000 / 0.0%	<i>non-contributing</i>	0.00000 / 0.0%	<i>non-contributing</i>
χ_8	-10.17657	0.00000 / 0.0%	<i>non-contributing</i>	0.00000 / 0.0%	<i>non-contributing</i>
χ_9	-10.17653	0.00000 / 0.0%	<i>non-contributing</i>	0.00000 / 0.0%	<i>non-contributing</i>
χ_{10}	-10.17652	0.00000 / 0.0%	<i>non-contributing</i>	0.00000 / 0.0%	<i>non-contributing</i>
χ_{11}	-10.17586	0.00000 / 0.0%	<i>non-contributing</i>	0.00000 / 0.0%	<i>non-contributing</i>
χ_{12}	-10.17586	0.00000 / 0.0%	<i>non-contributing</i>	0.00000 / 0.0%	<i>non-contributing</i>
χ_{13}	-0.87581	0.00031 / 2.2%	<i>depleting</i>	0.00017 / 2.3%	<i>depleting</i>
χ_{14}	-0.85459	0.00000 / 0.0%	<i>non-contributing</i>	0.00000 / 0.0%	<i>non-contributing</i>
χ_{15}	-0.78384	0.00028 / 1.9%	<i>depleting</i>	0.00014 / 1.9%	<i>depleting</i>
χ_{16}	-0.75827	0.00072 / 5.1%	<i>concentrating</i>	0.00034 / 4.5%	<i>depleting</i>
χ_{17}	-0.74841	0.00000 / 0.0%	<i>non-contributing</i>	0.00000 / 0.0%	<i>non-contributing</i>
χ_{18}	-0.72791	0.00000 / 0.0%	<i>non-contributing</i>	0.00000 / 0.0%	<i>non-contributing</i>
χ_{19}	-0.63238	0.00015 / 1.1%	<i>concentrating</i>	0.00004 / 0.5%	<i>concentrating</i>
χ_{20}	-0.62793	0.00188 / 13.2%	<i>concentrating</i>	0.00095 / 12.8%	<i>depleting</i>
χ_{21}	-0.59212	0.00000 / 0.0%	<i>non-contributing</i>	0.00000 / 0.0%	<i>non-contributing</i>
χ_{22}	-0.58592	0.00000 / 0.0%	<i>non-contributing</i>	0.00000 / 0.0%	<i>non-contributing</i>
χ_{23}	-0.54310	0.00198 / 13.9%	<i>concentrating</i>	0.00077 / 10.3%	<i>concentrating</i>
χ_{24}	-0.50360	0.00000 / 0.0%	<i>non-contributing</i>	0.00000 / 0.0%	<i>non-contributing</i>
χ_{25}	-0.48074	0.00237 / 16.6%	<i>concentrating</i>	0.00113 / 15.3%	<i>concentrating</i>
χ_{26}	-0.47350	0.00019 / 1.3%	<i>depleting</i>	0.00019 / 2.6%	<i>depleting</i>
χ_{27}	-0.44376	0.00000 / 0.0%	<i>non-contributing</i>	0.00000 / 0.0%	<i>non-contributing</i>
χ_{28}	-0.43615	0.00000 / 0.0%	<i>non-contributing</i>	0.00000 / 0.0%	<i>non-contributing</i>
χ_{29}	-0.43567	0.00273 / 19.1%	<i>concentrating</i>	0.00111 / 15.0%	<i>concentrating</i>
χ_{30}	-0.43051	0.00090 / 6.3%	<i>concentrating</i>	0.00050 / 6.8%	<i>concentrating</i>

Appendix I

Table S10 continues.

MO	Energy (a.u.)	Planar		Twisted	
		ED contribution (a.u.) / %-fraction	Classification based on 2nd derivative sign (λ_2)	ED contribution (a.u.) / %-fraction	Classification based on 2nd derivative sign (λ_2)
χ_{31}	-0.41671	0.00000 / 0.0%	<i>non-contributing</i>	0.00000 / 0.0%	<i>non-contributing</i>
χ_{32}	-0.39513	0.00000 / 0.0%	<i>non-contributing</i>	0.00000 / 0.0%	<i>non-contributing</i>
χ_{33}	-0.36916	0.00000 / 0.0%	<i>non-contributing</i>	0.00000 / 0.0%	<i>non-contributing</i>
χ_{34}	-0.36616	0.00000 / 0.0%	<i>non-contributing</i>	0.00000 / 0.0%	<i>depleting</i>
χ_{35}	-0.36285	0.00157 / 11.0%	<i>concentrating</i>	0.00083 / 11.2%	<i>concentrating</i>
χ_{36}	-0.34790	0.00118 / 8.3%	<i>concentrating</i>	0.00066 / 8.6%	<i>concentrating</i>
χ_{37}	-0.33466	0.00000 / 0.0%	<i>non-contributing</i>	0.00000 / 0.0%	<i>non-contributing</i>
χ_{38}	-0.29363	0.00000 / 0.0%	<i>non-contributing</i>	0.00000 / 0.0%	<i>non-contributing</i>
χ_{39}	-0.26531	0.00000 / 0.0%	<i>non-contributing</i>	0.00000 / 0.0%	<i>non-contributing</i>
χ_{40}	-0.25903	0.00000 / 0.0%	<i>non-contributing</i>	0.00024 / 3.3%	<i>concentrating</i>
χ_{41}	-0.23027	0.00000 / 0.0%	<i>non-contributing</i>	0.00034 / 4.6%	<i>depleting</i>

Appendix I

Table S11. MO-DI data (in e^- -pairs) for noncovalent interaction H7...H18 in the planar Bph.

MO	1–24 ^a	25	26	27	28	29	30	31	32	33	34	35	36	37	38	39	40	41
1–24	0.005 ^a	0.004	0.000	-0.002	0.000	0.005	0.001	-0.002	0.000	-0.002	0.000	0.004	0.001	-0.003	0.000	0.000	0.000	0.000
25	0.004	0.008	0.000	-0.006	0.000	0.009	0.002	-0.006	0.000	-0.004	0.000	0.006	0.002	-0.007	0.000	0.000	0.000	0.000
26	0.000	0.000	0.000	0.000	0.000	0.000	0.000	0.000	0.000	0.000	0.000	0.000	0.000	0.000	0.000	0.000	0.000	0.000
27	-0.002	-0.006	0.000	0.006	0.000	-0.008	-0.002	0.006	0.000	0.003	0.000	-0.005	-0.001	0.007	0.000	0.000	0.000	0.000
28	0.000	0.000	0.000	0.000	0.000	0.000	0.000	0.000	0.000	0.000	0.000	0.000	0.000	0.000	0.000	0.000	0.000	0.000
29	0.005	0.009	0.000	-0.008	0.000	0.012	0.003	-0.008	0.000	-0.005	0.000	0.008	0.002	-0.009	0.000	0.000	0.000	0.000
30	0.001	0.002	0.000	-0.002	0.000	0.003	0.001	-0.002	0.000	-0.001	0.000	0.002	0.001	-0.002	0.000	0.000	0.000	0.000
31	-0.002	-0.006	0.000	0.006	0.000	-0.008	-0.002	0.006	0.000	0.003	0.000	-0.005	-0.001	0.007	0.000	0.000	0.000	0.000
32	0.000	0.000	0.000	0.000	0.000	0.000	0.000	0.000	0.000	0.000	0.000	0.000	0.000	0.000	0.000	0.000	0.000	0.000
33	-0.002	-0.004	0.000	0.003	0.000	-0.005	-0.001	0.003	0.000	0.002	0.000	-0.003	-0.001	0.004	0.000	0.000	0.000	0.000
34	0.000	0.000	0.000	0.000	0.000	0.000	0.000	0.000	0.000	0.000	0.000	0.000	0.000	0.000	0.000	0.000	0.000	0.000
35	0.004	0.006	0.000	-0.005	0.000	0.008	0.002	-0.005	0.000	-0.003	0.000	0.006	0.001	-0.006	0.000	0.000	0.000	0.000
36	0.001	0.002	0.000	-0.001	0.000	0.002	0.001	-0.001	0.000	-0.001	0.000	0.001	0.001	-0.001	0.000	0.000	0.000	0.000
37	-0.003	-0.007	0.000	0.007	0.000	-0.009	-0.002	0.007	0.000	0.004	0.000	-0.006	-0.001	0.008	0.000	0.000	0.000	0.000
38	0.000	0.000	0.000	0.000	0.000	0.000	0.000	0.000	0.000	0.000	0.000	0.000	0.000	0.000	0.000	0.000	0.000	0.000
39	0.000	0.000	0.000	0.000	0.000	0.000	0.000	0.000	0.000	0.000	0.000	0.000	0.000	0.000	0.000	0.000	0.000	0.000
40	0.000	0.000	0.000	0.000	0.000	0.000	0.000	0.000	0.000	0.000	0.000	0.000	0.000	0.000	0.000	0.000	0.000	0.000
41	0.000	0.000	0.000	0.000	0.000	0.000	0.000	0.000	0.000	0.000	0.000	0.000	0.000	0.000	0.000	0.000	0.000	0.000
Diagonal	0.015 ^a	0.008	0.000	0.006	0.000	0.012	0.001	0.006	0.000	0.002	0.000	0.006	0.001	0.008	0.000	0.000	0.000	0.000
Off-diagonal	-0.004 ^a	0.001	0.000	-0.009	0.000	-0.002	0.002	-0.009	0.000	-0.004	0.000	0.001	0.002	-0.011	0.000	0.000	0.000	0.000
Total	0.011	0.008	0.000	-0.003	0.000	0.010	0.003	-0.003	0.000	-0.002	0.000	0.007	0.003	-0.003	0.000	0.000	0.000	0.000

^a MOs 1–24 were combined for the sake of brevity. The contributions made by diagonal elements of these MOs equal 0.015, whereas off-diagonal terms of only these MOs equal -0.01 to give a net contribution of 0.05. Interference with the remaining MOs (MOs 25–41) gives a positive, off-diagonal contribution of +0.006, so that the total contribution of MOs 1–24 equals 0.011.

Appendix I

Table S12. MO-DI data (in e^- -pairs) for noncovalent interaction H7...H18 in the twisted Bph.

MO	1–24 ^a	25	26	27	28	29	30	31	32	33	34	35	36	37	38	39	40	41
1–24	0.001 ^a	0.004	0.000	-0.002	0.000	0.005	0.001	-0.002	0.000	-0.002	0.000	0.004	0.001	-0.003	0.000	0.000	0.000	0.000
25	0.000	0.008	0.000	-0.007	0.000	0.008	0.003	-0.007	-0.001	-0.003	0.000	0.007	0.002	-0.007	0.000	0.000	0.000	0.000
26	0.000	0.000	0.000	0.000	0.000	0.000	0.000	0.000	0.000	0.000	0.000	0.000	0.000	0.000	0.000	0.000	0.000	0.000
27	0.001	-0.007	0.000	0.006	0.000	-0.007	-0.002	0.006	0.001	0.003	0.000	-0.006	-0.002	0.007	0.000	0.000	0.000	0.000
28	0.000	0.000	0.000	0.000	0.000	0.000	0.000	0.000	0.000	0.000	0.000	0.000	0.000	0.000	0.000	0.000	0.000	0.000
29	0.000	0.008	0.000	-0.007	0.000	0.009	0.003	-0.007	-0.001	-0.003	0.000	0.007	0.002	-0.008	0.000	0.000	0.000	0.000
30	0.000	0.003	0.000	-0.002	0.000	0.003	0.001	-0.002	0.000	-0.001	0.000	0.002	0.001	-0.002	0.000	0.000	0.000	0.000
31	0.001	-0.007	0.000	0.006	0.000	-0.007	-0.002	0.006	0.001	0.003	0.000	-0.006	-0.002	0.007	0.000	0.000	0.000	0.000
32	0.000	-0.001	0.000	0.001	0.000	-0.001	0.000	0.001	0.000	0.000	0.000	-0.001	0.000	0.001	0.000	0.000	0.000	0.000
33	0.000	-0.003	0.000	0.003	0.000	-0.003	-0.001	0.003	0.000	0.001	0.000	-0.003	-0.001	0.003	0.000	0.000	0.000	0.000
34	0.000	0.000	0.000	0.000	0.000	0.000	0.000	0.000	0.000	0.000	0.000	0.000	0.000	-0.001	0.000	0.000	0.000	0.000
35	0.000	0.007	0.000	-0.006	0.000	0.007	0.002	-0.006	-0.001	-0.003	0.000	0.006	0.002	-0.006	0.000	0.000	0.000	0.000
36	0.000	0.002	0.000	-0.002	0.000	0.002	0.001	-0.002	0.000	-0.001	0.000	0.002	0.001	-0.002	0.000	0.000	0.000	0.000
37	0.001	-0.007	0.000	0.007	0.000	-0.008	-0.002	0.007	0.001	0.003	-0.001	-0.006	-0.002	0.007	0.000	0.000	0.000	0.000
38	0.000	0.000	0.000	0.000	0.000	0.000	0.000	0.000	0.000	0.000	0.000	0.000	0.000	0.000	0.000	0.000	0.000	0.000
39	0.000	0.000	0.000	0.000	0.000	0.000	0.000	0.000	0.000	0.000	0.000	0.000	0.000	0.000	0.000	0.000	0.000	0.000
40	0.000	0.000	0.000	0.000	0.000	0.000	0.000	0.000	0.000	0.000	0.000	0.000	0.000	0.000	0.000	0.000	0.000	0.000
41	0.000	0.000	0.000	0.000	0.000	0.000	0.000	0.000	0.000	0.000	0.000	0.000	0.000	0.000	0.000	0.000	0.000	0.000
Diagonal	0.014 ^a	0.008	0.000	0.006	0.000	0.009	0.001	0.006	0.000	0.001	0.000	0.006	0.001	0.007	0.000	0.000	0.000	0.000
Off-diagonal	-0.011	-0.005	0.000	-0.007	0.000	-0.005	0.000	-0.007	0.000	-0.002	0.000	-0.003	0.001	-0.008	0.000	0.000	0.000	0.000
Total	0.003	0.003	0.000	-0.001	0.000	0.003	0.001	-0.001	0.000	-0.001	0.000	0.003	0.001	-0.001	0.000	0.000	0.000	0.000

^a MOs 1–24 were combined for the sake of brevity. The contributions made by diagonal elements of these MOs equal 0.014, whereas off-diagonal terms of only these MOs equal -0.013 to give a net contribution of 0.001. Interference with the remaining MOs (MOs 25–41) gives a positive, off-diagonal contribution of +0.002, so that the total contribution of MOs 1–24 equals 0.003.

Table S13. Summary of MO-ED & MO-DI data for H7...H18 in planar and twisted Bph

Classification based on λ_2	Planar		Twisted	
	Number of MOs	Contribution to $\rho(\text{CP})^a$	Number of MOs	Contribution to $\rho(\text{MDP})^a$
<i>Concentrating</i>	9	0.013	8	0.005
<i>Depleting</i>	3	0.001	7	0.002
<i>Non-contributing</i>	29	0.000	26	0.000
Delocalization	Contribution to DI^b		Contribution to DI^b	
<i>Overlapping</i>	0.064		0.060	
<i>Interference</i>	-0.033		-0.049	
<i>Net DI</i>	0.031		0.011	

^a in a.u.; ^b in e^- -pairs.

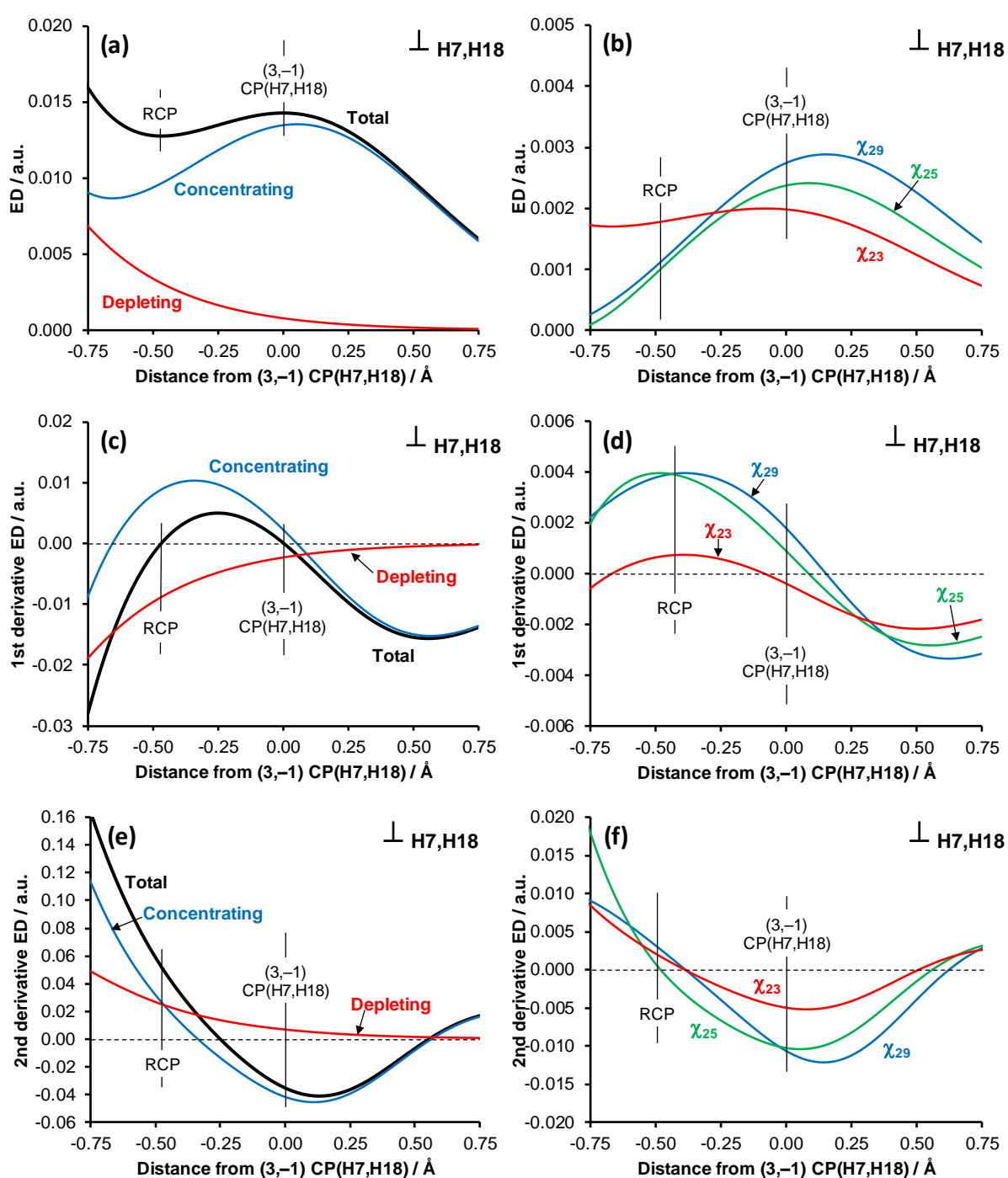


Figure S5. Decomposition of the total-ED (a), first derivative (c) and directional partial derivatives (e) along the λ_2 -eigenvector in the H7,H18 inter-nuclear region in planar biphenyl, as well as the subsequent decomposition of the concentrating density into the largest MO contributions (b,d,f)

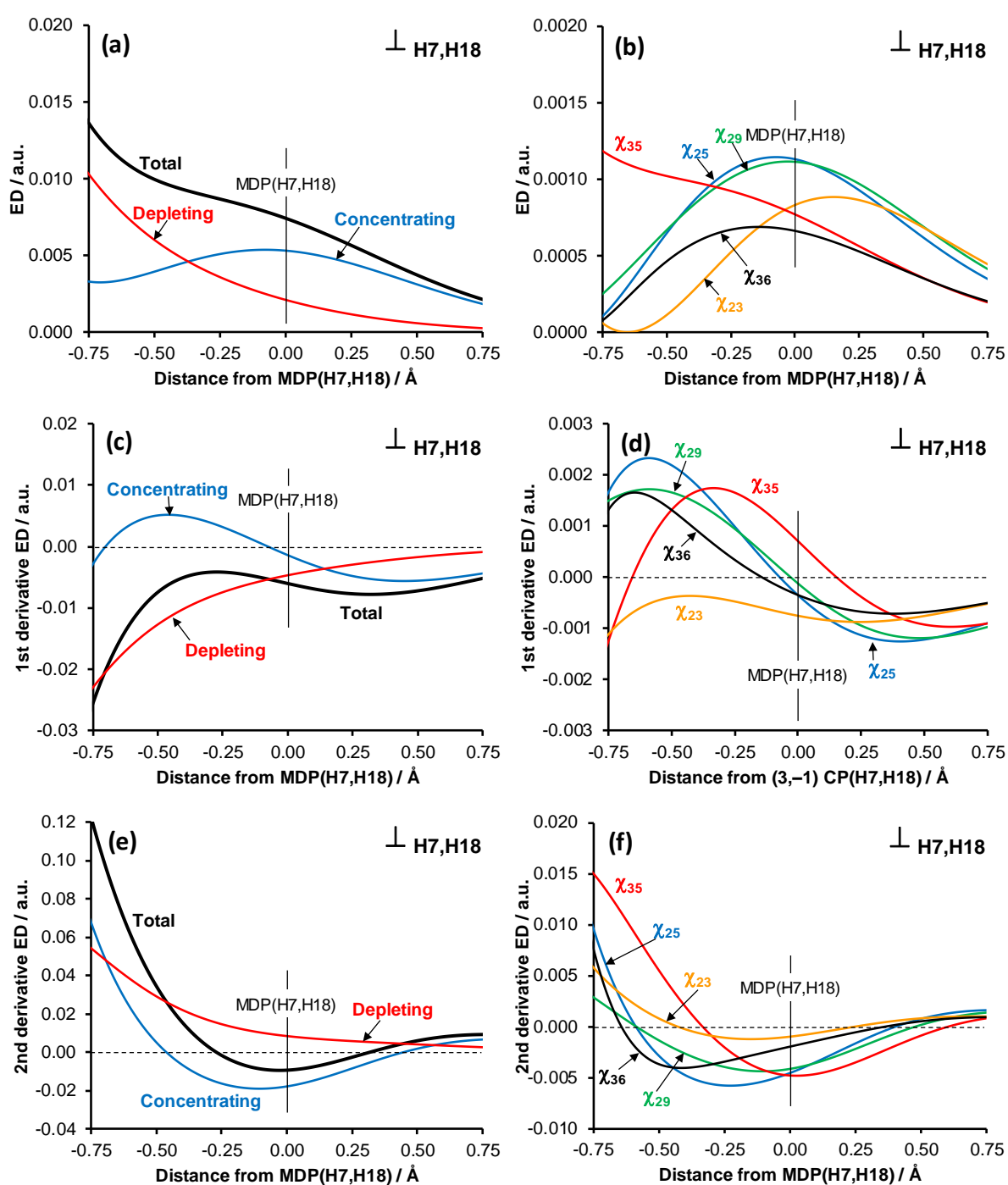


Figure S6. Decomposition of the total-ED (a), first derivative (c) and directional partial derivatives (e) along the λ_2 -eigenvector in the H7,H18 inter-nuclear region in twisted biphenyl, as well as the subsequent decomposition of the concentrating density into the largest MO contributions (b,d,f)

End of Part 5

Part 6 – Data pertaining to H ···H density bridges in Li₄H₄
Table S14. MO-ED data at (3,-1) CP(H2,H4), CP(H2,H5) and CP(H4,H5) in Li₄H₄.

MO	Energy (a.u.)	H2,H4		H2,H5		H4,H5	
		ED contribution (a.u.) / %-fraction	Classification based on 2nd derivative sign (λ_2)	ED contribution (a.u.) / %-fraction	Classification based on 2nd derivative sign (λ_2)	ED contribution (a.u.) / %-fraction	Classification based on 2nd derivative sign (λ_2)
χ_1	-10.19173	0.00013 / 0.8%	<i>Depleting</i>	0.00013 / 0.8%	<i>Depleting</i>	0.00013 / 0.8%	<i>Depleting</i>
χ_2	-10.19145	0.00005 / 0.3%	<i>Depleting</i>	0.00005 / 0.3%	<i>Depleting</i>	0.00003 / 0.2%	<i>Depleting</i>
χ_3	-10.17726	0.00002 / 0.1%	<i>Depleting</i>	0.00001 / 0.1%	<i>Depleting</i>	0.00010 / 0.7%	<i>Depleting</i>
χ_4	-10.17724	0.00006 / 0.4%	<i>Depleting</i>	0.00007 / 0.5%	<i>Depleting</i>	0.00000 / 0.0%	<i>Non-Contributing</i>
χ_5	-10.17720	0.00829 / 54.2%	<i>Concentrating</i>	0.00829 / 54.2%	<i>Concentrating</i>	0.00829 / 54.2%	<i>Concentrating</i>
χ_6	-10.17718	0.00000 / 0.0%	<i>Non-Contributing</i>	0.00158 / 10.4%	<i>Concentrating</i>	0.00516 / 33.8%	<i>Concentrating</i>
χ_7	-10.17658	0.00369 / 24.2%	<i>Concentrating</i>	0.00226 / 14.8%	<i>Concentrating</i>	0.00079 / 5.2%	<i>Concentrating</i>
χ_8	-10.17657	0.00305 / 20.0%	<i>Concentrating</i>	0.00290 / 19.0%	<i>Concentrating</i>	0.00079 / 5.2%	<i>Concentrating</i>

Appendix I

Table S15. MO-DI data for the H2,H5 atom-pair in Li₄H₄.

MO	MO1	MO2	MO3	MO4	MO5	MO6	MO7	MO8
MO1	0.000	0.000	0.000	0.000	0.001	0.000	0.000	0.000
MO2	0.000	0.000	0.000	0.000	0.000	0.000	0.000	0.000
MO3	0.000	0.000	0.000	0.000	0.000	0.000	0.000	0.000
MO4	0.000	0.000	0.000	0.000	0.000	0.000	0.000	0.000
MO5	0.001	0.000	0.000	0.000	0.207	-0.029	-0.057	-0.103
MO6	0.000	0.000	0.000	0.000	-0.029	0.009	0.009	0.016
MO7	0.000	0.000	0.000	0.000	-0.057	0.009	0.051	0.032
MO8	0.000	0.000	0.000	0.000	-0.103	0.016	0.032	0.092
Diagonal	0.000	0.000	0.000	0.000	0.207	0.009	0.051	0.092
Off-diagonal	0.000	0.000	0.000	0.000	-0.189	-0.004	-0.016	-0.055
Total	0.000	0.000	0.000	0.000	0.018	0.005	0.035	0.037

Table S16. Summary of MO-ED and MO-DI data for three H···H density bridges in Li₄H₄.

Classification based on λ_2	H2,H4		H2,H5		H4,H5	
	Number of MOs	Contribution to $\rho(\text{CP})^a$	Number of MOs	Contribution to $\rho(\text{CP})^a$	Number of MOs	Contribution to $\rho(\text{CP})^a$
<i>Concentrating</i>	3	0.015	4	0.015	4	0.015
<i>Depleting</i>	4	0.000	4	0.000	3	0.000
<i>Non-contributing</i>	1	0.000	0	0.000	1	0.000
Delocalization	Contribution to DI^b		Contribution to DI^b		Contribution to DI^b	
<i>Overlapping</i>	0.36		0.36		0.36	
<i>Interference</i>	-0.26		-0.26		-0.26	
<i>Net DI</i>	0.09		0.09		0.09	

^a in a.u.; ^b in e^- -pairs.

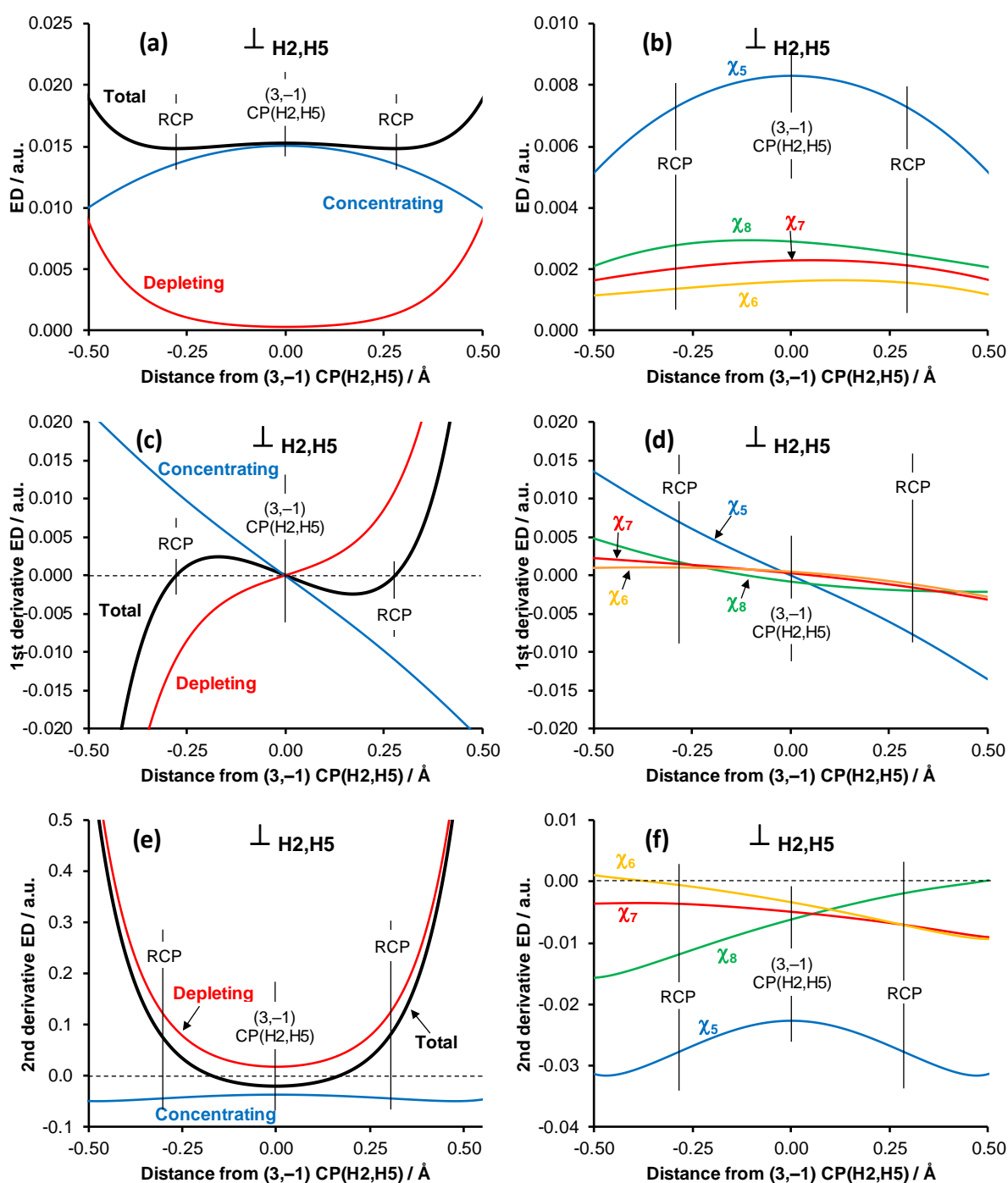


Figure S7. Decomposition of the total-ED (a), first derivative (c) and directional partial derivatives (e) along the λ_2 -eigenvector in the H₂,H₅ inter-nuclear region in Li₄H₄, as well as the subsequent decomposition of the concentrating density into the largest MO contributions (b,d,f).

End of Part 6

Appendix II

The CH \cdots HC interaction in biphenyl is a delocalized, molecular wide and entirely non-classical interaction: results from FALDI analysis

Published in:

Journal of Computational Chemistry **2021**. DOI: 10.1002/jcc.26491.

Supplementary Information

The CH...HC interaction in biphenyl is a delocalized, molecular-wide and entirely non-classical interaction: results from FALDI analysis

Thomas G. Bates, Jurgens H. de Lange* and Ignacy Cukrowski*

Department of Chemistry, Faculty of Natural and Agricultural Sciences, University of Pretoria, Lynnwood Road, Hatfield, Pretoria 0002, South Africa

*Correspondence to: Ignacy Cukrowski
Jurgens de Lange:

E-mail: ignacy.cukrowski@up.ac.za
E-mail: jurgens.delange@up.ac.za

Supplementary Information

Table of contents:	Page
Part 1. Cartesian Coordinates of all Molecules Studied	183
Part 2. Cross-Section Comparison Between MO- and FALDI-ED Method for Biphenyl	185
Part 3. Alternate Fragment Partitioning Scheme	188
Part 4. FALDI-ED Data for H7...H18 Interaction in Biphenyl	
Fragment Analysis	192
Diatomic Analysis	193

Part 1. Cartesian Coordinates of all molecules studied**Table S1.** Cartesian coordinates of planar biphenyl at the B3LYP/cc-pVDZ level.

Atom	X	Y	Z
C1	0.000000	0.747659	0.000000
C2	1.201002	1.486214	0.000000
C3	1.202756	2.881607	0.000000
C4	0.000000	3.592065	0.000000
C5	-1.202756	2.881607	0.000000
C6	-1.201002	1.486214	0.000000
H7	2.162178	0.972810	0.000000
H8	2.155610	3.416086	0.000000
H9	0.000000	4.684170	0.000000
H10	-2.155610	3.416086	0.000000
H11	-2.162178	0.972810	0.000000
C12	0.000000	-0.747659	0.000000
C13	1.201002	-1.486214	0.000000
C14	1.202756	-2.881607	0.000000
C15	0.000000	-3.592065	0.000000
C16	-1.202756	-2.881607	0.000000
C17	-1.201002	-1.486214	0.000000
H18	2.162178	-0.972810	0.000000
H19	2.155610	-3.416086	0.000000
H20	0.000000	-4.684170	0.000000
H21	-2.155610	-3.416086	0.000000
H22	-2.162178	-0.972810	0.000000

Molecular Energy = -463.330812 a.u.

Appendix II

Table S2. Cartesian coordinates of twisted biphenyl at the B3LYP/cc-pVDZ level.

Atom	X	Y	Z
C1	0.000000	0.743784	0.000000
C2	1.137590	1.468260	-0.402647
C3	1.137840	2.864563	-0.402880
C4	0.000000	3.569885	0.000000
C5	-1.137840	2.864563	0.402880
C6	-1.137590	1.468260	0.402647
H7	2.024118	0.929542	-0.744099
H8	2.030290	3.404597	-0.728007
H9	0.000000	4.662191	0.000000
H10	-2.030290	3.404597	0.728007
H11	-2.024118	0.929542	0.744099
C12	0.000000	-0.743784	0.000000
C13	1.137590	-1.468260	0.402647
C14	1.137840	-2.864563	0.402880
C15	0.000000	-3.569885	0.000000
C16	-1.137840	-2.864563	-0.402880
C17	-1.137590	-1.468260	-0.402647
H18	2.024118	-0.929542	0.744099
H19	2.030290	-3.404597	0.728007
H20	0.000000	-4.662191	0.000000
H21	-2.030290	-3.404597	-0.728007
H22	-2.024118	-0.929542	-0.744099

Molecular Energy = -463.333574 a.u.

End of Part 1

Part 2. Cross-section comparison between MO-ED and FALDI-ED method for Biphenyl

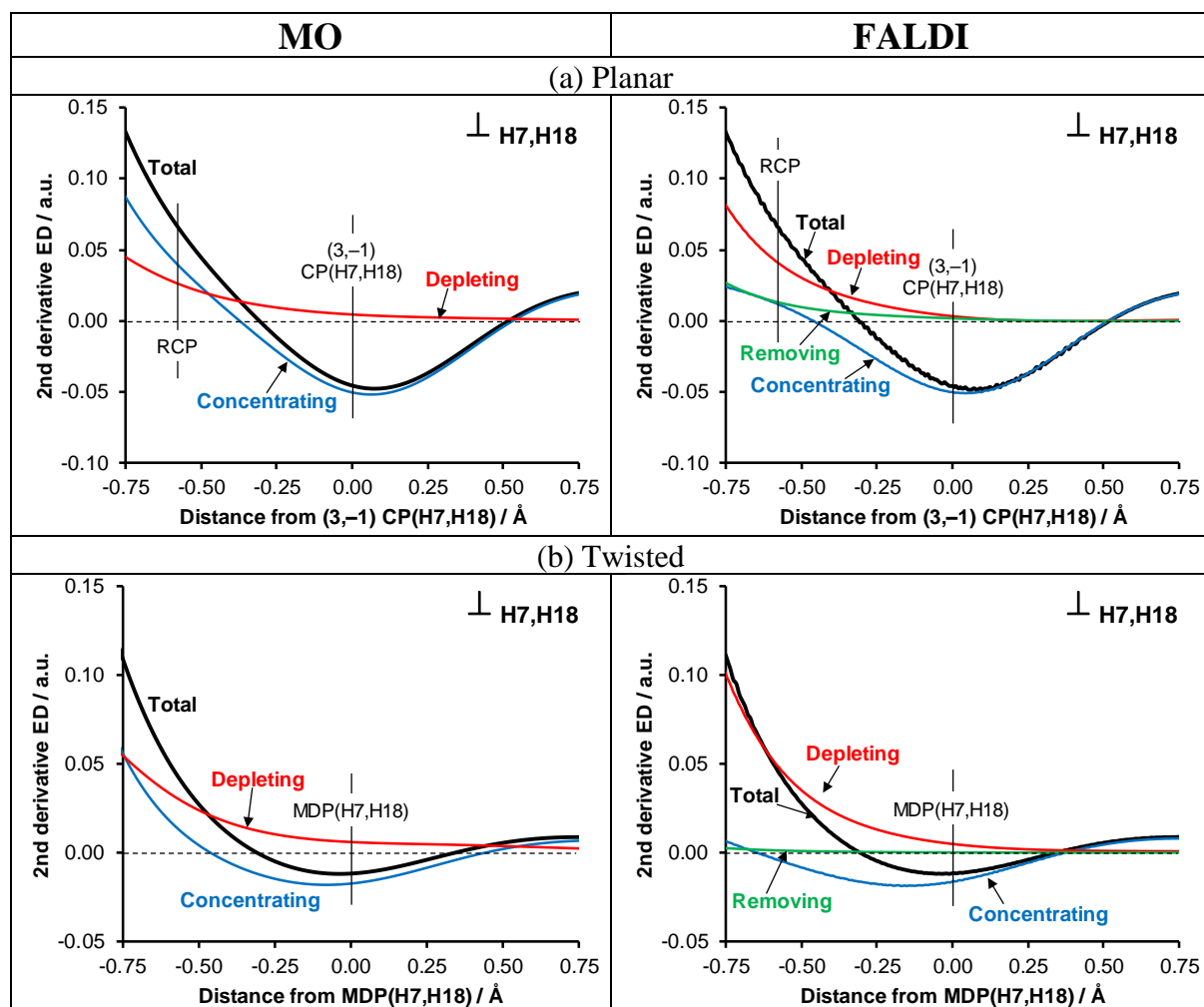


Figure S1 – Decomposition of the directional second partial derivative $\rho(\text{tot})$ along the λ_2 -eigenvector crossing (a) the CP(H7,H18) in planar conformer and (b) MDP(H7,H18) in twisted conformer of Bph to major contributions (concentrating, depleting, and removing) using MO and FALDI densities.

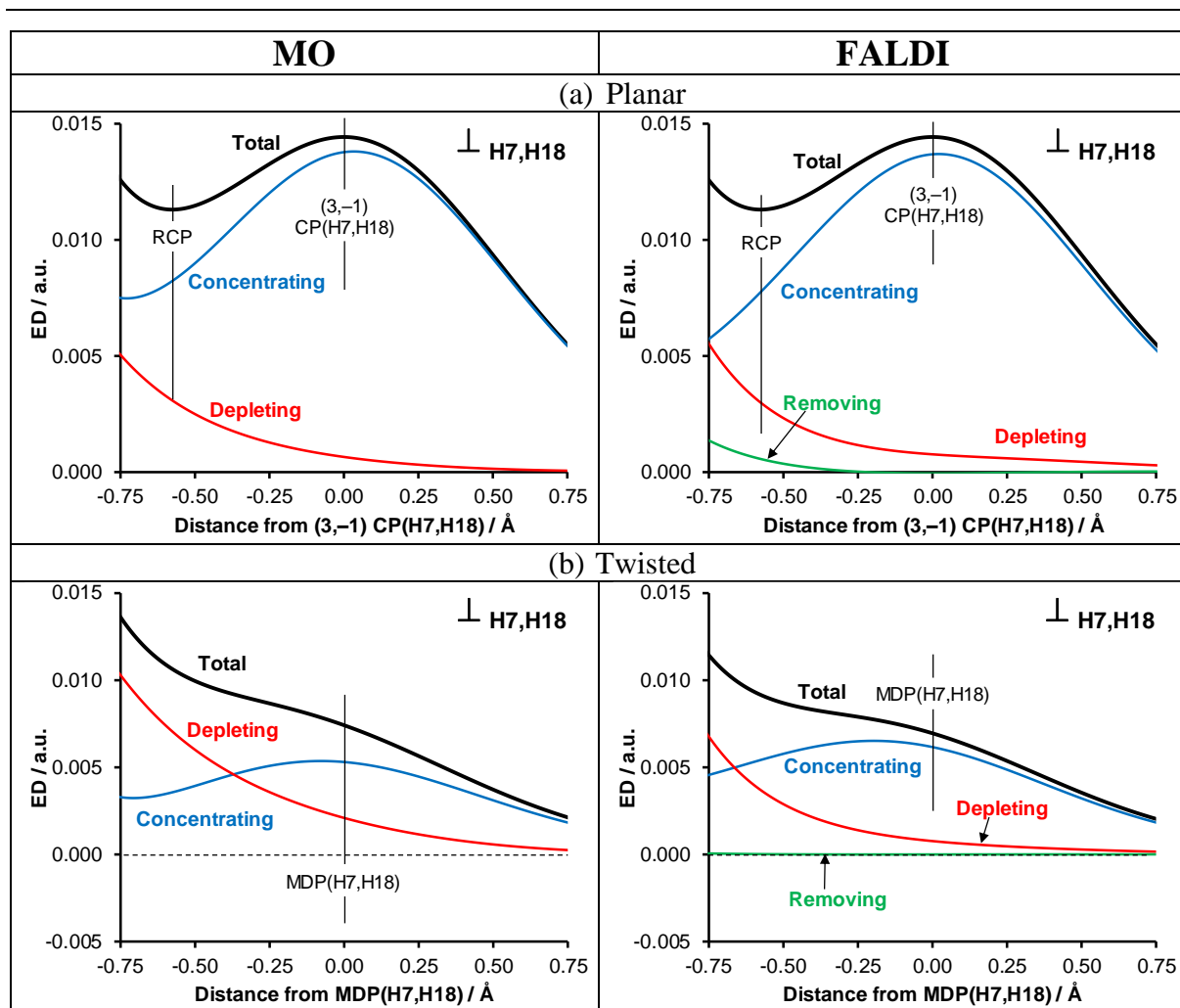


Figure S2 – Decomposition of the $\rho(\text{tot})$ along the λ_2 -eigenvector crossing (a) the CP(H7,H18) in planar conformer and (b) MDP(H7,H18) in twisted conformer of Bph to major contributions (concentrating, depleting, and removing) using MO and FALDI densities.

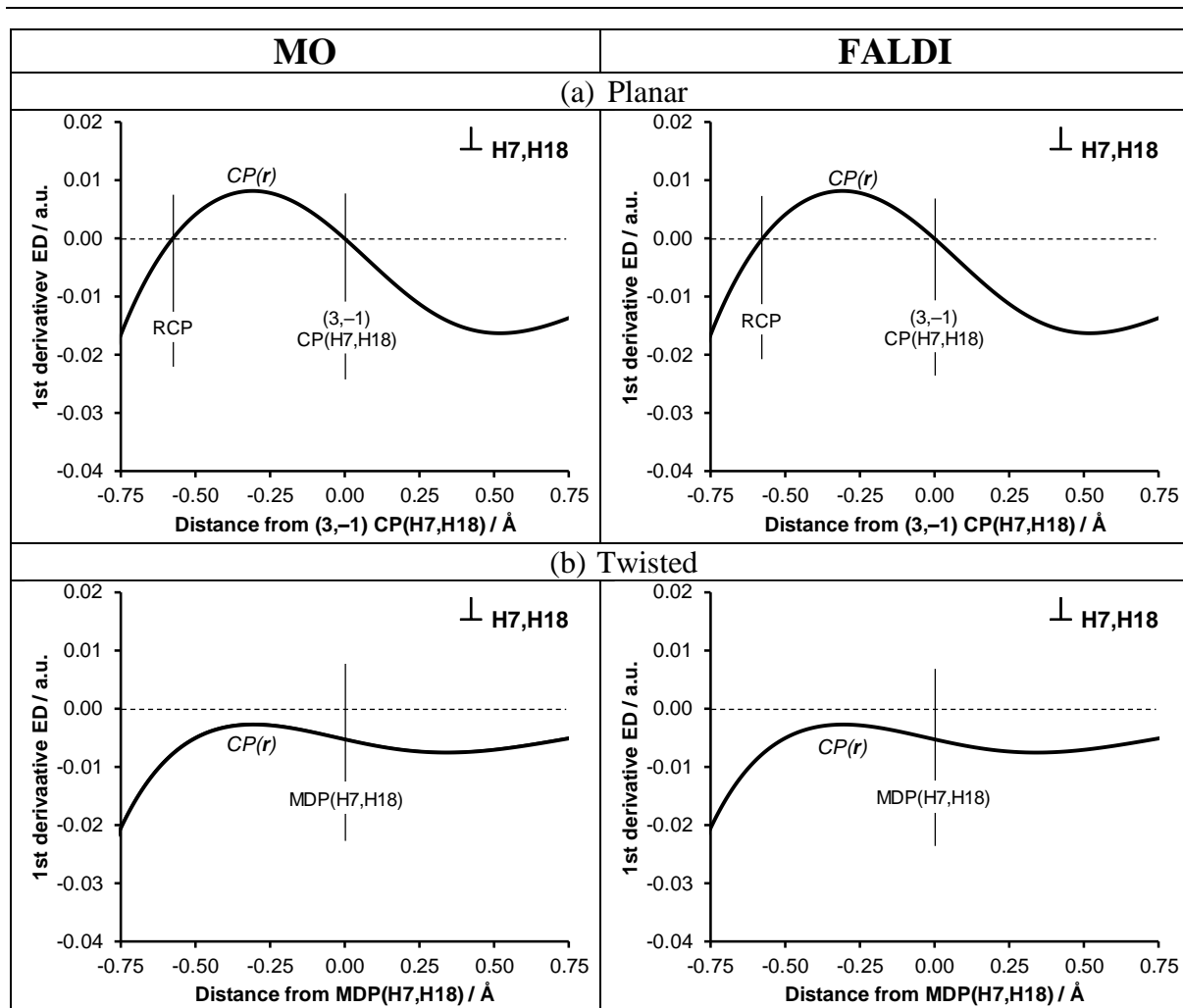
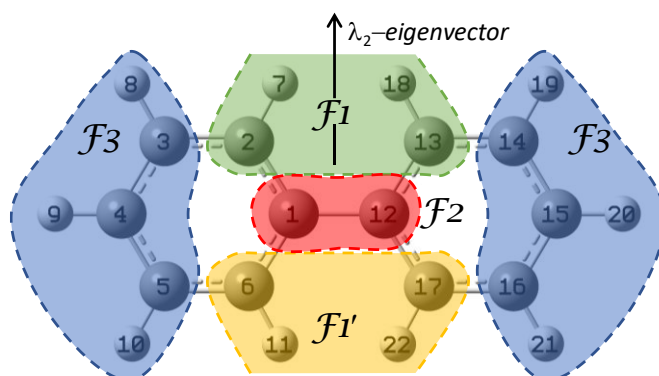


Figure S3 – $CP(\mathbf{r})$ function cross-sections along the λ_2 -eigenvector crossing the (a) $CP(H7,H18)$ in the planar conformer and (b) $MDP(H7,H18)$ in twisted conformer of Bph using MO and FALDI densities.

End of Part 2

Part 3. Alternate Fragment Partitioning Scheme

A different fragmentation scheme was performed, whereby the set of molecular fragments \mathcal{F} used in this work is shown in Scheme S1. Differing from the fragmentation scheme in the main body, this scheme groups the 4-centred bay-region into one fragment ($\mathcal{F}1$), and the other bay-region forms another fragment ($\mathcal{F}1'$). The remaining $\mathcal{F}3$ fragment encompasses 12 atoms of Bph that are not ‘directly’ involved in the steric contact.



Scheme S1. Definition of fragments for FALDI analysis. $\mathcal{F}1$: C2H...HC13 bay, $\mathcal{F}1'$: C6H...HC17 bay, $\mathcal{F}2$: C1-C12 linker, and $\mathcal{F}3$: combined fragment containing remainder of the molecule. The position and direction of the λ_2 -eigenvector used for cross-section analysis is also shown.

Cross-sections along the λ_2 -eigenvector for the H7...H18 region in planar Bph, as well as isosurfaces of the largest fragment contributions to the ED at CP(H7,H18), are shown in Figure 2. The largest contributor to the ED (62%) is the intra-fragment delocalization of fragment $\mathcal{F}1$. Electrons delocalized among the two CH groups creates a clean channel of delocalized density and results in a strong concentration of electrons at CP(H7,H18). However, two other components also contribute electrons in a concentrating fashion: the inter-fragment delocalized density between fragments $\mathcal{F}1$ and $\mathcal{F}3$, as well as between $\mathcal{F}1$ and $\mathcal{F}1'$ (22% and 4%, respectively).

Both of these components result in a very similar channel of delocalized density between the H-atoms. Finally, the only component that results in a significant depletion of density is the inter-fragment delocalization between $\mathcal{F}1$ and $\mathcal{F}2$ (contributing 10% to CP(H7,H18)).

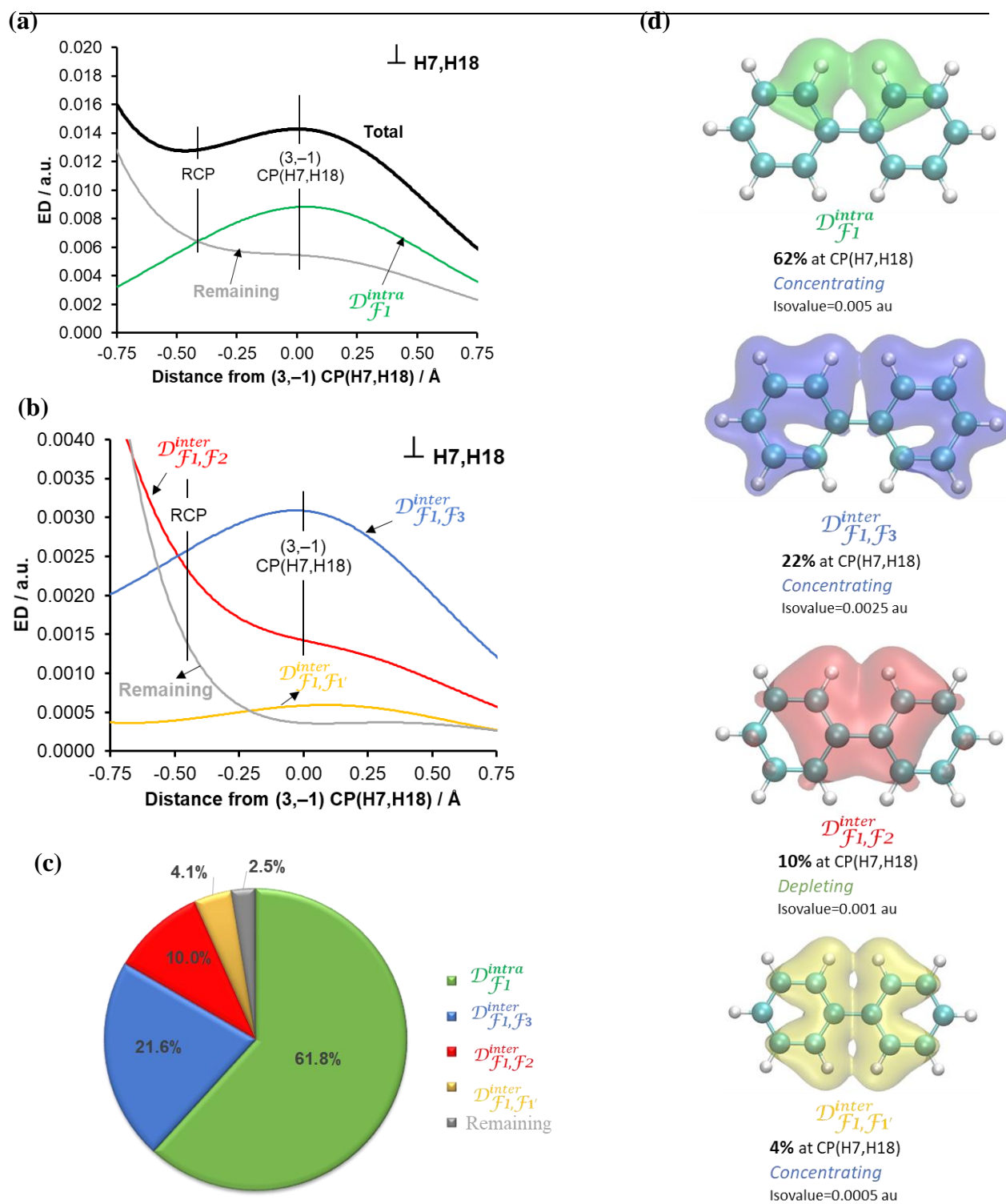


Figure S4. Decomposition of the (a) major and (b) minor FALDI fragment contributions to the ED of the CP(H7,H18) along the λ_2 -eigenvector in planar Bph. (c) provides the relative contributions to the ED at CP(H7,H18), and (d) isosurfaces of selected components.

Therefore, the fragment analysis reveals that the vast majority of the ED at CP(H7,H18) results from electron delocalization involving the two CH groups. Delocalization among themselves, as well as with the other CH...HC bay and the other remaining hydrocarbons results in a concentrating channel of delocalized ED. It is also interesting to note that the depletion of ED observed at CP(H7,H18) does not arise directly from the linker C-C bond, but rather from electrons delocalized between the linker and the bay CH...HC fragment. Finally, the fragment results clearly illustrates the molecular-wide nature of the density concentrated between the H,H atoms.

Performing the same analysis for the H...H region in twisted Bph reveals that the same four components make up the majority of the density at MDP(H7,H18) – Figure 3. The same contributions that concentrate/deplete ED in planar Bph also concentrate/deplete ED in twisted Bph. In fact, the only discernible differences between the two compounds are the relative magnitudes of each component, as well as their relative slopes.

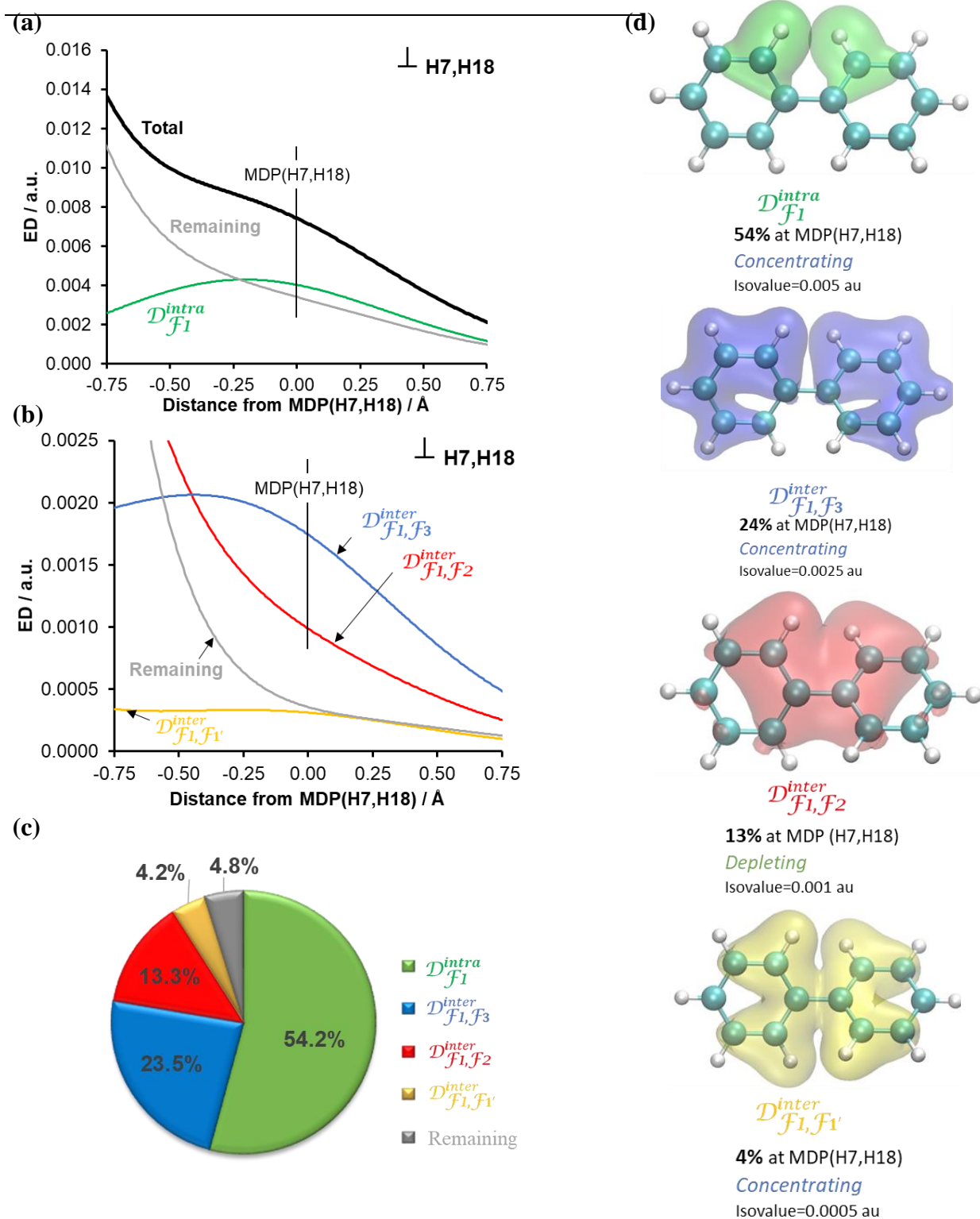


Figure S5. Decomposition of the (a) major and (b) minor FALDI fragment contributions to the ED of the MDP(H7,H18) along the λ_2 -eigenvector in twisted Bph. (c) provides the relative contributions to the ED at MDP(H7,H18), and (d) isosurfaces of selected components

End of Part 3

Part 4. FALDI-ED Data for H7...H18 Interaction in Biphenyl

FALDI Fragment Analysis

Table S3. FALDI fragment data at (3,-1) CP(H7,H18) or MDP(H7,H18) in planar and twisted biphenyl, respectively.

Fragment(s)	Planar		Twisted	
	ED contribution (a.u.) / %- fraction	Classification based on 2nd derivative sign (λ_2)	ED contribution (a.u.) / %- fraction	Classification based on 2nd derivative sign (λ_2)
$\mathcal{D}_{\mathcal{F}_1}^{intra}(\mathbf{r})$	0.00048 / 3.4	<i>concentrating</i>	0.00010 / 1.4	<i>concentrating</i>
$\mathcal{D}_{\mathcal{F}_2}^{intra}(\mathbf{r})$	-0.00003 / -0.2	<i>removing</i>	0.00005 / 0.6	<i>concentrating</i>
$\mathcal{D}_{\mathcal{F}_3}^{intra}(\mathbf{r})$	0.00001 / 0.1	<i>depleting</i>	0.00001 / 0.2	<i>depleting</i>
$\mathcal{D}_{\mathcal{F}_4}^{intra}(\mathbf{r})$	0.00030 / 2.1	<i>concentrating</i>	0.00019 / 2.6	<i>concentrating</i>
$\mathcal{D}_{\mathcal{F}_1, \mathcal{F}_2}^{inter}(\mathbf{r})$	0.00836 / 58.6	<i>concentrating</i>	0.00387 / 52.2	<i>concentrating</i>
$\mathcal{D}_{\mathcal{F}_1, \mathcal{F}_3}^{inter}(\mathbf{r})$	0.00048 / 3.4	<i>concentrating</i>	0.00023 / 3.0	<i>concentrating</i>
$\mathcal{D}_{\mathcal{F}_1, \mathcal{F}_4}^{inter}(\mathbf{r})$	0.00158 / 11.1	<i>concentrating</i>	0.00072 / 9.7	<i>concentrating</i>
$\mathcal{D}_{\mathcal{F}_2, \mathcal{F}_3}^{inter}(\mathbf{r})$	0.00094 / 6.6	<i>depleting</i>	0.00076 / 10.3	<i>depleting</i>
$\mathcal{D}_{\mathcal{F}_2, \mathcal{F}_4}^{inter}(\mathbf{r})$	0.00209 / 14.7	<i>concentrating</i>	0.00134 / 18.0	<i>concentrating</i>
$\mathcal{D}_{\mathcal{F}_3, \mathcal{F}_4}^{inter}(\mathbf{r})$	0.00005 / 0.4	<i>depleting</i>	0.00015 / 2.1	<i>depleting</i>

FALDI Diatomic Analysis**Table S4.** FALDI diatomic data at (3,-1) CP(H7,H18) or MDP(H7,H18) in planar and twisted biphenyl, respectively.

Atom-Pair	Planar		Twisted	
	ED contribution (a.u.) / %-fraction	Classification based on 2nd derivative sign (λ_2)	ED contribution (a.u.) / %-fraction	Classification based on 2nd derivative sign (λ_2)
C1,C2	0.00035 / 2.4	<i>depleting</i>	0.00029 / 4.2	<i>depleting</i>
C1,C3	0.00002 / 0.1	<i>depleting</i>	0.00002 / 0.3	<i>depleting</i>
C1,C4	0.00000 / 0.0	<i>depleting</i>	0.00001 / 0.2	<i>depleting</i>
C1,C5	0.00000 / 0.0	<i>depleting</i>	0.00000 / 0.1	<i>depleting</i>
C1,C6	0.00000 / 0.0	<i>removing</i>	0.00002 / 0.3	<i>depleting</i>
C1,H7	0.00018 / 1.2	<i>concentrating</i>	0.00007 / 1.0	<i>concentrating</i>
C1,H8	0.00000 / 0.0	<i>removing</i>	0.00000 / 0.0	<i>removing</i>
C1,H9	0.00000 / 0.0	<i>depleting</i>	0.00000 / 0.0	<i>depleting</i>
C1,H10	0.00000 / 0.0	<i>depleting</i>	0.00000 / 0.0	<i>depleting</i>
C1,H11	0.00000 / 0.0	<i>removing</i>	0.00000 / 0.0	<i>depleting</i>
C1,C12	0.00000 / 0.0	<i>depleting</i>	0.00001 / 0.2	<i>depleting</i>
C1,C13	0.00007 / 0.5	<i>concentrating</i>	0.00005 / 0.7	<i>concentrating</i>
C1,C14	0.00001 / 0.0	<i>concentrating</i>	0.00000 / 0.1	<i>concentrating</i>
C1,C15	0.00000 / 0.0	<i>depleting</i>	0.00000 / 0.0	<i>depleting</i>
C1,C16	0.00000 / 0.0	<i>depleting</i>	0.00000 / 0.0	<i>depleting</i>
C1,C17	0.00000 / 0.0	<i>removing</i>	0.00000 / 0.0	<i>depleting</i>
C1,H18	0.00008 / 0.6	<i>concentrating</i>	0.00004 / 0.5	<i>concentrating</i>
C1,H19	0.00000 / 0.0	<i>removing</i>	0.00000 / 0.0	<i>depleting</i>
C1,H20	0.00000 / 0.0	<i>depleting</i>	0.00000 / 0.0	<i>depleting</i>
C1,H21	0.00000 / 0.0	<i>removing</i>	0.00000 / 0.0	<i>depleting</i>
C1,H22	0.00000 / 0.0	<i>removing</i>	0.00000 / 0.0	<i>depleting</i>
C2,C3	0.00059 / 4.1	<i>concentrating</i>	0.00034 / 4.8	<i>concentrating</i>
C2,C4	0.00008 / 0.6	<i>concentrating</i>	0.00005 / 0.6	<i>concentrating</i>
C2,C5	0.00005 / 0.3	<i>concentrating</i>	0.00005 / 0.7	<i>concentrating</i>
C2,C6	0.00005 / 0.4	<i>concentrating</i>	0.00003 / 0.5	<i>depleting</i>
C2,H7	0.00413 / 28.7	<i>concentrating</i>	0.00178 / 25.6	<i>concentrating</i>
C2,H8	0.00006 / 0.4	<i>concentrating</i>	0.00003 / 0.4	<i>concentrating</i>
C2,H9	0.00005 / 0.3	<i>concentrating</i>	0.00002 / 0.3	<i>concentrating</i>
C2,H10	0.00002 / 0.1	<i>concentrating</i>	0.00001 / 0.2	<i>concentrating</i>
C2,H11	0.00002 / 0.2	<i>concentrating</i>	0.00001 / 0.2	<i>concentrating</i>
C2,C12	0.00007 / 0.5	<i>concentrating</i>	0.00005 / 0.7	<i>concentrating</i>
C2,C13	-0.00004 / -0.3	<i>removing</i>	0.00004 / 0.5	<i>concentrating</i>

Appendix II

Table S4 continues – FALDI diatomic data

C2,C14	0.00000 / 0.0	<i>concentrating</i>	0.00001 / 0.1	<i>concentrating</i>
C2,C15	0.00001 / 0.1	<i>concentrating</i>	0.00001 / 0.2	<i>concentrating</i>
C2,C16	0.00002 / 0.1	<i>concentrating</i>	0.00001 / 0.2	<i>concentrating</i>
C2,C17	0.00003 / 0.2	<i>concentrating</i>	0.00002 / 0.3	<i>concentrating</i>
C2,H18	0.00015 / 1.1	<i>concentrating</i>	0.00007 / 1.1	<i>concentrating</i>
C2,H19	0.00001 / 0.1	<i>concentrating</i>	0.00000 / 0.0	<i>concentrating</i>
C2,H20	0.00001 / 0.1	<i>concentrating</i>	0.00000 / 0.1	<i>concentrating</i>
C2,H21	0.00001 / 0.1	<i>concentrating</i>	0.00001 / 0.1	<i>concentrating</i>
C2,H22	0.00001 / 0.1	<i>concentrating</i>	0.00000 / 0.1	<i>concentrating</i>
C3,C4	0.00006 / 0.4	<i>concentrating</i>	0.00002 / 0.3	<i>concentrating</i>
C3,C5	0.00000 / 0.0	<i>concentrating</i>	0.00000 / 0.1	<i>concentrating</i>
C3,C6	0.00001 / 0.0	<i>concentrating</i>	0.00000 / 0.0	<i>concentrating</i>
C3,H7	0.00025 / 1.8	<i>concentrating</i>	0.00011 / 1.6	<i>concentrating</i>
C3,H8	0.00002 / 0.1	<i>concentrating</i>	0.00001 / 0.1	<i>concentrating</i>
C3,H9	0.00001 / 0.0	<i>concentrating</i>	0.00000 / 0.0	<i>concentrating</i>
C3,H10	0.00000 / 0.0	<i>concentrating</i>	0.00000 / 0.0	<i>concentrating</i>
C3,H11	0.00000 / 0.0	<i>concentrating</i>	0.00000 / 0.0	<i>concentrating</i>
C3,C12	0.00001 / 0.0	<i>concentrating</i>	0.00000 / 0.1	<i>concentrating</i>
C3,C13	0.00000 / 0.0	<i>concentrating</i>	0.00001 / 0.1	<i>concentrating</i>
C3,C14	0.00000 / 0.0	<i>removing</i>	0.00000 / 0.0	<i>removing</i>
C3,C15	0.00000 / 0.0	<i>depleting</i>	0.00000 / 0.0	<i>concentrating</i>
C3,C16	0.00000 / 0.0	<i>concentrating</i>	0.00000 / 0.0	<i>concentrating</i>
C3,C17	0.00000 / 0.0	<i>concentrating</i>	0.00000 / 0.0	<i>concentrating</i>
C3,H18	0.00003 / 0.2	<i>concentrating</i>	0.00001 / 0.2	<i>concentrating</i>
C3,H19	0.00000 / 0.0	<i>concentrating</i>	0.00000 / 0.0	<i>depleting</i>
C3,H20	0.00000 / 0.0	<i>concentrating</i>	0.00000 / 0.0	<i>concentrating</i>
C3,H21	0.00000 / 0.0	<i>concentrating</i>	0.00000 / 0.0	<i>concentrating</i>
C3,H22	0.00000 / 0.0	<i>concentrating</i>	0.00000 / 0.0	<i>concentrating</i>
C4,C5	0.00001 / 0.1	<i>concentrating</i>	0.00002 / 0.2	<i>concentrating</i>
C4,C6	0.00000 / 0.0	<i>concentrating</i>	0.00000 / 0.0	<i>depleting</i>
C4,H7	0.00013 / 0.9	<i>concentrating</i>	0.00005 / 0.8	<i>concentrating</i>
C4,H8	0.00000 / 0.0	<i>concentrating</i>	0.00000 / 0.0	<i>concentrating</i>
C4,H9	0.00001 / 0.1	<i>concentrating</i>	0.00001 / 0.1	<i>concentrating</i>
C4,H10	0.00000 / 0.0	<i>concentrating</i>	0.00000 / 0.0	<i>concentrating</i>
C4,H11	0.00000 / 0.0	<i>concentrating</i>	0.00000 / 0.0	<i>depleting</i>
C4,C12	0.00000 / 0.0	<i>depleting</i>	0.00000 / 0.0	<i>depleting</i>
C4,C13	0.00001 / 0.1	<i>concentrating</i>	0.00001 / 0.2	<i>concentrating</i>
C4,C14	0.00000 / 0.0	<i>depleting</i>	0.00000 / 0.0	<i>concentrating</i>
C4,C15	0.00000 / 0.0	<i>concentrating</i>	0.00000 / 0.0	<i>depleting</i>

Appendix II

Table S4 continues – FALDI diatomic data

C4,C16	0.00000 / 0.0	<i>concentrating</i>	0.00000 / 0.0	<i>depleting</i>
C4,C17	0.00000 / 0.0	<i>depleting</i>	0.00000 / 0.0	<i>depleting</i>
C4,H18	0.00001 / 0.1	<i>concentrating</i>	0.00001 / 0.1	<i>concentrating</i>
C4,H19	0.00000 / 0.0	<i>concentrating</i>	0.00000 / 0.0	<i>concentrating</i>
C4,H20	0.00000 / 0.0	<i>concentrating</i>	0.00000 / 0.0	<i>depleting</i>
C4,H21	0.00000 / 0.0	<i>concentrating</i>	0.00000 / 0.0	<i>concentrating</i>
C4,H22	0.00000 / 0.0	<i>concentrating</i>	0.00000 / 0.0	<i>concentrating</i>
C5,C6	0.00000 / 0.0	<i>depleting</i>	0.00000 / 0.0	<i>removing</i>
C5,H7	0.00003 / 0.2	<i>concentrating</i>	0.00002 / 0.2	<i>concentrating</i>
C5,H8	0.00000 / 0.0	<i>depleting</i>	0.00000 / 0.0	<i>concentrating</i>
C5,H9	0.00000 / 0.0	<i>concentrating</i>	0.00000 / 0.0	<i>concentrating</i>
C5,H10	0.00000 / 0.0	<i>depleting</i>	0.00000 / 0.0	<i>depleting</i>
C5,H11	0.00000 / 0.0	<i>depleting</i>	0.00000 / 0.0	<i>depleting</i>
C5,C12	0.00000 / 0.0	<i>depleting</i>	0.00000 / 0.0	<i>depleting</i>
C5,C13	0.00002 / 0.1	<i>concentrating</i>	0.00001 / 0.2	<i>concentrating</i>
C5,C14	0.00000 / 0.0	<i>concentrating</i>	0.00000 / 0.0	<i>concentrating</i>
C5,C15	0.00000 / 0.0	<i>concentrating</i>	0.00000 / 0.0	<i>depleting</i>
C5,C16	0.00000 / 0.0	<i>depleting</i>	0.00000 / 0.0	<i>concentrating</i>
C5,C17	0.00000 / 0.0	<i>depleting</i>	0.00000 / 0.0	<i>depleting</i>
C5,H18	0.00002 / 0.1	<i>concentrating</i>	0.00001 / 0.1	<i>concentrating</i>
C5,H19	0.00000 / 0.0	<i>concentrating</i>	0.00000 / 0.0	<i>concentrating</i>
C5,H20	0.00000 / 0.0	<i>concentrating</i>	0.00000 / 0.0	<i>concentrating</i>
C5,H21	0.00000 / 0.0	<i>depleting</i>	0.00000 / 0.0	<i>concentrating</i>
C5,H22	0.00000 / 0.0	<i>depleting</i>	0.00000 / 0.0	<i>concentrating</i>
C6,H7	0.00010 / 0.7	<i>concentrating</i>	0.00004 / 0.6	<i>concentrating</i>
C6,H8	0.00000 / 0.0	<i>concentrating</i>	0.00000 / 0.0	<i>removing</i>
C6,H9	0.00000 / 0.0	<i>concentrating</i>	0.00000 / 0.0	<i>concentrating</i>
C6,H10	0.00000 / 0.0	<i>depleting</i>	0.00000 / 0.0	<i>removing</i>
C6,H11	0.00000 / 0.0	<i>depleting</i>	0.00000 / 0.0	<i>depleting</i>
C6,C12	0.00000 / 0.0	<i>removing</i>	0.00000 / 0.0	<i>depleting</i>
C6,C13	0.00003 / 0.2	<i>concentrating</i>	0.00002 / 0.3	<i>concentrating</i>
C6,C14	0.00000 / 0.0	<i>concentrating</i>	0.00000 / 0.0	<i>concentrating</i>
C6,C15	0.00000 / 0.0	<i>depleting</i>	0.00000 / 0.0	<i>depleting</i>
C6,C16	0.00000 / 0.0	<i>depleting</i>	0.00000 / 0.0	<i>depleting</i>
C6,C17	0.00000 / 0.0	<i>removing</i>	0.00000 / 0.0	<i>depleting</i>
C6,H18	0.00003 / 0.2	<i>concentrating</i>	0.00001 / 0.1	<i>concentrating</i>
C6,H19	0.00000 / 0.0	<i>removing</i>	0.00000 / 0.0	<i>depleting</i>
C6,H20	0.00000 / 0.0	<i>concentrating</i>	0.00000 / 0.0	<i>depleting</i>
C6,H21	0.00000 / 0.0	<i>depleting</i>	0.00000 / 0.0	<i>depleting</i>

Appendix II

Table S4 continues – FALDI diatomic data

C6,H22	0.00000 / 0.0	<i>depleting</i>	0.00000 / 0.0	<i>depleting</i>
H7,H8	0.00007 / 0.5	<i>concentrating</i>	0.00003 / 0.4	<i>concentrating</i>
H7,H9	0.00005 / 0.4	<i>concentrating</i>	0.00002 / 0.3	<i>concentrating</i>
H7,H10	0.00002 / 0.1	<i>concentrating</i>	0.00001 / 0.1	<i>concentrating</i>
H7,H11	0.00005 / 0.3	<i>concentrating</i>	0.00002 / 0.3	<i>concentrating</i>
H7,C12	0.00008 / 0.6	<i>concentrating</i>	0.00004 / 0.5	<i>concentrating</i>
H7,C13	0.00015 / 1.1	<i>concentrating</i>	0.00007 / 1.1	<i>concentrating</i>
H7,C14	0.00003 / 0.2	<i>concentrating</i>	0.00001 / 0.2	<i>concentrating</i>
H7,C15	0.00001 / 0.1	<i>concentrating</i>	0.00001 / 0.1	<i>concentrating</i>
H7,C16	0.00002 / 0.1	<i>concentrating</i>	0.00001 / 0.1	<i>concentrating</i>
H7,C17	0.00003 / 0.2	<i>concentrating</i>	0.00001 / 0.1	<i>concentrating</i>
H7,H18	0.00051 / 3.5	<i>concentrating</i>	0.00010 / 1.5	<i>concentrating</i>
H7,H19	0.00001 / 0.1	<i>concentrating</i>	0.00000 / 0.1	<i>concentrating</i>
H7,H20	0.00000 / 0.0	<i>concentrating</i>	0.00000 / 0.0	<i>concentrating</i>
H7,H21	0.00001 / 0.1	<i>concentrating</i>	0.00000 / 0.1	<i>concentrating</i>
H7,H22	0.00001 / 0.0	<i>concentrating</i>	0.00000 / 0.1	<i>concentrating</i>
H8,H9	0.00000 / 0.0	<i>removing</i>	0.00000 / 0.0	<i>removing</i>
H8,H10	0.00000 / 0.0	<i>concentrating</i>	0.00000 / 0.0	<i>concentrating</i>
H8,H11	0.00000 / 0.0	<i>concentrating</i>	0.00000 / 0.0	<i>concentrating</i>
H8,C12	0.00000 / 0.0	<i>removing</i>	0.00000 / 0.0	<i>depleting</i>
H8,C13	0.00001 / 0.1	<i>concentrating</i>	0.00000 / 0.0	<i>concentrating</i>
H8,C14	0.00000 / 0.0	<i>concentrating</i>	0.00000 / 0.0	<i>depleting</i>
H8,C15	0.00000 / 0.0	<i>concentrating</i>	0.00000 / 0.0	<i>concentrating</i>
H8,C16	0.00000 / 0.0	<i>concentrating</i>	0.00000 / 0.0	<i>concentrating</i>
H8,C17	0.00000 / 0.0	<i>removing</i>	0.00000 / 0.0	<i>depleting</i>
H8,H18	0.00001 / 0.1	<i>concentrating</i>	0.00000 / 0.1	<i>concentrating</i>
H8,H19	0.00000 / 0.0	<i>concentrating</i>	0.00000 / 0.0	<i>concentrating</i>
H8,H20	0.00000 / 0.0	<i>concentrating</i>	0.00000 / 0.0	<i>concentrating</i>
H8,H21	0.00000 / 0.0	<i>concentrating</i>	0.00000 / 0.0	<i>concentrating</i>
H8,H22	0.00000 / 0.0	<i>concentrating</i>	0.00000 / 0.0	<i>concentrating</i>
H9,H10	0.00000 / 0.0	<i>concentrating</i>	0.00000 / 0.0	<i>concentrating</i>
H9,H11	0.00000 / 0.0	<i>depleting</i>	0.00000 / 0.0	<i>depleting</i>
H9,C12	0.00000 / 0.0	<i>depleting</i>	0.00000 / 0.0	<i>depleting</i>
H9,C13	0.00001 / 0.1	<i>concentrating</i>	0.00000 / 0.1	<i>concentrating</i>
H9,C14	0.00000 / 0.0	<i>concentrating</i>	0.00000 / 0.0	<i>concentrating</i>
H9,C15	0.00000 / 0.0	<i>concentrating</i>	0.00000 / 0.0	<i>depleting</i>
H9,C16	0.00000 / 0.0	<i>concentrating</i>	0.00000 / 0.0	<i>concentrating</i>
H9,C17	0.00000 / 0.0	<i>concentrating</i>	0.00000 / 0.0	<i>depleting</i>
H9,H18	0.00000 / 0.0	<i>concentrating</i>	0.00000 / 0.0	<i>concentrating</i>

Appendix II

Table S4 continues – FALDI diatomic data

H9,H19	0.00000 / 0.0	<i>concentrating</i>	0.00000 / 0.0	<i>concentrating</i>
H9,H20	0.00000 / 0.0	<i>concentrating</i>	0.00000 / 0.0	<i>concentrating</i>
H9,H21	0.00000 / 0.0	<i>concentrating</i>	0.00000 / 0.0	<i>concentrating</i>
H9,H22	0.00000 / 0.0	<i>concentrating</i>	0.00000 / 0.0	<i>concentrating</i>
H10,H11	0.00000 / 0.0	<i>depleting</i>	0.00000 / 0.0	<i>removing</i>
H10,C12	0.00000 / 0.0	<i>removing</i>	0.00000 / 0.0	<i>depleting</i>
H10,C13	0.00001 / 0.1	<i>concentrating</i>	0.00001 / 0.1	<i>concentrating</i>
H10,C14	0.00000 / 0.0	<i>concentrating</i>	0.00000 / 0.0	<i>concentrating</i>
H10,C15	0.00000 / 0.0	<i>concentrating</i>	0.00000 / 0.0	<i>concentrating</i>
H10,C16	0.00000 / 0.0	<i>depleting</i>	0.00000 / 0.0	<i>concentrating</i>
H10,C17	0.00000 / 0.0	<i>depleting</i>	0.00000 / 0.0	<i>depleting</i>
H10,H18	0.00001 / 0.1	<i>concentrating</i>	0.00000 / 0.1	<i>concentrating</i>
H10,H19	0.00000 / 0.0	<i>concentrating</i>	0.00000 / 0.0	<i>concentrating</i>
H10,H20	0.00000 / 0.0	<i>concentrating</i>	0.00000 / 0.0	<i>concentrating</i>
H10,H21	0.00000 / 0.0	<i>concentrating</i>	0.00000 / 0.0	<i>concentrating</i>
H10,H22	0.00000 / 0.0	<i>depleting</i>	0.00000 / 0.0	<i>depleting</i>
H11,C12	0.00000 / 0.0	<i>removing</i>	0.00000 / 0.0	<i>depleting</i>
H11,C13	0.00001 / 0.1	<i>concentrating</i>	0.00000 / 0.1	<i>concentrating</i>
H11,C14	0.00000 / 0.0	<i>concentrating</i>	0.00000 / 0.0	<i>concentrating</i>
H11,C15	0.00000 / 0.0	<i>concentrating</i>	0.00000 / 0.0	<i>concentrating</i>
H11,C16	0.00000 / 0.0	<i>depleting</i>	0.00000 / 0.0	<i>concentrating</i>
H11,C17	0.00000 / 0.0	<i>depleting</i>	0.00000 / 0.0	<i>depleting</i>
H11,H18	0.00001 / 0.0	<i>concentrating</i>	0.00000 / 0.1	<i>concentrating</i>
H11,H19	0.00000 / 0.0	<i>concentrating</i>	0.00000 / 0.0	<i>concentrating</i>
H11,H20	0.00000 / 0.0	<i>concentrating</i>	0.00000 / 0.0	<i>concentrating</i>
H11,H21	0.00000 / 0.0	<i>depleting</i>	0.00000 / 0.0	<i>depleting</i>
H11,H22	0.00000 / 0.0	<i>depleting</i>	0.00000 / 0.0	<i>removing</i>
C12,C13	0.00035 / 2.4	<i>depleting</i>	0.00029 / 4.2	<i>depleting</i>
C12,C14	0.00002 / 0.1	<i>depleting</i>	0.00002 / 0.3	<i>depleting</i>
C12,C15	0.00000 / 0.0	<i>depleting</i>	0.00001 / 0.2	<i>depleting</i>
C12,C16	0.00000 / 0.0	<i>depleting</i>	0.00000 / 0.1	<i>depleting</i>
C12,C17	0.00000 / 0.0	<i>removing</i>	0.00002 / 0.3	<i>depleting</i>
C12,H18	0.00018 / 1.2	<i>concentrating</i>	0.00007 / 1.0	<i>concentrating</i>
C12,H19	0.00000 / 0.0	<i>removing</i>	0.00000 / 0.0	<i>removing</i>
C12,H20	0.00000 / 0.0	<i>depleting</i>	0.00000 / 0.0	<i>depleting</i>
C12,H21	0.00000 / 0.0	<i>depleting</i>	0.00000 / 0.0	<i>depleting</i>
C12,H22	0.00000 / 0.0	<i>removing</i>	0.00000 / 0.0	<i>depleting</i>
C13,C14	0.00059 / 4.1	<i>concentrating</i>	0.00034 / 4.8	<i>concentrating</i>
C13,C15	0.00008 / 0.6	<i>concentrating</i>	0.00005 / 0.6	<i>concentrating</i>

Appendix II

Table S4 continues – FALDI diatomic data

C13,C16	0.00005 / 0.3	<i>concentrating</i>	0.00005 / 0.7	<i>concentrating</i>
C13,C17	0.00005 / 0.4	<i>concentrating</i>	0.00003 / 0.5	<i>depleting</i>
C13,H18	0.00413 / 28.7	<i>concentrating</i>	0.00178 / 25.6	<i>concentrating</i>
C13,H19	0.00006 / 0.4	<i>concentrating</i>	0.00003 / 0.4	<i>concentrating</i>
C13,H20	0.00005 / 0.3	<i>concentrating</i>	0.00002 / 0.3	<i>concentrating</i>
C13,H21	0.00002 / 0.1	<i>concentrating</i>	0.00001 / 0.2	<i>concentrating</i>
C13,H22	0.00002 / 0.2	<i>concentrating</i>	0.00001 / 0.2	<i>concentrating</i>
C14,C15	0.00006 / 0.4	<i>concentrating</i>	0.00002 / 0.3	<i>concentrating</i>
C14,C16	0.00000 / 0.0	<i>concentrating</i>	0.00000 / 0.1	<i>concentrating</i>
C14,C17	0.00001 / 0.0	<i>concentrating</i>	0.00000 / 0.0	<i>concentrating</i>
C14,H18	0.00025 / 1.8	<i>concentrating</i>	0.00011 / 1.6	<i>concentrating</i>
C14,H19	0.00002 / 0.1	<i>concentrating</i>	0.00001 / 0.1	<i>concentrating</i>
C14,H20	0.00001 / 0.0	<i>concentrating</i>	0.00000 / 0.0	<i>concentrating</i>
C14,H21	0.00000 / 0.0	<i>concentrating</i>	0.00000 / 0.0	<i>concentrating</i>
C14,H22	0.00000 / 0.0	<i>concentrating</i>	0.00000 / 0.0	<i>concentrating</i>
C15,C16	0.00001 / 0.1	<i>concentrating</i>	0.00002 / 0.2	<i>concentrating</i>
C15,C17	0.00000 / 0.0	<i>concentrating</i>	0.00000 / 0.0	<i>depleting</i>
C15,H18	0.00013 / 0.9	<i>concentrating</i>	0.00005 / 0.8	<i>concentrating</i>
C15,H19	0.00000 / 0.0	<i>concentrating</i>	0.00000 / 0.0	<i>concentrating</i>
C15,H20	0.00001 / 0.1	<i>concentrating</i>	0.00001 / 0.1	<i>concentrating</i>
C15,H21	0.00000 / 0.0	<i>concentrating</i>	0.00000 / 0.0	<i>concentrating</i>
C15,H22	0.00000 / 0.0	<i>concentrating</i>	0.00000 / 0.0	<i>depleting</i>
C16,C17	0.00000 / 0.0	<i>depleting</i>	0.00000 / 0.0	<i>removing</i>
C16,H18	0.00003 / 0.2	<i>concentrating</i>	0.00002 / 0.2	<i>concentrating</i>
C16,H19	0.00000 / 0.0	<i>depleting</i>	0.00000 / 0.0	<i>concentrating</i>
C16,H20	0.00000 / 0.0	<i>concentrating</i>	0.00000 / 0.0	<i>concentrating</i>
C16,H21	0.00000 / 0.0	<i>depleting</i>	0.00000 / 0.0	<i>depleting</i>
C16,H22	0.00000 / 0.0	<i>depleting</i>	0.00000 / 0.0	<i>depleting</i>
C17,H18	0.00010 / 0.7	<i>concentrating</i>	0.00004 / 0.6	<i>concentrating</i>
C17,H19	0.00000 / 0.0	<i>concentrating</i>	0.00000 / 0.0	<i>removing</i>
C17,H20	0.00000 / 0.0	<i>concentrating</i>	0.00000 / 0.0	<i>concentrating</i>
C17,H21	0.00000 / 0.0	<i>depleting</i>	0.00000 / 0.0	<i>removing</i>
C17,H22	0.00000 / 0.0	<i>depleting</i>	0.00000 / 0.0	<i>depleting</i>
H18,H19	0.00007 / 0.5	<i>concentrating</i>	0.00003 / 0.4	<i>concentrating</i>
H18,H20	0.00005 / 0.4	<i>concentrating</i>	0.00002 / 0.3	<i>concentrating</i>
H18,H21	0.00002 / 0.1	<i>concentrating</i>	0.00001 / 0.1	<i>concentrating</i>
H18,H22	0.00005 / 0.3	<i>concentrating</i>	0.00002 / 0.3	<i>concentrating</i>
H19,H20	0.00000 / 0.0	<i>removing</i>	0.00000 / 0.0	<i>removing</i>
H19,H21	0.00000 / 0.0	<i>concentrating</i>	0.00000 / 0.0	<i>concentrating</i>

Appendix II

Table S4 continues – FALDI diatomic data

H19,H22	0.00000 / 0.0	<i>concentrating</i>	0.00000 / 0.0	<i>concentrating</i>
H20,H21	0.00000 / 0.0	<i>concentrating</i>	0.00000 / 0.0	<i>concentrating</i>
H20,H22	0.00000 / 0.0	<i>depleting</i>	0.00000 / 0.0	<i>depleting</i>
H21,H22	0.00000 / 0.0	<i>depleting</i>	0.00000 / 0.0	<i>removing</i>

End of Part 4

Appendix III

NBOs Support MO and FALDI based 'Bonding' Description of CH \cdots HC Bond Paths in Planar Biphenyl

Prepared for submission to:

Journal of Computational Chemistry **2020**.

Supplementary Information

NBOs Support MO and FALDI based ‘Bonding’ Description of CH \cdots HC Bond Paths in Planar Biphenyl

Thomas G. Bates, Ignacy Cukrowski and Jurgens H. de Lange*

*Department of Chemistry, Faculty of Natural and Agricultural Sciences, University of Pretoria,
Lynnwood Road, Hatfield, Pretoria 0002, South Africa*

*Correspondence to: Jurgens de Lange: E-mail: jurgens.delange@up.ac.za

Supplementary Information

Table of contents:	Page
Part 1. Cartesian Coordinates of all Molecules Studied	202
Part 2. Cross-Section Comparison Between FALDI- and NBO-ED Method for Biphenyl	204
Part 3. Isosurfaces of the Major NBO Contributions	207

Part 1. Cartesian Coordinates of all molecules studied**Table S1.** Cartesian coordinates of planar biphenyl at the B3LYP/cc-pVDZ level.

Atom	X	Y	Z
C1	0.000000	0.747659	0.000000
C2	1.201002	1.486214	0.000000
C3	1.202756	2.881607	0.000000
C4	0.000000	3.592065	0.000000
C5	-1.202756	2.881607	0.000000
C6	-1.201002	1.486214	0.000000
H7	2.162178	0.972810	0.000000
H8	2.155610	3.416086	0.000000
H9	0.000000	4.684170	0.000000
H10	-2.155610	3.416086	0.000000
H11	-2.162178	0.972810	0.000000
C12	0.000000	-0.747659	0.000000
C13	1.201002	-1.486214	0.000000
C14	1.202756	-2.881607	0.000000
C15	0.000000	-3.592065	0.000000
C16	-1.202756	-2.881607	0.000000
C17	-1.201002	-1.486214	0.000000
H18	2.162178	-0.972810	0.000000
H19	2.155610	-3.416086	0.000000
H20	0.000000	-4.684170	0.000000
H21	-2.155610	-3.416086	0.000000
H22	-2.162178	-0.972810	0.000000

Molecular Energy = -463.330812 a.u.

Appendix III

Table S2. Cartesian coordinates of twisted biphenyl at the B3LYP/cc-pVDZ level.

Atom	X	Y	Z
C1	0.000000	0.743784	0.000000
C2	1.137590	1.468260	-0.402647
C3	1.137840	2.864563	-0.402880
C4	0.000000	3.569885	0.000000
C5	-1.137840	2.864563	0.402880
C6	-1.137590	1.468260	0.402647
H7	2.024118	0.929542	-0.744099
H8	2.030290	3.404597	-0.728007
H9	0.000000	4.662191	0.000000
H10	-2.030290	3.404597	0.728007
H11	-2.024118	0.929542	0.744099
C12	0.000000	-0.743784	0.000000
C13	1.137590	-1.468260	0.402647
C14	1.137840	-2.864563	0.402880
C15	0.000000	-3.569885	0.000000
C16	-1.137840	-2.864563	-0.402880
C17	-1.137590	-1.468260	-0.402647
H18	2.024118	-0.929542	0.744099
H19	2.030290	-3.404597	0.728007
H20	0.000000	-4.662191	0.000000
H21	-2.030290	-3.404597	-0.728007
H22	-2.024118	-0.929542	-0.744099

Molecular Energy = -463.333574 a.u.

End of Part 1

Part 2. Cross-Section Comparison Between FALDI- and NBO-ED Method for Biphenyl

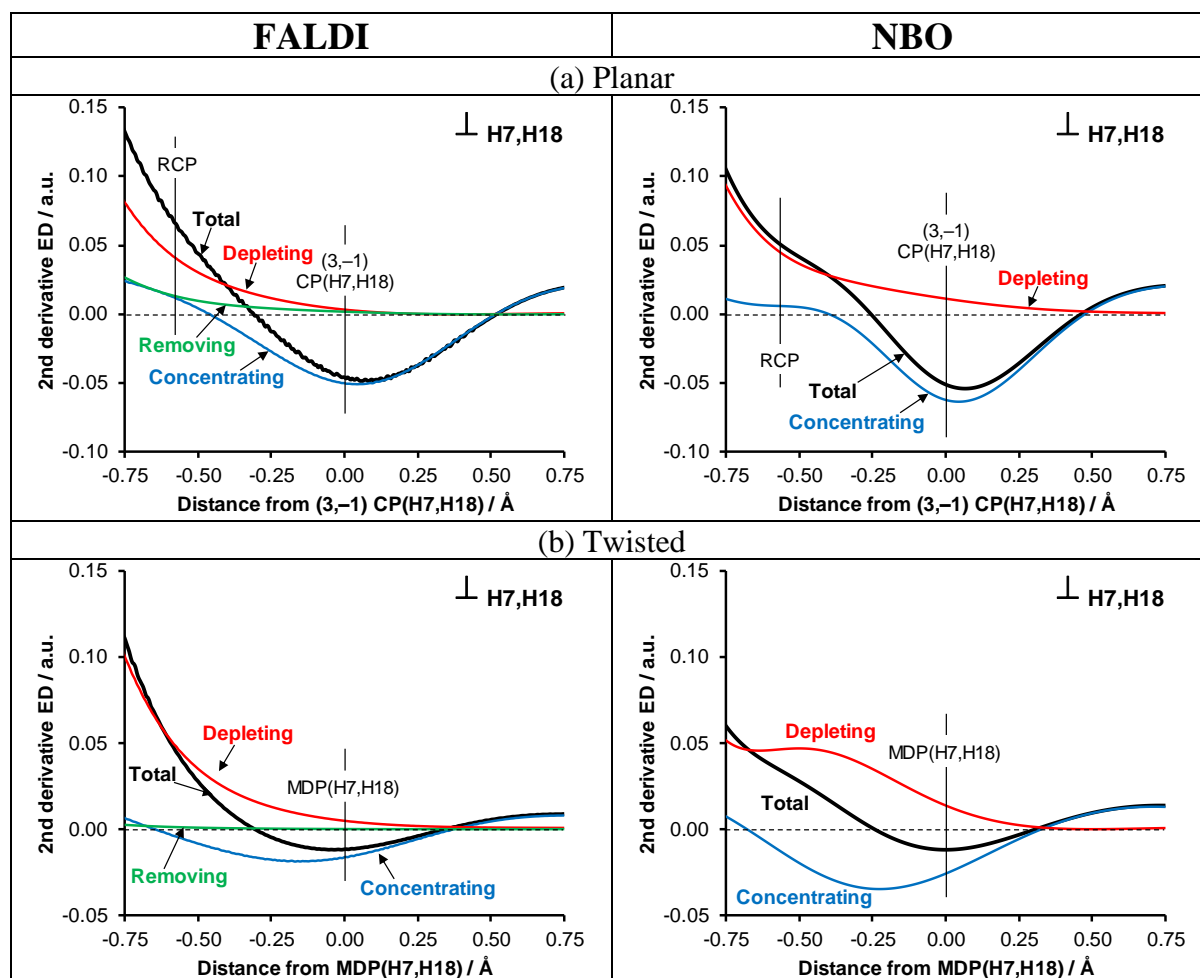


Figure S1 – Decomposition of the directional second partial derivative $\rho(\text{tot})$ along the λ_2 -eigenvector crossing (a) the CP(H7,H18) in planar conformer and (b) MDP(H7,H18) in twisted conformer of Bph to major contributions (concentrating, depleting, and removing) using FALDI and NBO methods.

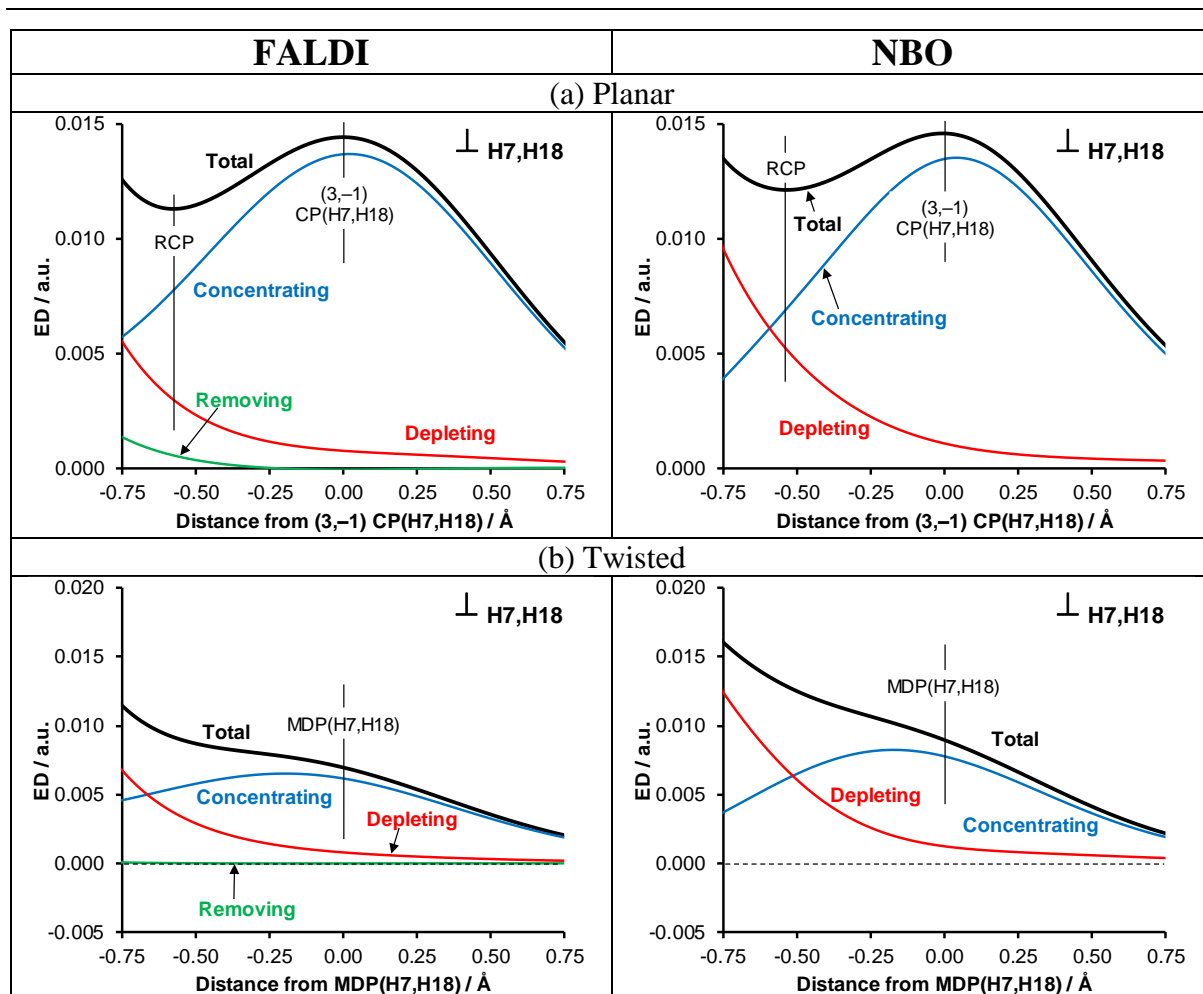


Figure S2 – Decomposition of the $\rho(\text{tot})$ along the λ_2 -eigenvector crossing (a) the CP(H7,H18) in planar conformer and (b) MDP(H7,H18) in twisted conformer of Bph to major contributions (concentrating, depleting, and removing) using FALDI and NBO methods.

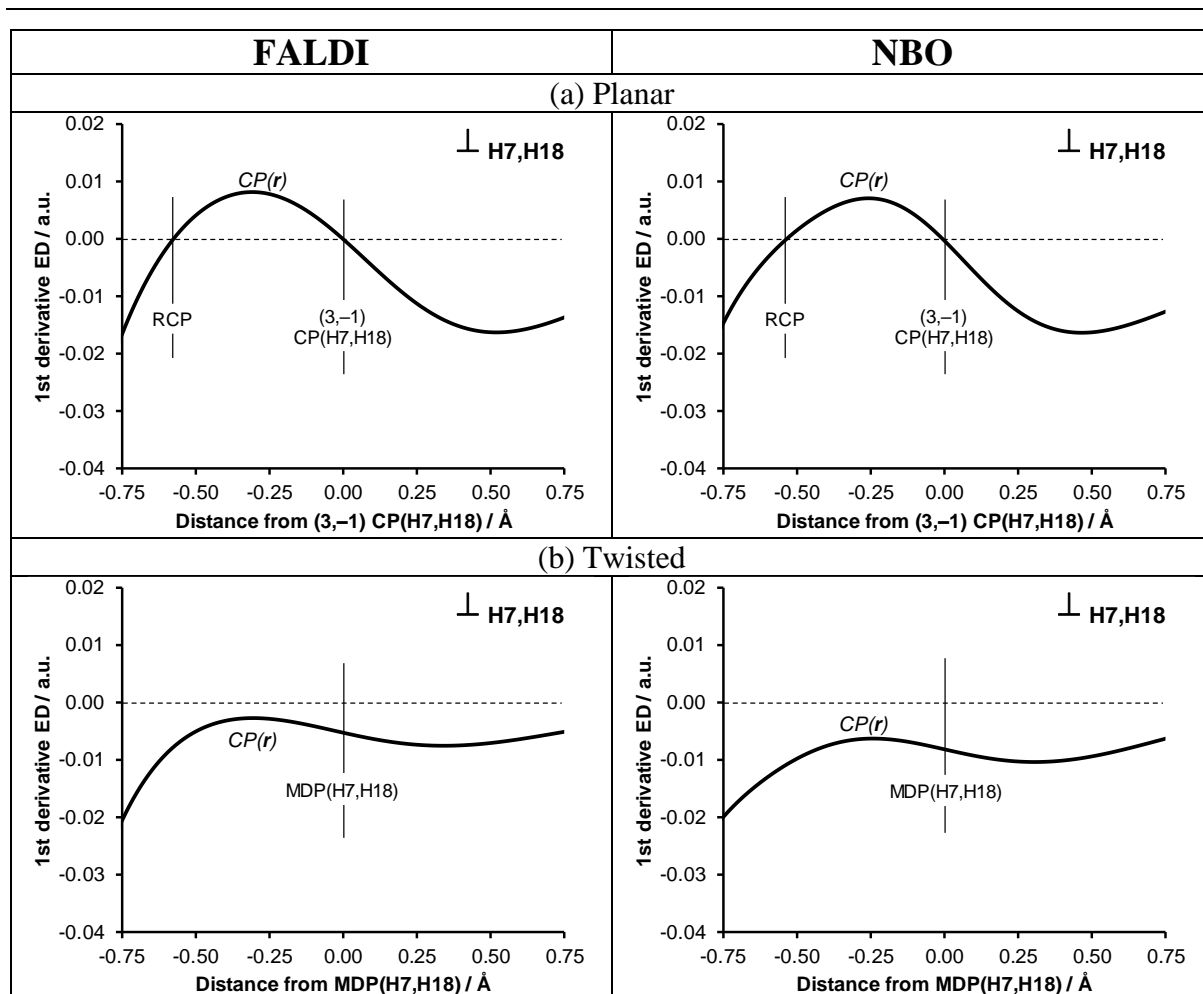
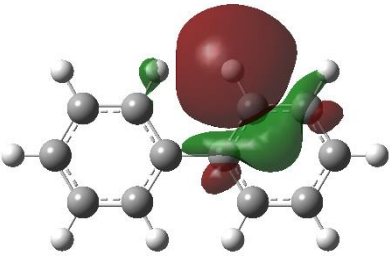
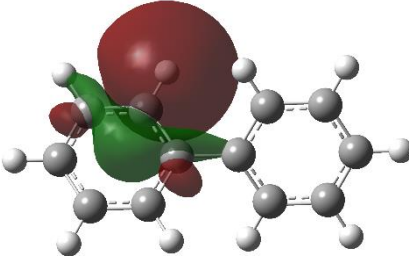
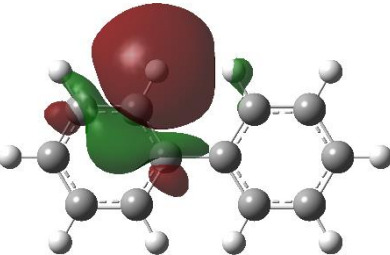
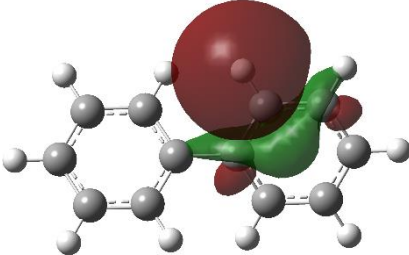
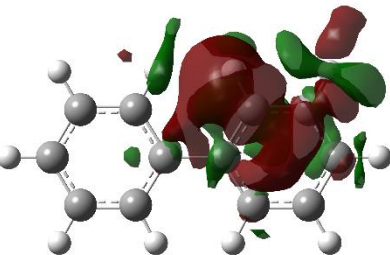
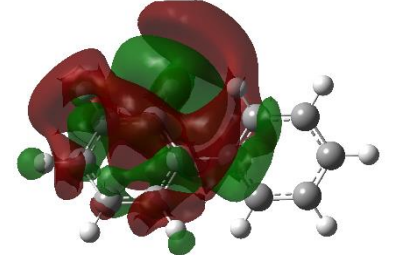
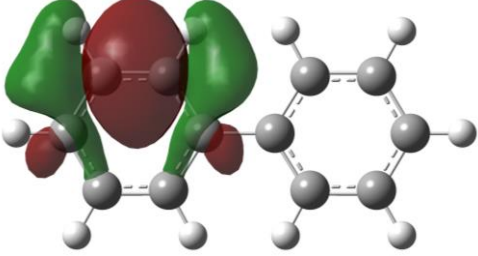
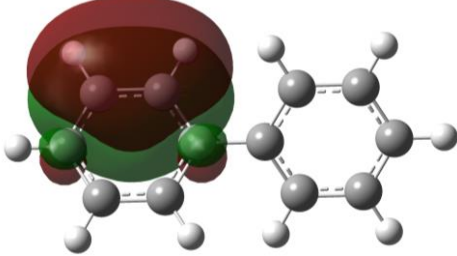
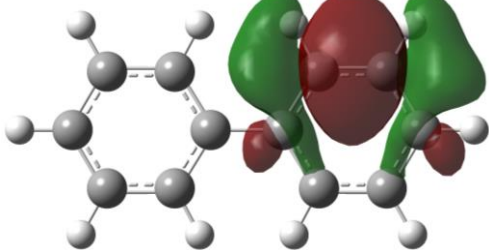
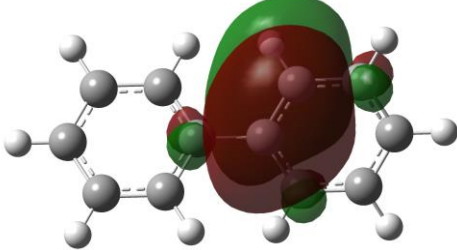


Figure S3 – $CP(\mathbf{r})$ function cross-sections along the λ_2 -eigenvector crossing the (a) CP(H7,H18) in the planar conformer and (b) MDP(H7,H18) in twisted conformer of Bph using FALDI and NBO methods.

End of Part 2

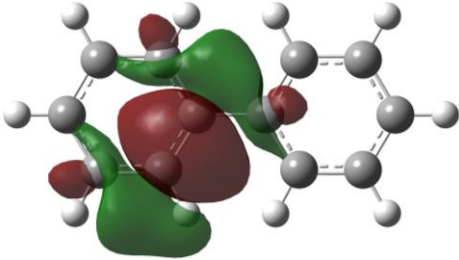
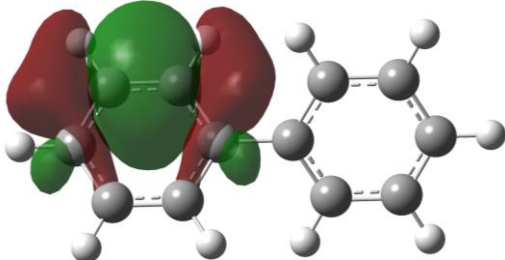
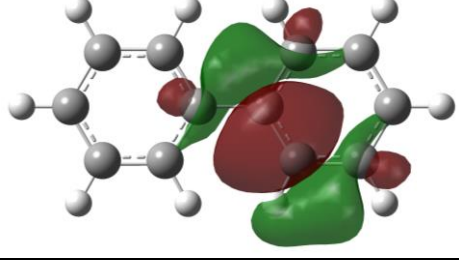
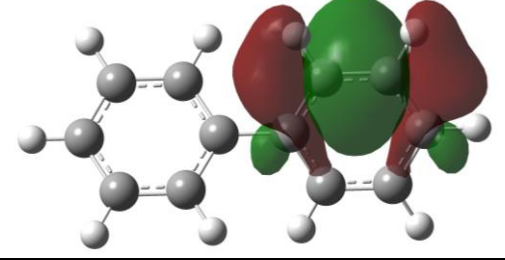
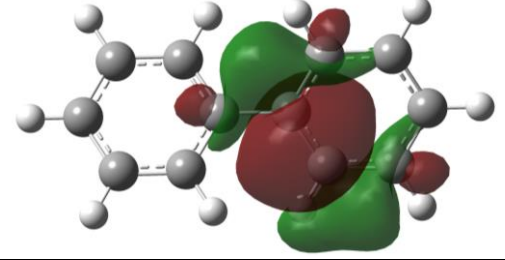
Part 3. Isosurfaces of the Major NBO Contributions

Table 3. Isosurfaces of the most significant NBO contributions (Isovalue 0.02 a.u.) at the (3,-1) CP(H7,H18) and MDP(H7,H18) in **planar** and **twisted** biphenyl, respectively.

Planar	Twisted
NBO; ED contribution a.u. / %-fraction, <i>nature</i>	
NBO 28; 0.00620 / 42.4, <i>conc</i>	NBO 35; 0.00265 / 29.5, <i>conc</i>
	
NBO 29; 0.00620 / 42.4, <i>conc</i>	NBO 32; 0.00265 / 29.5, <i>conc</i>
	
NBO 185; 0.00087 / 6.0, <i>conc</i>	NBO 109; 0.00227 / 25.2, <i>conc</i>
	
NBO 15; 0.00034 / 2.3, <i>depl</i>	NBO 37; 0.00016 / 1.8, <i>conc</i>
	
NBO 16; 0.00033 / 2.3, <i>depl</i>	NBO 41; 0.00035 / 3.9, <i>depl</i>
	

Appendix III

Table S3 continues – NBO isosurfaces

<p>NBO 22; 0.00011 / 0.8, <i>depl</i></p> 	<p>NBO 14; 0.00016 / 1.8, <i>depl</i></p> 
<p>NBO 21; 0.00011 / 0.8, <i>depl</i></p> 	<p>NBO 16; 0.00016 / 1.8, <i>depl</i></p> 
<p>–</p>	<p>NBO 21; 0.00010 / 1.2, <i>depl</i></p>
<p>–</p>	

End of Part 3